FUNDAMENTALS OF PVDF HOLLOW FIBER MEMBRANE FORMATION AND PERVAPORATION FOR ETHANOL-WATER SEPARATION

PANU SUKITPANEENIT

NATIONAL UNIVERSITY OF SINGAPORE

2011

FUNDAMENTALS OF PVDF HOLLOW FIBER MEMBRANE FORMATION AND PERVAPORATION FOR ETHANOL-WATER SEPARATION

PANU SUKITPANEENIT

(Msc., The Petroleum and Petrochemical College,

Chulalongkorn University, Thailand)

A THESIS SUBMITTED

FOR THE DEGREE OF DOCTOR OF PHILOSOPHY

DEPARTMENT OF CHEMICAL AND BIOMOLECULAR ENGINEERING

NATIONAL UNIVERSITY OF SINGAPORE

2011

ACKNOWLEDGEMENT

First of all, I would like to express my deepest gratitude and appreciation to my supervisor Prof. Chung Tai-Shung who introduced me into this fascinating area of membrane research. His excellent guidance, enthusiastic encouragement and invaluable support throughout my PhD study are invaluable. From him, I have learned and benefited greatly in not only research knowledge but also developed the necessary attitude of a qualified researcher.

I would also like to express my sincere appreciation to my PhD thesis committee members, Prof. Kawi Sibudjing, Prof. Tong Yen Wah, Prof. Yang Kun-Lin, Prof. Chen Shing Bor, and Prof. Lu, Xianmao. Their suggestions on my PhD proposal and thesis have been constructive throughout my candidature in NUS.

I would like to gratefully acknowledge the research scholarship and President's Graduate Fellowship offered by the National University of Singapore (NUS), which provided me a positive, conductive and professional atmosphere for conducting research study. I also wish to express my recognition to Agency for Science, Technology and Research (A*STAR) and National Research Foundation through the Competitive Research Program (NRF-CRP) for the financial support with the grant numbers of R-398-000-044-305 (A*STAR), R-279-000-288-305 (A*STAR), 092-139-0033 (A*STAR) and (R-279-000-311-281) (NRC-CRP), enabling this work to be successfully completed.

I would like to convey my personal appreciation to all former and current members of our research group, especially, Prof. Jiang Lanying, Dr. Natalia Widjojo, Dr. Low Bee Ting, Dr. Teoh May May, Dr. Peng Na, Dr. Wang Kaiyu, Dr. Wang Yan and Dr. Xiao Youchang for their invaluable suggestions, discussion and sharing of technical expertise. Special thanks are due to Ms. Chua Mei Ling, Ms. Zhong Peishan, Mr. Sina Bonyadi and Mr. Ong Yee Kang for their useful comments and suggestions on my research work. All members in Prof. Chung's group are cheerful and helpful to me, which have made my study in NUS enjoyable and memorable.

My sincere thanks are due to all staff members in the Department of Chemical and Biomolecular Engineering that have helped me in material purchasing, characterization techniques and given me professional suggestions. Speical appreciation goes to Mr. Ng Kim Poi for his help and expertise advice in fabrication of equipment setup and machinery. My gratitude is also extended to Mr. Lim Poh Chong at Institute of Materials Research and Engineering (IMRE) for his suggestion and help on XRD characterization and analysis.

Last but not least, I must express my grafefulness to my parents, my brothers and sister for their unconditional love and support, which makes my life and study meaningful.

TABLE OF CONTENTS

SUMMARY

The development of hollow fiber membranes with desirable morphology and separation performance in pervaporation processes for ethanol recovery has gained much attention in recent years due to its great potential in biofuel separations. In this thesis, a comprehensive study on the fabrication and pervaporation of poly(vinylidene fluoride) (PVDF) asymmetric hollow fiber membranes for ethanol-water separation is presented.

Firstly, the fundamental science and engineering of fabricating PVDF asymmetric hollow fiber membranes was established, with an emphasis on the correlation among membrane formation mechanism, membrane morphology, crystallinity and mechanical properties as functions of non-solvent additives and dope rheology in the phase inversion process. A series of non-solvents (i.e. water, methanol, ethanol, isopropanol) are used either as nonsolvent additives in the dope or as a component in the external coagulant. Depending on the strength of the non-solvent, the phase inversion of semi-crystalline PVDF membranes is dominated by liquid–liquid demixing or solid–liquid demixing accompanying crystallization. The precipitation mechanisms drastically influence the resultant morphology and mechanical integrity of the membranes. The membrane morphology transforms from an interconnected-cellular type to an interconnected-globule transition type with lower mechanical strengths when adding water, methanol, ethanol, or isopropanol into the spinning dopes or into the coagulation bath. The crystallinity and size of spherulitic globules in the morphology are controlled by the amounts of non-solvents presented in the systems. The rheological behavior of dope solutions was explored and the relationship between

elongation viscosity and mechanical properties has been elaborated. Analytical methods and molecular dynamics simulations were employed to provide insights mechanisms from the views of thermodynamic and kinetic aspects as well as the state of polymer chains involved in the phase inversion process. Interestingly, the conventional perspective of macrovoid-free membranes yielding better mechanical properties may not be applicable for semi-crystalline polymers like PVDF.

Secondly, the mass transport phenomenon in pervaporation of the ethanol/water system via PVDF hollow fiber membranes was investigated through the pore-flow model and a newly modified pore-flow model has been proposed. We have derived the governing equations and confirmed the mass transport mechanism in pervaporation of the ethanol/water system via PVDF asymmetric hollow fiber membranes following the modified pore-flow model. The modified pore-flow model differs from the old pore-flow model by factoring in the contribution of Knudsen flow to vapor transport, which was neglected by the pore-flow model. All transport parameters involved in the model equations are determined from the pervaporation experimental data of pure water and pure ethanol. The correlation of transport parameters to membrane pore size was explored and it was found that the pore size expansion (including the change of membrane surface morphology) is strongly dependent on the solvent in contact. The applicability of the pore-flow model and the modified pore-flow model was compared in predicting the pervaporation performance in terms of the permeate composition and the total mass flux in a water/ethanol mixture system. Results have shown that the modified pore-flow model shows a better prediction for the permeate composition than the pore-flow model, while both models exhibit an excellent prediction of total permeate mass flux. The significance of Knudsen flow contribution in vapor phase

transport as stated in the modified pore-flow model is discussed from the experimental and theoretical aspects.

Thirdly, we have further studied the feasilibity on the science of fabricating PVDF hollow fiber membranes with desirable morphology and pore size using the concept of the modified pore-flow model while elucidating the complicated relationship among membrane morphology, pore size, pore size distribution and separation performance. The variation of bore-fluid composition, air-gap distance and take-up speed results in membranes with various morphologies ranging from large-finger-like macrovoid to nearly perfect macrovoid-free structures. Interestingly, an increase in air-gap distance or take-up speed not only effectively suppresses the formation of macrovoids but also results in the reduction of membrane pore size and the narrowing of pore size distribution, hence leading to the enhancement of membrane performance. The permeation flux is found to be mainly controlled by the overall porosity and the contribution of large pore sizes of the membrane, while the selectivity or separation factor is greatly determined by membrane pore size and pore size distribution, which is consistent with the modified pore-flow model. The newly developed PVDF asymmetric hollow fiber membranes demonstrates remarkable high fluxes of 3,500–8,800 g m^{-2} h^{-1} and reasonable ethanol–water separation factors of 5–8 compared to existing polymeric-based pervaporation membranes.

Finally, we have demonstrated the design and engineering of poly(vinylidene fluoride) (PVDF)/nano-silica dual-layer hollow fibers as novel pervaporation membranes for ethanol recovery. The newly developed dual-layer hollow fiber membrane can exhibit a high separation factor of up to 29 with a sustainable high flux of 1,100 g m^{-2} h^{-1},

which lies within the separation performance regime of inorganic membranes. Central to this performance achievement is the synergy of (1) desirable membrane morphology, nano- pore size and high surface porosity of a thin-PVDF/nano-silica composite on a fully porous substrate accomplished by the dual-layer co-extrusion technology, and (2) optimal operating downstream pressure with the aid of controlled pervaporation transport. The membrane selectivity-downstream pressure dependence of PVDF/nano-silica hybrid membranes is comprehensible via a modified pore-flow model. This study may represent a new class of membranes for ethanol-water separation.

NOMENCLATURE

A	liquid transport parameter for a pure component system (mol m^{-1} s^{-1} Pa^{-1})
A_a	effective membrane area (m^2)
A_a	area of the amorphous phase
A_c	area of the crystalline phase
A_e, A_w	liquid transport parameters A of ethanol and water components, respectively
$A_{die\ swell}$	cross-section area of the nascent hollow fiber (cm^2)
A_{mem}	effective membrane area (m^2)
A_{mix}	liquid transport parameter for a binary system (mol m^{-1} s^{-1} Pa^{-1})
B	vapor transport parameter for a pure component system (mol m^{-1} s^{-1} Pa^{-2})
B_i, B_j	vapor transport parameters B of the i^{th} and j^{th} components, respectively
B_e, B_w	vapor transport parameters B of ethanol and water components, respectively
C	vapor transport parameter for a pure component system (mol m^{-1} s^{-1} Pa^{-1})
C_i, C_j	vapor transport parameter C of the i^{th} and j^{th} components, respectively
C_e, C_w	vapor transport parameter C of ethanol and water components, respectively
D	outer diameter of the hollow fiber (cm)
$D°_{NS\ in\ NMP}$	diffusion coefficient of non-solvent in almost pure NMP (10^{-6} cm^2 s^{-1})
F	total gas permeation rate (mol s^{-1})
G	gas permeance or gas permeation flux (mol m^{-2} Pa^{-1} s^{-1})
i.d.	inner diameter of the nascent hollow fiber at the die swell (mm)
I_o	intercept of the plot of G against mean pressures

J	total mass transferred over collecting time (g)
J_t	total permeation flux (g)
k_H	Henry's constant (mol m^{-3} Pa^{-1})
k'_H	proportionality constant in the vapor adsorption defined as the ratio of concentration in the adsorption layer to vapor pressure or (unit weight of polymer/volume of adsorbed gas molecule) x k_H (mol m^{-3} Pa^{-1})
K	power law coefficient constant
l	effective length of the module (cm)
L_0	initial length (cm)
L	air gap length at time t (cm)
M	molecular weight (kg mol^{-1})
M_i, M_j	molecular weight of the i^{th} and j^{th} components, respectively (kg mol^{-1})
M_e, M_w	molecular weight of ethanol and water components, respectively (kg mol^{-1})
n	power law index
n	number of fibers in one testing module
N_t	total number of pores per effective membrane area (m^{-2})
o.d.	outer diameter of the nascent hollow fiber at the die swell (mm)
Q_{dope}	dope flow rate (cm^3 s^{-1})
P_2	upstream pressure, pressure at the feed side (or the pore inlet) (Pa)
P_3	downstream pressure, pressure at the permeate side (or the pore outlet) (Pa)
P_*	saturation vapor pressure at the liquid-vapor phase boundary (Pa)
$P_{*,ethanol\text{-}water}$	total saturation vapor pressure at the liquid-vapor phase boundary for ethanol-water mixture system (Pa)

P_m	mean pressure (Pa)
P_d	downstream gas pressure (Pa)
P_u	upstream gas pressure (Pa)
$P_{i,3}$, $P_{j,3}$	partial vapor pressure of the i^{th} and j^{th} components at the permeate side (or the pore outlet), respectively (Pa)
$P_{i,*}$, $P_{j,*}$	partial vapor pressure of the i^{th} and j^{th} components in the saturated vapor, respectively (Pa)
$P_{e,3}$, $P_{w,3}$	partial vapor pressure of ethanol and water components at the permeate side (or the pore outlet), respectively (Pa)
$P_{e,*}$, $P_{w,*}$	partial vapor pressure of ethanol and water components in the saturated vapor, respectively (Pa)
ΔP	gas pressure difference across the membrane (Pa)
Q	molar flux (mol m^{-2} s^{-1})
$Q_{Knudsen}$	molar flux govern by Knudsen flow (mol m^{-2} s^{-1})
Q_{liquid}	molar flux in the liquid-phase transport (mol m^{-2} s^{-1})
$Q_{surface}$	molar flux govern by surface flow (mol m^{-2} s^{-1})
Q_{total}	total molar flux (mol m^{-2} s^{-1})
Q_{vapor}	molar flux in the vapor-phase transport (mol m^{-2} s^{-1})
$Q_{i,vapor}$, $Q_{j,vapor}$	molar flux of the i^{th} and j^{th} components in the vapor-phase transport, respectively (mol m^{-2} s^{-1})
$Q_{e,vapor}$,$Q_{w,vapor}$	molar flux of ethanol and water components in the vapor-phase transport, respectively (mol m^{-2} s^{-1})
r	mean pore size at the selective layer surface (m)
r_{max}	maximum pore size at the selective layer surface (m)
R	gas constant (8.314 m^3 Pa mol^{-1} K^{-1})

R_g	radius of gyration (Å)
S_o	slope of the plot of G against mean pressures
t	collecting time (s or h)
t	time (s)
t_a	thickness of the adsorption monolayer (m)
T_g	glass transition temperature (°C)
T	temperature (°C or K)
T_g	glass-transition temperature (°C or K)
V_0	initial velocity (cm s^{-1})
V_L	velocity of the nascent hollow fiber (which approximates to the free-fall velocity in this study) (cm s^{-1})
$V_{die\ swell}$	velocity of the nascent hollow fiber at the die swell region (cm s^{-1})
w_d	mass of the dry membrane (g)
w_w	mass of the kerosene-impregnated membrane (g)
W	mass flux (g m^{-2} s^{-1} or g m^{-2} h^{-1})
$W_{ethanol}$	ethanol permeate flux (g m^{-2} h^{-1})
W_{water}	*w*ater permeate flux (g m^{-2} h^{-1})
W_{total}	total mass flux (g $m^{-2}s^{-1}$ or g m^{-2} h^{-1})
X_e	mole fraction of ethanol in the feed
$X_{e,2}$, $X_{w,2}$	mole fraction of ethanol and water components at the feed side (or the pore inlet), respectively
$X_{e,*}$, $X_{w,*}$	mole fraction of ethanol and water components in the liquid at the liquid-vapor phase boundary, respectively
$X_{i,2,}$ $X_{j,2}$	mole fraction of the i^{th} and j^{th} components at the feed side (or the pore inlet), respectively

$X_{i,*}$, $X_{j,*}$	mole fraction of the i^{th} and j^{th} components in the liquid at the liquid-vapor phase boundary, respectively
X_w	mole fraction of the water in the feed
Y_e	mole fraction of ethanol in the permeate
$Y_{e,3}$, $Y_{w,3}$	mole fraction of ethanol and water components at the permeate side (or the pore outlet), respectively
$Y_{e,*}$, $Y_{w,*}$	mole fraction of ethanol and water components in the saturated vapor, respectively
$Y_{i,3}$, $Y_{j,3}$	mole fraction of the i^{th} and j^{th} components at the permeate side (or the pore outlet), respectively
$Y_{i,*}$, $Y_{j,*}$	mole fraction of the i^{th} and j^{th} components in the saturated vapor, respectively
Y_w	mole fraction of water in the permeate

Greek symbols

τ	shear stress (N m^{-2})
α	separation factor
$\alpha_{ethanol/water}$	ethanol-water separation factor
γ	shear rate (s^{-1})
δ	calculated solubility parameter in the whole system including PVDF and solvents ($MPa^{1/2}$)
δ	entire length of the pore or effective pore length (m)
δ_a	length of the liquid-filled section of the pore (m)

δ_b	length of the vapor-filled section of the pore (m)
δ_d	dispersive parameter ($MPa^{1/2}$)
δ_p	polar parameter ($MPa^{1/2}$)
δ_h	hydrogen bonding parameter ($MPa^{1/2}$)
δ_t	total solubility parameter ($MPa^{1/2}$)
$\Delta\delta_t$	the total solubility parameter difference defined as $\lvert \delta_{t(mixed\ solvent)} - \delta_{t(PVDF)} \rvert$ ($MPa^{1/2}$)
ε	porosity of the hollow fiber membrane (%)
$\dot{\varepsilon}$	elongation rate (s^{-1})
ε_s	surface porosity
η_L	viscosity of liquid (Pa s)
η_g	viscosity of gas (Pa s)
ρ	density of liquid (kg m^{-3} or g cm^{-3})
ρ_p	density of PVDF (g cm^{-3})
ρ_w	density of kerosene (g cm^{-3})
μ	surface viscosity of the vapor adsorption layer (Pa s)
θ	water contact angle (°)

Abbreviations

AFM	Atomic Force Microscope
CFD	Computational fluid dynamics
DDS	Dimethyldichlorosilane
DMAc	Dimethylacetamide

EDX	Energy Dispersion X-ray
ETBE	Ethyltertbutyl ether
FESEM	Field Emission Scanning Electron Microscopy
FO	Forward osmosis
IPA	Isopropanol
MF	Microfiltration
MTBE	Methyltertbutyl ether
NF	Nanofiltration
NMP	*N*-methyl-2-pyrrolidone
ODMS	α,ω-(3-bisaminopropyl) oligodimethyl siloxane
PAN	Polyacrylonitrile
PDMS	Polydimethylsiloxane
PEBA	Polyether block amide
PMDA	1,2,4,5-benzenetetracarboxylic dianhydride
PP	Polypropylene
PTFE	Polytetrafluoroethylene
PTMSP	Poly[1-(trimethylsilyl)-1-propyne]
PVA	Polyvinyl alcohol
PVDF	Poly(vinylidene fluoride)
PSI	Pervaporation separation index
RO	Reverse osmosis
TMVS	Trimethoxyvinylsilane
SBS	Styrene-butadiene-styrene block copolymer
SEM	Scanning Electron Microscopy
UF	Ultrafiltration

XRD	X-ray Diffraction
6FDA	5,5-[2,2,2-trifluoro-1-(trifluoromethyl) ethylidene] bis-1,3 isobenzenefurandione dianhydride

LIST OF TABLES

LIST OF FIGURES

CHAPTER ONE

INTRODUCTION

1.1 Membrane pervaporation and its historical development

A membrane applied in every separation process can be defined as a semi-permeable barrier that allows the preferential transport of one or more component(s) in the feed mixture, hence enabling a separation to occur [1]. Nowadays, membrane science and technology has gained an important place as an alternative to conventional separation techniques in a broad spectrum of applications related to energy, water production, environmental and health sciences. A variety of different membrane operations are employed in practice, which includes gas separation, pervaporation, microfiltration, nanofiltration, ultrafiltration, membrane dialysis, reverse osmosis, forward osmosis, membrane distillation, electrodialysis, and membrane contactors. The innovations and breakthroughs in membrane R&D has made a significant impact in industrial applications technically and commercially.

Pervaporation is an emerging membrane-based separation process for liquid/liquid separations. The term “pervaporation” is a combination of membrane permeation and evaporation in a process where the membrane acts as a selective barrier between the two phases, the liquid phase feed and the vapor phase permeate [2,3]. The schematic diagram of the pervaporation process is shown in Figure 1.1. In pervaporation, the liquid feed containing two or more components is placed in contact with one side of a membrane, which preferentially allows the permeation of one of the feed components. The permeate, enriched in this component, is removed as a vapor from the other side of

the membrane. This driving force of the process is the low vapor pressure on the permeate side of the membrane, which is generated by applying a vacuum (or purged gas) and condensing the permeate vapor. Mass transport through the membrane is induced by a chemical potential (partial pressure or/and concentration) difference between the liquid feed solution and the vapor permeate at each side of the membrane. The partial vaporization of feed components and a phase change across the membrane are unique features of this process. The separation achieved is proportional to the differences in permeation rates of individual components through the membrane, which are typically controlled by the complicated interactions among the feed components, the membrane material and thepermeate.

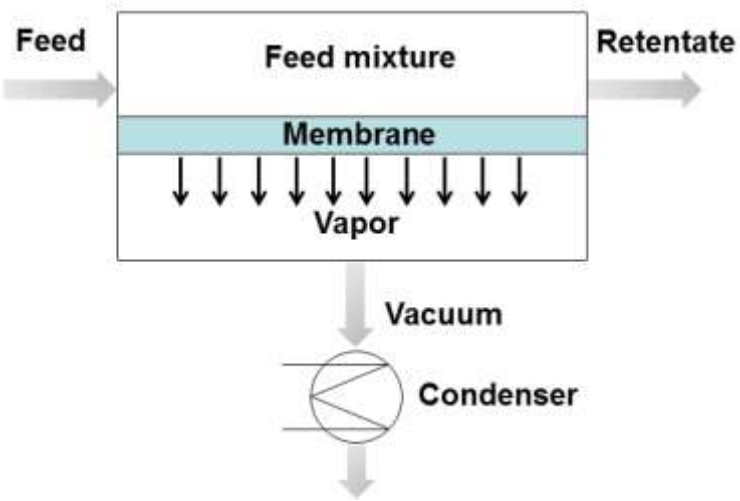

Figure 1.1 Schematic diagram of pervaporation process

The concept of pervaporation separation can be traced back to the 19th century when Kahlenberg first observed the selective transport of hydrocarbon/alcohol mixtures through a thin rubber sheet in 1906 [4]. However, it was Kober who first introduced the word ‘pervaporation’ in his paper published in 1917 about the selective permeation of water from aqueous solutions of albumin and toluene through cellulose nitrate

(Collodion) films [5]. Farber made the earliest attempt for separating and concentrating protein and enzyme solutions via pervaporation technique in 1935 [6]. Schwob investigated the dehydration of water/alcohol mixtures through a thin regenerated cellulose film (Cellophane) [7]. Heisler and coworkers in 1956 reported the first quantitative study of pervaporation separation of aqueous ethanol solution using a cellophane membrane [8].

Afterward, the process was studied in a systematic fashion by Binning and coworkers at American Oil Company between 1958 and 1962, based on their research on the separation of hydrocarbon mixtures through a polyethylene film [9-13]. However, the low permeation flux through homogenous dense films was a critical problem hindering the large-scale industrial applications of pervaporation in the early stage. The process was studied at Monsanto by Eli Perry and colleagues in the 1970s. Although the study was pursued for a number of years and several patents were issued [14-16], the process was not commercialized. Meanwhile, academic research on pervaporation for separating azeotropic mixtures was carried out by Neel and coworkers at the University of Toulouse [17,18].

A major breakthrough was achieved in early 1980s when Gesellschaft für Trenntechnik (GFT) Co., Germany (now owned by Sulzer Chemtech), developed the first commercial pervaporation membrane, which comprises a thin layer of cross-linked polyvinyl alcohol (PVA) supported on a porous polyacrylonitrile (PAN) substrate for the removal of water from concentrated alcohol solutions [19]. Apart from the success of commercial pervaporation plant for solvent dehydration, the removal of volatile organic compounds (VOCs) from contaminated water and the

recovery of expensive organics from waste streams were of great interest and have prompted the research on developing organo-selective pervaporation membranes which preferentially transfer organic compounds. This technology was developed by Membrane Technology and Research [20-23]; the first commercial membrane for organic compounds removal was produced in 1988 and the first commercial plant was sold in 1996. Figure 1.2 illustrates some of the scientific milestones in the development of pervaporation processes. Since 1995, more than 100 industrial pervaporation units were installed worldwide and around 260 European and US patents on pervaporation have been issued between 1980 and 1999 [24].

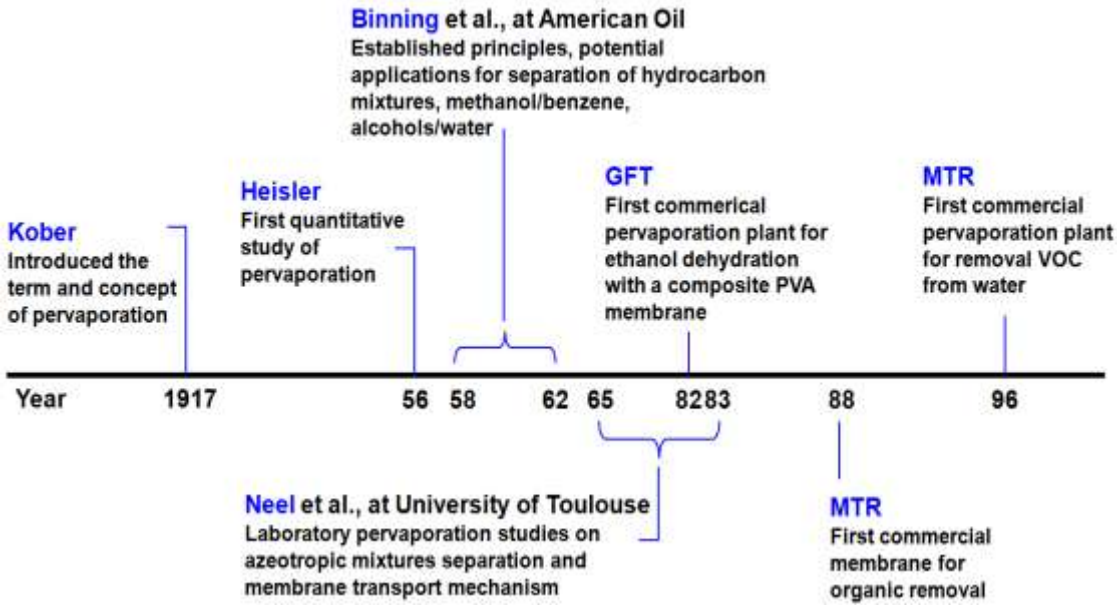

Figure 1.2 Scientific milestones in the development of pervaporation

1.2 Current industrial applications of membrane pervaporation

The industrial applications of pervaporation processes have been divided into three major areas: (1) dehydration of alcohols and other organic solvents; (2) removal of volatile organic components from aqueous mixtures and (3) separation of organic

mixtures. To date, the number of pervaporation applications on industrial-scale remains rather small and the majority of industrial pervaporation units are still for the dehydration of a limited number organic solvents [25-28]. Table 1.1 demonstrates the potential liquid separations that need technological breakthroughs and some existing applications that have been supported by commercially available pervaporation membranes. Some manufacturers of pervaporation systems, membranes, and their main applications are listed in Table 1.2.

Table 1.1 Potential liquid separations that need technological breakthroughs and some existing applications using commercially available pervaporation membranes

	Solvent dehydration	Removal of organics from aqueous solution	Organic-organic separation
Demanding breakthroughs	• Alcohols: Ethanol Isopropanol Butanols, etc	• Alcohols (biofuels) • Aromas • Methylene dichloride • Tetrachloro ethylene • Trichloro ethylene • Phenol	• Polar/Non-polar Methanol/toluene, Methanol/benzene Methanol/cyclohexane, Ethanol/benzene Ethanol/totulene, Isopropanol/totuene, Methanol/methyl ester or ether, Ethanol/ethyl ether
	• Acids		• Aromatic/Aliphatic Benzene/n-heptene, Benzene/n-hexane Toluene/n-octane, Toluene/n-heptane Toluene/n-hexane, Toluene/isooctane Styrene/ethyl benzene
	• Esters		• Aromatic/Alicyclic Benzene/cyclohexane, Toluene/cyclohexane
	• Ethers		• Isomeric Xylenes, C4-C8 alkanes isomers, C3-C4 alcohols
	• Tetrohydrofuran		• Others Carboxylic acid/ester/methanol Methanol/acetone Dimethyl carbonate/methanol Methanol/carbon tetrachloride Ethylacetate/carbon tetrachloride Acetonitrile/carbon tetrachloride
	• Ketones Acetone		
	• Others Dimethyl acetyl Phenol Ethylene glycol Methylisobutylketone Triethyl amine		
Available	• Ethanol; Isopropanol • Esters; Ethers; Triethyl amine	• Tetrachloro ethylene recovery in a dry-clean unit	• Methyl/methyl ester or methyl ether (e.g. Methyl tert butyl ether (MTBE)) • Ethanol/ethyl ether (e.g. Ethyl tert butyl ether (ETBE))

Table 1.2 Industrial suppliers of pervaporation system [29]

Company	Application	Membrane	Module design
Gesellschaft für Trenntechnik (GFT)	Solvent dehydration	Crosslinked PVA composite membranes	Plate and frame
Lurgi	Solvent dehydration	GFT PVA membranes	Plate and frame
British Petroleum (Kalsep)	Solvent dehydration	Composite membranes based on ion exchange polymers	Tubular, Plate and frame
Membrane Technology & Research (MTR)	Solvent recovery especially volatile organic compounds	Composite membranes	Spiral wound
Air products (Separex)	Organic-organic separation, i.e., methanol/MTBE	Cellulose acetate membranes	Spiral wound
Texaco	Solvent dehydration, i.e., ethylene glycol, isopropyl alcohol Organic-organic separation	Composite membranes	Plate and frame by GFT

1.2.1 Dehydration of alcohols and other organic solvents

Among the abovementioned kinds of applications, pervaporation is considered as a state-of-the-art technology used widely in large-scale applications for the dehydration of alcohols and organic solutions. Since alcohols and some organic solvents such as ethers and ketones are completely miscible with water and usually form azeotropes, the further dehydration of these solvents is needed to produce anhydrous grade chemicals. Pervaporation is more favorable and competitive than traditional azeotropic distillation using benzene trichloroethane as an additive or adsorption with desiccants [30]. So far, dehydration of alcohols mainly ethanol and isopropanol (IPA) is the most important application due to the high demand and usages in industries; anhydrous ethanol has gained more and more interest as a biofuel while IPA is an important solvent in pharmaceutical and electronic industries. The pervaporation technology for

dehydrating other solvents such as glycols, acetone and methylene chloride, etc is also gradually developing.

1.2.2 Removal of volatile organic compounds from water or solvent recovery

Another application of the pervaporation process is the removal or recovery of organic compounds from aqueous solutions, which can be applied in water purification, pollution control and solvent recovery. This application was first developed by Membrane Technology & Research (MTR), USA [21]. Different membranes have been used for this application according to the different solvents needed to be separated. Typical commercial organic solvent selective membranes mainly focus on the high selectivity for hydrophobic volatile solvents such as benzene, toluene and chloroform. Commonly adopted membranes are made from elastomers or rubbery polymers such as polydimethylsiloxane or silicon rubber, polybutadiene, natural rubber, polyether copolymers. Importantly, if the membrane has higher selectivity for hydrophilic polar solvents such as acetic acid, formic acid, acetone, methanol, ethanol, and other alcohols, pervaporation would be more widely applied for solvent recovery and it can compete with conventional distillation or solvent extraction. In this regards, the recovery of ethanol or organic products from a bioprocess could become another important area of the pervaporation. Nevertheless, most studies of this type of applications have been reported on a laboratory scale but have rarely been scaled up for industrial applications. The potential and development of membrane pervaporation for ethanol recovery is of interest and will be further reviewed in the next section.

1.2.3 Organic/organic separation

The separation of organic solvent mixtures is the least developed application of pervaporation compared to the other two applications. The lack of suitable membranes and modules which are stable during long term exposure to organic solvents at high temperature in this type of separation may be the key problem preventing its large-scale development. Though there are only two examples of industrial applications, which are methanol/methyltertbutyl ether (MTBE) and benzene/cyclohexane separations, this application indeed extends the potential of pervaporation technology by solving the difficult problem of separating pure organic mixtures, especially in the pertrochemical industry. The future goals are purification of the alkylether like ethyltertbutyl ether (ETBE), fuel octane enhancer without lead derivatives for protection of environment and extraction of aromatics from hydrocarbons (removal of aromatics from gasoline).

1.2.4 Commercially available pervaporation membranes

At present, the industrial manufacturers for pervaporation membranes are extremely scarce. The materials of existing commercial membranes are almost identical and the chemical structure of active layer is simple, that is PVA for dehydration and polydimethylsiloxane (PDMS) for organic removal. According to different applications, pervaporation membranes can be classified into three types: (1) hydrophilic membranes, (2) organophilic membranes and (3) organoselective membranes.

Table 1.3 Summary of existing commercial pervaporation membranes [24]

	Membrane	Structure	Comments
Hydrophilic membrane	PERVAP 2200	PVA cross-linked/PAN support	
	PERVAP 2201	PVA highly cross-linked/PAN	
	PERVAP 2202	PVA specially cross-linked/PAN	Dehydration of esters
	PERVAP 2205	PVA specially cross-linked/PAN	Dehydration of acids
	PERVAP 2210	PVA lightly cross-linked/PAN	Final dehydration of alcohols
	PERVAP 2510	PVA specially cross-linked/PAN	Dehydration of isopropanol
	CM-Celfa	PVA cross-linked/PAN	
	GKSS Simplex	Complex polyelectrolytes/PAN	
Organophilic membrane	PERVAP 1060	PDMS cross-linked/ PAN support	
	PERVAP 1070	PDMS cross-linked + silicalite/PAN	Recommended for highly water soluble organic species
	MTR 100	PDMS cross-linked /porous support	
	MTR 200	EPDM/PDMS cross-linked /porous support	Active layer: two layers
	GKSS POMS	POMS cross-linked/ porous support	
	GKSS PDMS	PDMS cross-linked/porous support	
	GKSS PEBA	PEBA/porous support	Extraction of phenols
Organoselective membrane	PERVAP 2256-1	Extraction of methanol	Separation methanol/methyl ester or methyl ether
	PERVAP 2256-2	Extraction of ethanol	Separation ethanol/ethyl ether

Table 1.3 summarizes the existing commercial membranes of pervaporation. The hydrophilic membranes were the first type of membranes to be used industrially for organic solvent dehydration by pervaporation. By modifying the active layer of these membranes with different chemical compositions and structures, these membranes are enabled to extract water with broad ranges of flux and selectivity. The majority of commercially available hydrophilic membranes are made of PVA with various types and contents of cross-linked agents. In contrast, the organophilic membranes have been developed more recently than the hydrophilic membranes and have been used less frequently industrially. The recovery of aromatic compounds by pervaporation is an important application for the organophilic membranes. The typical material for most commercially available organophilic membranes is PDMS.

In addition, although there are limited industrial applications for organoselective membranes, this type of membranes still receive high attention especially for solving separation problems in petrochemical industry. However, the industrial supply of pervaporation membrane for organic-organic separation is extremely scarce because the membrane design must be specifically tailored towards designated organic mixtures. Typical examples of industrial applications of organo-selective membranes have been reported by Sulzer Chemtech about two membranes for extracting methanol from methanol/methyl ester mixtures [24].

1.3 Membrane pervaporation for biofuel (bioethanol) separation

1.3.1 Significance of ethanol and water separation

Bioethanol is a prominent renewable fuel that is progressively gaining importance. At present, biofuel production is largely influenced by government policies that may either deter or boost the further penetration of biofuel in the energy consumption market [31]. For example, a 10 or 15% limit of ethanol gasoline is implemented by the Environmental Protection Agency in the United States [31]. It is projected that the global production of liquid biofuels will display a sizeable increment in the near future.

Liquid biofuels generally include methanol, ethanol, butanol and biodiesel. Methanol can be produced from solid biomass using bio-syngas obtained from the steam reforming process of biomass [32]. Biodiesel (methyl and ethyl esters) is mainly produced by the transesterification of vegetable and plant oils [33]. Ethanol and butanol are derived from the fermentation of starch or sugar crops [34]. Within these four, ethanol is the most abundantly produced biofuel at the present time in the global

energy market, particularly in Brazil and the United States. For instances, the ethanol produced by the United States can substitute 2% of the US gasoline supply, but it is expected to replace 30% of the gasoline demand by 2030, when the development of technologies for ethanol production from lignocellulosic feedstock has been projected to become a major contributor [35]. In addition, all the main industrialized countries have launched a program and legislation on a broad scale to use bioethanol as a fuel as can be seen via worldwide bioethanol production [36-38].

One of the major challenges is how to develop cost-effective technologies for bioethanol production in order to reduce production costs. Basically, the conversion process of cellulosic biomass to bioethanol mainly consists of 4 steps: (1) feedstock handling, (2) pretreatment and conditioning, (3) fermentation, and (4) biofuel product separation and purification. It has been reported that the "*separation and purification stage*" alone accounts for at least 40% (up to 80%) of the whole process cost [39]. To date, conventional distillation remains the dominant refinery separation scheme. However, it may no longer be economic and practical as the principal operation for biofuel purification and separation because of its energy intensive nature [40]. The use of membrane pervaporation appears to be a very promising, economic and practical approach [41-44]. Membrane pervaporation has been considered as one of the most effective and energy-saving process [44].

1.3.2 Membrane pervaporation for ethanol recovery

Typically, the final bioethanol separation and purification can be divided into 2 sub-stages: the 1st stage is the '*recovery*' stage, where bioethanol is separated and

concentrated from a dilute fermentation broth containing 5-15 wt% ethanol depending upon the microorganisms used and process conditions in fermentation, and the 2nd stage is the '*dehydration*' stage, where the resulting ethanol is further dehydrated in order to achieve high purification. Membrane pervaporation has demonstrated feasibility for bioethanol separation in both separation stages. Much effort has been devoted to the state of the art for biofuel dehydration purposes and a variety of proficient material candidates such as polyvinyl alcohol (current commercial-based membrane), polyamide, polyimide, etc are presented for industrial applications [45,46]. In contrast, the development of membrane pervaporation for biofuel recovery has yet to receive any breakthroughs in industrial practice although its clear economic and environmental benefits compared to conventional distillation-based separations. The current state-of- the-art for biofuel recovery via pervaporation, the challenges faced and future research directions are covered in a comprehensive review by Vane [43].

Table 1.4 summarizes the basic physiochemical properties of ethanol and water [47], the main chemical components involved in the separation. For alcohol recovery, the preferential transport of ethanol molecules across the membranes is required and organophilic materials are ideal for use. Membranes based on hydrophobic rubbery polymers are therefore good candidates for use in alcohol recovery, because of their excellent affinity for organics and high diffusivity attributed to the inherent hydrophobicity and polymer chain flexibility. In addition, the effect of solvent-induced swelling must be considered in the selection and design of membrane materials for pervaporation.

Table 1.4 Physicochemical properties of ethanol and water

Properties	Ethanol	Water
Chemical formula	C_2H_5OH	H_2O
Molecular weight, g mol^{-1}	46.1	18.0
Density, g cm^{-3}	0.789	1
Boiling point, °C	78.3	100.0
Vapor pressure at 20 °C, mmHg (kPa)	43.89 (5.9)	17.5 (2.33)
Azeotrope with water (wt% water)	4	-
Empirical polarity parameter ET (30), kcal mol^{-1}	51.9	63.1
Solubility parameter, $(MPa)^{1/2}$	26.5	47.8
Radius of gyration, Å	2.259	0.615

To date, the PDMS membrane originally developed and commercialized for organic removal applications has been extensively investigated and is currently regarded as the standard membrane material for ethanol recovery. Nevertheless, the absence of suitable alcohol-selective membrane materials with high separation performance has motivated the ongoing advancement and exploration of membrane materials with better separation and physicochemical properties.

1.4 Key challenges on the development of pervaporation membranes

One of major hurdles for the expansion of membrane pervaporation processes to the emerging markets is the lack of appropriate membranes. Without the development of a sufficient high performance membrane, pervaporation may unlikely to materialize as a viable alternative separation technique. Principally, one should screen and select materials to construct membranes which have superior separation factor and flux. Besides, membrane materials with desirable physicochemical properties such as good

mechanical integrity, chemical resistance and thermal stability are needed for the long-term durability and minimal solvent-induced swelling in harsh environment (e.g. high operating temperature) [26]. The other obstacle is due to the fact that a certain material often displays certain selectivity and/or permeability behavior for a specific mixture. In other words, different types of mixtures (i.e. compositions) require different types of membranes. Thus, the evaluation on material selection and tests may not be overlooked in designing membranes for specific separation purposes. Among the materials investigated or utilized for pervaporation, polymers are preferred and worthy or further study due to their superior advantages such as compactness, ease of fabrication and scale-up, lower material costs.

Membrane formation and module fabrication also play essential roles in determining the final membrane structure and corresponding separation performance. Typically, the formation of an anisotropic or asymmetric membrane structure comprising a very thin selective layer on a porous supporting layer is considered as the desired feature for ensuring a high flux, but must be optimized by overcoming problems such as large skin layer defects or structure integrity. At present, there are many types of membrane configurations available in the market, such as flat sheet composite membranes, polymeric hollow fibers, and inorganic tubular membranes. Hollow fiber membranes made of polymeric materials, which were firstly patented by Mahon [48] five decades ago, are highly competitive to flat and inorganic membranes because they provide a larger effective membrane area per unit volume of a membrane material, which can result in a higher productivity. However, it is not easy to fabricate hollow fiber membranes with both desirable morphology and separation performance. To successfully fabricate those new materials into useful hollow fiber membranes and

maximize materials potential, researchers must understand the intrinsic physicochemical properties of these new materials, manipulate the phase inversion process, and control dope rheological responses under various stresses during membrane formation in order to design membrane structure at molecular levels.

The success of membrane development is not only based on the advancements in membrane materials and fabrication techniques but also requires a proper understanding in the mass transport across the membrane. A fundamental study on mass transport mechanism typically provides in-depth knowledge in membrane structure design and manipulation, process operation optimization, and separation prediction, which found to be very crucial information for the industrial practice. Figure 1.3 summarizes key critical issues for a successful membrane-based pervaporation.

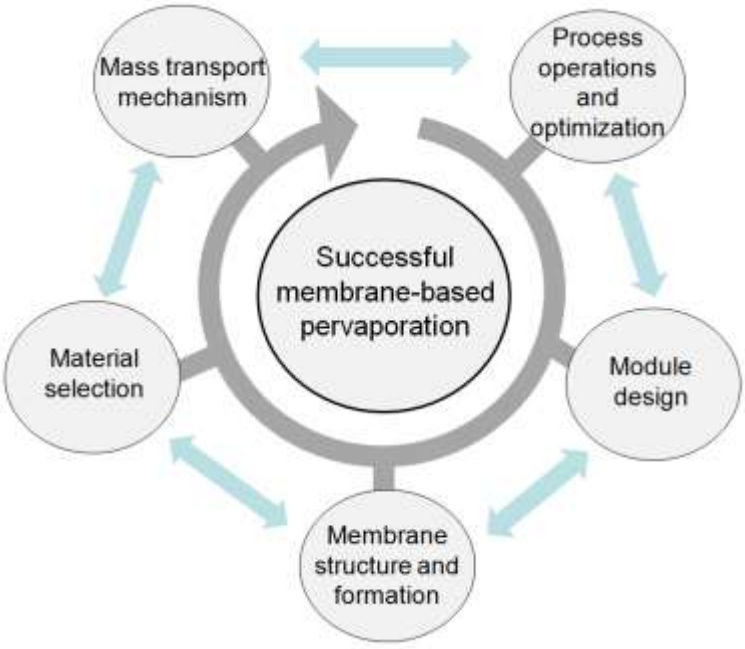

Figure 1.3 Key issues for a successful membrane-based pervaporation

1.5 Research objectives and thesis organization

The main objective of this research is to explore the science and engineering of fabricating poly(vinylidene fluoride) (PVDF) hollow fiber membranes as novel pervaporation membranes for ethanol recovery, which will be studied through: 1) studying the effect of spinning parameters, from aspects of phase inversion, crystallization and dope rheology, on the membrane formation, morphology and mechanical properties of PVDF hollow fiber membranes; 2) investigating the pervaporation mass transport in PVDF hollow fiber membranes and developing a suitable mathematics model for describing the transport mechanism and predicting membrane separation performance; 3) exploring the feasibility of fabricating PVDF hollow fiber membranes with desirable pore size and morphology for ethanol-water separation using the concept of the proposed modified pore-flow model; and 4) developing dual-layer hollow fiber membranes based on PVDF/silica composite and optimizing pervaporation operation conditions for separation performance enhancement.

Compared to conventional membrane materials investigated for alcohol recovery via pervaporation like poly(dimethyl siloxane) (PDMS), which is relatively weak in mechanical strengths and chemical resistance, PVDF brings together the superior mechanical properties, good thermal and chemical stabilities and highly hydrophobic nature, which are essential requirements for pervaporation membranes as they come into contact with liquid mixtures. In addition to these superior properties, the ease of fabrication into hollow fibers makes it more attractive. This is because hollow fiber membranes have the following advantages: (i) a larger membrane area per unit

membrane module volume, resulting in a higher permeation flow per unit volume; (ii) self-supporting structure, allowing the membrane to be a self-contained vacuum channel where the feed can be supplied from the shell side while vacuum is applied on the lumen side; and (iii) good flexibility and ease of handling during module fabrication and system operation. The ultimate goal of this thesis work is to achieve hollow fiber membranes with an excellent separation performance in both permeation flux and separation factor for the ethanol recovery, in addition to the in-depth knowledge on fundamentals of hollow fiber formation and pervaporation membrane transport.

This dissertation is organized and structured into eight chapters and two appendices. Chapter One provides an introduction of this dissertation including the background and historical development of membrane pervaporation, current industrial applications, and the great potential of the pervaporation for biofuel separation emphasizing on the ethanol recovery. In addition, a brief description of key challenges on the development of pervaporation membranes was introduced. The research objective and outline of this dissertation are also presented in this chapter.

Chapter Two covers the concept of the pervaporation process which includes mass transport mechanism, evaluation of membrane performance, membrane materials for ethanol recovery, design and engineering principles for polymeric membranes from aspects of membrane preparation, membrane morphology and structure, and module designs. In addition, the fundamentals of hollow fiber membrane formation and phase inversion mechanism are reviewed. The key elements and factors in hollow fiber spinning are also highlighted in this Chapter.

Chapter Three describes the experimental techniques employed in the entrie research progress. The materials, membrane preparation procedures, pervaporation experiments and membrane characterization are addressed in details.

Chapter Four presents the fundamental investigation on the science of fabricating PVDF asymmetric hollow fiber membranes. The effects of polymer dope composition, external coagulation composition and dope rheological properties on the membrane formation, membrane morphology, crystallinity and mechanical properties of PVDF hollow fiber membranes have been systematically explored. The analytical methods and molecular dynamics simulations are employed to gain insights phase inversion mechanisms and membrane morphology transformation from the views of thermodynamic and kinetic aspects as well as the behavior of polymer chains involved.

Chapter Five investigates the pervaporation of ethanol/water mixtures in PVDF asymmetric hollow fiber membranes. The pore-flow model and newly proposed modified pore-flow model have been applied to study the mass transport mechanism. The prediction of pervaporation experimental results using both models is presented in a parallel comparison. The discussion on the correlation among pore size, surface porosity and model transport parameters is included.

Chapter Six presents the fabrication of PVDF hollow fiber membranes with tunable and desirable morphology and pore size using the modified pore-flow concept. The effects of bore-fluid composition, air-gap distance and take-up speed on membrane morphology and ethanol-water separation performance have been investigated. A close

relationship among membrane morphology, pore size, pore size distribution and separation performance with in-depth science have been established. A comparison of pervaporation performance with other polymeric membranes in open literature is provided and the developed membranes showed an acceptable separation factor with outstanding permeation flux.

Chapter Seven presents the novel developed PVDF/nanosilica hollow fiber membranes with desirable membrane morphology and separation performance for ethanol recovery, which can be achieved by tuning spinning conditions and optimizing the operating downstream pressure based on the concept of the modified pore-flow model. The effects of hydrophobic silica nanoparticle and spinning parameters such as air-gap length, take-up speed, and silica nanoparticles have been investigated and optimized. The significance of downstream pressure on membrane separation and pervaporation mass transport is presented and the modified pore –flow model was used to predict and understand the pervaporation phenomenon. A comparison of the separation performance of developed hollow fiber membranes with various membranes available in the literature was highlighted. This study not only presents the development of high performance pervaporation membranes for ethanol recovery, but also provides the fundamental science and understanding of tunable pervaporation characteristics from the aspects of membrane morphological design and downstream pressure control.

General conclusions drawn from this research study are summarized in Chapeter Eight. In addition, some recommendations/suggestions for future research are included in this Chapter.

Appendices A and B describe the derivation of equations and parameters in the modified pore-flow model involved in Chapter Five and Chapter Seven, respectively.

REFERENCES

[1] M. Mulder, Basic Principles of Membrane Technology, Boston: Kluwer Academic Publishers (1996).

[2] H.L. Fleming, C.S. Slater, Pervaporation, in W.S.W. Ho and K.K. Sirkar edited, Membrane Handbook, New York: Van Nostrand Reinhold (1992).

[3] R.Y.M. Huang, Pervaporation membrane separation processes, New York: Elsevier (1991).

[4] L. Kahlenberg, On the nature of the process of osmosis and osmotic pressure with observations concerning dialysis, J. Phys. Chem. 10 (1906) 141.

[5] P.A. Kober, Pervaporation, perstillation and percrystallization, J. Am. Chem. Soc. 39 (1917) 944.

[6] L. Farber, Applications of pervaporation, Science 82 (1935) 158.

[7] Y. Schwob, Sur l´hémiperméabilité à l´eau, des membranes de cellulose régénérée. Thèse de Doctorat ès Sciences, Toulouse (France), 23 Mai 1949. E. Privat Editeur, 14 rue des Arts, Toulouse, 1950 (summarized in: La Nature, (1952).

[8] E.G. Heisler, A.S. Hunter, J. Siciliano, R.H. Treadway, Solute and temperature effects in the pervaporation of aqueous alcoholic solutions, Science 124 (1956) 77.

[9] R.C. Binning, F.E. James, Permeation, A new commercial separation tool, The Refiner Engineer, 30, n° 6 (1958) C_{14}-C_{15}.

[10] R.C. Binning, F.E. James, How separate by membrane permeation, Petroleum Refiner, 37, n° 5 (1958) 214.

[11] R.C. Binning, F.E. James, Permeation, a new way to separate mixture, Oil Gas J. 1958, 104.

[12] R.C. Binning, R.J. Lee, J.F. Jenning, E.C. Martin, Separation of liquid mixtures by permeation, Ind. Eng. Chem. 53 (1961) 45.

[13] R.C. Binning, Separation of mixtures, US Patent 2,981,680 (1961)

[14] W.F. Strazik, E. Perry, Process for the separation of styrene from ethyl benzene, US Patent 3,776,970 (1973).

[15] R. Chiang, Ballwin, E. Perry, Process for separating aqueous formaldehyde mixtures, US Patent 4,067,805 (1976).

[16] E. Perry, Membrane separation of organics from aqueous solutions, US Patent 4,218,312 (1980).

[17] P. Aptel, N. Challard, J. Cuny, J. Neel, Application of the pervaporation process to separate azeotropic mixtures, J. Membr. Sci. 1 (1976) 271.

[18] J. Neel, Q.T. Nguyen, R. Clement, L. Le Blanc, Fractionation of a binary liquid mixture by continuous pervaporation, J. Membr. Sci. 15 (1983) 43.

[19] G.F. Tusel, H.E.A. Bruschke, Use of pervaporation system in the chemical industry, Desalination 53 (1985) 327.

[20] J. Kaschemekat, J.G. Wijmans, R.W. Baker, I. Blume, Separation of organics from water using pervaporation, in Proceedings of the 3rd International Conference on Pervaporation Processes in the Chemical Industry, Nancy, France (1988) 405.

[21] I. Blume, J.G. Wijmans, R.W. Baker, The separation of dissolved organics from water by pervaporation, J. Membr. Sci. 49 (1990) 253.

[22] A.L. Athayde, R.W. Baker, R. Daniels, M.H. Le, J.H. Ly, Pervaporation for wastewater treatment, Chemtech 27 (1990) 253.

[23] G. Cox, R.W. Baker, Pervaporation for the treatment of small volume VOC-contaminated waste water streams, Indust. Wastewater, 6 (1998) 35.

[24] A. Jonquieres, R. Clement, P. Lochon, J. Neel, M. Dresch, B. Chretien, Industrial state-of-the-art of pervaporation and vapour permeation in the western countries, J. Membr. Sci. 206 (2002) 87.

[25] P. Shao, R.Y.M. Huang, Polymeric membrane pervaporation, J. Membr. Sci. 287 (2007) 162.

[26] B. Smitha, D. Suhanya, S. Sridhar, M. Ramakrishna, Separation of organic-organic mixtures by pervaporation — a review, J. Membr. Sci. 241 (2004) 1.

[27] R. Rautenbach, S. Klatt, J. Vier, State of the art of pervaporation: 10 years of industrial PV, in Proceedings of the 6th International Conference on the Pervaporation Process in Chemical Industry, Ottawa, Canada, Sept 27-30 (1992).

[28] W. Ji, S.K. Sikdar, Pervaporation using adsorbent-filled membranes, Ind. Eng. Chem. Res. 35 (1996) 1124.

[29] R.W. Baker, E.L. Clusser, W. Eykamp, W.J. Koros, R.L. Riley, H. Strathmann, Membrane separation systems, Recent developments and future directions, Noyes data corporation, Park Ridge, New Jersey, USA (1991).

[30] K. Scott, Handbook of Industrial Membranes, Kidlington, Oxford, UK (1995).

[31] U.S. Department of Energy, International Energy Outlook, Energy Information Administration, U.S. Department of Energy, Washington, D.C. (2009).

[32] V.D. Phillips, C. M. Kinoshita, D. R. Neill, P. K. Takashi. Thermochemical production of methanol from biomass in Hawaii, Appl. Energy. 35 (1990) 167.

[33] Y.C. Sharma, B. Singh, S. N. Upadhyay, Advancements in development and characterization of biodiesel: A review, Fuel 87 (2008) 2355.

[34] K.A. Gray, L. Zhao. M. Emptage, Bioethanol, Curr. Opin. Biotech., 10 (2006) 141.

[35] R.M. Neilson, The role of cellulosic ethanol in transportation, Summary of

presentation at Practical Paths: Climate Change and Beyond, Boise, Idaho (2007).

[36] T. Wiesenthal, G. Leduc, P. Christidis, B. Schade, L. Pelkmans, L. Govaerts, P. Georgopoulos, Biofuel support policies in Europe: lessons learnt for the long way ahead, Renewable Sustainable Energy Rev. 13 (2009) 789.

[37] M. Balat, H. Balat, C. Oz, Progress in bioethanol processing, Prog. Energy Combust. Sci. 34 (2008) 551.

[38] E.D. Larson, Biofuel production technologies: status, prospects and implications for trade and development, Report no. UNCTAD/DITC/TED/2007/10. United Nations Conference on Trade and Development, New York and Geneva; 2008.

[39] A.J. Ragauskas, C.K. Williams, B.H. Davison, G. Britovsek, J. Cairney, C.A. Eckert, W.J. Frederick Jr., J.P. Hallett. D.J. Leak, C.L. Liotta, J.R. Mielenz, R. Murphy, R. Templer, T. Tschaplinski, The path forward for biofuels and biomaterials, Science 311 (2006) 484.

[40] H.J. Huang, S. Ramaswamy, U. W. Tschirner, B. V. Ramarao, A review of separation technologies in current and future biorefineries, Sep. Purif. Technol. 62 (2008) 1.

[41] R.D. Noble and R. Agrawal, Separation research needs for the 21st century, Ind. Eng. Chem. Res. 44 (2005) 2887.

[42] K.K. Sirkar, Membrane separation technologies: Current developments, Chem. Eng. Commun. 157 (1997) 145.

[43] L.M. Vane, A review of pervaporation for product recovery from biomass fermentation processes, J. Chem. Technol. Biotechnol. 80 (2005) 603.

[44] L.M. Vane, Review: Separation technologies for the recovery and dehydration of alcohols from fermentation broths, Biofuels, Bioprod. Bioref. 2 (2008) 553.

[45] P.D. Chapman, T. Oliveira, A.G. Livingston, K. Li, Review: Membranes for the

dehydration of solvents by pervaporation, J. Membr. Sci. 318 (2008) 5.

[46] L.Y. Jiang, Y. Wang, T.S. Chung, X.Y. Qiao, J.Y. Lai, Polyimides membranes for pervaporation and biofuels separation, Prog. Polym. Sci. 34 (2009) 1135.

[47] B.T. Low, Y. Wang, T.S. Chung, Polymeric membranes for energy applications, Encylcopedia of polymer science and technology, John Wiley & Sons: New York (2010).

[48] H.I. Mahon, Permeability separatory apparatus and process using hollow fibers, US Patent 3,228,877 (1966).

CHAPTER TWO

BACKGROUND AND LITERATURE REVIEW

2.1 Mass transport mechanism in pervaporation membrane

The membrane in pervaporation acts as a barrier layer between a liquid and a vapor phase, regulating the transport of substances between the components; and a phase transition occurs from the feed to the permeate. The driving force for the mass transport is the chemical potential gradient (fugacity gradient for each species) across the membrane, which can be created by applying either a vacuum pump or an inert purge (normally air or steam) on the permeate side to maintain the permeate vapor pressure lower than the partial pressure of the feed liquid. Therefore, the selectivity is caused by fugacity differences between permeates as well as by permeability differences of the membrane towards different permeates. The ultimate separation performance to a liquid mixture is determined by 1) the physicochemical properties of feed mixtures and their own interactions, 2) the affinities of permeates toward the macromolecules of the membrane material, and 3) the physical structure of the membrane. Because of these complicated factors, the separation characteristics of pervaporation are far more complex than liquid filtration and gas separation membranes.

A proper understanding of the mass transport mechanism may effectively provide direct and useful information on the development of an appropriate membrane. There are many different views among membrane scientists regarding the pervaporation separation mechanism. From the view of microstructure, there are principally two

approaches for describing mass transport in pervaporation; one is the solution-diffusion [1] mechanism and the other is the pore flow mechanism [2]. Even though there are extremely different views between these two models concerning the presence of pores in the selective layer of the membrane, both theories agree that the complicated chemical and physical interactions among feed components as well as feed molecules and membranes play essential roles on controlling the overall separation performance.

2.1.1 Solution-diffusion mechanism

The solution-diffusion model is originally developed by Graham [3] for describing gas permeations, and has been widely adopted by the majority of membrane scientists in pervaporation due to its good agreement with experiments [1,4]. According to the model, pervaporation consists of three consecutive steps (as illustrated in Figure 2.1): (i) the sorption of the permeate from the feed liquid to the membrane, (ii) the diffusion of the permeate in the membrane and (iii) the desorption of the permeate to the vapor phase on the downstream side of the membrane. The selectivity and permeation rate are governed by the solubility and diffusivity of the feed components penetrating across the membrane. The solubility of a feed component in the membrane is determined primarily by the chemical nature of the membrane material and the permeating molecules, and this can be qualitatively estimated using the solubility parameter [5], whereas the diffusivity is dependent on chemical and physical aspects such as the size and shape of permeate molecules and mutual interactions between the permeate molecules and the membrane [6].

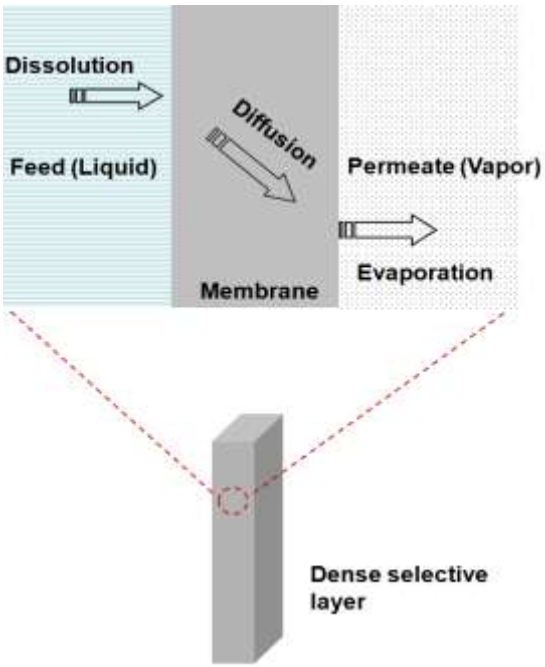

Figure 2.1 Schematic representation of the solution-diffusion mechanism in pervaporation transport

2.1.2 Pore-flow mechanism

The pore flow model is an alternative mechanism for describing the mass transport in pervaporation membranes. The model was first proposed by Okada and Matsuura [7]. Figure 2.2 depicts the schematic diagram of the pervaporation transport on the basis of pore-flow concept. The model was established based on the assumptions that there is a bundle of straight cylindrical pores with an effective length δ penetrating across the selective layer of the membrane and all pores are operating under an isothermal condition. According to the model, the mass transport mechanism in pervaporation consists of three successive steps: (i) the permeant transports through the liquid-filled portion of the pore with a distance δ_a, (ii) a liquid-to-vapor phase change takes place inside the pore, and (iii) the permeant transports through the vapor-filled portion of the pore with a distance δ_b. In other words, the pervaporation transport can be considered to be a combination of liquid-phase and vapor-phase transport in series. The

predictability of the models has been described through many studies using different membrane materials and various separating mixtures [8-10].

In this research study, the pore-flow concept has been employed to conduct a fundamental investigation on the pervaporation transport in membranes. For this reason the theoretical background and details, including derivation of governing equations on the basis of the pore-flow model will be further described in Chapter 5.

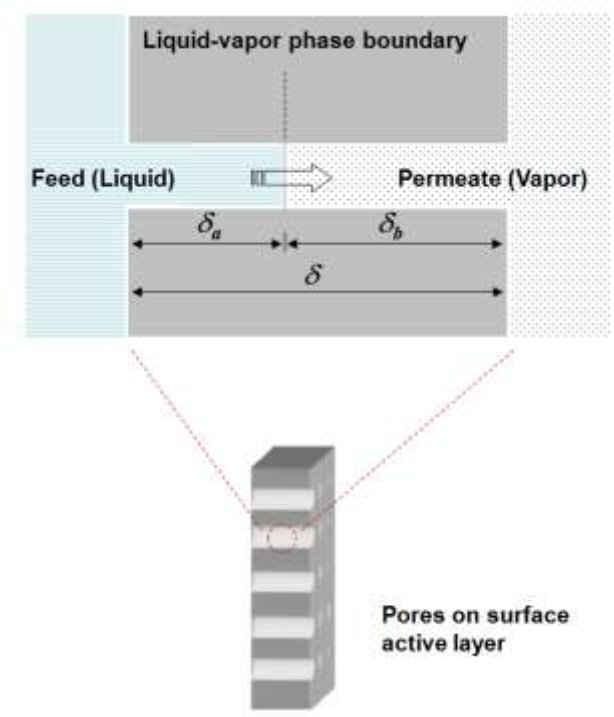

Figure 2.2 Schematic representation of the pore-flow mechanism in pervaporation transport

Apart from the above two models, several views have been proposed by other researchers with different mass transfer models and concepts. Binning and coworkers [11] suggested that the separation takes place in a boundary layer between the liquid and gas regimes in the membrane. Michaels et al. [12] interpreted the selectivity as a result of sieving by polymer crystals. Schrodt et al. [13] suggested that the hydrogen

bonding between the polymer and solvent components played an important role on achieving the membrane performance. Long et al. [14] considered that the diffusion and concentration gradients in different solvent components were the governing factors. Sourirajan and colleagues [15,16] regarded the pervaporation mechanism as a combination of reverse osmosis separation, followed by the evaporation and vapor transportation through capillary pores on the surface layer of a reverse osmosis membrane. Yoshikawa et al. [17-21] explained that the specific and selective separation of substances through a membrane might be realized by differences in the strength of the hydrogen bonding interaction, which led to a selective separation through a membrane.

2.2 Evaluation of pervaporation membrane performance

The selection of a pervaporation process is generally based on its capability to separate components from each other. There are two sets of interlinked parameters that have been widely used to describe this capability. The performance of a pervaporation membrane is typically characterized by flux (W_{total}) and separation factor (α) as defined by the following equations:

$$W_{total} = \frac{J}{A_a t} = \frac{Weight\ of\ permeant}{Membrane\ area\ x\ time} \tag{2.1}$$

$$\alpha_{ij} = \frac{y_i / y_j}{x_i / x_j} = \frac{ratio\ of\ components\ in\ permeate\ vapor}{ratio\ of\ components\ in\ feed\ solution} \tag{2.2}$$

where J is the total mass transferred over time t, A_a is the membrane area, subscripts i and j are two components in the binary system, x and y are the mole fractions of one component in the feed and permeate, respectively.

Because of the existence of a trade-off relationship between flux and separation factor, that is, the flux and separation factor normally perform in the opposite way, Huang and Yeom [22] introduced the term 'pervaporation separation index (PSI)' to evaluate the overall performance of a membrane. PSI was originally defined as a product of permeation flux and separation factor:

$$PSI = J_t \cdot \alpha \tag{2.3}$$

where J_t is the total permeation flux, and α is the separation factor. However, in this definition, the PSI can be large if the membrane has a high flux even when α is equal to 1. Thus, the definition of PSI was later modified as the product of J_t and $(\alpha - 1)$ [23].

$$PSI = J_t \cdot (\alpha - 1) \tag{2.4}$$

In most studies, flux and separation factor are the two main parameters reported, and widely used for the comparison purpose with the literature.

2.3 Membrane materials for ethanol recovery by pervaporation

While the great potential application of membranes in pervaporation processes for ethanol recovery has been recognized in particular for separating biofuels from dilute

fermentation broths, a lack of desirable membrane materials that possess a sufficient high selectivity/flux separation characteristic with a cost-effective fabrication has been a major hurdle that hinders the advancement of this technology in industrial practice. During the past three decades, several membrane materials ranging from polymeric, inorganic and composite (mixed-matrix) materials have been extensively investigated. The following section reviews the most attractive membrane materials and their corresponding separation performances for ethanol recovery.

2.3.1 Polymeric membrane materials

Polydimethylsiloxane (PDMS)

Poly(dimethylsiloxane) (PDMS) or often referred to as 'silicone rubber' is the most widely studied membrane material for ethanol recovery. Table 2.1 summarizes the separation performance of PDMS membranes reported in the literature. From the table, PDMS membranes exhibit ethanol-water separation factors in the range of 4-15. The variation of membrane selectivity and fluxes in PDMS membranes often arises from various factors including the source of the polymer starting materials (though called 'PDMS', there are often differences), the method of membrane casting, the degree of cross-linking, membrane module design and the testing conditions.

Table 2.1 Separation performance of PDMS membranes for ethanol recovery

Membrane material	Configuration	Feed composition (wt%)	*T* (°C)	Separation factor	Total flux (g m^{-2} h^{-1})	Ref.
PDMS polymers						
PDMS	Flat sheet	8/92	30	10.8	25	[24]
PDMS	Flat sheet	10/90	30	5.0	20	[24]
PDMS (GE 615 membrane)	Flat sheet	6/94	50	8.6	100	[26]
PDMS (Sulzer membrane)	Flat sheet	6/94	35	6.0	34	[27]
PDMS on cellulose acetate support	Flat sheet	5/95	40	8.5	1300	[28]
PDMS on Nylon support	Flat sheet	10/90	40	5.0	160	[29]
PDMS on PTFE support	Flat sheet	6/94	20	14.0	1530	[30]
PDMS on polyamide support	Flat sheet	4/96	40	8.5	1400	[31]
PDMS on polysulfone support	Flat sheet	4/96	40	4.5	1150	[29]
PDMS on polyimide support	Flat sheet	3/97	41	4.6	120	[32]
PDMS on microporous support (MTR membrane)	Flat sheet	6/94	25	5.5	39	[33]
PDMS/polysulfone composite	Hollow fiber	8/92	50	6.6	576	[34]
PDMS/PVDF/non-woven-fiber, multi-layer configuration	Flat sheet	5/95	60	15	450	[35]
PDMS on ZrO_2/Al_2O_3 ceramic support	Tubular	4.2/95.8	60	7.93	4190	[36]
PDMS on ZrO_2/Al_2O_3 ceramic support	Tubular	4.3/95.7	70	5.7	19500	[37]

To achieve the flux enhancement, PDMS composite membranes comprising a PDMS thin film layer coated on a porous support have been developed. Typically, a thinner PDMS selective layer results in a greater membrane flux [28,30,31,38]. The supporting porous material also plays an important role determining both flux and membrane selectivity. Shi and coworkers reported that using polyamide as a supporting layer results in the PDMS composite membrane with a better separation and flux than those fabricated with polysulfone [31]. In the recent work by Fenjuan and coworkers [37], the membranes consisting of a thin PDMS layer deposited on ZrO_2/Al_2O_3 porous ceramic supports can display a remarkable total flux of up to 19,500 g m^{-2} h^{-1} and separation factor of 5.7 for 4.3 wt% ethanol feed solution at 70 °C.

Table 2.2 Separation performance of modified PDMS membranes for ethanol recovery

Membrane material	Configuration	Feed composition (wt%)	*T* (°C)	Separation factor	Total flux ($g\ m^{-2}\ h^{-1}$)	Ref.
Modified PDMS polymers						
PPMS on cellulose acetate support	Flat sheet	5/95	40	6.2	1433	[39]
PDMS-styrene graft copolymer on PTFE support	Flat sheet	8.1/91.9	60	6.2	130	[40]
Plasma-induced grafted PDMS/PVDF composite	Flat sheet	10/90	35	5.1	1650	[41]
PDMS (Plasma-polymerized Tetramethoxysilane monomers)	Flat sheet	4/96	25	4.6	380	[42]
PDMS (Plasma-polymerized Hexamethyltrisiloxane monomers)	Flat sheet	4/96	25	5.0	320	[51]
PDMS (Plasma-polymerized hexamethyltrisiloxane PDMS membranes and treated with Octadecyldiethoxymethylsilane)	Flat sheet	4/96	25	18.0	15	[51]
Plasma-induced grafted TMVS/PVDF, coating by phosphate ester containing silicone copolymer	Flat sheet	10/90	30	4.6	2850	[43]
Plasma-induced grafted TMVS/PVDF, coating by phosphate ester containing silicone copolymer	Multi-layer flat sheet	10/90	30	31	900	[44]
PDMS-imide copolymers (synthesized from ODMS and PMDA)	Flat sheet	10/90	40	10.6	560	[45]
PDMS-imide copolymers (synthesized from ODMS and 6FDA)	Flat sheet	10/90	40	3.6	2120	[52]
PDMS-polystyrene interpenetrating polymer network on polyethersulfone ultrafiltration support	Flat sheet	10/90	60	5.5	160	[46]
PDMS-polysulfone block copolymers	Flat sheet	10/90	25	6.2	27	[47]

The chemical modification of PDMS membranes to improve alcohol/water separation properties has been extensively studied and some studies with an encouraging performance are listed in Table 2.2 Kashiwagi and coworkers [42] studied the modification of PDMS membranes using plasma-polymerization of silanes with different alkyl lengths. Silane monomers containing longer alkyl groups are better

modification reagents and the resultant membranes exhibit better ethanol/water permselectivity. Chang and Chang fabricated plasma-induced grafted TMVS/PVDF membranes, coating by phosphate ester containing silicone copolymer [44]. The membranes displayed the separation factor up to 31 with the flux of 900 g $m^{-2}h^{-1}$ for a feed mixture containing 10 wt% ethanol at 30 °C. Krea et al. synthesized polysiloxane-imide copolymers from α,ω-bis(3-aminopropyldimethyl) oligodimethylsiloxane (ODMS) and aromatic dianhydrides PMDA and 6FDA [45]. Compared to PDMS polymers, PDMS-imide comprising fluorinated imide blocks and siloxane blocks exhibit higher sorption affinities and selectivity for ethanol with enhanced mechanical properties. For the recovery of a feed solution containing 10 wt% ethanol at 60 °C, the separation factor of the PDMS-polystyrene interpenetrating polymer network on polyethersulfone ultrafiltration support is 5.5 and the permeation flux is 160 g $m^{-2}h^{-1}$ [46].

Poly [1-(trimethylsilyl)-1-propyne) (PTMSP)

Poly [1-(trimethylsilyl)-1-propyne) (PTMSP), a glassy polymer with a large free volume, has been explored for alcohol recovery. The pervaporation performances in terms of flux and separation factor of PTMSP membranes for ethanol/water separation were surveyed and summarized in Table 2.3.

Table 2.3 Separation performance of PTMSP and modified PTMSP membranes for ethanol recovery

Membrane material	Configuration	Feed composition (wt%)	*T* (°C)	Separation factor	Total flux ($g\ m^{-2}\ h^{-1}$)	Ref.
PTMSP polymers						
PTMSP	Flat sheet	6/94	30	19.9	325	[48]
PTMSP	Flat sheet	6/94-7/93	50	10.3	480	[49]
PTMSP	Flat sheet	6/94	75	9	700	[50]
PTMSP	Flat sheet	10/90	50	14.5	210	[51]
Modified PTMSP polymers						
PTMSP/PDMS graft copolymer	Flat sheet	7/93	30	28.3	62	[52]
Trimethylsilyl substituted PTMSP	Flat sheet	6/94-7/93	50	17.6	590	[55]
n-Decane substituted PTMSP	Flat sheet	6/94-7/93	50	17.8	430	[55]

The ethanol/water separation factor of PTMSP membranes falls in the range from 9 to 20. The flux with PTMSP is about threefold higher than the corresponding flux obtained with conventional PDMS under similar operation conditions. Overall, PTMSP membranes exhibit greater membrane selectivity and flux relative to conventional PDMS membranes. Nevertheless, it has not yet demonstrated a long-term stable separation performance. In fact, the selectivity and permeation flux of PTMSP membranes decline as a function of time and this phenomenon is probably due to the compaction of the polymer and/or the sorption of foulants within the membrane. The introduction of cross-linked structure to PTMSP membranes could be a feasible approach to accomplish a more stable membrane material and to strengthen the prospect of PTMSP membranes for alcohol recovery [53,54].

Other polymers

Tremendous effort has been expended on searching for other new polymeric materials with better separation characteristic than PDMS and PTMSP. These reported materials are very limited, which includes styrene-fluoroalkyl acrylate graft copolymer [24], polyorganophosphazene [29], styrene-butadinene-styrene block copolymers [32], polyurethaneurea [40], polyether block amide [55], poly(vinylidene fluoride) (PVDF) [56], Polytetrafluroethylene [57], Polypropylene [57]. Some examples of the alcohol/water separation performances of membranes fabricated from the materials are listed in Table 2.4.

Table 2.4 Separation performance of other hydrophobic membranes for ethanol recovery

Membrane material	Configura-tion	Feed composition (wt%)	*T* (°C)	Separation factor	Total flux ($g\ m^{-2}\ h^{-1}$)	Ref.
Other polymers						
Styrene-fluoroalkyl acrylate graft copolymer on PDMS support	Flat sheet	8/92	30	16.3-45.9	5-14	[24]
Polyorganophosphazene containing $–OC_2H_5$ pendant group on Nylon support	Flat sheet	10/90	40	2.0	130	[29]
Polyorganophosphazene containing $–OCH_2CF_3$ pendant group on Nylon support	Flat sheet	10/90	40	6.1	260	[29]
Polyorganophosphazene containting - $OCH_2CF_2CF_2CF_2H$ pendant group on Nylon support	Flat sheet	10/90	40	4.0	96	[29]
Polyurethaneurea containing PDMS	Flat sheet	10/90	40	8.6	130	[40]
Polyether block amide (PEBA® 2533, Antofina)	Flat sheet	5/95	23	2.5	118	[55]
Styrene-butadiene-styrene block copolymer (SBS), dense	Flat sheet	3/97	41	5.5	125	[32]
Styrene-butadiene-styrene block copolymer (SBS), porous	Flat sheet	3/97	41	3.5	1752	[32]

Besides above-mentioned materials, the fluorinated polyimides (PIs) synthesized from fluorine-containing (especially with bulky side groups, CF_3) monomers could also be

used as suitable membrane materials because of their unique hydrophobicity and relatively high free volume, which are important factors governing preferential sorption and diffusion of organics over water [58]. In most cases, membranes show a trade-off relationship in the separation performance; they possess either an improved separation factor with a significantly reduced flux or an enhanced flux with a lack of selectivity.

So far, only few specific cases have attained alcohol-water separation factors greater than that obtained by the common PDMS membranes. For instance, Kazuhiko and Kiyohide [24] reported that membranes fabricated using styrene-fluoroalkyl acrylate graft copolymer on a cross-linked PDMS support displayed an excellent ethanol/water separation factor of 46, which is significantly higher than the intrinsic PDMS separation factor of 11. Recently, Ghofar and Kokugan [57] investigated the pervaporation characteristics of microporous polytetrafluroethylene (PTFE) and polypropylene (PP) membranes for ethanol-water separation. They found that the resultant membranes are ethanol-selective and the ethanol-water separation factors could reach as high as 75 at an optimal downstream pressure condition. Even though such membranes in both examples display a promising separation performance, a further investigation and independent verification on the membrane performance may be required.

2.3.2 Inorganic membrane materials

Inorganic membranes based on silicalite-1 and hydrophobic zeolites typically display a greater alcohol/water separation factor and flux relative to polymer-based membranes.

A comprehensive summary on zeolite materials and the fundamentals of using zeolites for pervaporation applications is provided in a review by Bowen et al [59].

Table 2.5 Separation performance of silicalite-1 and hydrophobic zeolite membranes for ethanol recovery

Membrane material	Configura-tion	Feed composition (wt%)	*T* (°C)	Separation factor	Total flux ($g\ m^{-2}\ h^{-1}$)	Ref.
Silicalite-1						
Silicalite-1 on porous stainless steel support	Flat sheet	4/96	60	58	760	[60]
Silicalite-1 on porous stainless steel support	Flat sheet	5/95 (Fermented ethanol)	30	21	104	[61]
Silicalite-1 on Al_2O_3 support	Flat sheet	9.7/90.3	32	11.5	100	[62]
Silicalite-1 on porous α-Al_2O_3 tube support	Tubular	5/95	60	39	1510	[63]
Silicalite-1 on Mullite tubular support	Tubular	5/95	60	106	930	[64]
Silicalite-1 on α-Al_2O_3 tubular support	Tubular	5/95	60	89	1800	[65]
Silicalite-1 on Mullite tubular support	Tubular	10/90	60	72	2550	[66]
Silicalite-1 coated with PDMS on Stainless steel support	Flat sheet	10/90 (Fermented ethanol)	30	43	230	[67]
Silicalite-1 on stainless steel support	Flat sheet	4/96	30	26-51	150-330	[68]
Silicalite-1 coated with PDMS on stainless steel support	Flat sheet	4/96	30	125	140	[68]
Silicalite-1 on porous stainless steel disk support	Flat sheet	4.7/95.3	30	41	400	[69]
Silicalite-1 on porous stainless steel disk support	Flat sheet	4.6/95.4 (Fermented ethanol)	30	88	500	[69]
Silicalite-1 treated with silane, $C_8H_{17}SiCi_3$,on porous stainless steel disk support	Flat sheet	4/96	50	44	650	[70]
Silicalite-1 treated with silane, $C_{18}H_{37}SiCi_3$,on porous stainless steel disk support	Flat sheet	4/96	50	45	133	[70]
Other hydrophobic zeolite						
Ge-ZSM-5, on stainless steel support	Flat sheet	5/95	30	47	223	[71]
B-ZSM-5, on Al_2O_3-coated SiC multi-channel monolith support	Flat sheet	5/95	60	31	160	[72]
Ti-Silicalite, on α-Al_2O_3 capillary support	Tubular	5/95	45	16-62	700-2100	[73]

Table 2.5 shows the separation performance of silicalite-1 and other zeolite membranes investigated for ethanol recovery. From the table, the average ethanol/water separation factor of silicalite-1 membranes is approximately 100. Recent studies revealed that silicalite-1 membranes coated with thin PDMS layer can bring the separation factor up to 125 for ethanol/water pair [68]. Nevertheless, zeolite and silicalite-1 membranes are more difficult and costly to fabricate than polymeric membranes.

2.3.3 Composite or mixed-matrix membrane materials

An idea of incorporating zeolite/silicalite-1 into the polymer matrix is therefore of great recent interest as it combines the benefits of both materials; which include the exceptional high separation properties and thermal resistance of silicalite-1/zeolites with the desirable mechanical integrity, and the low price and ease of membrane fabrication of polymers. Several research groups have investigated silicalite-1/PDMS mixed-matrix membranes (MMMs) for alcohol/water recovery.

As summarized in Table 2.6, the separation factors of silicalite-1/PDMS membranes are in the range of 5-59 for ethanol/water separation. Importantly, the wide range in separation performance of the mixed matrix membranes is attributed to the difference in the silicalite-1 loading, particle size, source of silicalite-1, and membrane-casting protocols. Usually, loadings of 60 wt% or higher are required to deliver significant improvement in alcohol/water separation factors.

Table 2.6 Separation performance of silicalite-1/PDMS mixed-matrix membranes and other hybrid membranes for ethanol recovery

Membrane material	Particle size (μm)	Particle loading (%)	Feed composition (wt %)	*T* (°C)	Separation factor	Total flux (g m^{-2} h^{-1})	Ref.
Silicalite-1/PDMS							
Silicalite-1/PDMS	0.5-5	40	5-5.5/94.5-95	22.5	14.9	322	[74]
Silicalite-1/PDMS	0.5-5	60	5-5.5/94.5-95	22.5	16.5	449	[74]
Silicalite-1/PDMS	~1	60	5.3/94.7	50	21	105	[75]
Silicalite-1 filled PDMS on polyimide support	0.1-0.23	15	3/97	41	4.8	170	[32]
Silicalite-1 (UOP Inc.) /PDMS	1-10	70	7/93	22	29	52	[76]
Silicalite-1/PDMS	0.3-4	77	7/93	22	59	89	[76]
Silicalite-1/PDMS	~1	67	5.3/94.7	50	32	90	[75]
Hydrophobic zeolites/PDMS							
ZSM-5/PDMS CBV-28014, Zeolyst International) (Si/Al = 137)	~2.4	50	5/95	50	37	70	[77]
ZSM-5/PDMS, on polyimide support, CBV 3002 (Si/Al =240)	1-1.5	30	3/97	41	5.5	151	[32]
Other hybrid membranes							
Polyphosphazene nanotubes/PDMS	50 μm in length, 0.040 in diameter	10	10/90	40	10	476	[78]
Carbon black/PDMS	0.051	10	6/94	35	9	51	[79]
PTMSP/nano-silica	0.0045-0.0065	1.5	10/90	50	15.3	400	[51]

Besides mixed-matrix membranes based silicalite-1 or zeolite, new hybrid or composite membranes containing other different fillers such as polyphosphazene nanotubes [78], carbon black [79] and silica [51] have been studied, and their separation performances mostly fall in between the PDMS and silicalite-1/PDMS membranes.

Until now, only membranes based PDMS and silicalite-1/PDMS composites have been commercialized by Sulzer Chemtech (Neunkirchen, Germany), SolSep BV (Apeldoorn, Netherlands), Pervatech BV (Enter, Netherlands) [80], and regarded as the current benchmark materials for alcohol-selective membranes. Compared with works for ethanol/water separation, studies that report the separation of butanol and water using pervaporation membranes are relatively limited. The alcohol separation factors of the different membrane materials are of typical rank in the following order: PDMS < PTMSP < composite or mixed matrix membranes < Inorganic membranes. Ongoing works on the development and exploration of membranes with better separation and physicochemical properties for alcohol recovery is of paramount importance and necessary.

2.4 Design and engineering principles for polymeric pervaporation membranes

2.4.1 Membrane preparation method

A number of different techniques are available to prepare synthetic membranes [81], including sintering, stretching, track-etching, template leaching and phase inversion. Among those, phase inversion is a widely used method for preparing polymeric membranes. This is a very versatile technique that potentially allows various kinds of morphologies to be obtained. Most commercially available membranes are obtained by phase inversion.

Phase inversion is a process whereby a polymer is transformed in a controlled manner from a liquid to a solid state. The process of solidification is very often initiated by the transition from one liquid state into two liquids (liquid-liquid demixing). At a certain

stage during demixing, one of the liquid phases (the high polymer concentration phase) will solidify so that a solid matrix is formed [81]. By controlling the initial stage of phase transition, the membrane morphology can be controlled, i.e. porous as well as nonporous structure can be prepared. Four different techniques have been applied to achieve membrane formation by phase inversion as follows:

(i) Precipitation by solvent evaporation

The simplest technique for preparing phase inversion membranes is precipitation by solvent evaporation. In this method, polymer solution is cast on a suitable support such as a glass plate, nonporous (i.e. metal, glass or polymer such as polymethacrylate or polytetrafluoroethylene) or porous supports (i.e. nonwoven polyester). The solvent is allowed to evaporate in an inert (i.e. nitrogen) atmosphere, in order to exclude water vapor, allowing a dense homogeneous membrane to be formed.

(ii) Vapor induced precipitation [82]

This method applies a vapor atmosphere which consists of a non-solvent saturated with the same solvent used in the cast film. The high concentration of the solvent in the vapor phase prevents the evaporation of solvent from the cast film, while membrane formation occurs due to the penetration (diffusion) of non-solvent into the cast film which typically leads to form a porous membrane without a top skin layer.

(iii) Precipitation by controlled evaporation [81,83]

In the previous methods, polymer is dissolved only in a solvent. However, in this approach, polymer is dissolved in a mixture of solvent and non-solvent. If the solvent is more volatile than the non-solvent, the composition diagram shifts during the evaporation to a higher non-solvent and polymer content. This results in the polymer precipitation leading to the formation of a skinned membrane.

(iv) Thermal precipitation [81]

Polymer solution in a mixed or single solvent is cooled to enable phase separation. Evaporation of the solvent often allows the formation of a skinned membrane. This method is frequently used to prepare microfiltration membranes.

(v) Immersion precipitation [84,85]

Generally, a polymer solution is cast as a film on a support (glass plate or non-woven) with a casting knife. Then this film is immersed into a coagulation bath containing a non-solvent. At the moment of immersion, solvent diffuses out of the film, while non-solvent diffuses into the film. Due to polymer immiscibility with the non-solvent, its intrinsically high molecular weight and low diffusion coefficient, the relative velocity of the polymer molecules is very low. Therefore, diffusion takes place in a polymer frame of reference.

Typically, phase inversion via the immersion precipitation method is widely employed to produce pervaporation membranes with asymmetric structure comprising a relatively dense selective skin layer bonded on a porous substructure. The main

consideration of fabricating such a structure is to attain an excellent separation performance while maintaining high productivity. In this regard, the phase separation process by means of the immersion precipitation technique and the formation of the asymmetric structure will be further discussed in detail.

2.4.2 Types of membrane structures and configurations

The type of membrane structures and the membrane configurations significantly affect the separation performance of a membrane. Thus, it is important to design the membrane materials with an appropriate technique to obtain membranes with desirable morphology for a specific application. Membranes can be divided into two categories according to their structural characteristics which can have significant impacts on their separation characteristics: (i) symmetric and (ii) asymmetric membranes.

When the separating layer and the bulk support designed for mechanical strength are indistinguishable and show an integral, homogenous structure and composition in the direction of the membrane thickness, it is a symmetric or isotropic membrane [86,87]. Homogeneous and microporous membranes are the two typical examples of symmetric membranes. Particularly, a homogeneous membrane is referring to the dense membrane, which is intensively used in laboratory scale for the fundamental study of intrinsic membrane properties. It is commonly prepared through solution casting or phase inversion. Besides, microporous membranes consist of a solid matrix with defined pores, and the separation of the various chemical species is achieved strictly by a sieving mechanism with the pores and relative size of particles being the determining separation parameters. Most of the microporous membranes are manufactured through

the sintering of inorganic materials, or phase inversion from the three dope solution components (polymer-solvent-non-solvent) for polymeric materials. This type of membrane is employed for various separation tasks on a laboratory or industrial scale.

Asymmetric membranes are primarily used for pressure driven membrane processes. In contrast to the symmetric membranes, their structures compose of a very thin active skin layer on a highly porous substrate [86,87]. The main purpose of this support layer is to provide the membrane with sufficient mechanical strength and eliminate substantial substructure resistance of gas or vapor transport through the membrane. Phase inversion is mainly adopted to prepare asymmetric membranes. The porous structure is created by precipitation from a homogeneous polymer solution. On the other hand, composite membranes are in general an improvement over phase inversion membranes. The composite technique allows one to produce support and active (skin) layers from different materials, which are selected for optimum function in each case. A composite membrane is not necessarily restricted to two layers, but it can be fabricated with a number of regions or coating layers to meet the advanced separation characteristics required for a specific application. Figure 2.3 illustrates the structural differences among symmetric and asymmetric membranes [88].

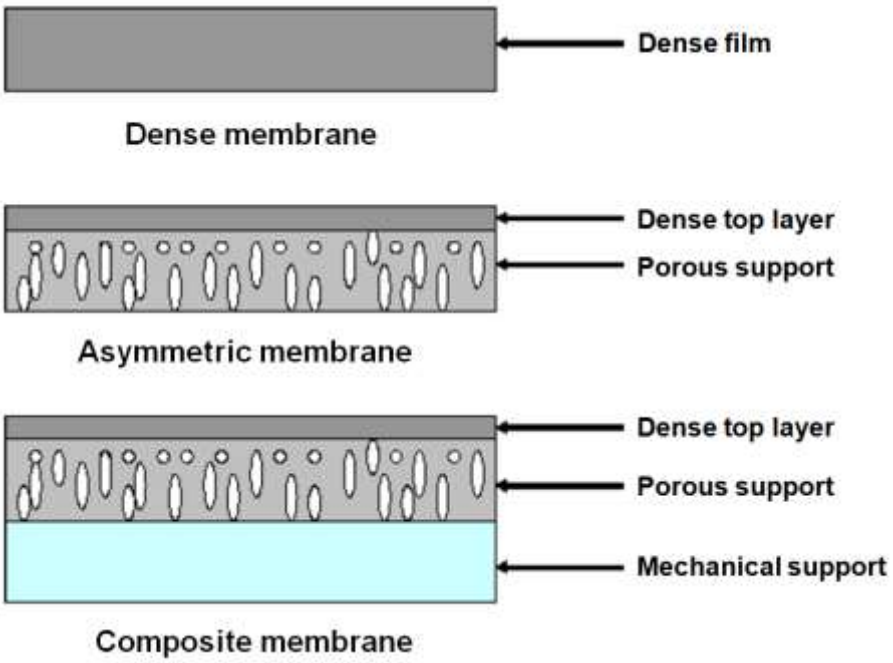

Figure 2.3 Typical membrane morphology

Based on the membrane morphology, there are two membrane configurations commonly used for pervaporation separation: (i) flat sheet membranes; and (ii) hollow fiber membranes.

Although a flat sheet membrane can be utilized to predict and tailor the desirable separation performance in the hollow fiber membranes, neither a flat sheet dense nor asymmetric membranes comparable to the hollow fiber membrane. To date, hollow fiber membranes are the most preferable configuration due to their high surface area and good mechanical resistance [2]. Therefore, the fabrication of single and dual-layer hollow fiber membranes will be the focus of this thesis. A detailed discussion on the hollow fiber membrane fabrication process and the criteria for fabrication of high performance hollow fiber membranes with designed morphology will be described in the next chapter.

2.4.3 Membrane module design

As mentioned previously, membranes in pervaporation and other membrane-based separation processes are available in both flat film and hollow fiber configurations. However, their utility is dependent on their incorporation into usable packages. Flat sheet membranes are usually contained in the plat-and-frame devices and spiral wound elements, whereas the modules of hollow fiber, tubular and capillary involved hollow fiber configuration. The vast majority of industrial membrane modules are constructed into five basic designs: plate-and-frame, spiral wound, hollow fiber, tubular and capillary. The three most general modules employed in industry will be discussed in the following sections.

(i) Plate-and-frame modules

Plate-and-frame design replicates conventional filtration setup. It is conceptually simple, which consists of a package of flat sheet membranes. Plate-and-frame module is easily fabricated and the area of the membranes in this configuration is well defined. The flat sheet membranes, mainly used for experimental purposes such as characterizing the intrinsic properties of membranes are stacked together like a multilayer sandwich in a frame. These types of modules consist of a cylindrical tube, spacer materials to separate the membrane envelopes and rubber gaskets to direct flow through the module and seal the assembly [86]. The plate-and-frame package design is illustrated by a schematic diagram shown in Figure 2.4.

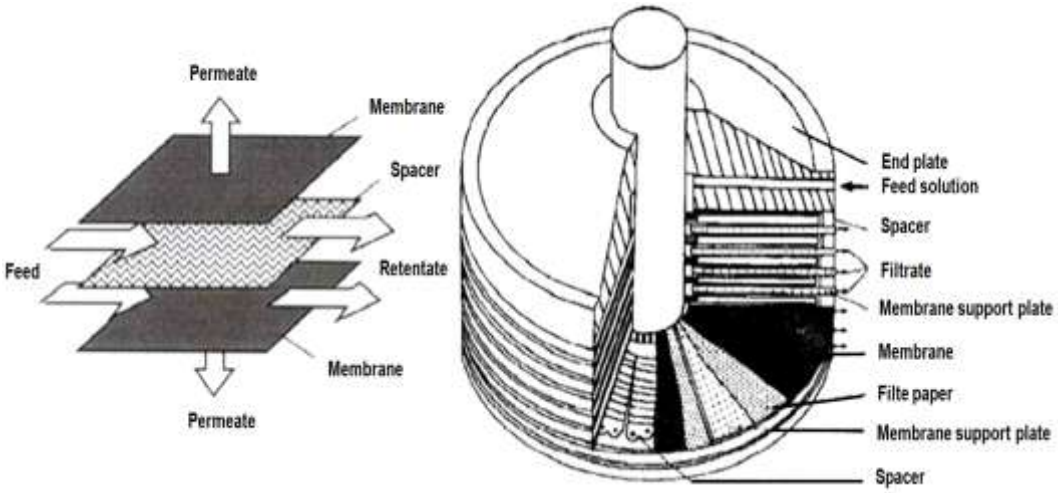

Figure 2.4 Schematic drawing of plate-and-frame module

Lowest surface area/unit separator volume (~100-400 m^2/m^3) is the major drawback of plate-and-frame module. These modules are favorable in reverse osmosis applications.

(ii) Spiral-wound module

The spiral-wound module maintains the simplicity of flat membranes fabrication, but it is the next logical step from a flat membrane. This element increases the packing density (membrane surface per module volume) remarkably to 300-1000 m^2/m^3 as compared to plate-and-frame module. As shown in Figure 2.5, the assembly consists of a sandwich of flat sheet membranes to form an envelope enclosing a separator/spacer in between to provide mechanical strength. The membranes envelope is wound around a central core of a perforate collecting tube. When a spiral-wound mode is in operation, the feed flows outside the membrane envelope, while the permeate moves toward the center of the module and is removed through the central collector [86].

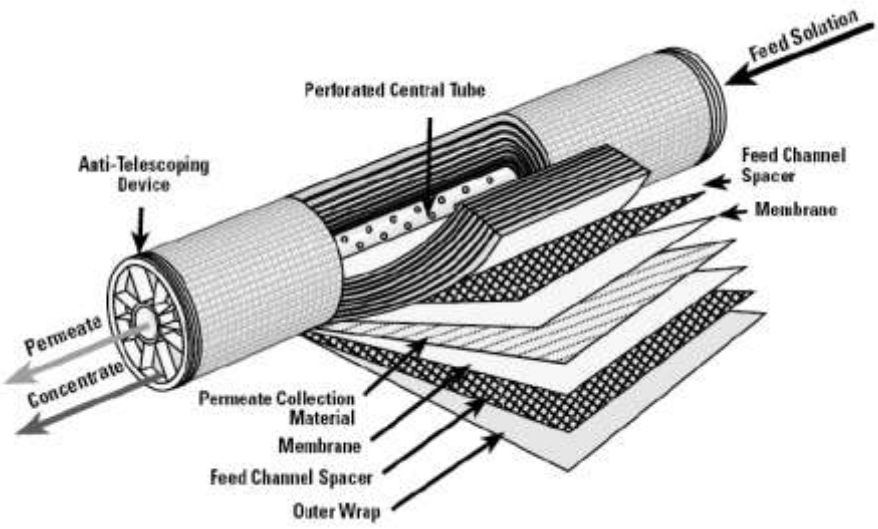

Figure 2.5 Schematic drawing of spiral-wound module

(iii)Hollow fiber module

A hollow fiber module consists of a large number of hollow fibers assembled together into a pressure vessel. The membranes are in the shape of thin hollow fiber tubes with very small diameter. The geometric arrangement of the hollow fiber module is similar to conventional heat-exchanger assembly, as presented in Figure 2.6. It offers a fairly high packing density with a maximum membrane surface area per unit volume as high as 10,000 m^2/m^3 [81,88]. Typically, the feed stream can enter either the shell side or lumen side and permeate is collected from the other side, depending on the fiber's dimension and mechanical properties.

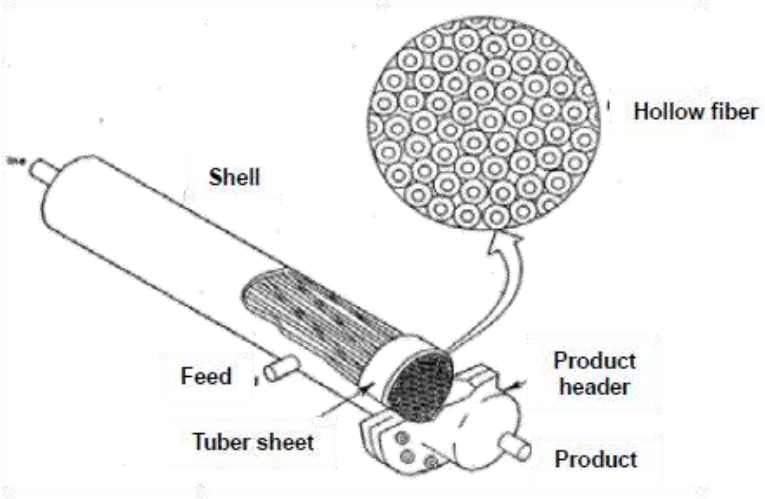

Figure 2.6 Schematic drawing of hollow fiber module

The selection and application of membrane modules principally depend on economic considerations, separation performance and practicability of the process (ease of cleaning, ease of maintenance, ease of operation, compactness of the system, scale and the possibility of membrane replacement).

2.5 Fundamentals of hollow fiber formation

2.5.1 Phase inversion mechanisms during the membrane formation

Asymmetric polymeric membranes, which consist of a dense skin layer integrally bonded with a relatively thick and asymmetric porous substructure, are usually prepared via the method of phase inversion. Before reviewing the technology development of hollow fiber formation, the fundamentals of phase inversion mechanisms will be discussed in this section. Phase inversion can be induced by non-solvent, vapor or temperature change. Among several techniques, the non-solvent induced phase separation or immersion precipitation is widely employed. During non-solvent induced phase inversion, a homogeneous (thermodynamically stable) polymer

solution is transformed into a polymer-rich phase (a high polymer concentration) and a polymer-lean phase (a high solvent concentration) to minimize the Gibbs free energy of mixing, ΔG_M, of the system [81]. For a simple ternary system consisting of a polymer, a solvent, and a non-solvent, the ΔG_M at constant pressure and temperature can be described using the Flory-Huggins theory [89] as the following equation:

$$\frac{\Delta G_m}{RT} = n_1 \ln \phi_1 + n_2 \ln \phi_2 + n_3 \ln \phi_3 + \chi_{12} n_1 \phi_2 + \chi_{13} n_1 \phi_3 + \chi_{23} n_2 \phi_3 \quad (2.5)$$

where n_i, φ_i, and χ_i are the number of moles, volume fraction and binary interaction parameter, respectively. The polymer-rich phase predominately constructs the membrane matrix, whereas the polymer-lean phase forms membrane pores. This phenomenon is typically regarded as liquid-liquid demixing.

Typically, the thermodynamic interactions between these three components in a simple ternary system and their transient states of phase transformation during phase inversion can be represented by a ternary phase diagram developed by Tompa in the late 1950s [90], following by Strathmann et al. [91] and Michaels [92] in the early 1970s.

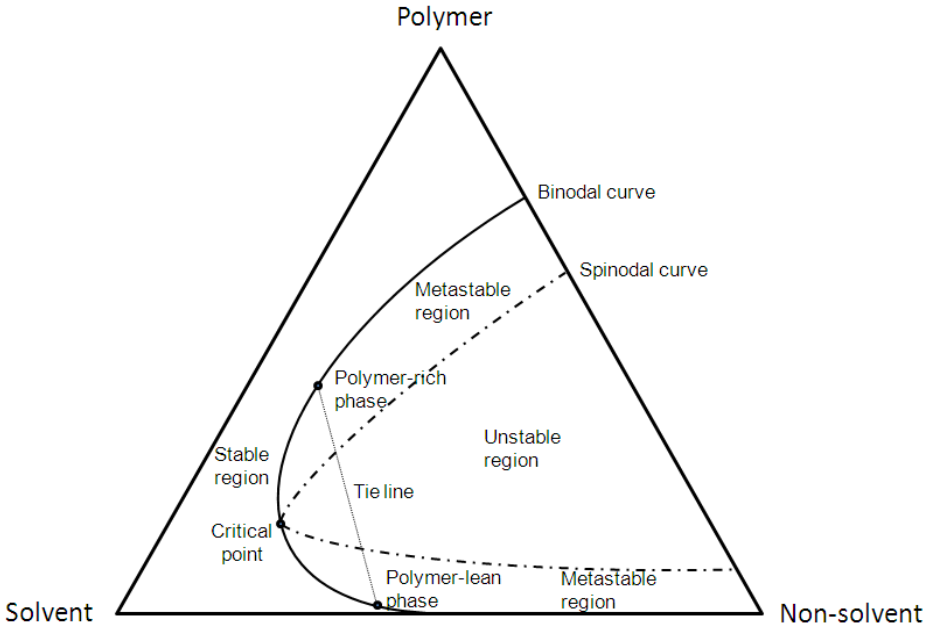

Figure 2.7 Typical ternary phase diagram of a polymer-solvent-nonsovlent system.

Figure 2.7 illustrates a typical ternary phase diagram where each corner of the triangle refers to each pure component and any point located inside the triangle represents a mixture of the three components. The essential elements of a phase-diagram include the binodal and spinodal curves, a critical point, tie-line, meta-stable region. The tie-line links two points on the binodal which are in thermodynamic equilibrium. One end-point of the tie-line represents the composition of polymer in a rich phase and the other end-point represents the composition of polymer in a lean phase. The intersected point between the binodal and the spinodal curve is referred to as the critical point.

2.5.1.1 Phase inversion of glassy polymers

Depending upon the thermodynamics of the system, the liquid-liquid phase separation may take place following one of the two mechanisms: (1) nucleation and growth and (2) spinodal decomposition [93]. The nucleation and growth is regarded as a

mechanism when a polymer solution departs from a thermodynamically stable condition and slowly enters a meta-stable region between the binodal and the spinodal curves in the phase diagram. In general, nucleation and growth of the polymer-rich phase in the lower meta-stable region which has low polymer concentrations leads to polymer powders or low-integrity polymer agglomerates which cannot be used as useful membranes. In contrast, nucleation and growth of the polymer-poor phase at high polymer concentrations in the upper meta-stable region results in porous membrane morphology [2]. Spinodal decomposition is another mechanism taking place when the system enters a thermodynamically unstable spinodal region by directly across the critical point or via the meta-stable region. In such a situation, spinodal decomposition originates, not from nuclei, but from concentration fluctuations of increasing amplitude. It is generally believed that spinodal decomposition yields "open-cell" or interconnected network structure, which is sometimes called a bicontinuous structure [93,94].

Most membrane scientists and engineers generally admit that the morphological change during membrane formation via liquid-liquid demixing may result from a combination of nucleation growth and spinodal decomposition [89,95-98]. The polymer solution may first develop its early membrane structure through the mechanism of nucleation growth, and then may or may not through spinodal decomposition. In addition, a nucleation mechanism could, in principle, take place after the spinodal decomposition depending on the precipitation path. It is important to point out that nucleation growth and spinodal decomposition can only help us qualitatively understand membrane formation and predict membrane morphology from the thermodynamic point of view. In reality, a phase inversion is a dynamics process

where each composition in the polymer-solvent-non-solvent system changes rapidly due to complicated mass transfer and convective flows among polymer, solvent and non-solvent during phase inversion. Thus, a further consideration including the kinetic point of view is necessary. For example, the ratio (referred as the k value) of solvent outflow to non-solvent inflow plays a crucial role on controlling membrane structure and overall porosity [2,89,99-101] as illustrated in Figure 2.8.

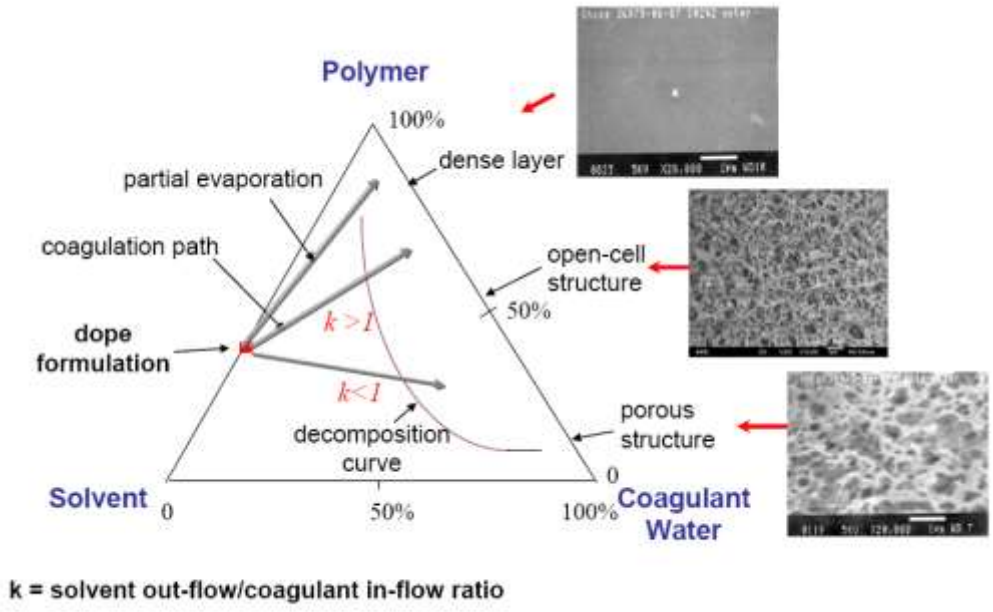

Figure 2.8 Schematic diagram of the relationship of dope composition and precipitation kinetics, and membrane morphology

Depending on the initial dope composition and the k value, the precipitation path may take place via the nucleation growth or the spinodal decomposition. Since k may not be constant across membrane thickness and its value is dependent on temperature and dope viscosity, it becomes difficult to microscopically predict the local membrane porosity. Therefore, Figure 2.8 can only be used as a qualitative understanding of the phase inversion.

Many mass transfer models have been proposed in order to better describe membrane formation during phase inversion [99,102-111]. Cohen et al. [109] and Reuvers et al. [110,111] are pioneers who proposed mass transfer models to explain the membrane formation at the interface between polymer solution and coagulation bath. Kim et al introduced the mass transfer formalism to study spinnodal decomposition mechanism during asymmetric membrane formation [112]. In the work published by Termonia [113], the polymer coagulation process is simulated using Monte Carlo diffusion model. The model is able to predict the different membrane morphologies ranging from dust-like, finger-like and sponge-like by changing the interaction parameters between solvent and non-solvent coagulant. He and coworkers recently reported that the change of asymmetric structure from island-like phase to continuous phase in a polymeric ultrafiltration membrane may be likely resulted from the mechanism transition of phase separation from spinodal decomposition to nucleation growth, based on the computer simulation results observed [114]. An attempt to investigate the effect of polymer chain length and solvent size on the kinetics of membrane formation during phase inversion using dynamic simulation was recently studied by Wang and coworkers [115].

Reuvers and coworkers studied phase inversion during membrane formation by measuring light transmission and proposed two different mechanisms; namely instantaneous and delayed demixing which principally lead to the formation of different asymmetric membrane structures [110,111]. They reported that membranes consisting of a thin layer full of porous nodular structure on top of a macrovoid-filled open-cell substructure obtained under an instantaneous liquid-liquid demixing process are generally used for ultrafiltration (UF) and hyperfiltration; while membranes with a

relatively thick dense top layer with a closed-cell substructure acquired from the delayed liquid-liquid demixing process are principally used for gas and pervaporation applications if the substructure resistance can be kept low. However, as time goes by, most modern UF membranes tend to have a macrovoid-free structure because of the advantages of enhanced mechanical strengths and long-term stability, while gas separation and pervaporation membranes prefer an open-cell substructure to minimize the transport resistance and solvent swelling. Many studies reported that the instantaneous demixing in the inner or outer skin during the hollow fiber spinning may possible to achieve membranes with a dense thin layer if the polymer concentration is sufficient high [107,108]. These findings are consistent with the common perception that usually a high polymer concentration above its critical polymer concentration is needed in order to fabricate effective hollow fiber membranes for gas and pervaporation separations [101].

In fact, phase inversion is much more complex if it involves other solidification process in addition to liquid-liquid demixing. Contradictory explanations can be easily seen in the literature, especially on the formation mechanism of a skin selective layer: (1) nucleation and growth to form a small polymer-rich phase followed by the coarsening of nucleus [116]; (2) spinodal decomposition to form nodules at the interface [117], (3) spinodal composition followed by densification by capillary forces in the air-gap region of the dry-wet process [118], (4) gelation induced via vitrification (glass transition state) [119,120]; or (5) crystallization (for crystallizable polymers) interrupting a liquid-liquid demixing process [121,122]. Despite the differing views in describing the formation of a skin layer in hollow fiber membranes with respect to individual polymer-solvent-non-solvent systems, there remains a general guideline that

the polymer concentration at a contact interface with a strong non-solvent will increase rapidly and generates a sufficient high viscosity that eventually forms the selective skin structure of the asymmetric membranes.

Since the selective skin has different meanings or definitions in terms of interstitial space, d-space, pore size, and porosity for different separation systems, it is our hypothesis that phase inversion mechanisms to form the selective or functional separation skin may be quite different for pore-flow based membranes (i.e., MF, UF, NF) and for solution-diffusion based membranes (i.e., RO, gas separation and most pervaporation). The formation mechanisms of loose RO, some NF and FO membranes may be a combination of these two models. In addition, demixing is a phenomenon but an ambiguous scientific term to describe the phase inversion compared to the definitions of nucleation growth and spinodal decomposition. Future works should focus not only on the mechanism of dense-layer formation for different systems, but also integrate demixing with nucleation growth and spinodal decomposition.

2.5.1.2 Phase inversion of semi-crystalline polymers

Extensive studies on the fundamentals of membrane formation have been devoted to glassy (or amorphous) polymers e.g. cellulose acetate, polyamide, polysulfone, polyimide and others. However, the knowledge learned from glassy polymers may not be fully applicable for describing the membrane formation from semi-crystalline polymers. For glassy polymers, precipitation during the phase inversion is predominantly governed by liquid–liquid demixing whereas for semi-crystalline polymers, both liquid–liquid demixing and solid–liquid demixing accompanying with

crystallization control the precipitation. The phase separation of a semi-crystalline polymer is more complicated since solid-liquid demixing occurs together with the liquid-liquid demixing. There is a clear difference in membrane morphology resulting from liquid-liquid demixing and solid-liquid demixing. Typically, liquid–liquid demixing results in cellular morphology with pores created from the polymer-lean phase, which are surrounded by the polymeric matrix formed by the polymer-rich phase. In contrast, the solid–liquid demixing results in interlinked semi-crystalline particle or globular structure [123-125].

The rate of polymer crystallization has to be considered as well. Although the solid-liquid demixing is thermodynamically favorable over liquid-liquid demixing, this cannot simply imply that the solid-liquid demixing is kinetically preferential over liquid-liquid demixing. Many previous and recent studies on various semi-crystalline polymers i.e., polylactide [122], nylon [126,127], poly(ethylene-co-vinyl alcohol) [128], polyvinylidene fluoride (PVDF) [129-132] have proven that the influence of crystallization on membrane structure is critical when the demixing process is delayed.

2.5.2 The limitations of Flory-Huggins equations for hollow fiber membrane formation

Although the Flory-Huggins theory for polymer solutions derived in 1942 has been widely adopted for the study of phase inversion during the formation of asymmetric flat membranes, Chung [89] pointed out that the original Flory-Huggins thermodynamics may not be fully capable of describing the appropriate Gibbs free energy for the state of as-spun hollow fibers. It is well known that the major difference

between hollow fiber and flat membrane fabrications is that the phase inversion process for hollow fiber formationusually takes place non-isothermally under tension or elongational stress. In other words, the limitations of using Flory-Huggins theory to estimate the Gibbs free energy for the solution states during hollow fiber membrane formation are due to the existence of (1) non-isothermal conditions in the air gap, (2) the additional forces applied upon the as-spun hollow fiber solutions (nascent fibers); namely, the gravity induced by its own weight and stress induced by the take-up unit, and (3) non-Newtonian viscoelastic fluid behavior along the spinning line. Consequently, at least two additional terms have to be included in the equation if the fiber is spun isothermally; one is the work done by the external stresses on the as-spun nascent fiber and the other is an extra entropy change induced by these stresses. The external stresses and viscoelastic behavior may counterbalance their effects on (1) phase instability and separation; and (2) molecular orientation. Therefore, future works on mathematic modeling of phase separation should include external stresses and viscoelastic behavior into consideration. Otherwise, those mathematic models would have very limited applications for real cases.

2.6 Key elements and factors in hollow fiber spinning

Even though there are many commercially available hollow fiber membranes used in various industries, there are mainly three key elements determining the potential and applications of a hollow fiber membrane; namely, (1) the pore size and pore size distribution of the functional separation or selective layer, (2) the chemistry, mechanical and physicochemical properties of the membrane material; and (3) the thickness of the functional separation or selective layer and its substructure morphology. In addition to governing the intrinsic permeability and selectivity for

aqueous, chemical and gas separations under the solution-diffusion mechanism, material chemistry and physics play important roles in determining (1) the spinnability and mechanical strengths, (2) the inherent hydrophilicity / hydrophobicity and fouling tendency for water reuse, desalination and protein separation, (3) bio-compatibility for medical uses, and (4) chemical resistance and stability for applications in harsh environments. Once a potential material with proper strengths and balanced physicochemical properties is chosen for membrane development, membrane scientists must molecularly design the hollow fiber membrane via phase inversion to ensure that it has a desirable pore size, narrow pore size distribution, ultrathin selective layer and open-cell sponge-like substructure morphology. However, the phase inversion process is not a straight forward process; it strongly depends on membrane's material chemistry and physicochemical properties.

Commercially available polymeric hollow fiber membranes are usually spun from a hot spinneret with a short air-gap distance and a moderate high take-up speed. Figure 2.9 illustrates a typical hollow fiber spinning line for the fabrication of polymeric hollow fibers via non-solvent induced phase inversion and Figure 2.10 shows the enlarged schematic nearby the spinneret.

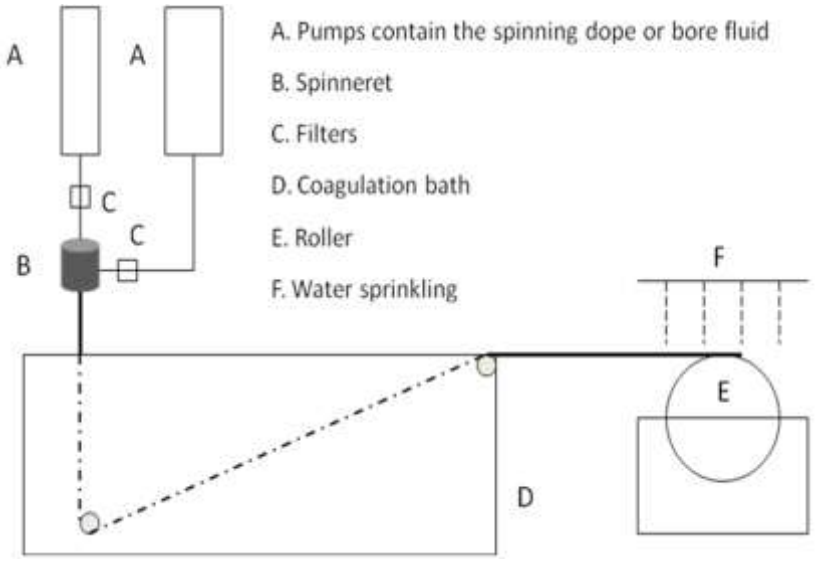

Figure 2.9 Schematic diagram of hollow fiber spinning line

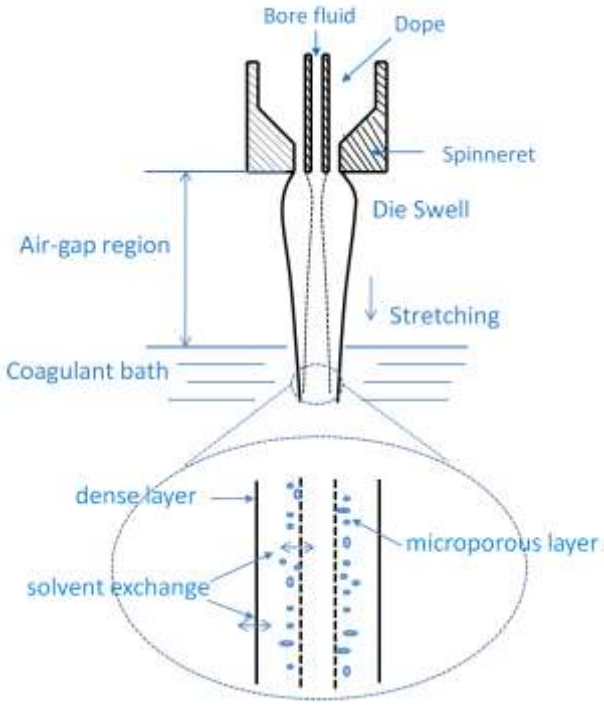

Figure 2.10 Schematic diagram of area nearby the spinneret and the formation of nascent hollow fiber during phase inversion

Once the dope solution is prepared and degassed, the hollow fiber spinning process usually consists of the following steps: (1) metering the spinning dope and bore fluid simultaneously by different precision pumps; (2) conveying the spinning solution

through a spinneret under shear and possibly converging flows; (3) internal coagulation taking place when the bore fluid meets the dope exiting from the spinneret; (4) solvent evaporation from the outer nascent membrane surface in the air-gap region; (5) moisture-induced early phase separation in the outer nascent membrane surface in the air-gap region; (6) stretch by gravity and elongational forces induced by the take-up unit; (7) fully phase inversion or solidification induced by the external coagulation bath; and (8) solvent exchange or additional post-treatments to remove residual solvents or prevent pores from collapse.

The major effects of the key factors that are illustrated in Figure 2.10 on membrane structure development can be described as follows. Solid concentration is an important parameter that plays a crucial role on overall fiber morphology and porosity. Usually, a higher solid concentration (often refers to polymer concentration) is required to form hollow fiber membranes for gas separation or pervaporation than those needed to form hollow fibers for water related separation applications such as ultrafiltration (UF) or microfiltration (MF). This guideline arises from the fact that polymer solutions with a higher solid concentration usually have a higher viscosity and tend to induce chain entanglement, which can effectively reduce micro-defects and porosity in the membrane matrix.

During the precipitation of a nascent hollow fiber, the size of solvent molecules greatly determines the precipitation path and fiber morphology: a smaller molecule facilitates a faster solvent exchange process, or vice versa. The coagulation rate is also strongly dependent on the solubility parameter difference between the dope solution and the coagulant: an increase in solubility parameter difference enhances the coagulation rate.

In general, a thick and relatively porous skin is formed if the coagulation rate is slow (which is referred as delayed demixing), while a thin but relatively dense layer is formed with a fast coagulation (also referred as instantaneous demixing). Since there are two coagulations taking place almost simultaneously in the hollow fiber formation, membrane scientists can alter and engineer the location of the selective layer and its properties and cross-section morphology by properly adjusting solubility parameter differences between the dope solution and the inner /outer coagulants.

Since most of the parameters mentioned above, such as dope viscosity, solubility parameter and coagulation rate are a function of temperature, both the temperatures of the spinneret and the coagulation bath therefore significantly affect fiber morphology. Usually, an increase in dope temperature results in a reduction in dope viscosity while an increase in coagulation bath temperature results an increase in solvent exchange rate and solubility [133-134].

The gravity induced by the fiber's own weight and the external tensional stretching forces by the take-up unit must be considered especially for the spinning process involving a high air-gap distance or a high take-up speed because their effects on the structure of external surface and cross-section of hollow fibers are significant. Taking the polyimide hollow fiber in Figure 2.11(a) as an example, the wet-spun hollow fiber (no air-gap) has a tight external surface morphology, while the dry-jet wet-spun fiber with a long air-gap results in a three-dimensional open-cell structure [89].

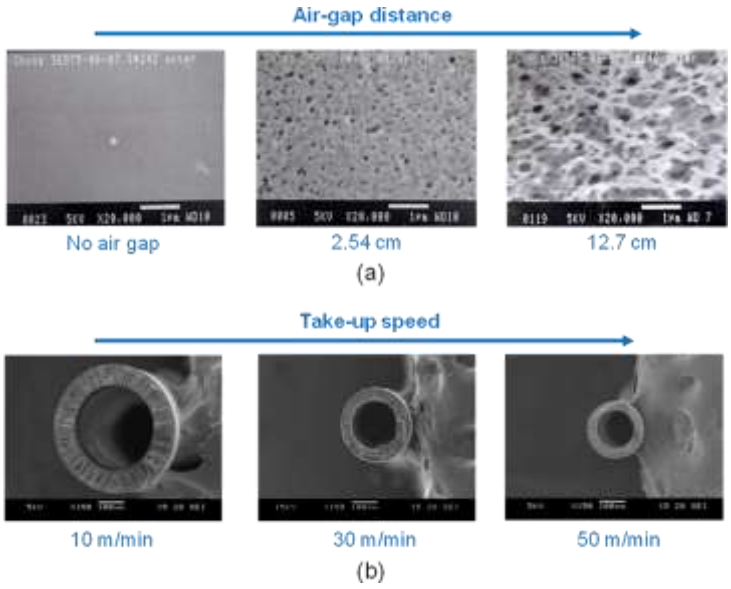

Figure 2.11 The effect of air-gap distance and take-up speed on hollow fiber morphology (a) SEM external surface images of 6FDA/6FDAM polyimide membranes with various air-gap lengths, (b) SEM cross-section images of P84 polyimide membranes with various take-up speeds.

This phenomenon may arise not only from the fact that different precipitation paths taking place during the wet-spinning and dry-jet wet-spinning processes, but also from elongation-induced chain orientation, packing and de-lamination. Figure 2.4(b) demonstrates that the macrovoid formation in a hollow fiber strongly depends on the take-up speed, and sponge-like hollow fibers can be produced in high speed spinning [135]. In addition to altering the state of as-spun solutions, the external elongational stresses probably contribute three effects on the nascent hollow fiber: (1) creating extra phase instability, (2) facilitating phase separation, and (3) inducing orientation and packing. The first two reasons will either shorten the time for a solution moving from the binodal boundary to the spinodal boundary or reduce the distance of precipitation path between binodal and spinodal boundaries, while the last one results in an oriented polymer chain structure. However, if the air-gap distance or take-up speed is too large, defects by tearing chains apart may also be created because of the excessive gravity and elongational stresses.

REFERENCES

[1] J.G. Wijmans, R.W. Baker, The solution-diffusion model: a review, J. Membr. Sci. 107 (1995) 1.

[2] T. Matsuura, Synthetic Membrane and Membrane Separation Process, CRC Press: Boca Raton, New York (1995).

[3] T. Graham, On the law of diffusion of gases, Philos. Mag. 32 (1866) 401.

[4] X. Feng, R.Y.M. Huang, Liquid separation by membrane pervaporation: a review, Ind. Eng. Chem. Res. 36 (1997) 1048.

[5] X. Feng, R.Y.M. Huang, Estimation of activation energy for permeation in pervaporation processes, J. Membr. Sci. 118 (1996) 127.

[6] H. Eustache, G. Histi, Separation of aqueous organic mixtures by pervaporation and analysis by mass-spectrometry or a coupled gas chromatograph-mass spectrometer, J. Membr. Sci. 8 (1980) 105.

[7] T. Okada and T. Matsuura, A new transport model for pervaporation, J. Membr. Sci. 59 (1991) 133.

[8] T. Okada, M. Yoshikawa, T. Matsuura, A study on the pervaporation of ethanol/water mixtures on the basis of pore flow model, J. Membr. Sci. 59 (1991)151.

[9] S. Deng, B. Shiyao, S. Sourirajan, T. Matsuura, A study of the pervaporation of isopropyl alcohol/water mixtures by cellulose acetate membranes, J. Colloid Interface Sci. 136 (1990) 283.

[10] T. Okada, T. Matsuura, Predictability of transport equations for pervaporation on the basis of pore-flow mechanism, J. Membr. Sci. 70 (1992) 163.

[11] R.C. Binning, R.J. Lee, I. Joseph, F. Jennings, E.C. Martin, Separation of liquid

mixtures by permeation, Ind. Eng. Chem. 53 (1961) 45.

[12] A.S. Michaels, R.F. Baddour, H.J. Bixler, C.Y. Choo, Conditioned polyethylene as a permselective membrane, Ind. Eng. Chem. Process Des. Dev. 1 (1962) 14.

[13] V.N. Schrodt, R.F. Sweeny, A. Rose, Division of Industrial and Engineering Chemistry, 144th Meeting, ACS, Los Angeles, March 1963.

[14] R.B. Long, Liquid permeation through plastic films, Ind. Eng. Chem. Fundamentals, 4 (1965) 445.

[15] S. Sourirajan, B. Shiyo, T. Matsuura, Proceeding of the Second International Conference on Pervaporation Processed in Chemical Industry, San Antonio, Texas, March 8-11, R. Bakish Ed. (1987) 9.

[16] S. Sourirajan, T. Matsuura, Reverse Osmosis and Ultrafiltration/Process Principles, Chapter 4, National Research Council of Canada, Ottawa (1985).

[17] M. Yoshikawa, T. Yukoshi, K. Sanui, N. Ogata, Separation of water and ethanol by pervaporation through poly(acrylic acid-co-acrylonitrile) membrane, J. Polym. Sci., Polym. Lett. 22 (1984) 473.

[18] M. Yoshikawa, H. Yokoi, K. Sanui, N. Ogata, Pervaporation of water-ethanol mixture through poly(maleimide-co-acrylonitrile) membrane, J. Polym. Sci. Polym. Lett. 22 (1984) 125.

[19] M. Yoshikawa, H. Yokoi, K. Sanui, N. Ogata, Selective separation of water-alcohol binary mixture through poly(maleimide-co-acrylonitrile) membrane, J. Polym. Sci: Polym. Lett. 22 (1984) 2159.

[20] M. Yoshikawa, T. Yukoshi, K. Sanui, N. Ogata, Selective separation of water ethanol mixture through synthetic-polymer membranes having carboxylic-acid as a functional-group, J. Polym. Sci: Part A: Polym. Chem. 24 (1986) 1585.

[21] M. Yoshikawa, N. Ogata, T. Shimidzu, Polymer membrane as a reaction field. 3. Effect of membrane polarity on selective separation of a water ethanol binary mixture through synthetic-polymer membranes, J. Membr. Sci. 26 (1986) 107.

[22] R.Y.M. Huang, C.K. Yeom, Pervaporation separation of aqueous mixtures using crosslinked poly (vinyl alcohol) (PVA). II. Permeation of ethanol-water mixtures, J. Membr. Sci. 51 (1990) 273.

[23] R.Y.M. Huang, X.S. Feng, Dehydration of isopropanol by pervaporation using aromatic polyetherimide membranes, Sep. Sci. Technol. 28 (1993) 2035.

[24] I. Kazuhiko, M. Kiyohide, Pervaporation of ethanol-water mixture through composite membranes composed of styrene-fluoroalkyl acrylate graft copolymers and crosslinked polydimethylsiloxane membrane, J. Appl. Polym. Sci. 34 (1987) 437.

[25] M.C. Conclaves, G.S.S Marquez, F. Galembeck, Pervaporation and dialysis of water-ethanol solution by using silicone rubber-membrane, Sep. Sci. Technol. 18 (1983) 893.

[26] B. Moermans, W.D. Beuckelaer, I.F.J. Vankelecom, R. Ravishankar, J.A. Martens, P.A. Jacobs, Incorporation of nano-sized zeolites in membranes, Chem. Commun. 24 (2000) 2467.

[27] I.F.J. Vankelecom, D. Depré, S.D. Beukelaer, J.B. Uytterhoeven, Influence of zeolites in PDMS membranes: Pervaporation of water/alcohol mixtures. J. Phys. Chem. 99 (1995) 13193.

[28] L. Li, Z. Xiao, S. Tan, L. Pu, Z. Zhang, Composite PDMS membrane with high flux for the separation of organics from water by pervaporation, J. Membr. Sci. 243 (2004) 177.

[29] Y. Huang, J. Fu, Y. Pan, X. Huang, X. Tang, Pervaporation of ethanol aqueous

solution by polyphosphazene membranes: Effect of pendant groups, Sep. Purif. Technol. 66 (2009) 504.

[30] Y. Mori, T. Inaba, Ethanol production from starch in a pervaporation membrane bioreactor using clostridium thermohydrosulfuricum, Biotechnol. Bioeng. 36 (1990) 849.

[31] E. Shi, W. Huang, Z. Xiao, D. Li, M. Tang, Influence of binding interface between active and support layers in composite PDMS membranes on permeation performance, J. Appl. Polym. Sci. 104 (2007) 2468.

[32] A. Dobrak, A. Figoli, S. Chovau, F. Galiano, S. Simone, I.F.J. Vankelecom, E. Drioli, B. Van der Bruggen, Performance of PDMS membranes in pervaporation: Effect of silicalite fillers and comparison with SBS membranes, J. Colloid Interf. Sci. 346 (2010) 254.

[33] S.L. Schmidt, M.D. Myers, S.S. Kelley, J.D. McMillan, N. Padukone, Evaluation of PTMSP membranes in achieving enhanced ethanol removal from fermentations by pervaporation, Appl. Biochem. Biotech. 63-65 (1997) 469.

[34] J. Guo, G. Zhang, W. Wu, S. Ji, Z. Qin, Z. Liu, Dynamically formed inner skin hollow fiber polydimethylsiloxane/polysulfone composite membrane for alcohol permselective pervaporation, Chem. Eng. J. 158 (2010) 558.

[35] X. Zhan, J. Li, J. Huang, C. Chen, Enhanced pervaporation performance of multi-layer PDMS/PVDF composite membrane for ethanol recovery from aqueous solution, Appl. Biochem. Biotechnol. 160 (2010) 632.

[36] F. Xiangli, W. Wei, Y. Chen, W. Jin, N. Xu, Optimization of preparation conditions for polydimethylsiloxane (PDMS)/ceramic composite pervaporation membranes using response surface methodology, J. Membr. Sci. 311 (2008) 23.

[37] X. Fenjuan, C. Yiwei, J. Wangin, X. Nanping, Polydimethylsiloxane

(PDMS)/ceramic composite membrane with high flux for pervaporation of ethanol-water mixtures, Ind. Eng. Chem. Res. 46 (2007) 2224.

[38] J. Huang and M.M. Meagher, Pervaporative recovery of n-butanol from aqueous solutions and ABE fermentation broth using thin-film silicalite-filled silicone composite membranes, J. Membr. Sci. 195 (2001) 231.

[39] Y. Luo, S. Tan, H. Wang, F. Wu, X. Liu, L. Li, Z. Zhang, PPMS composite membranes for the concentration of organics from aqueous solutions by pervaporation, Chem. Eng. J. 137 (2008) 496.

[40] S. Takegemi, H. Yamada, S. Tusujii, Pervaporation of ethanol/water mixture using novel hydrophobic membrane containing polydimethylsiloxane, J. Membr. Sci. 75 (1992) 93.

[41] C.L. Chang, P.Y. Chang, Performance enhancement of silicone/PVDF composite membranes for pervaporation by reducing cross-linking density of the active silicone layer, Desalination 192 (2006) 241.

[42] T. Kashiwagi, K. Okabe, K. Okita, Separation of ethanol from ethanol/water mixtures by plasma-polymerized membranes from silicone compounds, J. Membr. Sci. 36 (1988) 353.

[43] C.L. Chang, M.S. Chang, Preparation of composite membranes of functionalized silicone polymers and PVDF for pervaporation of ethanol–water mixture, Desalination 148 (2002) 39.

[44] C.L. Chang, M.S. Chang, Preparation of multi-layer silicone/PVDF composite membranes for pervaporation of ethanol aqueous solutions, J. Membr. Sci. 238 (2004) 117.

[45] M. Krea, D. Roizard, N. Moulai-Mostefa, D. Sacco, New copolyimide membranes with high siloxane content designed to remove polar organics from

water by pervaporation, J. Membr. Sci. 241 (2004) 55.

[46] L. Liang, E. Ruckenstein, Pervaporation of ethanol–water mixtures through polydimethylsiloxane–polystyrene interpenetrating polymer network supported membranes, J. Membr. Sci. 114 (1996) 227.

[47] K. Okamoto, A. Butsuen, S. Tsuru, S. Nishioka, K. Tanaka, H. Kita, S. Asakawa, Pervaporation of water–ethanol mixtures through polydimethylsiloxane block-copolymer membranes, Polym. J. 19 (1987) 747.

[48] A.G. Fadeev, S.S. Kelley, I.D. McMillan, Y.A. Selinskaya, V.S. Khotimsky, V.V. Volkov, Effect of yeast fermentation by-products on poly[1-(trimethylsilyl)-1-propyne] pervaporative performance, J. Membr. Sci. 214 (2003) 229.

[49] Y. Nagase, Y. Takamura, K. Matsui, Chemical modification of poly(substitutedacetylene). V. Alkylsilylation of poly(1-trimethylsilyl-1-propyne) and improved liquid separating property at pervaporation, J. Appl. Polym. Sci. 42 (1991) 185.

[50] J.R. Gonzalez-Velasco, J.A. Gonzalez-Marcos, C. Lopez-Dehesa, Pervaporation of ethanol–water mixtures through poly(1-trimethylsilyl-1-propyne) (PTMSP) membranes, Desalination 149 (2002) 61.

[51] S. Claes, P. Vandezande, S. Mullens, R. Leysen, K.D. Sitter, A. Andersson, F.H.J. Maurer, H. Van den Rul, R. Peeters, M.K. Van Bael, High flux composite PTMSPsilica nanohybrid membranes for the pervaporation of ethanol/water mixtures, J. Membr. Sci. 351 (2010) 160.

[52] Y. Nagase, K. Ishihara, K. Matsui, Chemical modification of poly(substitutedacetylene): II. Pervaporation of ethanol/water mixture through poly(1-trimethylsilyl-1-propyne)/poly(dimethylsiloxane) graft copolymer membrane, J. Poly. Sci. Part B: Polym. Phys. 28 (1990) 377.

[53] C.J. Ruud, J. Jia, G.L. Baker, Synthesis and characterization of poly[(1-trimethylsilyl-1-propyne)-co-(1-(4-azidobutyldimethylsilyl)-1-propyne)] copolymers, Macromolecules, 33 (2000) 8184.

[54] J. Jia and G.L. Baker, Cross-linking of poly(1-trimethylsilyl-1-propyne) membranes using bis(aryl azides), J. Appl. Polym. Sci. Part B: Polym. Phys. 36 (1998) 959.

[55] F. Liu, L. Liu, X. Feng, Separation of acetone-butanol-ethanol (ABE) from dilute aqueous solutions by pervaporation, Sep. Purif. Technol. 42 (2005) 273.

[56] P.N. Pintauro, K. Jian, Integral asymmetric fluoropolymer pervaporation membranes and method of making the same, US Patent 5,387,378 (1995).

[57] A. Ghofar, T. Kokugan, The pervaporation mechanism of dilute ethanol solution by hydrophobic porous membranes, Biochem. Eng. J. 18 (2004) 235.

[58] X. Jiang, J. Gu, Y. Shen, S. Wang, X. Tian, New fluorinated siloxane-imide block copolymer membranes for application in organophilic pervaporation, Desalination 265 (2011) 74.

[59] T.C. Bowen, R.D. Noble, J.L. Falconer, Fundamentals and applications of pervaporation through zeolite membranes, J. Membr. Sci. 245 (2004) 1.

[60] T. Sano, H. Yanagishita, Y. Kiyozumi, F. Mizukami, K. Haraya, Separation of ethanol/water mixture by silicalite membrane on pervaporation, J. Membr. Sci. 95 (1994) 221.

[61] T. Ikegami, D. Kitamoto, H. Negishi, K. Haraya, H. Matsuda, Y. Nitanai, N. Koura, T. Sano, H. Yanagishita, Drastic improvement of bioethanol recovery using a pervaporation separation technique employing a silicone rubber-coated silicalite membrane, J. Chem. Tech. Biotechnol. 78 (2003) 1006.

[62] Q. liu, R.D. Noble, J.L. Falconer, H.H. Funke, Organics/water separation by

pervaporation with a zeolite membrane, J. Membr. Sci. 117 (1996) 163.

[63] D. Shen, W. Xiao, J. Yang, N. Chu, J. Lu, D. Yin, J. Wang, Synthesis of silicalite-1 membrane with two silicon source by secondary growth method and its pervaporation performance, Sep. Purif. Technol. 76 (2011) 308.

[64] X. Lin, X. Chen, H. Kita, K. Okamoto, Synthesis of silicalite tubular membranes by in situ crystallization, AIChE J. 49 (2003) 237.

[65] X. Lin, H. Kita, K.I. Okamoto, Silicalite membrane preparation, characterization and separation performance, Ind. Eng. Chem. Res. 40 (2001) 4069.

[66] X. Lin, H. Kita, K.I. Okamoto, A novel method for the synthesis of high performance silicalite membranes, Chem. Comm. 19 (2000) 1889.

[67] T. Ikegami, H. Yanagishita, D. Kitamoto, H. Negishi, K. Haraya, T. Sano, Concentration of fermented ethanol by pervaporation using silicalite membranes coated with silicone rubber, Desalination, 149 (2002) 49.

[68] H. Matsuda, H. Yanagishita, H. Negishi, D. Kitamoto, T. Ikegami, K. Haraya, T. Nakane, Y. Idemoto, N. Koura, T. Sano, Improvement of ethanol selectivity of silicalite membrane in pervaporation by silicone rubber coating, J. Membr. Sci. 210 (2002) 433.

[69] M. Nomura, T. Bin, S.I. Nakao, Selective ethanol extraction from fermentation broth using a silicalite membrane, Sep. Purif. Technol. 27 (2002) 59.

[70] T. Sano, M. Hasegawa, S. Ejiri, Y. Kawakami, H. Yanagishita, Improvement of the pervaporation performance of silicalite membranes by modification with a silane coupling reagent, Microporous Mater. 5 (1995) 179.

[71] S. Li, V.A. Tuan, J.L. Falconer, R.D. Noble, Properties and separation performance of Ge-ZSM-5 membranes, Micropor. Mesopor. Mat. 58 (2003)

137.

[72] T.C. Bowen, H. Kalipcilar, J.L. Falconer, R.D. Noble, Pervaporation of organic/water mixtures through B-ZSM-5 zeolite membranes on monolith supports, J. Membr. Sci. 215 (2003) 235.

[73] V. Sebastian, J. Motuzas, R.W.J. Dirrix, R.A. Terpstra, R. Mallada, A. Julbe, Synthesis of capillary titanosilicalite TS-1 ceramic membranes by MW-assisted hydrothermal heating for pervaporation application, Sep. Purif. Technol. 75 (2010) 249.

[74] H.J.C. te Hennepe, D. Bargeman, M.H.V. Mulder, C.A. Smolders, Zeolite-filled silicone rubber membranes Part 1. Membrane preparation and pervaporation results, J. Membr. Sci. 35 (1987) 39.

[75] S. Yi, Y. Su, Y. Wan, Preparation and characterization of vinyltriethoxysilane (VTES) modified silicalite-1/PDMS hybrid pervaporation performance and its application in ethanol separation from dilute aqueous solution, J. Membr. Sci. 360 (2010) 341.

[76] M.D. Jia, K.V. Peinemann, R.D. Behling, Preparation and characterization of thin-film zeolite-PDMS composite membranes, J. Membr. Sci. 73 (1992) 119.

[77] L.M. Vane, V.V. Namboodiri, T.C. Bowen, Hydrophobic zeolite-silicone rubber mixed matrix membranes for ethanol-water separation: Effect of zeolite and silicone component selection on pervaporation performance, J. Membr. Sci. 308 (2008) 230.

[78] Y. Huang, P. Zhang, J. Fu, Y. Zhou, X. Huang, X. Tang, Pervaporation of ethanol aqueous solution by polydimethylsiloxane/polyphosphazene nanotube nanocomposite membranes, J. Membr. Sci. 339 (2009) 85.

[79] I.F.J. Vankelecom, J.D. Kinderen, B.M. Dewitte, J.B. Uytterhoeven,

Incorporation of hydrophobic porous fillers in PDMS membranes for use in pervaporation, J. Phys. Chem. B 101 (1997) 5182.

[80] P. Peng, B. Shi, Y. Lan, A review of membrane materials for ethanol recovery by pervaporation, Sep. Sci. Technol. 46 (2011) 234.

[81] M. Mulder, Basic principles of membrane technology, Dordrecht: Kluwer Academic Publishers (1996).

[82] H. Strathmann, K. Koch, P. Amar, R.W. Baker, The formation mechanism of asymmetric membranes, Desalination 16 (1975) 179.

[83] J.D. Ferry, Ultrafilter membranes and ultrafiltration, Chem. Rev. 18 (1936) 373.

[84] R.E. Kesting, Synthetic polymeric membranes, New York: McGraw Hill (1985).

[85] M.A. Frommer, D. Lancet, H.K. Lonsdale, H.E. Podall, Reverse osmosis membrane research, New York: Plenum Press (1972).

[86] D.R. Paul and Y.P. Yampol'skii, Polymeric gas separation membranes, Boca Raton: CRC Press (1994).

[87] W.J. Koros, G.K. Fleming, Membrane-based gas separation, J. Membr. Sci. 83 (1993) 1.

[88] C.J. Geankopolis, Membrane separation processes: In transport processes and unit operations, Prentice-Hall, Inc., American (1995) p 745.

[89] L. Yilmaz, A.J. McHugh, Analysis of nonsolvent-solvent-polymer phase diagrams and their relevance to membrane formation modeling, J. Appl. Polym. Sci. 31 (1986) 997.

[90] H. Tompa, Polymer solutions, London: Butterworths Scientific Publications (1956).

[91] H. Strathmann, P. Scheible, R.W. Baker, A rationale for the preparation of Loeb-Sourirajan-type cellulose acetate membranes, J. Appl. Polym. Sci. 15

(1971) 811.

[92] A.S. Michaels, High flow membrane, US Patent 3,615,024 (1971).

[93] O. Olabisi, L.M. Robeson, M.T. Shaw, editors, Polymer-polymer miscibility, New York: Academic Press (1979).

[94] R. Saxena, G.T. Caneba, Studies of spinodal decomposition in a ternary polymer-solvent-nonsolvent system, Polym. Eng. Sci. 42 (2002) 1019.

[95] T.S. Chung, The limitations of using Flory-Huggins equation for the states of solutions during asymmetric hollow fiber formation, J. Membr. Sci. 126 (1997) 19.

[96] G.R. Fernandes, J.C. Pinto, R. Nobrega, Modeling and simulation of the phase-inversion process during membrane formation, J. Appl. Polym. Sci. 82 (2001) 3036.

[97] A.J. Reuvers, J.W.A. van den Berg, C.A. Smolders, Formation of membranes by means of immersion precipitation. Part I. A model to describe mass transfer during immersion precipitation, J. Membr. Sci. 34 (1987) 45.

[98] A.J. Reuvers, C.A. Smolders, Formation of membranes by means of immersion precipitation. Part II. The mechanism of formation of membranes prepared from the system cellulose acetate-acetone-water, J. Membr. Sci. 34 (1987) 67.

[99] C.S. Tsay, A.J. McHugh, Mass transfer modeling of asymmetric membrane formation by phase inversion, J. Polym. Sci. B Polym. Phys. 28 (1990) 1327.

[100] L. Yilmaz, A.J. McHugh, Modeling of asymmetric membrane formation. II. The effects of surface boundary conditions, J. Appl. Polym. Sci. 35 (1988) 1969.

[101] T.S. Chung, S.K. Teoh, X.D. Hu, Formation of ultrathin high-performance polyethersulfone hollow fiber membranes, J. Membr. Sci. 133 (1997) 161.

[102] T.S. Chung, S.K. Teoh, Breaking the limitation of composition change during isothermal mass-transfer processes at the spinodal, J. Membr. Sci. 130 (1997) 141.

[103] S.S. Shojaie, W.B. Krantz, A.R. Greenberg, Dense polymer film and membrane formation via dry-cast process. Part I. Model development, J. Membr. Sci. 94 (1994) 255.

[104] L. Yilmaz, A.J. McHugh, Modeling of asymmetric membrane formation. I. Critique of evaporation models and development of a diffusion equation formalism for the quench period, J. Membr. Sci. 28 (1986) 287.

[105] L. Yilmaz, A.J. McHugh, Modeling of asymmetric membrane formation. II. The effects of surface boundary conditions, J. Appl. Polym. Sci. 35 (1988) 1969.

[106] S.P. Sun, K.Y. Wang, D. Rajarathnam, T.A. Hatton, T.S. Chung, Polyamide-imide nanofiltration hollow fiber membranes with elongation-induced nano-pore evolution, AIChE J. 56 (2010) 1481.

[107] I. Pinnau, Recent advances in the formation of ultrathin polymeric membranes for gas separation, Polym. Adv. Tech. 5 (1994) 733.

[108] J.A. van't Hof, Wet spinning of asymmetric hollow fibre membranes for gas separation, Ph.D. Thesis, University of Twenty, Enschede, The Netherlands, (1988).

[109] C. Cohen, G.B. Tanny, S. Prager, Diffusion-controlled formation of porous structures in ternary polymer systems, J. Polym. Sci. Polym. Phys. Ed. 17 (1979) 477.

[110] A.J. Reuvers, J.W.A van den Berg, C.A. Smolders, Formation of membranes by means of immersion precipitation. Part I. A model to describe mass transfer

during immersion precipitation, J. Membr. Sci. 34 (1987) 45.

[111] A.J. Reuvers, C.A. Smolders, Formation of membranes by means of immersion precipitation. Part II. The mechanism of formation of membranes prepared from the system cellulose acetate-acetone-water, J. Membr. Sci. 34 (1987) 67.

[112] Y.D. Kim, J.Y. Kim, H.K. Lee, S.C. Kim, A new modeling of asymmetric membrane formation in rapid mass transfer system, J. Membr. Sci. 190 (2001) 69.

[113] Y. Termonia, Monte Carlo diffusion model of polymer coagulation, Phys. Rev. Lett. 72 (1994) 3678.

[114] X. He, C. Chen, Z. Jiang, Y. Su, Computer simulation of formation of polymeric ultrafiltration membrane via immersion precipitation, J. Membr. Sci. 371 (2011) 108.

[115] X. Wang, H. Qian, L. Chen, Z. Lu, Z. Li, Dissipative particle dynamics simulation on the polymer membrane formation by immersion precipitation, J. Membr. Sci. 311 (2008) 251.

[116] H. Strathmann, K. Kock, P. Amar, R.W. Baker, The formation mechanism of asymmetric membranes, Desalination 16 1(975) 179.

[117] W.J. Koros, I. Pinnau, Membrane formation for gas separation process. In: D.R. Paul, Y.P. Yampol'skii, editors, Polymeric gas separation membranes, Boca Raton, FL: CRC Press (1994).

[118] I. Pinnau, W.J. Koros, A qualitative skin layer formation mechanism for membranes made by dry/wet phase inversion, J. Polym. Sci. B Polym. Phys. 31 (1993) 419.

[119] A.J. Reuvers, F.W. Altena, C.A. Smolders, Demixing and gelation behavior of ternary cellulose acetate solutions, J. Polym. Sci. B Polym. Phys. 24 (1986) 793.

[120] J.Y. Kim, Y.D. Kim, T. Kanamori, H.K. Lee, K.J. Baik, S.C. Kim, Vitrification phenomena in polysulfone/NMP/water system, J. Appl. Polym. Sci. 71 (1999) 431.

[121] I.M. Wienk, R.M. Boom, M.A.M. Beerlage, A.M.W. Bulte, C.A. Smolders, H. Strathmann, Recent advances in the formation of phase inversion membranes made from amorphous or semi-crystalline polymers, J. Membr. Sci. 113 (1996) 361.

[122] P.V.D Witte, P.J. Dijkstra, J.W.A. van den Berg, J. Feijen, Phase separation processes in polymer solutions in relation to membrane formation, J. Membr. Sci. 117 (1996) 1.

[123] T.H. Young, D.J. Lin, J.J. Gau, W.Y. Chuang, L.P. Cheng, Morphology of crystalline Nylon-6,10 membranes prepared by the immersion-precipitation process: competition between crystallization and liquid-liquid phase separation. Polymer 40 (1999) 5011.

[124] H. Matsuyama, M. Teramoto, R. Nakatani, T. Maki, Membrane formation via phase separation induced by penetration of nonsolvent from vapor phase. II. Membrane morphology, J. Appl. Polym. Sci. 74 (1999) 171.

[125] P. van de Witte, H. Esselbrugge, P.J. Dijkstra, J.W.A. van den Berg, J. Feijen, Phase transitions during membrane formation of polylactides. I. A morphological study of membranes obtained from the system polylactide-chloroform-methanol, J. Membr. Sci. 113 (1996) 223.

[126] A.M.W. Bulte, B. Folkers, M.H.V. Mulder, C.A. Smolders, Membranes of semicrystalline aliphatic polyamide nylon 4,6: Formation by diffusion-induced phase separation, J. Appl. Polym. Sci. 50 (1993) 13.

[127] C.H. Shih, C.C. Gryte, L.P. Cheng, Morphology of membranes formed by the

isothermal precipitation of polyamide solutions from water/formic acid systems, J. Appl. Polym. Sci. 96 (2005) 944.

[128] T.H. Young, Y.H. Huang, L.Y. Chen, Effect of solvent evaporation on the formation of asymmetric and symmetric membranes with crystallizable EVAL polymer, J. Membr. Sci. 164 (2000) 111.

[129] Y. Doi, H. Matsumura, Polyvinylidene fluoride porous membrane and a method for producing the same, US Patent 5,022,990 (1991).

[130] S. Rajabzadeh, T. Maruyama, T. Sotani, H. Matsuyama, Preparation of PVDF hollow fiber membrane from a ternary polymer/solvent/nonsolvent system via thermally induced phase separation (TIPS) method, Sep. Purif. Tech. 63 (2008) 415.

[131] T.H. Young, L.P. Cheng, D.J. Lin, L. Fane, W.Y. Chuang, Mechanisms of PVDF membrane formation by immersion-precipitation in soft (1-octanol) and harsh (water) nonsolvents, Polymer 40 (1999) 5315.

[132] M.G. Buonomenna, P. Macchi, M. Davoli, E. Drioli, Poly(vinylidene fluoride) membranes by phase inversion: the role the casting and coagulation conditions play in their morphology, crystalline structure and properties, Eur. Polym. J. 43 (2007) 1557.

[133] N. Peng, T.S. Chung, J.Y. Lai, The rheology of Torlon® solutions and its role in the formation of ultra-thin defect-free Torlon® hollow fiber membranes for gas separation, J. Membr. Sci. 326 (2009) 608.

[134] T.S. Chung, E.R. Kafchinski, The effects of spinning conditions on asymmetric 6FDA/6FDAM polyimide hollow fibers for air separation, J. Appl. Polym. Sci. 65 (1997) 1555.

[135] N. Peng, T.S. Chung, K.Y. Wang, Macrovoid evolution and critical factors to

form macrovoid-free hollow fiber membranes, J. Membr. Sci. 318 (2008) 363.

CHAPTER THREE

EXPERIMENTAL

3.1 Materials

3.1.1 Polymer

Commercially available poly(vinylidene fluoride) (PVDF), Kynar HSV 900 (specific gravity = 1.77, T_g = -38 °C) was purchased from Arkema Inc. and used as the membrane material in this research study. The polymer was dried in a vacuum oven at 60 °C overnight prior to use. The chemical structure of PVDF is shown in Figure 3.1.

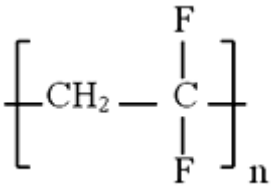

Figure 3.1 Chemical structure of Poly(vinylidene fluoride) (PVDF)

3.1.2 Inorganic filler

Hydrophobic silica, AEROSIL® R 972 (Average particle size =16 nm; specific surface area (BET) = 110±20 m^2 g^{-1}; tapped density ~ 0.50 g l^{-1}, SiO_2 content ≥ 99.8 wt%, spherical shape with free of pores) was provided by Evonik Degussa Chemicals (Germany) and employed as the inorganic filler for fabricating nanocomposite hollow fiber membranes. Its high hydrophobicity (water contact angle ~ 105º [1] is attributed to the surface modification with Dimethyldichlorosilane (DDS). Silica was dried at 60 °C in a vacuum oven overnight before use.

3.1.3 Organic solvents

N-methyl-2-pyrrolidone (NMP), employed as the solvent for polymer dope preparation, was supplied by Merck with analytical grade. Methanol, ethanol, isopropanol (IPA) were purchased from Merck and utilized as non-solvent additives in the polymer dope or as components in the external coagulant for hollow fiber membrane fabrication. Analytical grade ethanol from Tedia and Merck were used to conduct the pervaporation experiment. All the chemicals were used as received.

3.2 Polymer dope preparation

For the polymer dope preparation, a desired amount of dehydrated PVDF powder was dissolved in NMP. The polymer solution was then subsequently stirred at 60 °C for 24 h to ensure complete dissolution of the polymer in NMP. To prepare a dope with non-solvent additives, the homogenous PVDF/NMP solution was allowed to cool to ambient temperature before adding the non-solvent. The cooling is to prevent the evaporation of used non-solvents, i.e. methanol and ethanol [2]. The PVDF/NMP/non-solvent mixture was stirred at room temperature for 24 h. All the dope solutions were degassed for 24 h and placed into the ISCO syringe pump overnight before spinning.

For the heterogeneous PVDF/NMP dope containing silica, a slight modification on the dope preparation was made as follows; the desired amount of silica nanoparticles was firstly dispersed into NMP and the mixture was then stirred continuously for 24 h under an agitation of 400-500 rpm in order to break down particle aggregations and to

enhance the dispersion of the particles [3]. After that, PVDF was slowly added into the dispersed nano-silica/NMP mixture and stirred for 24 h. All the dope solutions were degassed in an ultrasonic bath for several hours and then in the ISCO syringe pumps for another 12 h prior to fiber spinning.

The polymer dope compositions vary depending on the properties of the dopes and will be described in each chapter individually.

3.3 Single-layer and dual-layer hollow fiber membrane fabrications

The dope solution spinning and non-solvent induced phase inversion processes were adopted in this study to fabricate hollow fiber membranes with either pristine PVDF or the PVDF/silica composite membrane material. Figure 3.2 illustrates the schematic diagram of lab-scale hollow fiber spinning line applied in this research and the enlarged picture of extruded nascent fiber at the outlet of the spinneret. The real pilot scale spinning line was supplied by the Motianmo Technology Ltd. Company from Tianjin, China. The detailed experimental set-up and procedures have been documented elsewhere [4,5]

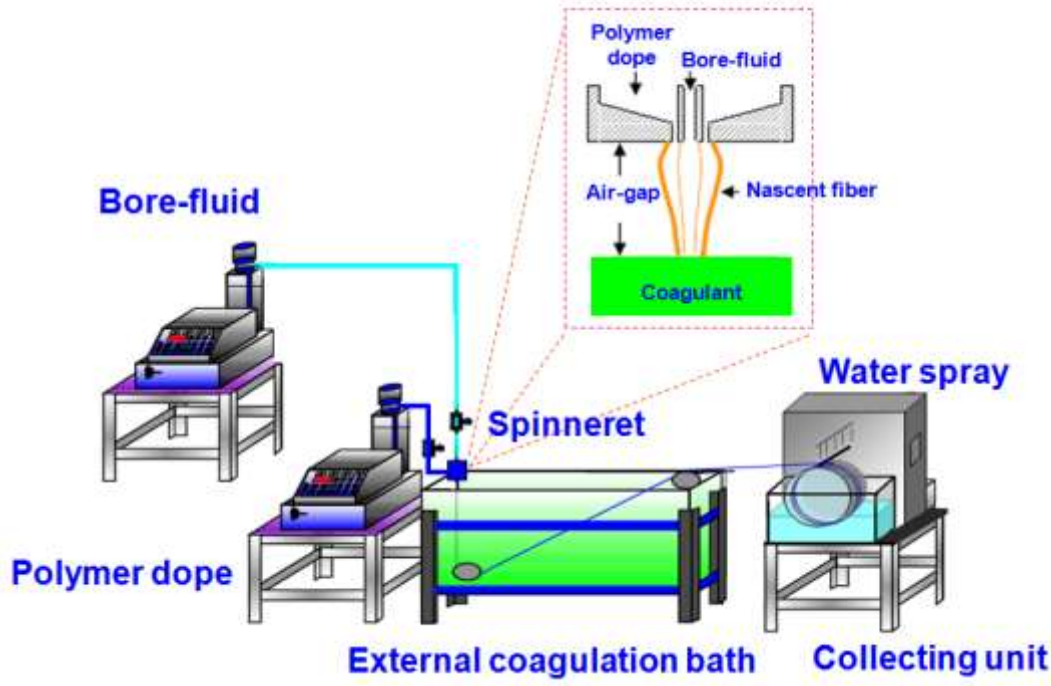

Figure 3.2 Schematic diagram of lab-scale hollow fiber spinning line and a magnification of extruded nascent fiber at the outlet of the spinneret

By applying pressures from the ISCO syringe pump, the dope solutions were extruded through the channels of the spinneret and exited at the orifice to form the nascent hollow fibers, while a bore fluid was extruded at the same time from the center channel of the spinneret to form the bore or the lumen. Right before entering the chamber of the spinneret, the fluids went through a package of 15 μm sintered metal filters (Swagelok®). The fibers in this stage are called nascent hollow fibers.

After extruding out of the spinneret, the nascent polymeric fibers first experience the air-gap region before entering the coagulation bath comprising of water or alcohol/water mixtures. The fibers were then phase separated and solidified by the diffusive removal of the solvent and/or addition of non-solvent in the coagulant bath (Figure 3.2). This process is known as dry-jet wet spinning. Lastly, the as-spun fibers were then cut into segments around 1-m in length, and immersed in water for at least 3

days to ensure thorough removal of residual solvent and additives. Subsequently, the hollow fibers were dried in a Freeze-dryer (Thermo Electron Co. Modulyo D-230) with vacuum for 24 h before further characterization and study. The details on spinning parameters and conditions employed for different fibers will be individually elaborated in the following chapters.

3.4 Characterization of rheological properties of spinning dope solutions

The rheological behavior of dope solutions was characterized by an advanced rheological extension system (ARES) (Rheometrics, USA) and a capillary rheometer (SMART RHEO 2000 CEAST, Italy). The shear viscosity of PVDF solutions at low shear rates was measured using ARES with a 25 mm cone-and-plate geometry at 25 °C. The steady-state controlled shear rate mode was altered in the range of 1-100 s^{-1}. The power law model was applied to fit the rheological data and to express the relationship between shear stress τ (N m^{-2}) and shear rate γ (s^{-1}) as follows:

$$\tau = K\gamma^n \tag{3.1}$$

where K is the power law coefficient constant and n is the power law index.

The shear viscosity of the solutions at high shear rates (i.e. 100-10000 s^{-1}) was studied by Capillary Rheometer (SMART RHEO 2000 CEAST, Italy). Two capillary stubs with a diameter of 1 mm and respective length/diameter (L/D) ratios of 10 and 30 were used. The elongation viscosity was calculated based on the method proposed by

Cogswell which utilizes the relationship between the pressure drop and flow rate of a polymer melt or solution flowing through a thin capillary die [6].

3.5 Molecular simulation

Materials Studio 4.3 from Accelrys Inc. was applied for molecular dynamics simulations. Repeat units of poly(vinylidene fluoride) (PVDF) were constructed using the Build function. For constructing the polymer, 100 repeat units were used. Isotactic polymer configuration with random torsion and head-to-tail orientation was assumed for simulating the polymer chains. Energy minimization of the polymer chain was performed prior to amorphous cell construction.

To simulate the polymer and mixed solvent systems, the amorphous cell module was utilized for construction using compass forcefield. In order to investigate the effect of mixed solvent environment on the polymer conformation, one polymer chain was used for construction with the desired amount of NMP and non-solvent based on mole fraction ratio. The amorphous cell was subjected to fine convergence with maximum iterations of 10,000 before proceeding with molecular dynamics simulation by the Discover module. An equilibrium stage temperature of 298 K and equilibrium time of 5.0 ps were used. Isothermal-isobaric (NPT) ensemble was used for the simulation. A total of 100,000 steps with a step time of 1.0 fs and a dynamics time of 100 ps were employed. The radius of gyration of the PVDF chain and the solubility parameter of each system were determined using the Analysis function of the amorphous cell module.

3.6 Membrane characterization

3.6.1 Scanning Electron Microscope (SEM)

The cross-section, inner and outer surface morphologies of hollow fiber membranes were observed using scanning electron microscopy (SEM JEOL JSM-5600LV) and field emission scanning electron microscopy (FESEM JEOL JSM-6700LV). The samples for the cross-section characterization were immersed and fractured in liquid nitrogen. After adhering all the specimens on the stub using a double-side conductive carbon tape, the specimens were further dried under vacuum overnight. All samples were coated with platinum using a sputtering coater (JEOL LFC-1300) before characterization.

3.6.2 Energy Dispersion of X-ray (EDX)

X-ray energy dispersive spectrometry (EDX Oxford INCA) equipped with Scanning Electron Microscope (SEM JEOL JSM-5600LV) was used to analyze their surface elemental content. The mapping mode was applied to detect the existence of certain elements as well as to examine the elemental distribution profile; the area-scan and line-scan spectrums were performed on the composite hollow fiber's outer surface and cross-section, respectively.

3.6.3 X-ray Diffraction (XRD)

X-ray diffraction (XRD) characterization (Bruker D8 series, GADDS (General Area Detector Diffraction System) was carried out to investigate the crystallinity of hollow

fiber membranes. A small piece of the fiber was adhered onto the sample holder using a double-side adhesive tape. Ni-filtered Cu Kα with a radiation wavelength λ =1.54 Å was used at 40 kV and 40 mA.

The crystallinity of hollow fiber membranes was determined by a peak deconvolution method [7]. The diffraction peaks at 2θ = 18.2 and 20.4° were decomposed into amorphous and crystalline regions by a curve fitting technique of TOPAS analysis software. The crystallinity is defined as the area of crystalline phases divided by the total area of crystalline phases and amorphous phases as follows:

$$\text{The crystallinity (\%)} = \frac{A_c}{A_c + A_a} x100 \qquad (3.2)$$

where A_c is the area of the crystalline phase and A_a is the area of the amorphous phase.

3.6.4 Atomic Force Microscope (AFM)

The membrane surface topology was examined using a Nanoscope III atomic forace microscope (AFM) equipped with 1533D scanner (Digital Instruments, California, USA). For each sample, an area of 10 μm x 10 μm was scanned in a tapping mode. Various roughness parameters such as the mean roughness (R_a), the root mean square (R_{ms}) roughness, and the maximum roughness (R_{max}) were determined using the Nanoscope software.

3.6.5 Mechanical Property Test

The mechanical properties (i.e. extension at break, tensile strain and Young's modulus) of the hollow fiber membranes were measured using an Instron 5542 tensile testing instrument at room temperature. Each sample was clamped at the both ends with an initial gauge length of 25 mm. A testing speed of 50 mm min^{-1} was used. At least five fiber samples were tested for each spinning condition.

3.6.6 Contact angle measurement

The contact angle of the PVDF hollow fiber membranes at 25 °C was measured using a KSV Sigma 701 Tensiometer (KSV Instruments Ltd., Finland) [8]. The fiber was brought into vertical contact with a reservoir of deionized water and the advancing contact angle was calculated with the aid of computer software.

3.7 Membrane pore size, pore size distribution and porosity determinations

3.7.1 Gas permeation method

The mean pore size and effective surface porosity of PVDF hollow fiber membranes were characterized using the gas permeation method. The experimental apparatus and procedures for hollow fiber design have been described elsewhere [9]. Each module consists of two fibers with an effective length of about 5 cm. Pure nitrogen was used as the test gas. The gas permeation rate was measured using a soap-bubble flow meter at various transmembrane pressure differences from 0 to 103.42 kPa at room temperature. The gas permeance, *G*, was determined using the following equation:

$$G = \frac{F}{A_a \Delta P} = \frac{F}{n\pi D l \Delta P} \tag{3.3}$$

where G is the gas permeance (mol m^{-2} Pa^{-1} s^{-1}), F is the total gas permeation rate (mol s^{-1}), A_a is the effective membrane area (m^2), n is the number of fibers in one testing module, D is the outer diameter of the hollow fiber (cm), l is the effective length of the modules (cm), and ΔP is the gas pressure difference across the membrane (Pa).

In a porous asymmetric hollow fiber membrane, the gas transport mechanism can be considered as the combination of Knudsen flow and Poiseuille flow [10-12]. By assuming cylindrical pores in the selective skin layer, the total gas permeance can be calculated as follows:

$$G = \frac{2}{3}\left(\frac{8RT}{\pi M}\right)^{1/2} \frac{1}{RT}\frac{r\varepsilon_s}{\delta} + \frac{P_m}{8\eta_g RT}\frac{r^2\varepsilon_s}{\delta} \tag{3.4}$$

or rewritten as the following:

$$G = I_o + S_o P_m \tag{3.5}$$

where r is the mean pore size of the membrane (m), ε_s is the surface porosity, δ is the effective pore length (m), η_g is the viscosity of gas (Pa s), R is the gas constant (8.314 m^3 Pa mol^{-1} K^{-1}), P_m is the mean pressure (Pa) which is equal to $(P_u+P_d)/2$, P_u is upstream gas pressure (Pa), P_d is downstream gas pressure (Pa), M is molecular weight of the gas (kg mol^{-1}) and T is the absolute temperature (K).

The mean pore size can be calculated from the intercept (I_o) and slope (S_o) as follows by plotting G against mean pressure according to the equation (3.5) as follows:

$$r = \frac{16}{3}\left(\frac{S_o}{I_o}\right)\left(\frac{8RT}{\pi M}\right)^{1/2}\eta_g \qquad (3.6)$$

Similarly, the effective surface porosity (ε_s/δ) can be obtained with the aid of the slope (S_o):

$$\frac{\varepsilon_s}{\delta} = \frac{8\eta_g RTS_o}{r^2} \qquad (3.7)$$

There is a clear distinction between the term "effective surface porosity", which is defined as ε_s/δ in the equation (3.7), and the term "surface porosity, ε_s". The former has a unit of "m^{-1}" while the latter has no unit.

3.7.2 Capillary Flow Porometry analysis

The maximum pore size (pore size at the bubble point), mean pore size and pore size distribution were determined using a 1500 AE Capillary Flow Porometer (Porous Materials Inc., USA) [13]. A wetting liquid, Galwick with a surface tension of 15.9 dynes cm^{-1}, was used to fill the membrane pores. The hollow fibers were soaked in the liquid for at least 24 h to ensure that all pores were completely filled. The wetted fibers were then mounted on the sample chamber and the nitrogen gas was allowed to flow

into the chamber gradually. The bubble point was defined as the point where the increased nitrogen pressure overcame the capillary force of the fluid within the largest pore. After exceeding the bubble point, the pressure was increased continuously and the nitrogen permeation rate was measured until no more wetting liquid remained in the pores. The nitrogen pressures and permeation flow rates through the dry sample were also recorded. The mean pore size was calculated at the flow pressure corresponding to the intersection of the wet flow and one-half of the dry flow curves [14]. In other words, it is defined as the pore size obtained at which fifty percent of the flow is contributed by larger pores and the rest of the flow belongs to the smaller pores.

3.7.3 Overall porosity measurement

The membrane porosity is determined by impregnating hollow fibers with kerosene for two days. The impregnated fibers were blotted between tissue papers to remove any excess kerosene in the lumen side and on the outer surface of the fibers. For each spinning condition, three membrane samples were employed to estimate the porosity. The mass of the fibers before and after immersing in kerosene was obtained using a digital microbalance. The porosity of the hollow fiber membrane (ε) is defined as the pore volume divided by the total volume of the hollow fiber as follows [15]:

$$\varepsilon = \frac{(w_w - w_d)/\rho_w}{(w_w - w_d)/\rho_w + (w_d/\rho_p)})x100\% \quad (3.8)$$

where w_w is the mass of the kerosene-impregnated membrane (g), w_d is the mass of the dry membrane (g), ρ_w is the kerosene density (0.82 g cm^{-3}) and ρ_p is the density of

PVDF (1.77 g cm^{-3}). In the determination of the membrane porosity, it was assumed that all the pores in the hollow fibers were completely filled with kerosene.

3.8 Pervaporation study

3.8.1 Membrane module fabrication

The hollow fibers were fabricated into modules for pervaporation tests. Two pieces of fibers were assembled into the module holder which consists of two Swagelok stainless steel male run tees connected by a PFA tube. Both ends of the module were sealed with a slow cure epoxy resin (KS Bond EP231, Bondtec). The modules were mounted onto the pervaporation set-up with the shell side in contact with the feed solution and the effective length of the fiber of approximately 15 cm.

3.8.2 Pervaporation set-up for hollow fiber membranes

Pervaporation experiments with the hollow fiber membranes were conducted using a laboratory scale pervaporation unit and the details of the apparatus have been described elsewhere [16]. Figure 3.3 shows the schematic layout of the pervaporation apparatus for the hollow fiber membranes.

In this study, at least three modules with same fabrication conditions were examined for each pervaporation condition. Two liters of an ethanol/water mixture with a recirculation rate of 30 l h^{-1} was used as the feed solution. The operating temperature was controlled at designed temperature throughout the experiment. The upstream

pressure was at atmospheric pressure (101.325 kPa) while the downstream pressure was controlled by a vacuum pump (Edward RV5, USA).

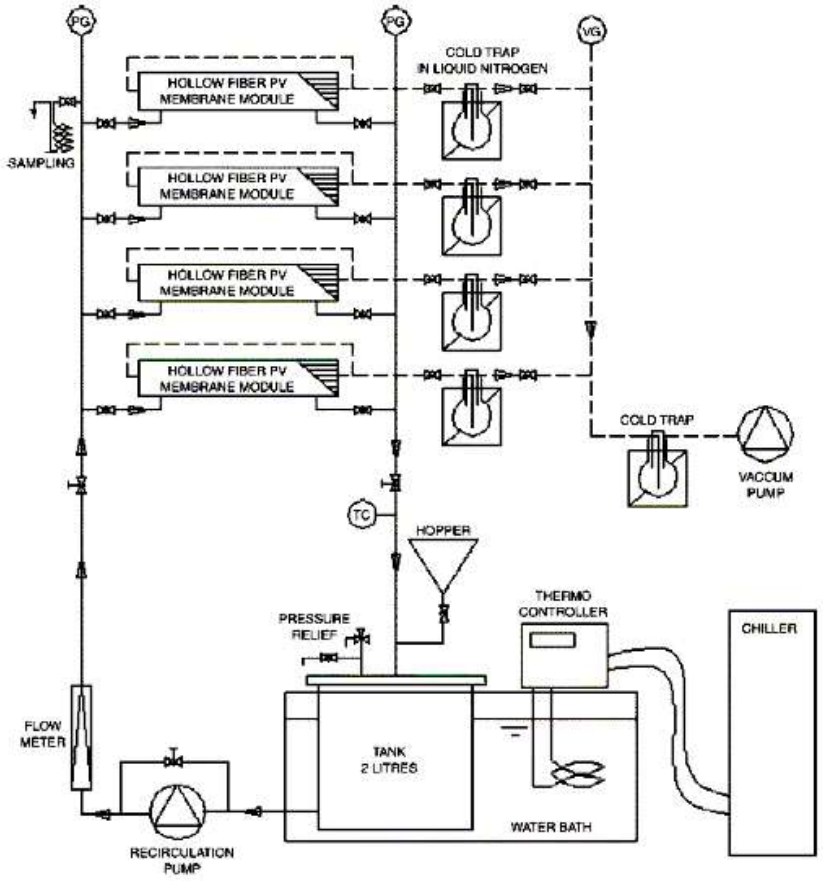

Figure 3.3 Schematic layout of the pervaporation apparatus for the hollow fiber membranes

The total permeate (downstream) pressure was regulated by introducing bleed air via an adjustable valve and the pressure was measured using Digital Vacuum Regulator (Vacuubrand, USA), both are located between the cold trap and the vacuum pump. In our experiments, the downstream pressure is varied from low to high pressure. There was no liquid observed in the permeate side as long as the downstream pressure was kept below the saturated vapor pressure. When the downstream pressure was increased to a certain value (close to and above saturated vapor pressure), the presence of

condensed liquid in the permeate line was clearly observed. To avoid the misleading results from this phenomenon due to the fact that some accumulated permeates could possibly not reach the cold trap, the condensed permeates were collected for analyses by applying a full vacuum (with turning off the valve near the module) for a very short time (< 1 min) to suck all condensed permeate from the tube to the cold trap. Since the time applied for this practice is short, the effect of membrane swelling under untreated vacuum can be neglected. The system was stabilized for 1 h before the collection of samples to account for system dynamics. According to the observation in this study, 1 h was sufficient for both the permeate flux and composition to reach a steady state.

The permeate vapor was condensed in a cold trap which was immersed in liquid nitrogen. The sample was collected at 1 h interval for 4 h and weighed by a Mettler Toledo balance. The sample compositions were analyzed with three parallel injections by a Hewlett-Packard GC 6890 with a HP-INNOWAX column (packed with cross-linked polyethylene glycol) and a TCD detector. The feed content varied less than 1 wt% during the entire experiment and can be therefore considered as a constant because of the large quantity of feed solution in comparison with the permeate sample. The total flux, W_{total} (g m^{-2} h^{-1}) and separation factor, $\alpha_{ethanol/water}$ were calculated.

REFERENCES

[1] L. Forny, K. Saleh, R. Denoyel, I. Pezron, Contact angle assessment of hydrophobic silica nanoparticles related to the mechanisms of dry water formation, Langmuir 26 (2010) 2333.

[2] D. Wang, K. Li, W.K. Teo, Porous PVDF asymmetric hollow fiber membranes prepared with the use of small molecular additives, J. Membr. Sci. 178 (2000) 13.

[3] L.Y. Jiang, T.S. Chung, S. Kulprathipanja, Fabrication of mixed matrix hollow fibers with intimate polymer-zeolite interface for gas separation, AIChE J. 52 (2006) 2898.

[4] T.S. Chung, Z.L. Xu,W.H. Lin, Fundamental understanding of the effect of air-gap distance on the fabrication of hollow fiber membranes, J. Appl. Polym. Sci. 72 (1999) 379.

[5] K.Y. Wang, D.F. Li, T.S. Chung, S.B. Chen, The observation of elongation dependent macrovoid evolution in single- and dual-layer asymmetric hollow fiber membranes, Chem. Eng. Sci. 59 (2004) 4657.

[6] F.N. Cogswell, Converging flow of polymer melts in extrusion dies, Polym. Eng. Sci. 12 (1972) 64.

[7] D.J. Lin, H.H. Chang, T.C. Chen, Y.C. Lee, L.P. Cheng, Formation of porous poly(vinylidene fluoride) membranes with symmetric or asymmetric morphology by immersion precipitation in the water/TEP/PVDF system, Eur. Polym. J. 42 (2006) 1581.

[8] M.M. Teoh, T.S. Chung, Membrane distillation with hydrophobic macrovoid-free PVDF-PTFE hollow fiber membranes, Sep. Purif. Technol. 66 (2009) 229.

[9] T.S. Chung, S.K. Teoh, X. Hu, Formation of ultrathin high-performance

polyethersulfone hollow-fiber membranes, J. Membr. Sci. 133 (1997) 161.

[10] J.M.S. Henis, M.K. Tripodi, Composite hollow fiber membranes for gas separation: the resistance model approach, J. Membr. Sci. 8 (1981) 233.

[11] K. Li, J.F. Kong, D. Wang, W.K. Teo, Tailor-made asymmetric PVDF hollow fiber for soluble gas removal, AIChE J. 45 (1999)1211.

[12] D. Wang, K. Li, W.K. Teo, Preparation and characterization of polyvinylidene fluoride (PVDF) hollow fiber membranes, J. Membr. Sci. 163 (1999) 211.

[13] K.Y. Wang, S.W. Foo, T.S. Chung, Mixed matrix PVDF hollow fiber membranes with nanoscale pores for desalination through direct contact membrane distillation, Ind. Eng. Chem. Res. 48 (2009) 4474.

[14] A. Jena, K. Gupta, Flow Porometry: What can Flow porometry do for us? Porous Materials, Inc., Ithaca, NY, USA (2002).

[15] X. Li, T. Wang, Z. Lu, C. Xiao, Morphology changes of polyvinylidene fluoride membrane under different phase separation mechanisms, J. Membr. Sci. 320 (2008) 477.

[16] L.Y. Jiang, T.S. Chung, R. Rajagopalan, Dehydration of alcohols by pervaporation through polyimide Matrimid? asymmetric hollow fibers with various modifications Chem. Eng. Sci. 63 (2008) 204.

CHAPTER FOUR

MOLECULAR ELUCIDATION OF MORPHOLOGY AND MECHANICAL PROPERTIES OF PVDF HOLLOW FIBER MEMBRANES FROM ASPECTS OF PHASE INVERSION, CRYSTALLIZATION AND RHEOLOGY

4.1 Introduction

Poly(vinylidene fluoride) (PVDF) has gained considerable attention as one of promising polymeric membrane materials due to its outstanding chemical and physical properties. The key advantages of PVDF include its highly hydrophobic nature and excellent chemical resistance against corrosive chemicals such as acids and halogens [1]. Typically, PVDF comprises of crystalline phases along with amorphous and/or rubbery regions which respectively provides the thermal stability and flexibility of the membranes [2]. Compared to other hydrophobic materials such as polytetrafluoroethylene (PTFE) and polypropylene (PP), PVDF possesses better processability since it is soluble in common organic solvents. PTFE and PP membranes are usually fabricated by thermal and stretching methods and the resultant membranes are relatively symmetric [3-4]. In contrast, PVDF hollow fibers with favorable asymmetric structure can be fabricated via the dry-wet phase-inversion process. With these superior properties, PVDF has been considered for utilization in various membrane-based separations e.g. micro/nano/ultra-filtration [5-6], membrane distillation [7-9], pervaporation [10] and membrane gas absorption [11-12].

To date, there have been extensive studies that report the preparation, morphology and performance of flat sheet PVDF membranes [13-23]. Conversely, there are relatively

less studies devoted to the fabrication and characterization of PVDF asymmetric hollow fiber membranes [24-29]. For large scale applications, the hollow fiber configuration is generally preferred over the flat sheet. It should be noted that the formation of flat-sheet membranes cannot be simply extended for hollow fiber membranes due to the differences involved in the fabrication process. One essential difference is the dope formulation which affects the dope viscosity. Generally, a polymer dope with viscosity of a few hundred centipoises ($x10^{-1}$ Pa s) is sufficient for casting a flat-sheet membrane while the minimum dope viscosity required for spinning hollow fibers is an order of magnitude higher i.e. a few thousand centipoises ($x10^{0}$ Pa s) [30]. Moreover, the phase inversion for hollow fiber membranes is considerably more complicated than for flat-sheet membranes. Neglecting the moisture-induced phase inversion involved in the membrane fabrication, phase inversion starts from the top surface of a cast film after immersing in a coagulation bath. Conversely, for hollow fiber membranes produced via the dry-jet wet-spinning process, phase inversion starts immediately at the lumen side upon extrusion from a spinneret by the internal coagulant. Subsequently, the contact of the nascent fibers with the external coagulant similarly induces phase separation at the outer surface of the hollow fibers. In view of the importance of PVDF hollow fibers for industrial applications, it is certainly worthwhile to study the fundamentals of membrane formation and to bridge membrane morphology with chain coils, dope rheology and phase inversion mechanisms.

Generally, macrovoids in hollow fiber membranes are undesirable because they are the roots of weak mechanical points possibly leading to membrane failure under high pressures or continuously vibration and backwashing operations. Therefore, hollow fiber membranes with favorable macrovoid-free structure have received great

academic and industrial interest. The development of hollow fiber membranes with macrovoid-free structure has been thoroughly investigated for many membrane materials. Nevertheless, the majority of studies is focused on glassy polymers e.g. cellulose acetate, polyamide, polyimide [31-33] and the concept may not be fully applicable to semi-crystalline polymers e.g. PVDF. For glassy polymers, precipitation in the phase inversion is governed dominantly by liquid-liquid demixing whereas for semi-crystalline polymers, both liquid-liquid demixing and solid-liquid demixing accompanying with crystallization control the precipitation. Typically, liquid-liquid demixing results in cellular morphology with pores created from the polymer-lean phase, which are surrounded by the polymeric matrix formed by the polymer-rich phase. In contrast, solid-liquid demixing results in interlinked semi-crystalline particle structure [34-36]. With this difference, is it possible to produce macrovoid-free PVDF hollow fiber membranes? In a recent work by Bonyadi et al. [37], a new approach involving the use of solvent-dope solution co-extrusion was proposed for fabricating highly porous and macrovoid-free PVDF hollow fiber membranes. However, one must also answer if the macrovoid-free morphology made from the solid-liquid phase inversion process is a preferred structure for PVDF hollow fiber membranes with good mechanical properties. Since the development of macrovoid-free PVDF hollow fibers has yet been well explored, it would be interesting to investigate the relationship among membrane formation, membrane morphology, and their mechanical properties.

The rheological behavior of polymer dope solutions under shear and elongation flows during hollow fiber spinning is another parameter that influences membrane morphology. Chung et al. [38-43] found that the shear rate within the spinneret plays an important role on hollow fiber membrane morphology. Ren et al. [29] studied the

influences of PVDF dope rheology on membrane morphology. They found that increasing the shear rate in the spinning process resulted in a larger mean pore size and a wider pore size distribution. In addition to the shear rate experienced in hollow fiber spinning, the elongation rate induced by the gravity of the nascent fibers in the air gap is inevitable [44]. Therefore, the elongation viscosity of polymer solution with respect to the elongation rate must be considered. It has been revealed in some studies that the elongation viscosity of polymer solutions affects membrane morphology and mechanical properties to a larger extent compared to shear viscosity. Ekiner and Vassilatos [45] studied the rheology behavior of polyaramide dope solutions for hollow fiber spinning and observed an elongation hardening phenomenon i.e. elongation viscosity hardens with increasing elongation rates. Polymer dopes with elongation hardening behavior may produce hollow fibers with denser morphology, lesser macrovoids and better mechanical properties. Peng et al. [46] observed similar extension thinning and thickening phenomena for different grades of Torlon® poly(amide-imide), which is dependent on the degree of hydrogen bonding. These studies prove the importance and influence of dope rheology on the formation of macrovoid-free hollow fibers.

Therefore, the objectives of this study are to conduct fundamental investigation on the science of fabricating poly(vinylidene fluoride) (PVDF) hollow fiber membranes with/without macrovoids and to elucidate the relationship among membrane morphology, crystallinity, mechanical properties, non-solvent additives, and dope rheology in the phase inversion process. The effects of polymer concentration, external coagulation bath and non-solvent additive on membrane morphology will be systematically investigated. To our best knowledge, the fundamental rheological

behavior of PVDF dope solution for hollow fiber membrane fabrication has not been reported in the literature. Similarly, no reports are available on the correlations between membrane morphology, polymer dope rheology and mechanical properties of PVDF hollow fiber membranes. It is believed that this pioneering work will significantly enhance the understanding of PVDF hollow fiber formation and improve the PVDF membrane production in the industry.

4.2 Experimental

4.2.1 Spinning dope composition and preparation

Figure 4.1 shows the shear viscosity of PVDF/NMP solutions as a function of polymer concentration at a shear rate 10 s^{-1}. The two linear portions of the viscosity curve are extrapolated and the polymer concentration corresponding to the intersection point of the two lines is defined as the critical concentration.

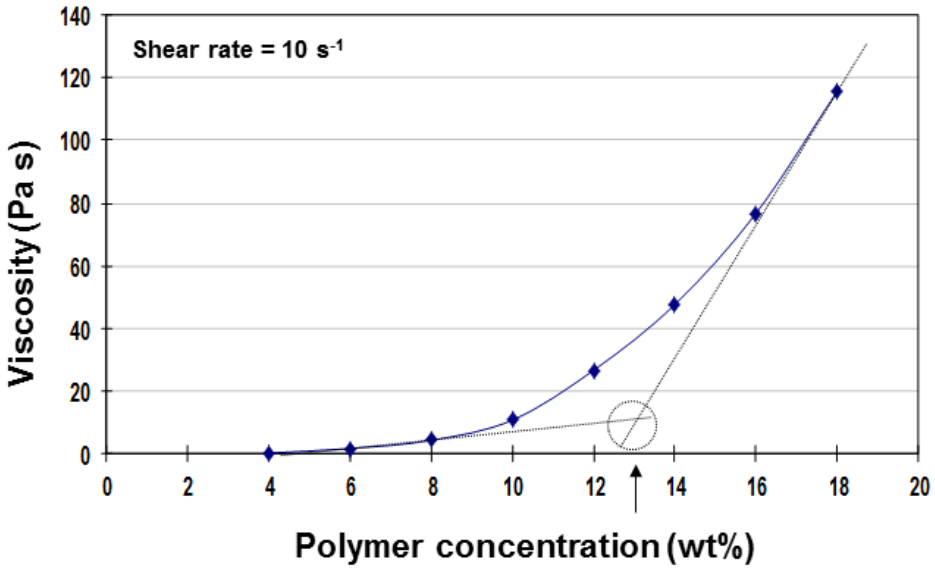

Figure 4.1 The critical concentration of PVDF/NMP dope solution.

Based on Figure 4.1, the critical polymer concentration is about 13 wt%. It has been hypothesized by Chung et al. that at or above the critical concentration, the polymer exhibits significant chain entanglement which aids the formation of dense skin with minimal defects on the hollow fibers [47]. A 13 wt% polymer solution was chosen as the first trial but defects were clearly visible on the outer skin of the as-spun hollow fiber membranes. Therefore, in order to obtain hollow fibers with dense skin morphology, a dope solution of 15 wt% PVDF HSV 900/NMP (above critical concentration) was employed for further investigation.

4.2.2 Hollow fiber spinning condition

The hollow fibers were fabricated by a dry-jet wet-spinning process which involves the extrusion of a polymer dope through a spinneret. In this study, the dope and bore fluid flow rates were kept constant during spinning. Bore fluid with a high NMP concentration was employed to reduce the inner layer resistance. Depending on the free fall velocity of each spinning condition, the corresponding take-up velocity in the range of 2-4.5 m/min was used. Table 4.1 lists the sample identification code, dope compositions and spinning conditions.

Table 4.1 Spinning conditions for PVDF hollow fiber membranes

Spinning code	Spinning Condition[a]			
	Dope solution composition (wt%)	Bore-fluid composition (wt%)	External coagulant composition (wt%)	
The effect of polymer dope concentrations				
P-15	PVDF/NMP 15/85			
P-17	PVDF/NMP 17/83	NMP/water 90/10	Tap water	
P-19	PVDF/NMP 19/81			
The effect of external coagulations				
M-10			Water/methanol	90/10
M-20			Water/methanol	80/20
M-50			Water/methanol	50/50
E-10			Water/ethanol	90/10
E-20	PVDF/NMP 15/85	NMP/water 90/10	Water/ethanol	80/20
E-50			Water/ethanol	50/50
I-10			Water/isopropanol	90/10
I-20			Water/isopropanol	80/20
I-50			Water/isopropanol	50/50
The effect of non-solvent additives				
W-2-add	PVDF/NMP/water 15/83/2			
M-10-add	PVDF/NMP/methanol 15/75/10	NMP/water 90/10	Tap water	
E-10-add	PVDF/NMP/ethanol 15/75/10			

[a] Bore fluid flow rate: 0.6 $cm^3 min^{-1}$; dope flow rate: 2.0 $cm^3 min^{-1}$; air gap distance: 1 cm; spinneret dimensions (OD/ID): 1.2/0.8 mm; coagulant bath and spinning temperature: 25 °C; relative humidity: 65%.

4.2.3 Determination of shear and elongation rates experienced during hollow fiber spinning

The shear rate profile of each polymer solution in the spinneret was estimated by the computational fluid dynamics (CFD) model reported by Qin [40] and Cao et al [44]. This CFD model accounts for the flow of a fluid which obeys the power law within a concentric annulus. The The shear rate at the outermost of the spinneret outlet was selected for consideration. Table 4.2 lists the empirical power law equations and Figure 4.2 shows the shear rate profiles for various polymer dope solutions used in this study. From the results, the shear rates experienced in the spinning process fall in the range of 1700-2000 s^{-1}.

Table 4.2 Power law equations for the polymer dope solutions

Spinning code	Power-law equation at 25 °C
The effect of polymer concentrations	
P-15	$\tau = 44.71 \lvert\gamma\rvert^{0.657}$
P-17	$\tau = 89.31 \lvert\gamma\rvert^{0.621}$
P-19	$\tau = 141.74 \lvert\gamma\rvert^{0.577}$
The effect of non-solvent additives	
W-2-add	$\tau = 50.64 \lvert\gamma\rvert^{0.633}$
M-10-add	$\tau = 140.78 \lvert\gamma\rvert^{0.463}$
E-10-add	$\tau = 83.28 \lvert\gamma\rvert^{0.548}$

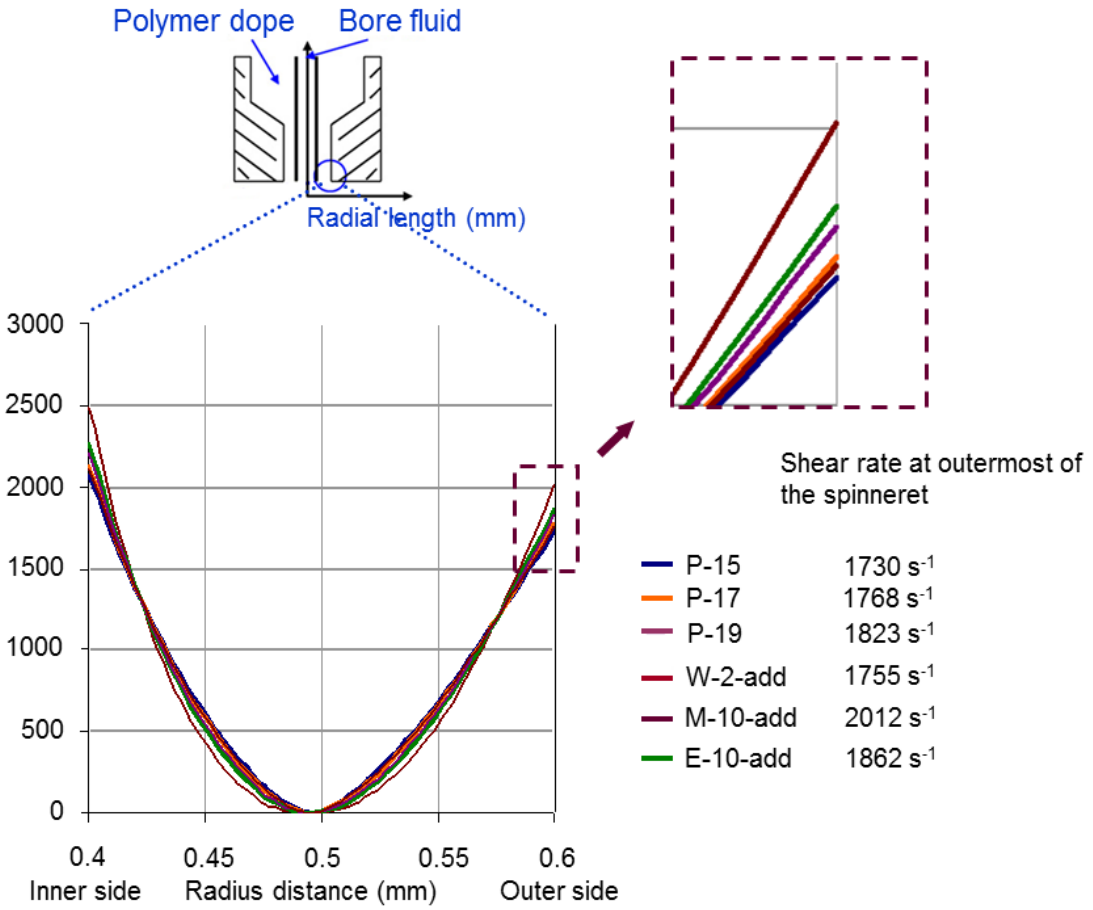

Figure 4.2 Shear rate profiles of different polymer dope solutions in the spinneret.

In the dry-jet wet spinning process, the elongation rate is dependent on the location of the nascent hollow fiber along the spinning line. Typically, the elongation rate is induced by the gravity of the nascent fiber and the elongation stretch by the take-up unit. It is revealed that the elongation rate experienced at the air- gap region plays an important role on determining membrane morphology and separation performance, compared to other locations in the spinning process. This is due to the fact at the air-gap region the nascent fiber has not been yet fully solidified and the induced elongation rate can significantly affect the phase inversion mechanism and corresponding membrane structure. On the other hand, after passing through the external coagulation bath where a rapid phase inversion is taken place resulting in relatively fixed final fiber's structure. As a consequence, the elongation rate experienced along the external coagulation can be treated as a constant and most of the times its influences on the membrane formation and separation properties can be neglected.

In this study, all the fibers were spun under free-falling conditions. Hence, the elongation rate is induced by the gravity of the nascent fibers in the air gap (1 cm) region. The elongation rate is dependent on spinning parameters i.e. dope flow rate and take-up velocity. A definition of the elongation rate ($\dot{\varepsilon}$) is represented by equation (4.1) [48] and can be rewritten in different formats by equations (4.2)-(4.4) as follows.

$$In\frac{L}{L_0} = \dot{\varepsilon} t \tag{4.1}$$

$$In\frac{L/t}{L_0/t} = \dot{\varepsilon} t \tag{4.2}$$

$$In\frac{V_L}{V_{die\ swell}} = \dot{\varepsilon}\frac{L}{V_L} \qquad (V_L = \frac{L}{t} \ and \ V_0 = V_{die\ swell}) \tag{4.3}$$

$$\dot{\varepsilon} = \left(In\frac{V_L}{V_{die\ swell}} \right)\frac{V_L}{L} \tag{4.4}$$

where L_0 (cm) is the initial length, L (cm) is the air gap length at some later time t (s) and V_0 (cm s^{-1}) is the initial velocity. V_L (cm s^{-1}) is the velocity of the nascent hollow fiber (which approximates to the free-fall velocity in this study), $V_{die\ swell}$ (cm s^{-1}) is the velocity of the nascent hollow fiber at the die swell region. $V_{die\ swell}$ is calculated by equation (4.5).

$$V_{die\ swell} = \frac{Q_{dope}}{A_{die\ swell}} = \frac{Q_{dope}}{\frac{\pi}{4}\left(o.d.^2 - i.d.^2\right)_{die\ swell}} \tag{4.5}$$

where Q_{dope} (cm^3 s^{-1}) is the dope flow rate and $A_{die\ swell}$ (cm^2) is the cross-section area of the nascent hollow fiber calculated by the outer diameter (*o.d.*) and inner diameter (*i.d.*) at the die swell. The *o.d.* of the fiber is estimated from the die swell images taken by a digital camera (Canon EOS 350) with a MP-E65 mm high magnification lens. The fiber *i.d.* cannot be observed clearly from the images and hence, the *i.d.* is assumed to be equal to the inner diameter of the spinneret. Figure 4.3 shows the die swell image of the 15 wt% PVDF/NMP solution and the calculated outer diameter is 1.447 mm. Based on equations (4.1) to (4.5), the calculated elongation rate is about 6.5 s^{-1}. The same approach is used to determine the elongation rates for the other polymer dopes and their values are in the range of 6- 10 s^{-1}.

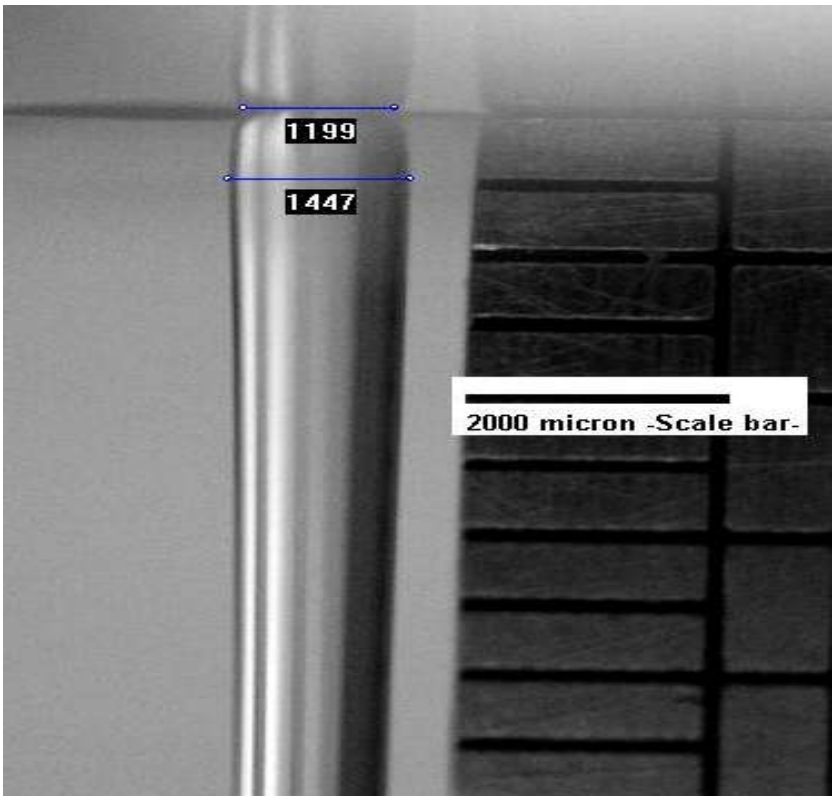

Figure 4.3 Image of the die swell phenomenon for the 15 wt% PVDF/NMP dope solution.

4.3 Results and discussion

4.3.1 Phase diagrams of PVDF/NMP/non-solvent system

Thermodynamic analysis reveals the effect of interaction potentials on the mixing and demixing of blended components, which are often demonstrated by phase diagrams. Figure 4.4 shows the ternary phase diagrams of PVDF/NMP/non-solvent systems at 25 °C, which are constructed based on the cloud-point measurements. It should be noted that the cloud points are represented by the gelation points resulting from both liquid-liquid and solid-liquid (accompanying with crystallization) demixing of the polymer solution [49]. As shown in Figure 4.4, the gelation boundary for the PVDF/NMP/water system is closer to the polymer-solvent axis as compared to the other PVDF/NMP/non-solvent systems. In other words, only a small amount of water is needed to disturb the

solution system equilibrium and induce the polymer precipitation. The results suggest that the thermodynamic stability of the PVDF/NMP/non-solvent systems follows the sequence: water < methanol < ethanol < IPA. Therefore, water is a strong non-solvent while alcohols are weak non-solvents for the PVDF/NMP system.

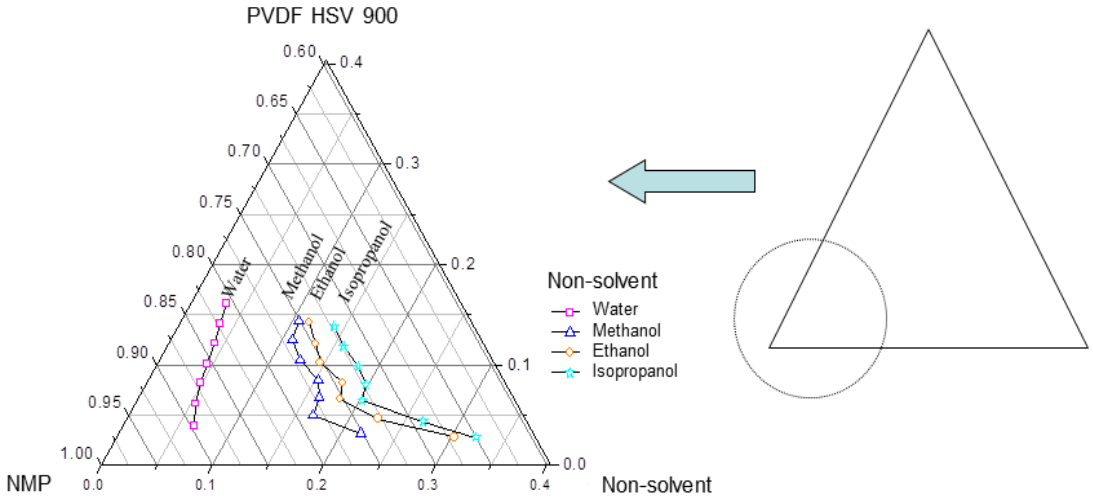

Figure 4.4 Phase diagram of ternary PVDF/NMP/non-solvent systems at 25 °C.

4.3.2 Membrane morphology

4.3.2.1 The effect of polymer dope concentrations

Figure 4.5 shows the cross-section and outer surface morphologies of PVDF hollow fiber membranes spun from various PVDF/NMP dope concentrations and coagulated in water. With reference to Figure 4.5, regardless of the polymer concentration used, finger-like macrovoids are present in the bulk of the hollow fiber membranes, underneath a dense skin surface. At 15 wt% PVDF/NMP (Figure 4.5a), the intrusion of water is very severe and in fact, it occurs across the entire membrane thickness as shown by the size of finger-like macrovoids. As the polymer concentration increases from 17 wt% to 19 wt% (Figure 4.5b-c), water intrusion is suppressed to a certain

extent and the finger-like macrovoid structure near the lumen side of the hollow fiber becomes sponge-like. This is attributed to the greater viscoelasticity of a more concentrated polymer solution which prohibits the immediate convective type solvent exchange in an instantaneous liquid-liquid phase separation process [50]. However, for the PVDF/NMP system which we are considering here, further increase in the polymer concentration beyond 19 wt% is not feasible. In fact, for a polymer concentration of 21 wt%, gelation occurs and complete degassing before spinning is not possible. Hence, increasing the polymer concentration can reduce but does not completely eliminate the macrovoid formation.

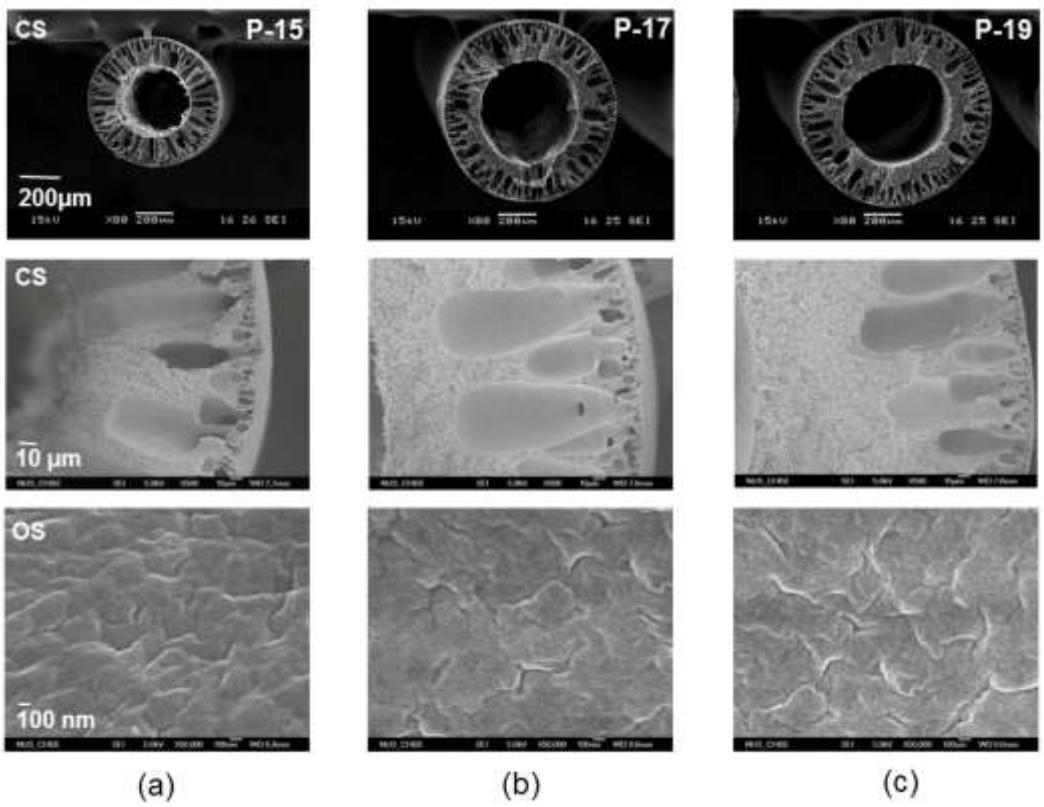

Figure 4.5 Cross-section and outer surface morphologies of hollow fiber membranes spun from PVDF/NMP with different polymer concentrations (a) P-15 (b) P-17 and (c) P-19 (CS = cross-section, OS= outer surface).

4.3.2.2 The effect of external coagulations

It is well known that the external coagulant plays an important role in membrane formation by phase inversion processes. The effect of external coagulants on the morphology of the PVDF hollow fiber membranes are demonstrated in Figures 4.6 and 4.7.

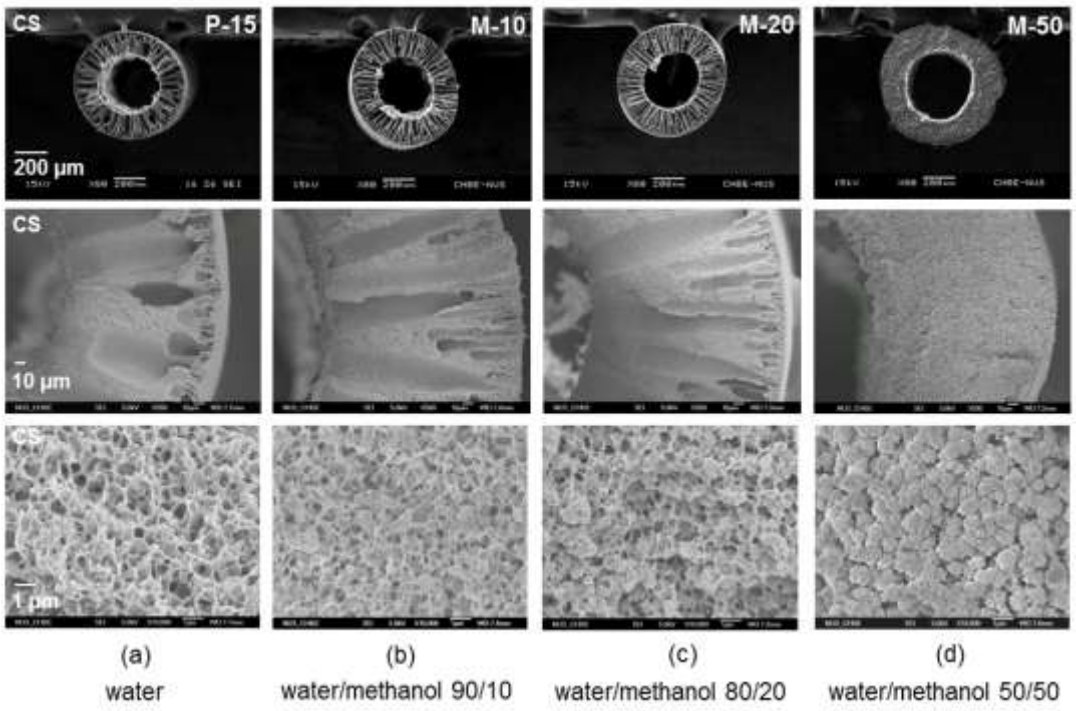

Figure 4.6 The cross-section morphology of hollow fiber membranes spun from 15 wt% PVDF/NMP with various compositions of water/methanol external coagulant (a) P-15 (b) M-10 (c) M-20 and (d) M-50.

Figure 4.6 depicts the cross-section morphology of hollow fibers spun from 15 wt% PVDF/NMP solution using 0, 10, 20 and 50 wt% methanol/water as the coagulants. When pure water is used as the coagulant, the membrane structure comprises mainly finger-like macrovoids and a small portion with cellular morphology. This morphological feature indicates that the precipitation is dominated by instantaneous

liquid-liquid demixing. With 10 and 20 wt% methanol/water mixtures as the coagulants, the size of finger-like macrovoids is reduced compared to that using pure water as the coagulant. When the methanol content is further increased to 50 wt%, a macrovoid-free structure is obtained. By observing the cross section morphology under high magnifications (Figure 4.6, third row), it is apparent that the membrane structure is gradually transformed from an interconnected-cellular type (P-15) to an interconnected-globule transition type (M-10, M-20) and finally a globule type structure (M-50). It has been reported that the globule-type structure consists of spherical globules made of semi-crystalline PVDF [19,23,36]. Figure 4.7 illustrates the membrane morphology with different compositions of ethanol/water as the external coagulants, respectively. The change in morphology here is similar to the observation when methanol/water is used as the coagulant i.e. increasing alcohol content eliminates macrovoids.

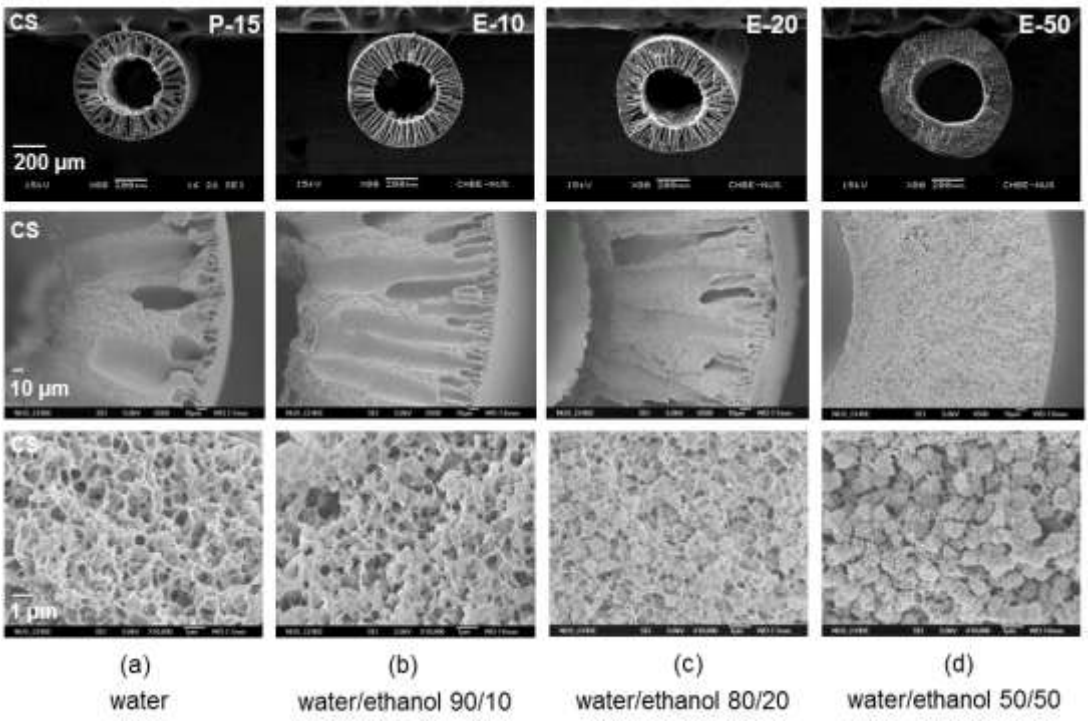

Figure 4.7 The cross-section morphology of hollow fiber membranes spun from 15 wt% PVDF/NMP with various compositions of water/ethanol external coagulant (a) P-15 (b) E-10 (c) E-20 and (d) E-50.

The difference in membrane morphology is resulted from the use of different coagulants that result in delayed demixing accompanying with crystallization during the phase inversion. When pure water is used as the coagulant, the demixing process occurs rapidly and there is insufficient time to induce crystallization. Hence, the liquid-liquid demixing controls the phase separation. However, by introducing methanol or ethanol in the coagulant, the liquid-liquid demixing process is delayed, and the accompanying crystallization process occurs (often referred as solid-liquid demixing). With increasing alcohol content in the coagulant, the phase separation process is eventually dominated by the solid-liquid demixing.

Figure 4.8 shows the XRD spectra of hollow fiber membranes spun from polymer dopes with different methanol/water content. The results reveal that the degree of crystallinity increases with methanol content. This result is consistent with the change in membrane morphology resulting from different extent of crystallization during the demixing process. For all cases, there is a strong peak at $2\theta = 20.4°$ which is attributed to the diffraction of the (200) and (110) planes. Weaker diffraction peaks at 36.2° and 41.0° are also present. This XRD pattern corresponds to the β crystalline phase of PVDF [51]. Previous studies have reported that the formation of PVDF β-crystalline structure from solutions is favored at temperatures below 70 °C [52].

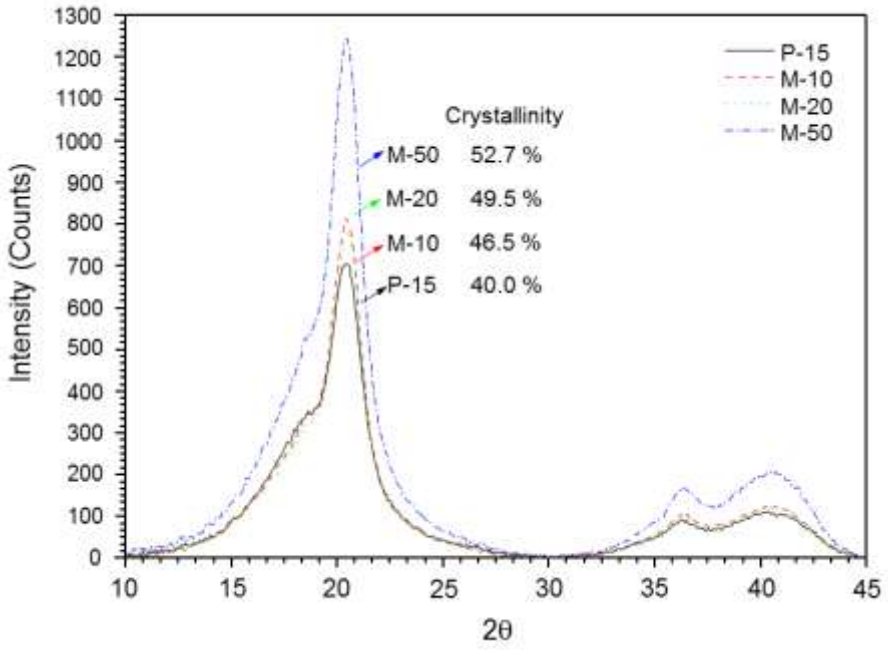

Figure 4.8 XRD patterns of the hollow fiber membranes spun with various compositions of water/methanol external coagulants.

Another significant finding is that the size of spherulitic globules is slightly increased when the coagulant component is changed from methanol to ethanol and IPA as shown in Figure 4.9. Table 4.3 summarizes their sizes of spherulitic globules which were estimated from the SEM image analysis with an assumption that the globules are uniform spherical shapes. For each spinning condition, the cross-section SEM image at high magnification (10,000x) was employed and the average particle size was determined from at least fifteen spots at different locations in the image as illustrated in Figure 4.10. From the results, the size of the spherulitic globules is dependent on the time allowed for crystallization i.e. a longer time favors the formation of a larger globule. The addition of alcohol in the coagulant intensifies the delayed demixing which allows a greater extent of crystallization. The enhancement in delayed demixing by the non-solvents follows the sequence IPA> ethanol > methanol > water, which is in agreement with the phase diagram (Figure 4.4).

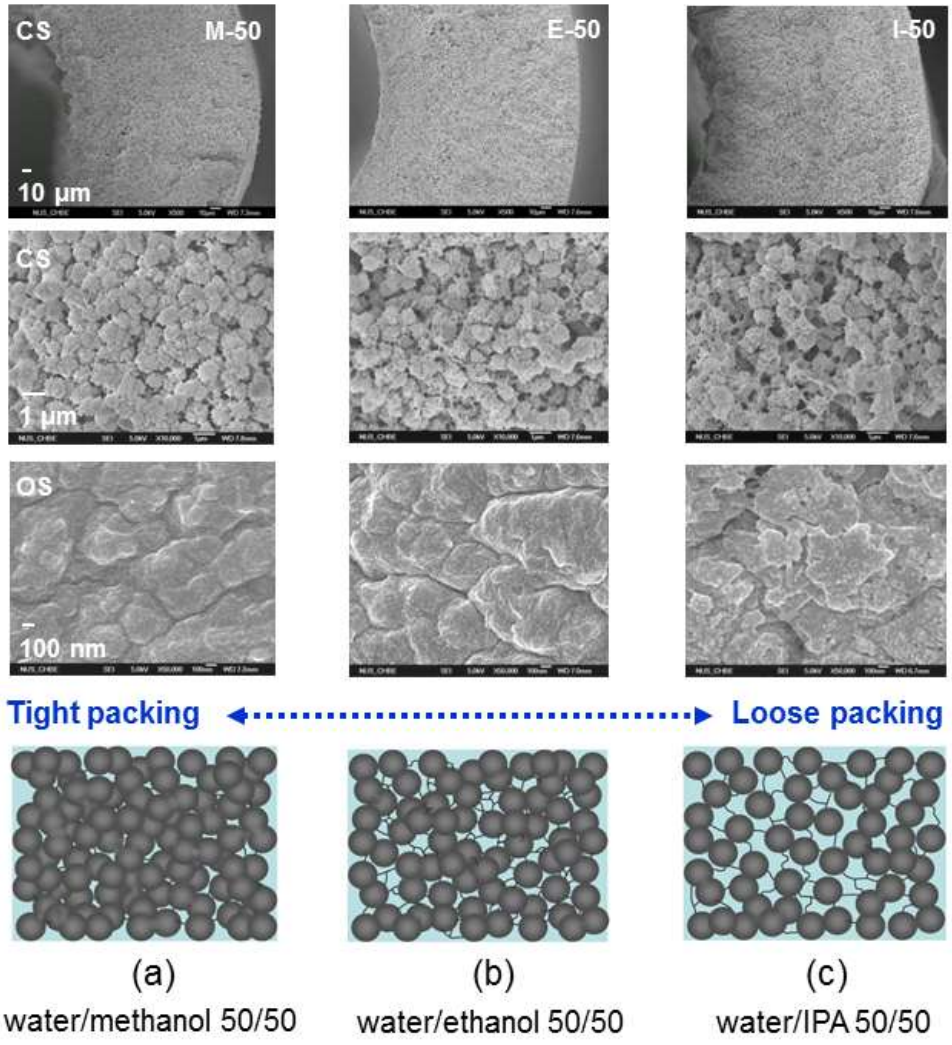

Figure 4.9 Comparison of the morphology and schematic model for macrovoid-free PVDF hollow fiber membranes (a) M-50, (b) E-50 and (c) I-50.

Table 4.3 Spherulitic particle size in PVDF hollow fiber membranes

Spinning code	Mean spherulitic particle size (μm)
The effect of external coagulants	
M-50	0.947± 0.090
E-50	1.017± 0.105
I-50	1.137± 0.116
The effect of non-solvent additives	
M-add-10	0.399± 0.044
E-add-10	0.679± 0.195

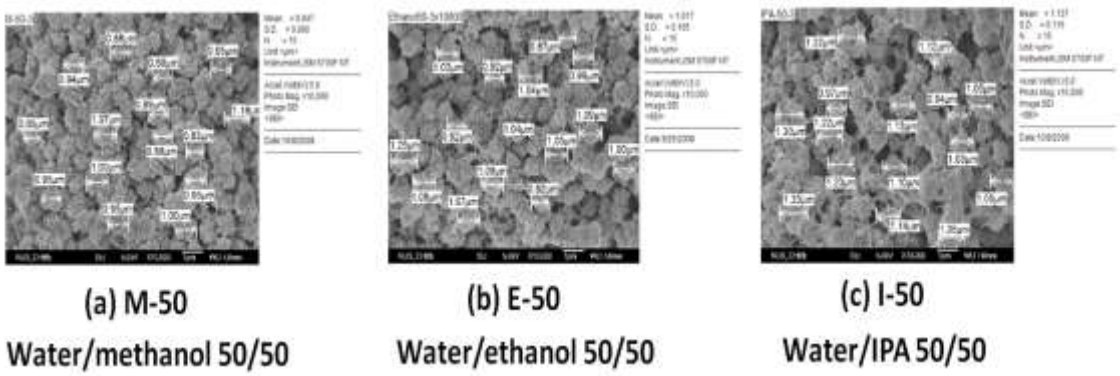

Figure 4.10 The determination of a mean spherulitic particle size from SEM image analysis of PVDF hollow fiber membranes (a) M-50, (b) E-50 and (c) I-50.

Table 4.4 summarizes the solubility parameters for the non-solvents and solvents used in this work. The difference in solubility parameters between PVDF and the non-solvents is of the order (PVDF-water) > (PVDF-methanol) > (PVDF-ethanol) > (PVDF-IPA). A larger difference in solubility parameter usually implies a faster precipitation rate i.e. a shorter time for crystallization to occur. From the kinetics point of view, it is possible to correlate the exchange diffusion process of solvent/non-solvent with the demixing process. Generally, a higher diffusion of a non-solvent in a solvent results in a faster precipitation. Consistent with experiments, the diffusion coefficients of non-solvents (i.e. water and alcohols) with respect to the solvent (i.e. NMP) follow the order: water > methanol > ethanol > IPA as summarized in Table 4.5.

Table 4.4 Solubility parameters of polymers, solvent and non-solvents [53]

Chemicals	Solubility parameters ($MPa^{1/2}$)			
	δ_d	δ_p	δ_h	δ_t
Water	15.60	16.00	42.30	47.80
Methanol	15.10	12.30	22.30	29.60
Ethanol	15.80	8.80	19.40	26.50
Isopropanol (IPA)	15.80	6.10	16.40	23.50
N-Methyl-2-pyrrolidone	18.00	12.30	7.21	22.90
Poly(vinylidene fluoride)	-	-	-	14.15[a]
	-	-	-	17.75[b]
	17.20	12.50	9.20	23.20[c]

δ_d, dispersive parameter, δ_p, polar parameter, δ_h, hydrogen bonding parameter, δ_t, total solubility parameter

[a] simulated using material studio (synthia) based on the Van Krevelen equation
[b] simulated using material studio (synthia) based on the Fedors equation
[c] from reference [54] based on solubility test

Table 4.5 Properties of solvent and non-solvents [55,56]

	Water	Methanol	Ethanol	Isopropanol (IPA)	NMP
Molecular volume[a] ($Å^3$)	30	67	97	127	160
Boiling point (°C)	100	64.5	78	82	202
Vapor pressure (mmHg at 20 °C)	17.5	96	43.89	33	-
Specific gravity	1.00	0.792	0.789	0.790	1.026
Viscosity (10^{-3} Pa s)	1.00	0.60	1.22	2.40	1.65
$D^{\circ}_{NS\ in\ NMP}$[b] (10^{-6} cm^2 s^{-1})	18.0	12.6	10.5	9.6	-

[a] The volume per molecule is calculated by the molecular weight divided by the density and Avogadro number
[b] The diffusion coefficient of non-solvent in almost pure NMP

Zuo et al. [57] investigated the precipitation rate in terms of the delayed time for a 14 wt% PVDF/dimethylacetamide (DMAc) solution in various alcohol coagulation baths by a light transmission technique. They found that the delayed time increases gradually

when the coagulation bath changed from methanol to ethanol and IPA. Their findings are in agreement with our observation.

Therefore, from the thermodynamics and kinetics aspects, it can be concluded that water induces the most rapid precipitation among the non-solvents employed in this study while the alcohols effectively delay the demixing process and result in the formation of spherulitic globules in the as-spun PVDF hollow fiber membranes.

4.3.2.3 The effect of non-solvent additives in spinning solutions

The effects of adding water, methanol and ethanol in spinning dopes on membrane morphology were examined and presented in Figure 4.11. Three dope solutions containing 15 wt% PVDF were prepared. The concentration of the non-solvent additives in each dope solution is 2 wt% water, 10 wt% methanol and 10 wt% ethanol, respectively. The required amount of water additive is much lower than methanol and ethanol. Based on the ternary phase diagram (Figure 4.4), the desired amounts of water and methanol were chosen close to their gelation lines while the amount of ethanol was selected to be the same as methanol for the purpose of comparison. When water is used as the additive, the membrane structure comprises finger-like macrovoids with a dense skin surface (Figure 4.11a). This observed morphology is similar to the previous case (Figure 4.7a) where a binary PVDF/NMP mixture (i.e. no additive) is used as the dope and water as the external coagulant. However, compared Figure 4.11a with Figure 4.7a, slightly more macrovoids are present when water is introduced as a dope additive. In a study by Wang et al. [26], it has been found that water as an additive in the PVDF/DMAc system may promote the macrovoids formation due to the weak interactions between water and PVDF. In addition, the compatibility among the water

additive, water external coagulant, and/or NMP/water bore fluid possibly enhances instantaneous demixing. The addition of water is, therefore, believed to have suppressed the polymer interaction and favored liquid-liquid demixing.

The membrane structure is significantly different when methanol and ethanol are used as the additives. In both cases, the resulting membranes comprise packed spherulitic globule structures in the inner substrate and small voids underneath the dense outer skin as shown in Figures 4.11b and c.

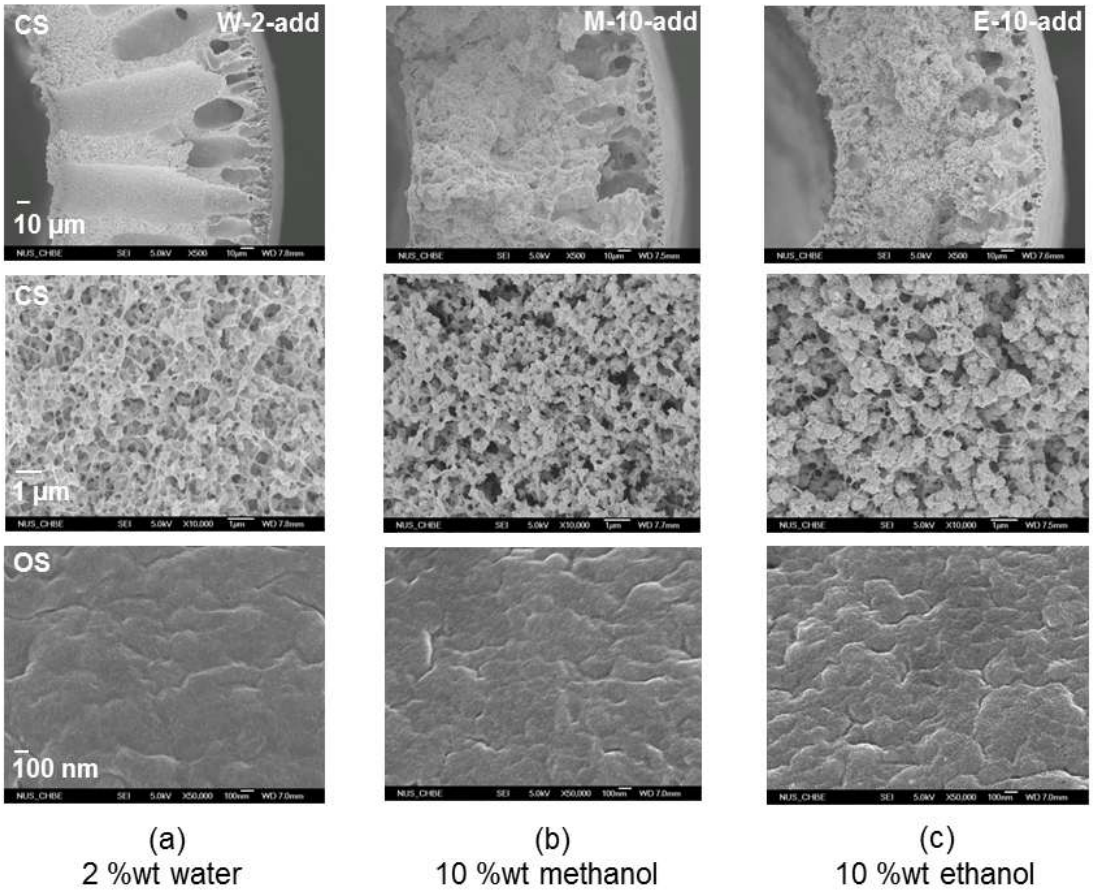

Figure 4.11 Cross-section and outer surface morphologies of hollow fiber membranes spun from 15 wt% PVDF/NMP solutions with different non-solvent additives (a) W-2-add, (b) M-10-add and (c) E-10-add.

The change in morphological structure when a non-solvent is added into a dope is similar to those when the same non-solvent is added into the external coagulant. Therefore, the same concept of delay demixing occurring with crystallization discussed in Section 4.3.2.2 is applicable. However, they have different spherulitic globule sizes. As tabulated in Table 4.3, the spherulitic globule size is about 0.40 μm and 0.68 μm for methanol and ethanol as the additive, respectively. Their corresponding spherulitic globule sizes increase to 0.95 μm and 1.02 μm, respectively, when methanol and ethanol are added as a component in the external coagulant.

This interesting phenomenon is resulted from different amounts of non-solvents present in the systems. Because of constrain in the phase diagram, one cannot add too much non-solvent in a dope solution, while a large amount of non-solvent can be added into the external coagulant. As a result, the amount of non-solvent in contact with the polymer dope during phase inversion is much more in the latter case. Hence, there is more severe delayed demixing, resulting in a larger spherulitic globule size. The XRD diffraction patterns shown in Figure 4.12 also support our hypothesis. The membranes (i.e., M-50, E-50) spun with a non-solvent as a component in the external coagulant have higher crystallinity than those (i.e., W-2-add, M-10-add, E-10-add) when the same non-solvent is employed as an additive in the dope. In addition, all aforementioned samples have higher crystallinity than the controlled one (P-15).

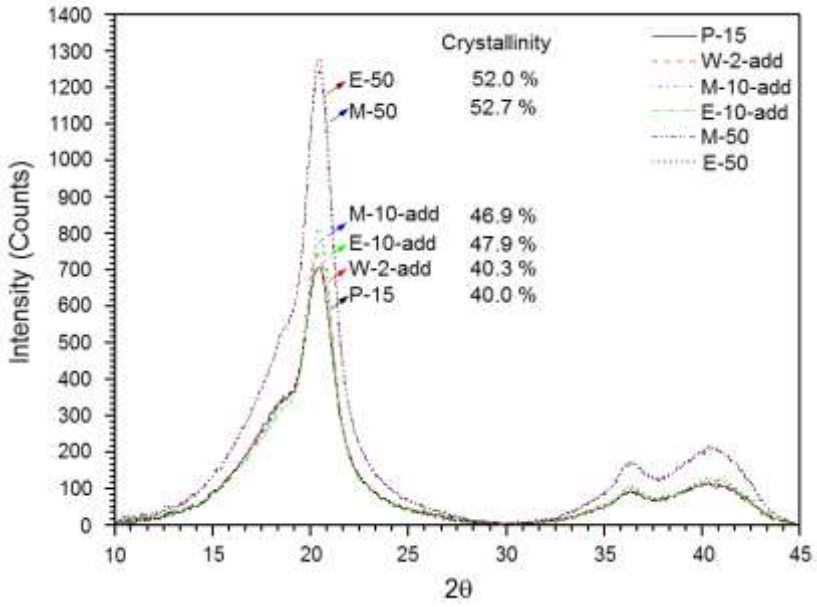

Figure 4.12 XRD patterns of the hollow fiber membranes spun with different spinning conditions.

4.3.3 The rheology of spinning dope solution

4.3.3.1 The effect of polymer dope concentrations

Figure 4.13 illustrates the shear and elongation viscosities as a function of shear and elongation rates for PVDF/NMP dope solutions with different polymer concentrations. The white dotted rectangular areas are the shear and elongation rates applied in our spinning conditions. All dope solutions exhibit shear and strain–thinning behavior over the shear and elongation rates tested. With increasing polymer concentration, the shear and elongation viscosities tend to increase. This is attributed to the enhanced viscoelastic properties of the dopes when the polymer concentration increases. At a higher polymer concentration, there is a greater degree of chain entanglement which creates more resistance to stretching and sliding polymer chains, thereby increasing the shear and elongation viscosities. When the shear and elongation viscosity is higher, it

is more difficult for the coagulant to penetrate the polymer matrix. Therefore, macrovoids formation is suppressed as illustrated in Figure 4.5.

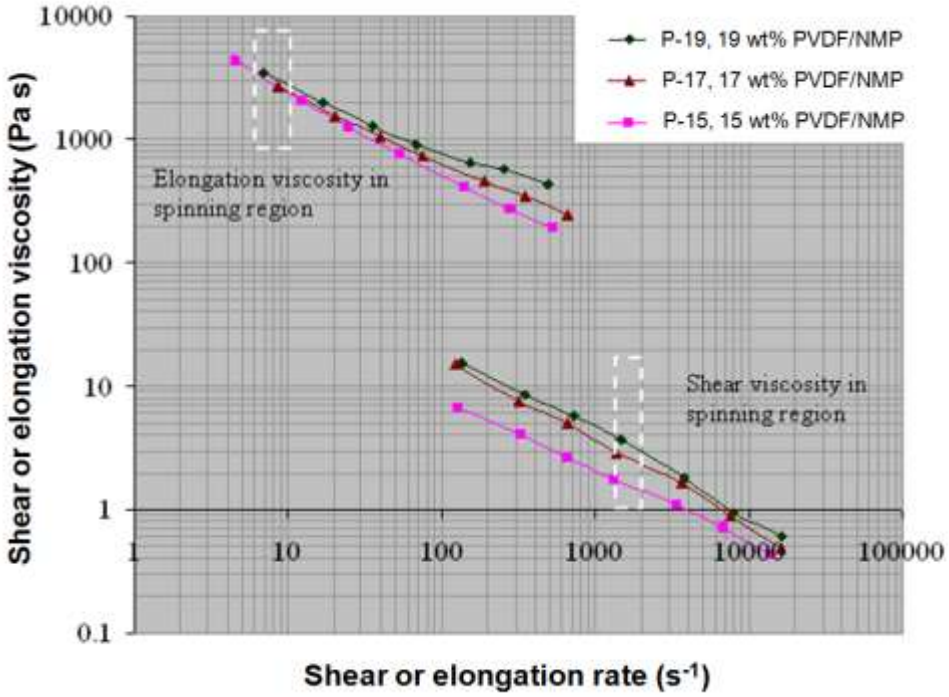

Figure 4.13 Shear and elongation viscosities as a function of shear and elongation rates for PVDF/NMP solutions with different polymer concentrations.

4.3.3.2 The effect of non-solvent additives in spinning dopes

Figure 4.14 presents the shear and elongation viscosities as a function of shear and elongation rates for PVDF/NMP dope solutions with different non-solvent additives. Similar to the binary PVDF/NMP system, the ternary dope solutions exhibit shear-thinning behavior regardless of the type of additives used. The addition of non-solvent increases the shear viscosity of the polymer solution.

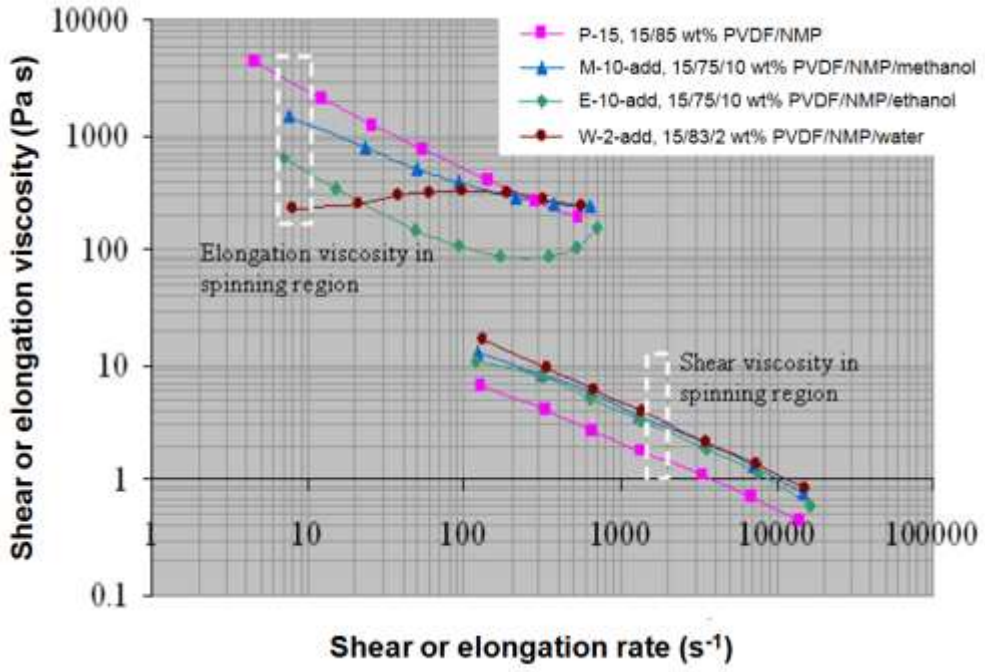

Figure 4.14 Shear and elongation viscosities as a function of shear and elongation rates for PVDF/NMP solutions with different non-solvent additives.

This phenomenon can be explained by considering the initial state of the polymer dope. It is hypothesized that the non-solvent induced phase separation possibly occurred in the polymer dope [49] even before the dry-jet wet spinning and this increases the viscosity of the solution. Table 4.6 lists the difference in solubility parameter between PVDF and the mixed solvent/non-solvent. Generally, a larger difference in the solubility parameter indicates a higher possibility of non-solvent induced phase separation. With reference to Table 4.6, the solubility parameter difference is the largest for the PVDF/NMP/water system which accounts for the highest shear viscosity (even though the calculated solubility parameters for PVDF from different methods may vary significantly).

Table 4.6 Solubility parameters of mixed solvents

Mixed Solvent[a]	δ_t [b] (mixed solvent) (MPa)$^{1/2}$	$\Delta\delta_t$ [c] (MPa)$^{1/2}$		
		$\delta_{t(PVDF)}$ = 14.15 (based on Van Krevelen eqn., material studio (Synthia))	$\delta_{t(PVDF)}$ = 17.75 (based on Fedors eqn., material studio (Synthia))	$\delta_{t(PVDF)}$ = 23.20 (based on solubility test from Ref. [54])
Water/NMP (2:83)	25.82	11.67	8.07	2.62
Methanol/NMP (10:75)	24.86	10.71	7.11	0.50
Ethanol/NMP (10:75)	23.70	9.55	5.95	0.50

[a] the solvent and non-solvent are mixed by a fixed weight ratio
[b] δ_t of the mixed solvent is calculated based on mole fraction %
[c] $\Delta\delta_t = | \delta_{t(mixed\ solvent)} - \delta_{t(PVDF)} |$

Contradictory to the effect of non-solvent additives on shear viscosity, the addition of non-solvent additives decreases the elongation viscosity as shown in Figure 4.14. This phenomenon can be adequately explained by considering the conformation of polymer chains in the mixed solvent/non-solvent environment. Generally, polymer chains exist in a highly coiled state with limited inter-chain entanglement in the presence of a poor solvent. Conversely, the polymer chains tend to be extended and entangle with neighboring chains when in contact with a good solvent. Since the degree of chain entanglement is greater when the polymer is in contact with a good solvent, the elongation viscosity is higher. Molecular dynamics simulations were conducted for PVDF in different solvent/non-solvent systems and the radius of gyration of the polymer chain is computed. The radius of gyration (R_g) represents the distance from the centre of gravity of a polymer chain to the end of the chain. If the polymer chain is in a highly coiled state, the corresponding radius of gyration will be small. Figure 4.15 shows the simulated images and the corresponding radius of gyration of PVDF in different environments. The radius of gyration for PVDF/NMP/methanol is larger than PVDF/NMP/ethanol and PVDF/NMP/water. This finding supports the idea that a larger radius of gyration results in a higher elongation viscosity. The simulated

solubility parameter (δ) of PVDF/mixed solvent systems shown in Figure 4.15 is in the same order as the solubility parameter of mixed solvents ($\delta_{t\ (mixed\ solvent)}$) in Table 4.6. This implies that our simulation may be able to represent the true PVDF/NMP/non-solvent systems investigated in this study.

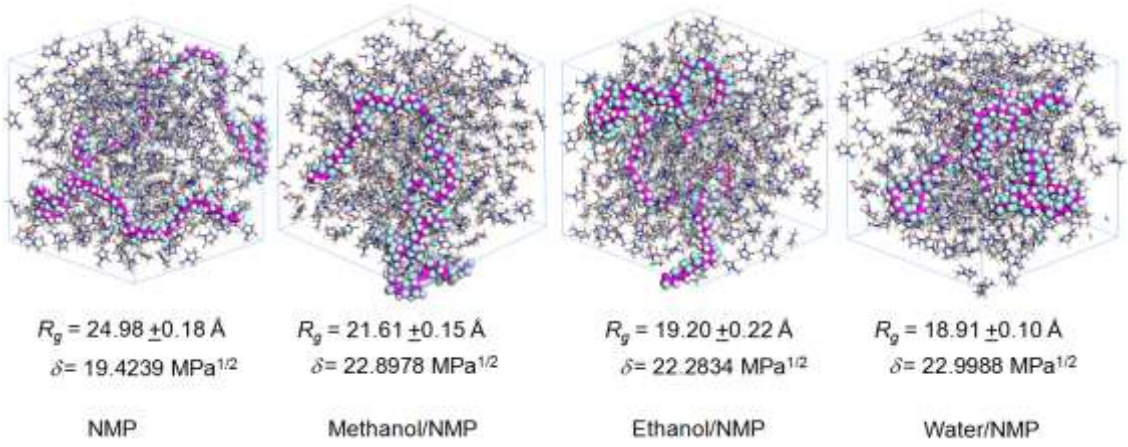

Figure 4.15 Snapshots from the molecular dynamic simulations showing the PVDF chain conformation in different mixed solvents environment (δ is the calculated solubility parameter in the whole system including PVDF and solvents).

Another interesting observation is all polymer dopes, other than the one containing water as the non-solvent additive, exhibit strain thinning behavior. This may imply that weak molecular interactions are dominant in the processes of chain stretching and sliding in these systems under elongation. However, for the PVDF/NMP/water system, its elongation viscosity increases with increasing elongation rate. This may arise from hydrogen bonding or strong interactions between NMP and water that result in greater resistance for chain stretching and sliding.

4.3.4. Porosity, mechanical properties and rheology of hollow fiber membranes

Table 4.7 lists the fiber dimensions, porosity and mechanical properties of all hollow fiber membranes in this study. In terms of mechanical properties, all hollow fiber membranes exhibit ductile behavior as indicated by the relatively small tensile strength and large extension at break.

Table 4.7 Fiber dimensions, porosity and mechanical properties of PVDF hollow fiber membranes

Spinning dope ID	Outer/Inner diameter (μm)	Wall thickness (μm)	Porosity (%)	Tensile strength (MPa)	Extension at break (%)	Young's Modulus (MPa)
The effect of polymer concentrations						
P-15	680/400	140	82.3 ± 0.8	2.78 ± 0.13	65.30 ± 2.73	54.00 ± 4.00
P-17	920/520	200	78.8 ± 0.2	3.18 ± 0.03	75.24 ± 3.16	55.20 ± 2.28
P-19	980/540	220	77.7 ± 0.5	3.68 ± 0.08	133.58 ± 6.52	84.33 ± 6.19
The effect of external coagulations						
M-10	740/400	150	79.1 ± 0.1	2.81 ± 0.08	69.57 ± 0.76	59.60 ± 0.89
M-20	760/400	180	78.1 ± 0.2	2.17 ± 0.05	58.39 ± 3.16	47.50 ± 1.00
M-50	780/400	190	71.0 ± 0.4	1.53 ± 0.10	90.31 ± 5.50	35.20 ± 1.10
E-10	790/400	190	78.8 ± 0.2	2.60 ± 0.09	56.80 ± 4.65	58.40 ± 3.58
E-20	760/400	180	77.1 ± 0.4	2.21 ± 0.12	55.18 ± 2.02	42.80 ± 3.35
E-50	800/420	190	73.1 ± 0.6	1.38 ± 0.05	89.44 ± 5.32	25.60 ± 0.89
I-10	780/400	190	79.1 ± 0.1	2.19 ± 0.06	55.89 ± 1.60	56.80 ± 4.38
I-20	760/400	180	76.9 ± 0.4	2.18 ± 0.07	53.41 ± 2.24	42.40 ± 2.19
I-50	800/400	200	73.8 ± 0.4	0.85 ± 0.04	56.99 ± 2.33	21.60 ± 2..19
The effect of non-solvent additives						
W-2-add	680/360	160	80.1 ± 0.3	2.32 ± 0.07	110.51 ± 3.48	44.20 ± 1.48
M-10-add	700/400	150	79.8 ± 0.3	1.37 ± 0.02	46.79 ± 1.64	35.60 ± 1.14
E-10-add	720/380	170	77.7 ± 0.9	0.79 ± 0.01	36.51 ± 2.73	22.40 ± 2.61

Similar behavior of PVDF hollow fibers fabricated by phase inversion has been reported in previous studies [58]. A different attempt from the previous study was made to correlate the effects of polymer concentrations, external coagulants and non-solvent additives on the mechanical properties of as-spun hollow fiber membranes. A comparison of their Young's modulus which represents tensile stiffness of hollow fibers is depicted in Figure 4.16. There seems to be a direct relationship between the

Young's modulus and the elongation viscosity of the polymer dope. An exception is observed when water is used as a non-solvent additive in the dope. This is possibly due to (1) only 2% water presented in the W-2-add sample, while 10% non-solvents in M-10-add and E-10-add samples, and (2) different membrane morphologies resulted from alcohol and water solvent additives.

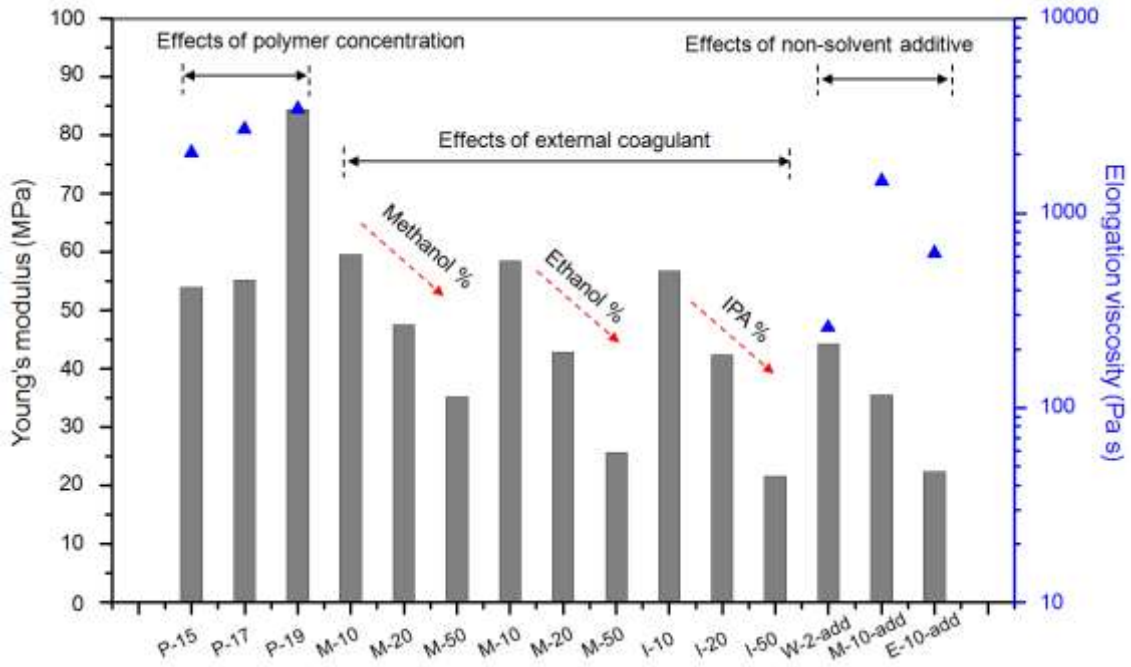

Figure 4.16 Correlation between the Young's modulus of hollow fiber membranes and the elongation viscosity of dope solutions.

The overall porosity of the resultant fibers is in the range of 70-83%. Membranes with finger-like macrovoid structure results in higher porosity while macrovoid-free membranes with globule structure have lower porosity. Several interesting and novel points are worthy of mention. Hollow fiber membranes with finger-like macrovoids possess better mechanical properties than those with macrovoid free structure. This result is in contrary to the common perception that macrovoids represents weak

mechanical points. This interesting finding can be related to the micro-structural morphology and rheology of polymer solutions as discussed in the later section.

The relationship between porosity and tensile properties of these PVDF hollow fibers as function of non-solvent additives and external coagulant chemistry is interesting. For hollow fibers spun from dopes containing no water such as P17-P19, porosity decreases while all tensile properties (strength, modulus and extension at break) increase with an increase in PVDF concentration in the spinning dope. However, both porosity and most tensile properties (strength and modulus) decrease with an increase in alcohol concentration in the external coagulant. The effect of external alcohols on lowering tensile strength and modulus follows the order: methanol < ethanol < IPA. As illustrated in Figure 4.9, the membrane morphology changes from tight to loose globule- packing and the porosity increases while tensile properties decrease with increasing the strength of alcohols (methanol < ethanol < IPA). To fabricate a well-packed interconnected globule type structure, three strategies are proposed, namely: (1) to use a strong non-solvent as a coagulant, i.e. methanol/water mixture, which results in a better mechanical strength as shown in Table 4.7; (2) to fabricate PVDF hollow fiber membranes via thermally induced phase separation (TIPS) with diluent mixture since this approach induces the well-interconnected globule type structure in PVDF membranes [59]; (3) to apply heat treatment. Sipsas et al. reported that heat-treated membranes show uniform crystallinity as well as high mechanical strength without significant changes on the overall morphology [60].

The sharp difference in the relationship between porosity and mechanical strengths is resulted from the combination effects of membrane morphology and dope rheology.

Hollow fiber membranes spun from dopes containing no water comprise interconnected-cellular type structure show greater mechanical properties. This type of morphology can be obtained by increasing the polymer concentration or introducing a strong non-solvent (like water) to induce instantaneous demixing. Conversely, the membranes with spherulitic globule structure show weaker mechanical properties. This kind of structure is obtained from the delayed demixing process accompanying crystallization by using a weak external coagulant or weak non-solvent additive. However, the smaller radius of gyration or coil size resulting from non-solvent additives also facilitates crystallization within a short range and reduces mutual interactions among spherulitic globules as illustrated by the schematic model in Figure 4.9. Therefore, the rheological properties and the state of polymer chains, dope composition, and coagulant chemistry are intertwined complicatedly and simultaneously to affect the resultant membrane morphology and mechanical properties.

4.4 Conclusions

Polymer dope composition (i.e. solid content and type of non-solvent additives) and coagulant composition (i.e. nature of non-solvent and relative amount of solvent/non-solvent) are significant parameters which influence the resultant morphology and mechanical properties of PVDF hollow fiber membranes. The use of a weak non-solvent (i.e. methanol, ethanol or IPA) as an additive or a component in the external coagulant induces delayed demixing and crystallization. The resultant membranes are macrovoid-free with globule structure comprising spherulitic crystallites. Due to the thermodynamics and kinetics factors, the enhancement in delayed demixing by the non-

solvents follows the sequence IPA> ethanol > methanol > water. The spherulitic globule size increases as the strength and amount of non-solvent in the system increase. Despite the macrovoid-free structure, the membrane with spherulitic globule packing exhibits a lower mechanical strength than those with interconnected-cellular type morphology. Interestingly, the conventional perspective of macrovoid-free membranes yielding better mechanical properties may not be applicable for semi-crystalline polymers like PVDF. The addition of a non-solvent in a spinning dope increases shear viscosity, while decreases elongation viscosity. The state of polymer chains involved in the phase inversion is further supported through the analytical methods and molecular dynamics simulations. The mechanical strength of as-spun fibers tends to increase as the elongation viscosity of the polymer dope increases. Therefore, the dope composition, rheology, and coagulant composition determine the membrane morphology and mechanical strength, which is vital for fabricating PVDF hollow fibers with desirable properties.

REFERENCES

[1] A.J. Lovinger, in: D.C. Bassett (Ed.), Poly(vinylidene fluoride), Development in Crystalline Polymers, vol. 1, London: Applied Science (1982).

[2] J.E. Dohany, L.E. Robb, Polyvinylidene fluoride, in: Kirk-Othmer Encyclopedia of Chemical Technology, vol. 11, 3rd ed., New York: Wiley (1980).

[3] A.J. Castro, Method for making microporous products, US Patent 4,247,498 (1981).

[4] N. Chlubek, M. Tomaszewska, Some properties of hydrophobic membranes for distillation, Environ. Prot. Eng. 15 (1989) 95.

[5] C. Güell, R.H. Davis, Membrane fouling during microfiltration of protein mixtures, J. Membr. Sci. 119 (1996) 269.

[6] M. Khayet, C.Y. Feng, K.C. Khulbe, T. Matsuura, Preparation and characterization of polyvinylidene fluoride hollow fiber membranes for ultrafiltration, Polymer 43 (2002) 3879.

[7] K. Schneider, T.S. Van Gassel, Membrane distillation, Chem. Eng. Technol. 56 (1984) 514.

[8] S. Bonyadi, T.S. Chung, Flux enhancement in membrane distillation by fabrication of dual layer hydrophilic-hydrophobic hollow fiber membranes, J. Membr. Sci. 306 (2007) 134.

[9] K.Y. Wang, T.S. Chung, M. Gryta, Hydrophobic PVDF hollow fiber membranes with narrow pore size distribution and ultra-thin skin for the fresh water production through membrane distillation, Chem. Eng. Sci. 63 (2008) 2587.

[10] K. Jian, P.N. Pintauro, Asymmetric PVDF hollow-fiber membranes for organic/water pervaporation separations, J. Membr. Sci. 135 (1997) 41.

[11] K. Li, J.F. Kong, D. Wang, W.K. Teo, Tailor-made asymmetric PVDF hollow fibers for soluble gas removal. AIChE J. 45 (1999) 1211.

[12] S. Atchariyawut, C. Feng, R. Wang, R. Jiraratananon, D.T. Liang, Effect of membrane structure on mass-transfer in the membrane gas-liquid contacting process using microporous PVDF hollow fibers, J. Membr. Sci. 285 (2006) 272.

[13] M. Sugihara, M. Fujimoto, T. Uragami, Effect of casting solvent on permeation characteristics of polyvinylidene fluoride membranes, Polym. Prepr. (Am. Chem. Soc. Div. Polym. Chem.) 20 (1979) 999.

[14] T. Uragami, M. Fujimoto, M. Sugihara, Studies on syntheses and permeabilites of special polymer membranes-24. Permeation characteristics of poly(vinylidene fluoride) membranes, Polymer 21 (1980) 1047.

[15] A. Bottino, G. Capannelli, S. Munari, Effect of coagulation medium on properties of sulphonated polyvinylene fluoride membranes, J. Appl. Polym. Sci. 30 (1985) 3009.

[16] A. Bottino, G. Capannelli, S. Munari, Factors affecting the structure and properties of asymmetric polymeric membranes, in: E. Drioli, M. Nakagaki (Eds.), Membrane and Membrane Processes, Plenum Press, New York (1986).

[17] A. Bottino, G. Camera-Roda, G. Capannelli, S. Munari, The formation of microporous polyvinylidene difluoride membranes by phase separation, J. Membr. Sci. 57 (1991) 1.

[18] A. Bottino, G. Capannelli, S. Munari, A. Turturro, High performance ultrafiltration membranes cast from LiCl doped solutions, Desalination 68 (1988) 167.

[19] T.H. Young, L.P. Cheng, D.J. Lin, L. Fane, W.Y. Chuang, Mechanisms of PVDF membrane formation by immersion-precipitation in soft (1-octanol) and harsh (water) nonsolvents, Polymer 40 (1999) 5315.

[20] H. Matsuyama, M. Teramoto, R. Nakatani, T. Maki, Membrane formation via phase separation induced by penetration of nonsolvent from vapor phase. II. Membrane morphology, J. Appl. Polym. Sci. 74 (1999) 171.

[21] M.L. Yeow, Y.T. Liu, K. Li, Morphological study of Poly(vinylidene fluoride) asymmetric membranes: Effects of the solvent, additive, and dope temperature, J. Appl. Polym. Sci. 92 (2004) 1782.

[22] E. Fontananova, J.C. Jansen, A. Cristiano, E. Curcio, E. Drioli, Effect of additives in the casting solution on the formation of PVDF membranes, Desalination 192 (2006) 190.

[23] M.G. Buonomenna, P. Macchi, M. Davoli, E. Drioli, Poly(vinylidene fluoride) membranes by phase inversion: the role the casting and coagulation conditions play in their morphology, crystalline structure and properties, Eur. Polym. J. 43 (2007) 1557.

[24] D. Wang, K. Li, W.K. Teo, Preparation and characterization of polyvinylidene fluoride (PVDF) hollow fiber membranes, J. Membr. Sci. 163 (1999) 211.

[25] J. Kong, K. Li, Preparation of PVDF hollow-fiber membranes via immersion precipitation, J. Appl. Polym. Sci. 81 (2001) 1643.

[26] D. Wang, K. Li, W.K. Teo, Porous PVDF asymmetric hollow fiber membranes prepared with the use of small molecular additives, J. Membr. Sci. 178 (2000) 13.

[27] M. Khayet, The effects of air gap length on the internal and external morphology of hollow fiber membranes, Chem. Eng. Sci. 58 (2003) 3091.

[28] S. Rajabzadeh, T. Maruyama, T. Sotani, H. Matsuyama, Preparation of PVDF hollow fiber membrane from a ternary polymer/solvent/nonsolvent system via thermally induced phase separation (TIPS) method, Sep. Purif. Technol. 63 (2008) 415.

[29] J. Ren, R. Wang, H.Y. Zhang, Z. Li, D.T. Liang, J.H. Tay, Effect of PVDF dope rheology on the structure of hollow fiber membranes used for CO_2 capture, J. Membr. Sci. 281 (2006) 334.

[30] D. Wang, Polyethersulfone hollow fiber gas separation membranes prepared from solvent systems containing non-solvent-additives, Ph.D. Thesis, Department of Chemical Engineering, National University of Singapore (1995).

[31] O.M. Ekiner, G. Vassilatos, Polyaramide hollow fibers for hydrogen/methane separation-spinning and properties, J. Membr. Sci. 53 (1990) 259.

[32] N. Peng, T.S. Chung, K.Y. Wang, Macrovoid evolution and critical factors to form macrovoid-free hollow fiber membranes, J. Membr. Sci. 318 (2008) 363.

[33] D.T. Clausi, W.J. Koros, Formation of defect-free polyimide hollow fiber membranes for gas separations, J. Membr. Sci. 167 (2000) 79.

[34] D.R. Lloyd, K.E. Kinzer, H.S. Tseng, Microporous membrane formation via thermally induced phase separation. I. solid-liquid phase separation, J. Membr. Sci. 52 (1990) 239.

[35] T.H. Young, D.J. Lin, J.J Gau, W.Y. Chuang, L.P. Cheng, Morphology of crystalline Nylon-6,10 membranes prepared by the immersion-precipitation process: Competition between crystallization and liquid-liquid phase separation, Polymer 40 (1999) 5011.

[36] L.P. Cheng, T.H. Young, L. Fang, J.J. Gau, Formation of particulate microporous poly(vinylidene fluoride) membranes by isothermal immersion

precipitation from the 1-octanol/dimethylformamide/poly(vinylidene fluoride) system, Polymer 40 (1999) 2395.

[37] S. Bonyadi, T.S. Chung. Highly porous and macrovoid-free PVDF hollow fiber membranes for membrane distillation by a solvent-dope solution co-extrusion approach, J. Membr. Sci. 331 (2009) 66.

[38] T.S. Chung, W.H. Lin, R.H. Vora, The effect of shear rates on gas separation performance of 6FDA-durene polyimide hollow fibers, J. Membr. Sci. 167 (2000) 55.

[39] T.S. Chung, S.K. Teo, W.W.Y. Lau, M.P. Srinivasan, Effect of shear stress within the spinneret on hollow fiber membrane morphology and separation performance, Ind. Eng. Chem. Res. 37 (1998) 3930 and 4903.

[40] J.J. Qin, R. Wang, T.S. Chung, Investigation of shear stress effect within a spinneret on flux, separation and thermochanical properties of hollow fiber ultrafiltration membrane, J. Membr. Sci. 175 (2000) 197.

[41] K.Y. Wang, T. Matsuura, T.S. Chung, W.F. Guo, The effects of flow angle and shear rate within the spinneret on the separation performance of poly(ethersulfone) (PES) ultrafiltration hollow fiber membranes, J. Membr. Sci. 22 (2004) 67.

[42] N. Widjojo, T.S. Chung, Thickness and air gap dependence of macrovoid evolution in phase-inversion asymmetric hollow fiber membranes, Ind. Eng. Chem. Res. 45 (2006) 7618.

[43] N. Peng, T.S. Chung, The effects of spinneret dimension and hollow fiber dimension on gas separation performance of ultra-thin defect-free Torlon® hollow fiber membranes, J. Membr. Sci. 310 (2008) 455.

[44] C. Cao, T.S. Chung, S.B. Chen, Z. Dong, The study of elongation and shear

rates in spinning process and its effect on gas separation performance of Poly(ether sulfone) (PES) hollow fiber membranes, Chem. Eng. Sci. 59 (2004) 1053.

[45] O.M. Ekiner, G. Vassilatos, Polyaramide hollow fibers for H2/CH4 separation II. Spinning and properties, J. Membr. Sci. 186 (2001) 71.

[46] N. Peng, T.S. Chung, J.Y. Lai, The rheology of Torlon® solutions and its role in the formation of ultra-thin defect-free Torlon® hollow fiber membranes for gas separation, J. Membr. Sci. 326 (2009) 608.

[47] T.S. Chung, S.K. Teoh, X.D. Hu, Formation of ultrathin high-performance polyethersulfone hollow fiber membranes, J. Membr. Sci 133 (1997) 181.

[48] R.K. Gupta, Polymer and composite rheology, second edition, revised and expanded, Marcel Dekker, Inc. New York, 2000, p. 8.

[49] L.P. Cheng, D.J. Lin, C.H. Shih, A.H. Dwan, C.C. Gryte, PVDF membrane formation by diffusion-induced phase separation-morphology prediction based on phase behavior and mass transfer modeling, J. Polym. Sci. B: Polym. Phys. 37 (1999) 2079.

[50] C.A. Smolders, A.J. Reuvers, R.M. Boom, I.M. Wienk, Microstructures in phase-inversion membranes. Part 1. Formation of macrovoids, J. Membr. Sci. 73 (1992) 259.

[51] H. Horibe and M. Taniyama, Poly(vinylidene fluoride) crystal structure of poly(vinylidene fluoride) and poly(methyl methacrylate) blend after annealing, J. Electrochem. Soc. 153 (2006) G119.

[52] R. Gregorio, Determination of the α, β and γ crystalline phase of poly(vinylidene fluoride) films prepared at different conditions, J. Appl. Polym. Sci. 100 (2006) 3272.

[53] C.M. Hansen, Hansen solubility parameter, A User's Handbook, CRC Press, New York (1999).

[54] A. Bottino, G. Capannelli, S. Munari and A. Turturro, Solubility parameters of poly(vinylidene fluoride), J. Polym. Sci. B: Polym. Phys. 26 (1988) 785.

[55] R.Y.M. Huang, N.R. Jarvis, Separation of liquid mixtures by using polymer membranes. II. Pervaporation of aqueous alcohol solutions through cellophane and poly(vinyl alcohol), J. Appl. Polym. Sci. 14 (1970) 2341.

[56] J.A. Van't Hof, A.J. Reuvers, R.M. Boom, H.H.M. Rolevink, C.A. Smolders, Preparation of asymmetric gas separation membrnaes with high selectivity by a dual-bath coagulation method, J. Membr. Sci. 70 (1992) 17.

[57] D.Y. Zuo, B.K. Zhu, J.H. Cao, Y.Y. Xu, Influence of alcohol-based nonsolvents on the formation and morphology of PVDF membranes in phase inversion process, Chinese. J. Polym. Sci. 24 (2006) 281.

[58] Y. Doi, H. Matsumura, Polyvinylidene fluoride porous membrane and a method for producing the same, US Patent 5,022,990 (1991).

[59] G.L. Ji, L.P. Zhu, B.K. Zhu, C.F. Zhang, Y.Y. Xu, Structure formation and characterization of PVDF hollow fiber membrane prepared via TIPS with diluent mixture, J. Membr. Sci. 319 (2008) 264.

[60] I.P. Sipsas, I. Rothmann, I. Joffee, Uniform polyvinylidene difluoride membranes, US Patent 5,198,505 (1993).

CHAPTER FIVE

MODIFIED PORE-FLOW MODEL FOR PERVAPORATION MASS TRANSPORT IN PVDF HOLLOW FIBER MEMBRANES FOR ETHANOL-WATER SEPARATION

5.1 Introduction

Pervaporation is a separation process in which a liquid feed containing two or more components comes into contact with one side of a membrane while vacuum (or purged gas) is applied on the other side to produce a permeate vapor [1]. The phenomenon of pervaporation was first discovered by Kober in 1917 [2] and the potential applications of the pervaporation process were subsequently explored by Farber [3] and Binning and co-workers [4]. Recently, pervaporation has emerged as one of the promising processes for biofuel separation in addition to various liquid mixture separations such as dehydration of organic solvents, recovery of organic compounds from aqueous solutions and separation of organic mixtures [5-8].

To date, there have been several models proposed to describe the mass transport in pervaporation, and the solution-diffusion model is the most widely-accepted model [9,10]. According to the solution-diffusion model, pervaporation consists of three successive steps: (i) the permeant dissolves in the feed side of the membrane; (ii) the permeant diffuses though the membrane; and (iii) the permeant evaporates as vapor at the downstream side of the membrane. The productivity and separation selectivity between different permeants are not only dependent on the solubility and diffusivity of each permeant but also on their solubility and diffusivity ratios through the membrane.

Excellent agreements between experimental data and theoretical predictions by means of the solution-diffusion model have been reported for both defect-free dense flat membranes and asymmetric membranes consisting of a thin defect-free dense-selective layer [10-22].

Although the solution-diffusion model has been well established for membrane pervaporation process, there are still some unclear points regarding how and where the evaporation or actual phase change from liquid to vapor takes place. These have been pointed out and discussed in many previous studies [10, 23-25]. In addition, to our best knowledge, there is still no proper explanation elucidating this fundamental phenomenon of pervaporation process on the basis of solution-diffusion model with no further modification [25-27]. Consequently, the pore-flow model proposed by Okada and Matsuura [23] is an alternative model to investigate the mass transport phenomena occurring during pervaporation. The model assumes that straight cylindrical pores exist across the membrane and the pervaporation is taking place in the pore. Unlike the solution-diffusion mechanism, this distinguishing feature takes into account (i) the permeant transports through the liquid-filled portion of the pore, (ii) a liquid-to-vapor phase change takes place inside the pore, (iii) the permeant transports through the vapor-filled portion of the pore [23]. If the pervaporation membrane really comprises micropores, the pore-flow model apparently follows the actual operation dynamics because its mass transport mechanism consists of liquid transport and vapor transport in series.

There are extremely different views among leading membrane scientists between these two models concerning the presence of pores in pervaporation membranes.

Conventional wisdom implies that any pores in the membrane bulk and surface different from the d-space or free volume of polymer chains may be considered as voids and defects, respectively. The voids may enhance the permeability, while the surface defects may lower the membrane from acquiring its maximal (ideal) selectivity. Following the gas separation membranes, the solution-diffusion model has been vastly used to describe the permeation phenomenon of a liquid mixture through pervaporation membranes. The effectiveness of the solution-diffusion mechanism through the membrane's defect-free dense-selective layer relies on the thermally agitated motion of chain segments within the dense layer. Penetrant molecules diffuse and jump across the membrane via transient gaps among chains from the upstream to the downstream without the use of any voids and defects for mass transport [28].

In contrast to the solution-diffusion model, the pore-flow model aims at elucidating the permeation phenomenon of a liquid mixture through a porous asymmetric membrane [29]. Since the phase inversion process tends to create defective asymmetric membranes consisting of a thin defective dense-selective layer and an asymmetric substructure [30-32], the pore-flow model seems to be more relevant for some asymmetric membranes prepared from the phase inversion process. Works published by Jian and Pintauro on poly(vinylidene fluoride) (PVDF) membranes are typical examples [33-35]. They reported that PVDF membranes with an asymmetric structure had a greater separation factor and permeation flux than PVDF membranes with a dense symmetric structure for the separation of organic compounds from water. Depending on casting conditions, the pore size in the dense layer varied from 58 to 850 Å. When the pore size increased, the water permeation flux increased while the separation factor decreased for the benzene/water mixtures separation [34]. The same

observation was also found in the case of PVDF asymmetric hollow fiber membranes where pore size played an important role on pervaporation performance [35].

We have been a strong supporter for the use of solution-diffusion mechanism for pervaporation [15-17,20,21]. Recently, PVDF asymmetric hollow fiber membranes fabricated in our previous work [36] have been employed to investigate their potential for biofuel recovery using a 5 wt% ethanol/water mixture as a model solution. The performance of the membranes is summarized in Table 5.1.

Table 5.1 Separation performance of PVDF hollow fiber membranes on separation of ethanol/water mixture via pervaporation

Spinning Condition[a] Dope composition (wt%)	Silicone rubber coating[b]	Permeate composition (wt%)		Pervaporation performance[c]	
		Ethanol	Water	Total flux (kg m^{-2} h^{-1})	Separation factor $\alpha_{ethanol/water}$
15/85 PVDF/NMP	No	20.95	79.05	7.91	5.06
17/83 PVDF/NMP	No	17.95	82.05	5.70	4.18
19/81 PVDF/NMP	No	11.66	88.34	5.22	2.53
15/85 PVDF/NMP	Yes	5.87	94.13	1.83	1.19

[a] Bore fluid flow rate: 0.6 ml min^{-1}; dope flow rate: 2.0 ml min^{-1}; air gap distance: 1 cm; Bore-fluid: NMP/water (90/10 wt%); spinneret dimensions (OD/ID): 1.2/0.8 mm; water coagulant bath and spinning temperature: 25 °C; relative humidity: 65%.
[b] Hollow fiber membranes are immersed in 3 wt% silicone rubber in hexane solution for 3 min.
[c] Feed composition: 5 wt% ethanol/water mixture; recirculation flow rate is 30 L h^{-1}; operating temperature is 40 °C

It can be seen that the PVDF hollow fiber membrane spun with a higher polymer dope concentration tends to have a lower total flux and separation factor. This phenomenon seems to contradict with our understanding from the solution-diffusion approach; typically, a higher polymer dope concentration results in the membranes with a thicker dense skin, hence its selectivity is expected to improve [21]. Another interesting finding is that the selectivity of the membrane with 15/85 wt% PVDF/NMP dope

concentration, which is the highest compared to other compositions, dropped significantly after silicone rubber coating. In general, coating by silicone rubber has been employed in gas separation and pervaporation membranes as an effective way to seal the defects or pores on the surface of the membrane and to recover the dense-layer selectivity. Evidently, data shown in this Table imply that the solution-diffusion model may not be appropriate to describe the pervaporation transport for this case. This surprising discrepancy motivates us to investigate the pervaporation transport of PVDF hollow fiber membranes on the basis of pore-flow model.

Clearly, there are two types of pervaporation membranes co-existing; one without pores and the other with pores. The solution-diffusion model is applicable for those membranes without pores, but not applicable for those with pores. Therefore, the objective of this study is to conduct a fundamental investigation on the pervaporation transport phenomena of PVDF asymmetric hollow fiber membranes on the basis of the pore-flow model. To our best knowledge, this is the first time that the pore-flow concept is used to describe the mass transport in PVDF asymmetric hollow fiber membranes and the model can be modified to analyze membranes with a wider range of pore size. The relationship among pore size, surface porosity and transport parameters will be expressed in quantitative terms. In addition, the prediction of pervaporation performance using pore-flow and modified pore-flow models is presented in a parallel comparison. The representative feed employed in this study is a mixture of ethanol and water.

5.2. Background: The pore-flow model and derivation of the modified pore-flow model

5.2.1 Pore-flow model

The pore-flow model was proposed by Okada and Matsuura [23] and was established based on the assumptions that the membrane pores are all straight and cylindrical with an effective length δ penetrating across the selective layer of the membrane and that all the pores are operating under an isothermal condition. Figure 5.1 illustrates the schematic representation of the pore-flow model in the pervaporation transport within an asymmetric hollow fiber; the liquid-filled section of the pore with a distance δ_a refers to the section of the pore where the permeant flows by liquid-phase transport, while the vapor-filled section with a distance δ_b refers to the section of the pore where the permeant flows by vapor-phase transport. The evaporation takes place at the boundary between liquid- and vapor- sections; therefore, the pervaporation transport can be considered to be a combination of liquid-phase and vapor-phase transport in series.

Considering the mass transport of a single component system, the liquid transport is described by the Darcy's equation and the mass transport in terms of molar flux can be expressed as

$$Q_{liquid} = \frac{A}{\delta_a}(P_2 - P_*) \qquad where \quad A = \frac{\pi r^4 \rho N_t}{8\eta_L M} \tag{5.1}$$

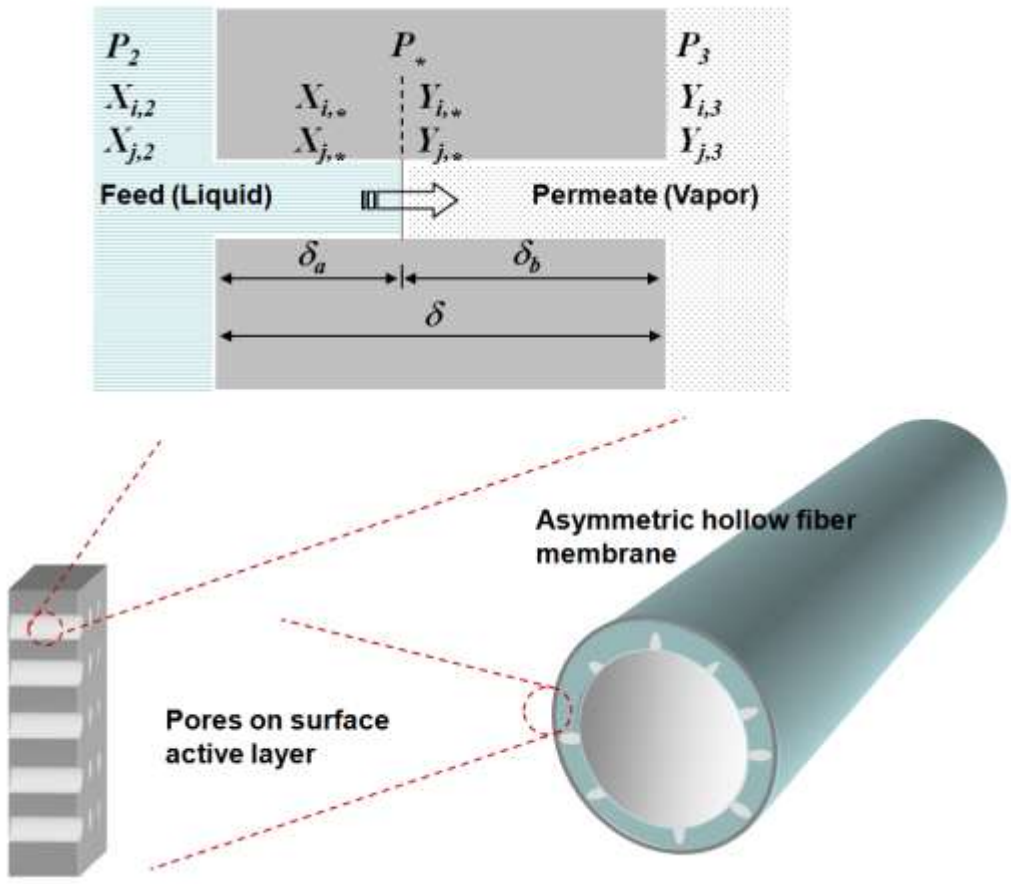

Figure 5.1 Schematic representation of the pore-flow model in pervaporation transport within asymmetric hollow fiber membranes.

For the vapor transport, the pore-flow first assumes the surface flow mechanism is prevailing while other gas flow mechanisms are negligible. According to the surface flow mechanism, the pore is filled with an adsorption layer of vapor molecules on the pore wall. Further assumptions of the validity of Henry's law and monolayer adsorption have to be made in simplifying the formulation of equation (5.2). The detailed derivation of equation (5.2) can be found elsewhere [23, 37] and finally written as:

$$Q_{vapor} = Q_{surface} = \frac{B}{\delta_b}(P_*^2 - P_3^2) \qquad where \quad B = \frac{\pi(2rt_a - t_a^2)^2 t_a N_t}{8r}\frac{RT}{\mu}(k_H^{'})^2 \qquad (5.2)$$

where Q is the molar flux (mol.m^{-2}.s^{-1}), P_2 and P_3 are the upstream and downstream pressure (Pa), respectively, P_* is the saturation vapor pressure (Pa) at the liquid-vapor boundary, r and k'_H are the mean pore size in the membrane and a proportionality constant involved in the vapor adsorption, respectively. N_t is the total number of pores per effective membrane area (m^{-2}). μ is the surface viscosity which refers to the flow resistance of vapor molecules adsorbed on the pore wall (Pa s). A high surface viscosity indicates a strong interaction between adsorbed vapor molecules and the membrane pore, leading to a decrease on vapor permeation flux. Definitions of other symbols are given in the notation.

Since both liquid and gas fluxes are equivalent to the total flux as expressed in the following equation,

$$Q_{total} = Q_{liquid} = Q_{vapor} \tag{5.3}$$

and

$$\delta = \delta_a + \delta_b \tag{5.4}$$

Combining equations (5.1), (5.2), (5.3) and (5.4), the equation to calculate total flux is expressed as

$$Q_{total} = \frac{A}{\delta}(P_2 - P_*) + \frac{B}{\delta}(P_*^2 - P_3^2) \qquad when \quad P_3 < P_* \tag{5.5}$$

Equation (5.5) is valid under the condition that $P_3 < P_*$. When $P_3 \geq P_*$, the entire length of the pore is saturated with liquid. Hence, the equation for total flux is deduced and given by

$$Q_{total} = \frac{A}{\delta}(P_2 - P_3) \qquad when \quad P_3 \geq P_* \tag{5.6}$$

The ratio of the length of the liquid-filled portion to the entire length of membrane pore can be represented by

$$\frac{\delta_a}{\delta} = \frac{\frac{A}{\delta}(P_2 - P_*)}{\frac{A}{\delta}(P_2 - P_*) + \frac{B}{\delta}(P_*^2 - P_3^2)} \tag{5.7}$$

Similarly, the ratio of the length of the vapor-filled portion to the entire length of membrane pore can be expressed as

$$\frac{\delta_b}{\delta} = \frac{\frac{B}{\delta}(P_*^2 - P_3^2)}{\frac{A}{\delta}(P_2 - P_*) + \frac{B}{\delta}(P_*^2 - P_3^2)} \tag{5.8}$$

In the case of a binary system containing components *i* and *j*, the equations can be derived based on the assumption that no separation occurs within the liquid-filled section of the pore. Therefore, the equation can be written in a similar fashion to equation (5.1) as follows,

$$Q_{liquid} = \frac{A_{mix}}{\delta_a}(P_2 - P_*) \tag{5.9}$$

In the vapor-filled section of the pore, vapor transport for component *i* and *j* in the system can be expressed in an analogous fashion to equation (5.2) by considering the partial pressure of each component as a driving force. The expressions for component *i* and *j* are respectively given by

$$Q_{i,vapor} = \frac{B_i}{\delta_b}(P_{i,*}^2 - P_{i,3}^2) \tag{5.10}$$

$$Q_{j,vapor} = \frac{B_j}{\delta_b}(P_{j,*}^2 - P_{j,3}^2) \tag{5.11}$$

Equation (5.12) denotes the total molar flux for a two-component system in a similar manner as equation (5.5) and can be expressed as

$$Q_{total} = \frac{A_{mix}}{\delta}(P_2 - P_*) + \frac{B_i}{\delta}(P_{i,*}^2 - P_{i,3}^2) + \frac{B_j}{\delta}(P_{j,*}^2 - P_{j,3}^2) \tag{5.12}$$

The total mass flux can then be written by

$$W_{total} = \left[\frac{A_{mix}}{\delta}(P_2 - P_*) + \frac{B_i}{\delta}(P_{i,*}^2 - P_{i,3}^2) + \frac{B_j}{\delta}(P_{j,*}^2 - P_{j,3}^2)\right] \times (M_i Y_{i,3} + M_j Y_{j,3}) \tag{5.13}$$

If evaporation is assumed to occur at the pore inlet so that the pore is filled with vapor, the first term in equation. (5.13) can be eliminated and thus the equation will be reduced to

$$W_{total} = \left[\frac{B_i}{\delta}(P_{i,*}^2 - P_{i,3}^2) + \frac{B_j}{\delta}(P_{j,*}^2 - P_{j,3}^2) \right] \times (M_i Y_{i,3} + M_j Y_{j,3}) \tag{5.14}$$

The mole fraction of the i^{th} component at the permeate side can be represented by equation (5.15)

$$Y_{i,3} = \frac{Q_{i,vapor}}{Q_{i,vapor} + Q_{j,vapor}} = \frac{(P_{i,*}^2 - P_{i,3}^2)}{(P_{i,*}^2 - P_{i,3}^2) + \frac{B_j}{B_i}(P_{j,*}^2 - P_{j,3}^2)} \tag{5.15}$$

5.2.2 Modified Pore-flow model

The concept and general assumptions of the pore-flow model as aforementioned in Section 5.2.1 are still applicable in the modified pore-flow model. The difference, however, is that the modified pore-flow model includes the contribution of Knudsen flow in the vapor transport while the pore-flow model neglects it. The original pore-flow model is limited to the case of membranes with small pores in the range of Angstrom up to 1.5 nm [23]. In such case, the negation of Knudsen flow is possible. However, in this study, the modified pore-flow model is proposed to describe the mass transport at larger pore sizes where the Knudsen flow may be more dominant. In other words, the interaction between vapor and pore wall contributed from the Knudsen

mechanism cannot be neglected. The importance of Knudsen flow will be further discussed in the results and discussion section.

The molar flux contributed from the Knudsen diffusion can be expressed as

$$Q_{Knudsen} = \frac{C}{\delta_b}(P_* - P_3) \qquad where \quad C = \frac{2}{3}\left(\frac{8RT}{\pi M}\right)^{1/2} \frac{\pi r^3 N_t}{RT} \tag{5.16}$$

Then the vapor transport is the total sum of surface flow and Knudsen flow contributions and as follows:

$$Q_{vapor} = Q_{surface} + Q_{Knudsen} \tag{5.17}$$

$$Q_{vapor} = \frac{B}{\delta_b}(P_*^2 - P_3^2) + \frac{C}{\delta_b}(P_* - P_3) \tag{5.18}$$

Similar to the derivation of equations (5.5) and (5.6), the total molar flux can be expressed as

$$Q_{total} = \frac{A}{\delta}(P_2 - P_*) + \frac{B}{\delta}(P_*^2 - P_3^2) + \frac{C}{\delta}(P_* - P_3) \qquad when \quad P_3 < P_* \tag{5.19}$$

$$Q_{total} = \frac{A}{\delta}(P_2 - P_3) \qquad when \quad P_3 \geq P_* \tag{5.20}$$

The ratio of the length of the liquid-filled portion and of the length of the vapor-filled portion to entire length of membrane pore can be expressed by equations. (5.21) and (5.22), respectively

$$\frac{\delta_a}{\delta} = \frac{\frac{A}{\delta}(P_2 - P_*)}{\frac{A}{\delta}(P_2 - P_*) + \frac{B}{\delta}(P_*^2 - P_3^2) + \frac{C}{\delta}(P_* - P_3)} \tag{5.21}$$

$$\frac{\delta_b}{\delta} = \frac{\frac{B}{\delta}(P_*^2 - P_3^2) + \frac{C}{\delta}(P_* - P_3)}{\frac{A}{\delta}(P_2 - P_*) + \frac{B}{\delta}(P_*^2 - P_3^2) + \frac{C}{\delta}(P_* - P_3)} \tag{5.22}$$

For a binary system, the liquid transport can still be expressed by equation (5.9) whereas the vapor transports for the components *i* and *j* are expressed by equations (5.23) and (5.24), respectively.

$$Q_{i,vapor} = \frac{B_i}{\delta_b}(P_{i,*}^2 - P_{i,3}^2) + \frac{C_i}{\delta_b}(P_{i,*} - P_{i,3}) \tag{5.23}$$

$$Q_{j,vapor} = \frac{B_j}{\delta_b}(P_{j,*}^2 - P_{j,3}^2) + \frac{C_j}{\delta_b}(P_{j,*} - P_{j,3}) \tag{5.24}$$

Therefore, the total molar flux for a two-component system can be represented as

$$Q_{total} = \frac{A_{mix}}{\delta}(P_2 - P_*) + \frac{B_i}{\delta}(P_{i,*}^2 - P_{i,3}^2) + \frac{C_i}{\delta}(P_{i,*} - P_{i,3}) + \frac{B_j}{\delta}(P_{j,*}^2 - P_{j,3}^2) + \frac{C_j}{\delta}(P_{j,*} - P_{j,3}) \tag{5.25}$$

And the total weight flux can be written by

$$W_{total} = \left[\begin{array}{l} \frac{A_{mix}}{\delta}(P_2 - P_*) + \frac{B_i}{\delta}(P_{i,*}^2 - P_{i,3}^2) + \frac{C_i}{\delta}(P_{i,*} - P_{i,3}) + \\ \frac{B_j}{\delta}(P_{j,*}^2 - P_{j,3}^2) + \frac{C_j}{\delta}(P_{j,*} - P_{j,3}) \end{array} \right] \times \left(M_i Y_{i,3} + M_j Y_{j,3}\right) \tag{5.26}$$

When evaporation takes place at the pore inlet, the first term of the right-hand side in equation (5.26) can be eliminated and the total weight flux can be rewritten as

$$W_{total} = \left[\begin{array}{l} \frac{B_i}{\delta}(P_{i,*}^2 - P_{i,3}^2) + \frac{C_i}{\delta}(P_{i,*} - P_{i,3}) + \frac{B_j}{\delta}(P_{j,*}^2 - P_{j,3}^2) + \\ \frac{C_j}{\delta}(P_{j,*} - P_{j,3}) \end{array} \right] \times \left(M_i Y_{i,3} + M_j Y_{j,3}\right) \tag{5.27}$$

The mole fraction of the i^{th} component at the permeate side can be expressed as

$$Y_{i,3} = \frac{\frac{B_i}{\delta}(P_{i,*}^2 - P_{i,3}^2) + \frac{C_i}{\delta}(P_{i,*} - P_{i,3})}{\frac{B_i}{\delta}(P_{i,*}^2 - P_{i,3}^2) + \frac{C_i}{\delta}(P_{i,*} - P_{i,3}) + \frac{B_j}{\delta}(P_{j,*}^2 - P_{j,3}^2) + \frac{C_j}{\delta}(P_{j,*} - P_{j,3})} \tag{5.28}$$

Tables 5.2 and 5.3 summarize all equations derived from both the pore-flow and the modified pore-flow models for pure and binary systems, respectively. As shown in Tables 5.2 and 5.3, the focus of this study utilizes water and ethanol as the i^{th} and j^{th} components respectively for the investigation of the newly developed pore-flow model in pervaporation membranes.

Table 5.2 Comparison of the equations derived from pore-flow and modified pore-flow models for a pure system

Pore-flow model	Modified pore-flow model
Pure system • Total molar flux	
$Q_{total} = Q_{liquid} + Q_{vapor}$	$Q_{total} = Q_{liquid} + Q_{vapor}$
$Q_{total} = Q_{liquid} + Q_{surface}$	$Q_{total} = Q_{liquid} + Q_{surface} + Q_{knudsen}$
$Q_{total} = \frac{A}{\delta}(P_2 - P_*) + \frac{B}{\delta}(P_*^2 - P_3^2)$ when $P_3 < P_*$	$Q_{total} = \frac{A}{\delta}(P_2 - P_*) + \frac{B}{\delta}(P_*^2 - P_3^2) + \frac{C}{\delta}(P_* - P_3)$ when $P_3 < P_*$
$Q_{total} = \frac{A}{\delta}(P_2 - P_3)$ when $P_3 \geq P_*$	$Q_{total} = \frac{A}{\delta}(P_2 - P_3)$ when $P_3 \geq P_*$
• The ratio of the length of the liquid-filled portion to the entire pore length	
$\frac{\delta_a}{\delta} = \frac{\frac{A}{\delta}(P_2 - P_*)}{\frac{A}{\delta}(P_2 - P_*) + \frac{B}{\delta}(P_*^2 - P_3^2)}$	$\frac{\delta_a}{\delta} = \frac{\frac{A}{\delta}(P_2 - P_*)}{\frac{A}{\delta}(P_2 - P_*) + \frac{B}{\delta}(P_*^2 - P_3^2) + \frac{C}{\delta}(P_* - P_3)}$
• The ratio of the length of the vapor-filled portion to the entire pore length	
$\frac{\delta_b}{\delta} = \frac{\frac{B}{\delta}(P_*^2 - P_3^2)}{\frac{A}{\delta}(P_2 - P_*) + \frac{B}{\delta}(P_*^2 - P_3^2)}$	$\frac{\delta_b}{\delta} = \frac{\frac{B}{\delta}(P_*^2 - P_3^2) + \frac{C}{\delta}(P_* - P_3)}{\frac{A}{\delta}(P_2 - P_*) + \frac{B}{\delta}(P_*^2 - P_3^2) + \frac{C}{\delta}(P_* - P_3)}$

Table 5.3 Comparison of the equations derived from pore-flow and modified pore-flow models for a binary system

Pore-flow model	Modified pore-flow model
Binary system	
• Total molar flux	
$Q_{total} = \frac{A_{mix}}{\delta}(P_2 - P_*) + \frac{B_w}{\delta}(P_{w,*}^2 - P_{w,3}^2) + \frac{B_e}{\delta}(P_{e,*}^2 - P_{e,3}^2) \quad when\ P_3 < P_*$	$Q_{total} = \frac{A_{mix}}{\delta}(P_2 - P_*) + \frac{B_w}{\delta}(P_{w,*}^2 - P_{w,3}^2) + \frac{C_w}{\delta}(P_{w,*} - P_{w,3}) + \frac{B_e}{\delta}(P_{e,*}^2 - P_{e,3}^2) + \frac{C_e}{\delta}(P_{e,*} - P_{e,3}) \quad when P_3 < P_*$
$Q_{total} = \frac{A_{mix}}{\delta}(P_2 - P_3) \quad when\ P_3 \geq P_*$	$Q_{total} = \frac{A_{mix}}{\delta}(P_2 - P_3) \quad when\ P_3 \geq P_*$
• The mole fraction of water in permeate side, $Y_{w,3}$	
$Y_{w,3} = \frac{Q_{w,vapor}}{Q_{w,vapor} + Q_{e,vapor}}$	$Y_{w,3} = \frac{Q_{w,vapor}}{Q_{w,vapor} + Q_{e,vapor}}$
$Y_{w,3} = \frac{(P_{w,*}^2 - P_{w,3}^2)}{(P_{w,*}^2 - P_{w,3}^2) + \frac{B_e}{B_w}(P_{e,*}^2 - P_{e,3}^2)}$	$Y_{w,3} = \frac{\frac{B_w}{\delta}(P_{w,*}^2 - P_{w,3}^2) + \frac{C_w}{\delta}(P_{w,*} - P_{w,3})}{\frac{B_w}{\delta}(P_{w,*}^2 - P_{w,3}^2) + \frac{C_w}{\delta}(P_{w,*} - P_{w,3}) + \frac{B_e}{\delta}(P_{e,*}^2 - P_{e,3}^2) + \frac{C_e}{\delta}(P_{e,*} - P_{e,3})}$
• Total mass flux in permeate side, W_{total}	
Without A_{mix}	
$W_{total} = \left[\frac{B_w}{\delta}(P_{w,*}^2 - P_{w,3}^2) + \frac{B_e}{\delta}(P_{e,*}^2 - P_{e,3}^2)\right] \times (M_w Y_{w,3} + M_e Y_{e,3})$	$W_{total} = \left[\frac{B_w}{\delta}(P_{w,*}^2 - P_{w,3}^2) + \frac{C_w}{\delta}(P_{w,*} - P_{w,3}) + \frac{B_e}{\delta}(P_{e,*}^2 - P_{e,3}^2) + \frac{C_e}{\delta}(P_{e,*} - P_{e,3})\right] \times (M_w Y_{w,3} + M_e Y_{e,3})$
With A_{mix}	
$W_{total} = \left[\frac{A_{mix}}{\delta}(P_2 - P_*) + \frac{B_w}{\delta}(P_{w,*}^2 - P_{w,3}^2) + \frac{B_e}{\delta}(P_{e,*}^2 - P_{e,3}^2)\right] \times (M_w Y_{w,3} + M_e Y_{e,3})$	$W_{total} = \left[\frac{A_{mix}}{\delta}(P_2 - P_*) + \frac{B_w}{\delta}(P_{w,*}^2 - P_{w,3}^2) + \frac{C_w}{\delta}(P_{w,*} - P_{w,3}) + \frac{B_e}{\delta}(P_{e,*}^2 - P_{e,3}^2) + \frac{C_e}{\delta}(P_{e,*} - P_{e,3})\right] \times (M_w Y_{w,3} + M_e Y_{e,3})$

5.3 Experimental

5.3.1 Polymer dope preparation and hollow fiber fabrication

PVDF was dissolved in NMP up to a concentration of 15 wt% for the preparation of the polymer dope. To ensure complete dissolution of PVDF in NMP, the solution was stirred continuously at 60 °C for 24 h. In this work, the PVDF hollow fiber membranes were fabricated by the dry-jet wet spinning process as described in Chapter 3. The spinning parameters and conditions of PVDF hollow fiber membranes are listed in Table 5.4.

Table 5.4 Spinning parameters and conditions of PVDF hollow fiber membranes

Spinning parameters	Conditions
Dope composition (wt%)	Kynar HSV 900/NMP 15/85
Bore fluid solution (wt%)	NMP/DI Water 95/5
Dope flow rate (ml min^{-1})	2.0
Bore flow rate (ml min^{-1})	0.6
Air gap length (cm)	1.0
Take up speed (m min^{-1})	Free flow (2.0 m min^{-1})
External coagulant	Tap Water
Experiment temperature (°C)	Ambient (25±1)
Spinneret dimension (mm)	OD = 1.2, ID = 0.8, L = 5.0
Post treatment	Freeze dried for 24 h

5.3.2 Pervaporation study

In this study, three modules were examined for each pervaporation condition. Two liters of an ethanol/water mixture was used as the feed solution with a recirculation rate of 30 l h^{-1}. The operating temperature was maintained at 40 °C throughout the

experiment. The details of pervaporation set-up and other operating procedures can be found in Chapter 3.

5.4 Results and discussion

5.4.1 Membrane characterization

The typical morphology of PVDF hollow fiber membranes is shown in Figure 5.2. It can be observed from the overall cross-section SEM image (Figure 5.2a) that the spun hollow fiber membrane has an asymmetric structure comprising of a thicker substrate with a finger-like macrovoid structure and a thinner skin with a relatively dense structure. The inner surface (Figure 5.2b) of the hollow fiber has a porous structure which is desirable for minimizing the substructure resistance [38]. In contrast, the outer surface (Figure 5.2c) is relatively dense and apparently has small voids or defects (formed at the edge of nodules) distributed on the rough surface and these voids or defects can be regarded as pores on the membrane surface.

Furthermore, as illustrated in Figures 5.2d and 5.2e, it can be observed that there is a layer of small voids lying beneath the dense skin and the penetration of voids through the top skin layer can be observed at high magnifications (Figure 5.2d). Interestingly, this structural feature coincides with the conceptual structure in the viewpoint of the pore-flow model. As shown in Figure 5.2c, the pore size at the outer surface cannot be observed clearly from the FESEM images even at a high magnification (x 50,000). Moreover, pore characterization using FESEM can be misleading due to interference generated by the platinum-coating step [39].

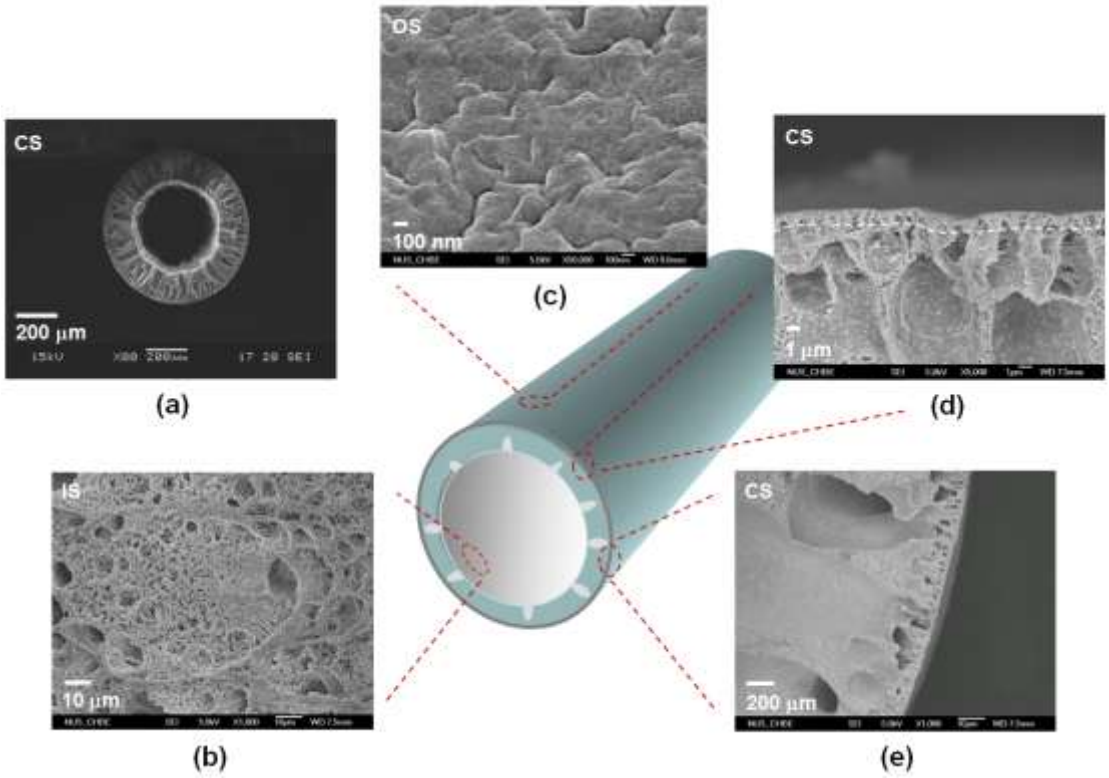

Figure 5.2 SEM and FESEM images of hollow fiber membranes (a) overall cross-section (b) inner surface (c) outer surface (d) partial cross-section at high magnification (e) partial cross-section at low magnification (CS = cross-section, OS = outer surface, IS = inner surface).

Therefore, gas permeation tests and measurements using the porometer were carried out in this study to characterize the pore size. The information on pore size is tabulated in Table 5.5 which includes the maximum pore size, mean pore size and effective surface porosity of PVDF hollow fiber membranes.

Table 5.5 Mean pore size, maximum pore size and effective surface porosity of PVDF hollow fiber membranes

Membrane	Porometer		Gas permeation test	
	Maximum Pore size, r_{max} (at the bubble point) (μm)	Mean pore size, r (μm)	Mean pore size, r (μm)	Effective surface porosity, ε_s/δ (m^{-1})
PVDF hollow fiber membranes	0.0775	0.0659	0.0523	3.31×10^4

From the result, the mean pore size determined from gas permeation method is 0.0523 μm. It is of the same order of magnitude as the mean pore size (0.0659 μm) and the maximum pore size (0.0775 μm) determined using the porometer. The effective surface porosity, which is related to the number of pores on the surface membrane, is 3.31×10^4 m^{-1}. The contact angle at the outer surface of hollow fiber membranes is 87.4±2°, which is consistent with those reported in the literature [40]. The high contact angle (~90°) value reflects the high hydrophobicity of PVDF membranes.

5.4.2 Pervaporation of pure water and pure ethanol

The pervaporation experiment was carried out for each individual component as separate pure-component systems to determine the liquid and vapor transport parameters (A/δ, B/δ and C/δ) in the pore-flow model (Equations (5.5) and (5.6)) and the modified pore-flow model (Equations (5.19) and (5.20)). The experimental data for pure water and pure ethanol flux, as illustrated in Figures 5.3 and 5.4 respectively, were obtained from the monitoring of the change in total flux at different downstream pressures.

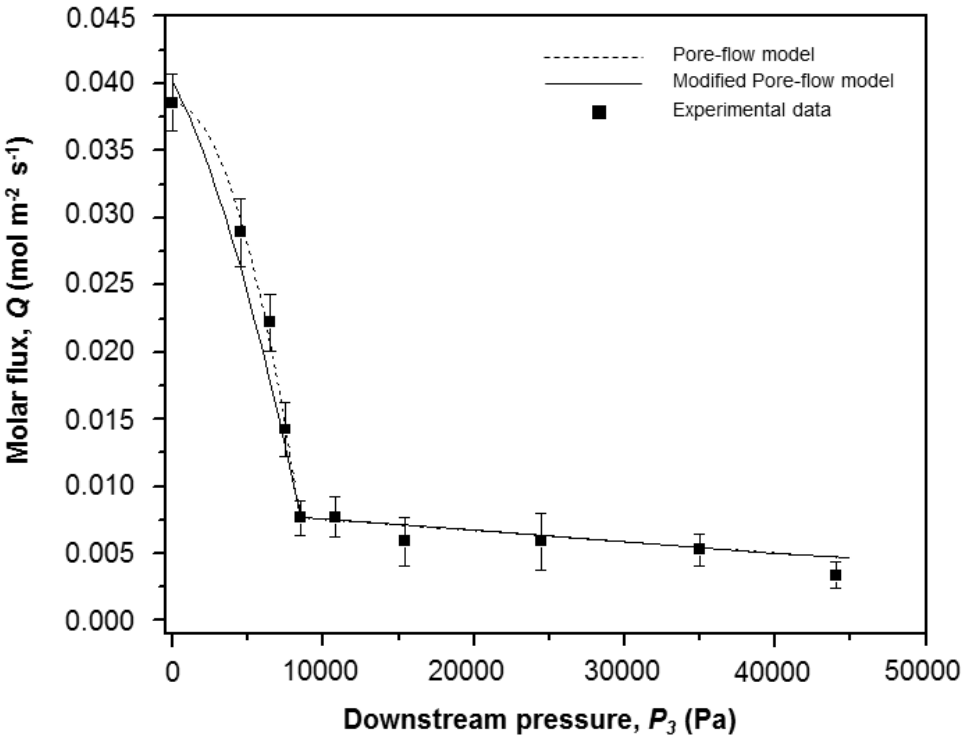

Figure 5.3 Total molar flux at various downstream pressures in the pervaporation of pure water

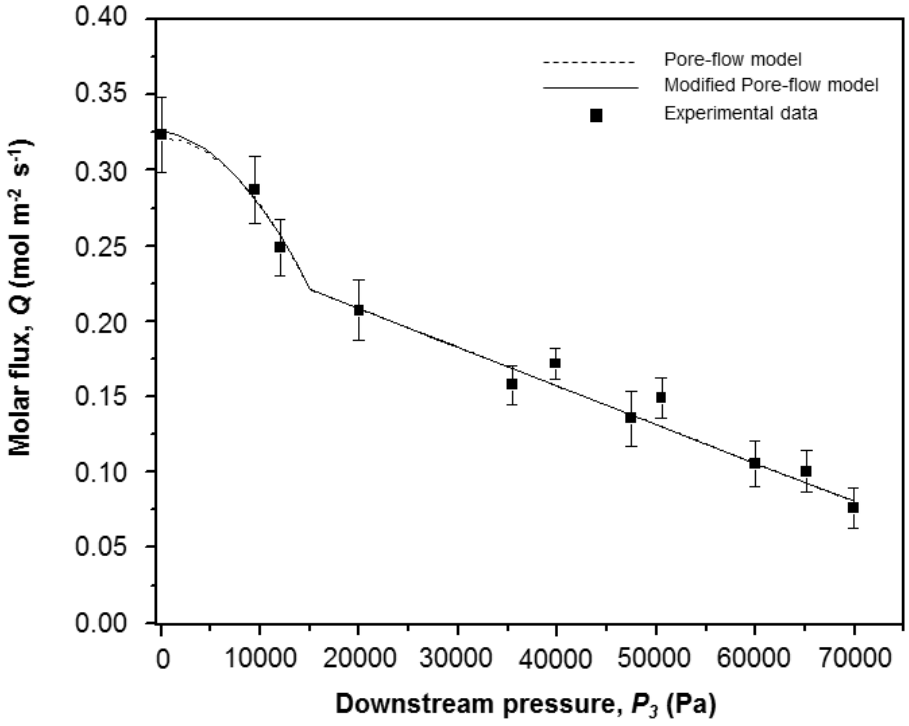

Figure 5.4 Total molar flux at various downstream pressures in the pervaporation of pure ethanol

In both cases it can be seen that the molar flux first decreases parabolically to a point of inflection and then further decreases linearly with an increase in downstream pressure. This is in consistent with the mathematical equations developed by the pore-flow model [24]. The first portion occurring at relatively low downstream pressures reflects the combination of liquid and vapor transport while the second portion occurring at relatively high downstream pressures is predominantly that of liquid transport. Thus, the inflection point corresponds to the saturation vapor pressure of the component.

Figures 5.3 and 5.4 also illustrate the total flux for pure systems calculated on the basis of the pore-flow model (Equations (5.5) and (5.6)) and the modified pore-flow model (Equations (5.19) and (5.20)). The calculations of total flux were done using the liquid and vapor parameters listed in Table 5.6 and all transport parameters A/δ, B/δ, C/δ and P_* were attained by fitting experimental data to the respective models; Equations (5.5) and (5.6) for pore-flow model and equations (5.19) and (5.20) for the modified pore-flow model. The saturation vapor pressures (P_*) used in both models for pure water and pure ethanol were 8500 Pa and 15000 Pa, respectively. These values are in agreement with the saturation vapor pressure of water (7425 Pa) and ethanol (17943 Pa) at 40 °C as calculated by the Antoine equation [41]. In addition, it can be observed that the liquid transport parameters (A/δ) for both water and ethanol obtained by means of the original and modified pore-flow model are the same values while the vapor transport parameters (B/δ, C/δ) are different. The B/δ values in the modified pore-flow model are lower than those in the pore-flow model for both pure component systems. The decreased B/δ values with the additional parameter C/δ reflect the main feature of

the modified pore-flow model which is the addition of the Knudsen diffusion vapor transport.

Table 5.6 Liquid and vapor transport parameters of the pure component system based on the pore-flow model and the modified pore-flow model

Model	Pure component	Parameters in model equations[a]					
		Liquid transport	Vapor transport		Saturation vapor pressure	The ratio[b]	
		A/δ (mol m^{-2} s^{-1} Pa^{-1})	B/δ (mol m^{-2} s^{-1} Pa^{-2})	C/δ (mol m^{-2} s^{-1} Pa^{-1})	P_s (Pa)	δ_d/δ	δ_δ/δ
Pore-flow model	Water	8.25×10^{-8}	4.28×10^{-10}	-	8500	0.20	0.80
	Ethanol	2.56×10^{-6}	4.45×10^{-10}	-	15000	0.69	0.31
Modified pore-flow model	Water	8.25×10^{-8}	1.86×10^{-10}	2.25×10^{-6}	8500	0.19	0.81
	Ethanol	2.56×10^{-6}	3.95×10^{-10}	1.08×10^{-6}	15000	0.68	0.32

[a] refer to equations (5.5) and (5.6) for the pore-flow model and equations (5.19) and (5.20) for the modified pore-flow model, respectively.

[b] refer to equations (5.7) and (5.8) for the pore-flow model and equations (5.21) and (5.22) for the modified pore-flow model, respectively.

Another finding is that the liquid transport parameters for pure water ($A/\delta = 8.25 \times 10^{-8}$) are always lower than those for pure ethanol ($A/\delta = 2.56 \times 10^{-6}$), which may be attributed to the hydrophobic and swelling properties of PVDF hollow fiber membranes. It is clearly observed during the experiment that the fibers showed no swelling in pure water but exhibited high swelling in pure ethanol. The same phenomenon has been reported in previous studies [42]. Based on the observations of membrane swelling; it appears that the liquid transport parameters calculated are also intrinsically influenced by the hydrophobicity and the swelling property of the resulting membrane.

Table 5.6 also tabulates the δ_a/δ and δ_b/δ ratios, which are related to the position where evaporation is taking place in the pore. From the data, there is only a slight difference between the δ_a/δ (or δ_b/δ) calculated using pore-flow or modified pore-flow models. The δ_a/δ ratio for water system (~0.20) is found to be always smaller than the ratio determined for ethanol system (~0.68). This result reveals that in the case for water, the evaporation (liquid-vapor phase boundary) occurs near the pore inlet while in the case for ethanol, the evaporation is shifted further from the pore inlet. This result is in agreement with the observation of pore size expansion due to the influences of hydrophobicity and swelling property of the membrane. In other words, the pore size expansion of membranes under ethanol system causes more liquid to enter the pore before evaporation takes place subsequently.

The transport parameters in both the pore-flow and modified pore-flow models can be used to estimate pore sizes of the membranes, as shown in Table 5.7. The pore size predicted from the liquid transport parameter is lower (4.9×10^{-10} m) in the water system compared to the pore size (6.3×10^{-9} m) predicted in the ethanol system. Hence, this result shows that the pore size and possibly membrane surface morphology change significantly depending on the solvent system. A smaller pore size is estimated from the pure water system resulting from the low interaction between water molecules and PVDF membranes, while a higher pore size is estimated from the pure ethanol system resulting from the strong interaction between the ethanol molecules and the PVDF polymer. The finding is consistent with the Kokugan's studies that hydrophobic membranes preferentially attract ethanol molecules and repel water molecules [43]. In addition, the swelling of the PVDF membrane, as mentioned previously, may be the key reason to account for the overall pore size expansion when it comes in contact with

pure ethanol. Swelling, typically cause the pore size to increase [44] and its effect may be dominant particularly in case of soft or low glass-transition temperature (T_g) polymers (T_g of PVDF is -37 °C). It has to be noted that pore size determination from the B/δ parameter may not be easily calculated due to the unavailability of some fundamental data which are directly involved in the formulation of equation (5.2), like the adsorption layer thickness (t_a) and the adsorption constant (k'_H). Nevertheless, the same trend can be expected.

Table 5.7 Pore size calculated from transport parameters in the pore-flow and modified pore-flow models compared with the pore size obtained from gas permeation tests

Model	Pure component	A/δ (mol m^{-2} s^{-1} Pa^{-1})	r^a (m)	C/δ (mol m^{-2} s^{-1} Pa^{-1})	r^b (m)	r (m) (Gas permeation test)
Pore-flow model	Water	8.25×10^{-8}	4.86×10^{-10}	-		5.23×10^{-8}
	Ethanol	2.56×10^{-6}	6.26×10^{-9}	-		5.23×10^{-8}
Modified pore-flow model	Water	8.25×10^{-8}	4.86×10^{-10}	2.25×10^{-6}	4.37×10^{-10}	5.23×10^{-8}
	Ethanol	2.56×10^{-6}	6.26×10^{-9}	1.08×10^{-6}	3.35×10^{-10}	5.23×10^{-8}

[a] Calculated from $r = \left[\left(\frac{A}{\delta} \right) \frac{8\eta M}{\rho} \frac{1}{(\varepsilon_s / \delta)} \right]^{1/2}$; the detailed derivation of equation and the calculation for water and ethanol systems are given in Appendix A.1

[b] Calculated from $r = \frac{3}{2} \left(\frac{C}{\delta} \right) \left(\frac{\pi M}{8RT} \right)^{1/2} \frac{RT}{(\varepsilon_s / \delta)}$; the detailed derivation of equation and the calculation for water and ethanol systems are given in Appendix A.2

5.4.3 Pervaporation of ethanol/water mixtures

The mole fractions of water in the permeate vapor, $Y_{w,3}$ predicted from equation (5.15) (for the pore-flow model) and equation (5.28) (for the modified pore-flow model) with the transport parameters listed in Table 5.6 are presented in comparison with the experimental data for the pervaporation of ethanol/water mixtures as shown in Figure 5.5.

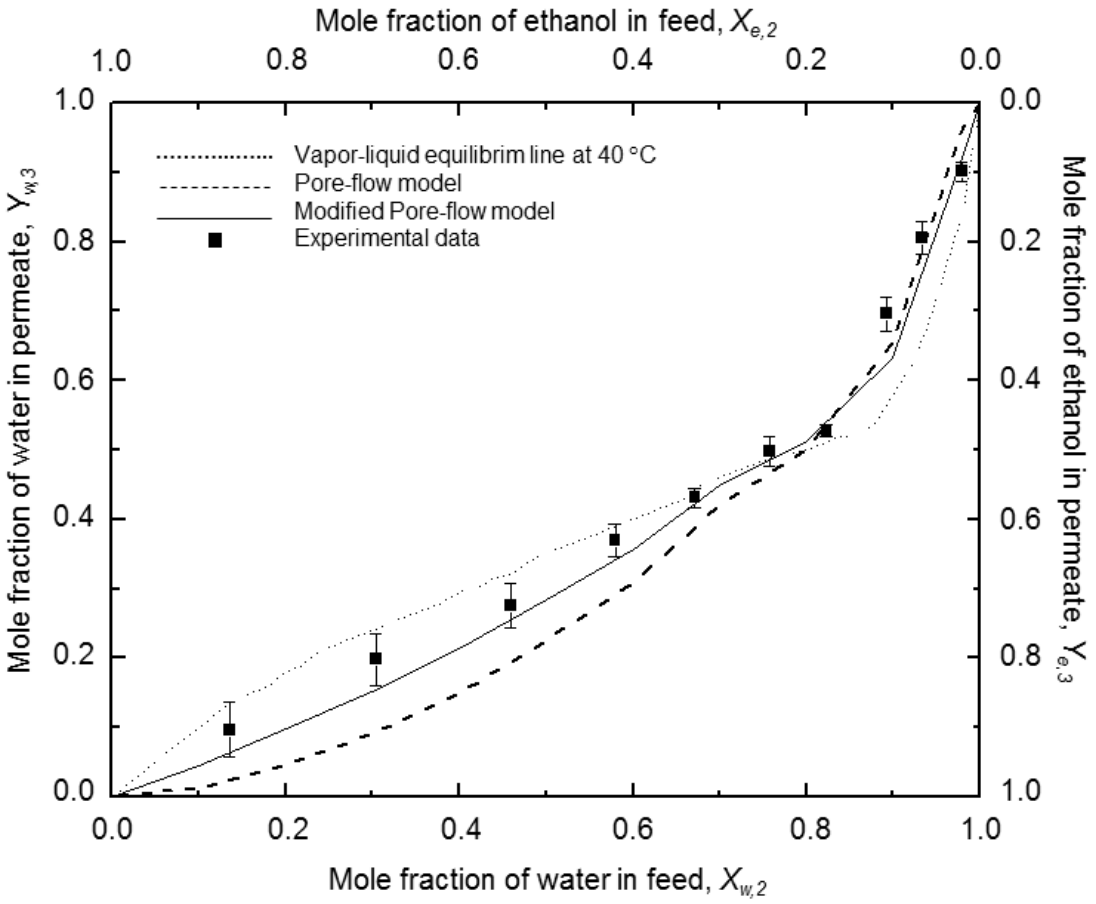

Figure 5.5 Comparison of water mole fraction at the permeate side obtained from experiment with that predicted from pore-flow and modified pore-flow models. Upstream pressure, P_2 = 101325 Pa, Downstream pressure, P_3 = 0 Pa, Temperature = 40 °C.

It can be seen at any point that the water mole fraction in the permeate vapor is lower than the water mole fraction in the feed regardless of the experimental or the predicted data, while on the other hand, the ethanol content in the permeate vapor has been enriched to be greater than any feed ethanol concentration. The curve pattern predicted from both models is similar to that reported for ethanol-selective membranes in Okada and coworkers' studies [23]; the curve intersected with the liquid-vapor equilibrium line at the feed mole fraction around 0.8 for the pore-flow model and around 0.75 for the modified pore-flow model. With reference to Figure 5.5, when the water mole fraction in the feed is high ($X_{w,2}$ > 0.75), the data predicted from both pore-flow and

modified pore-flow models are acceptable in line with the experimental data. However, when the water mole fraction in the feed is lower than 0.75 ($X_{w,2}$ < 0.75), the data predicted by the pore-flow model shows an obvious deviation from experimental data while the one predicted by the modified pore-flow model still shows a satisfactory correlation with the experimental data. Therefore, the modified pore-flow model can be said to provide a better prediction of the permeate composition compared to the pore-flow model.

Figure 5.6 demonstrates the total mass flux at the permeate side, W_{total}, as a comparison between the data predicted from the pore-flow model and the modified pore-flow model with the data obtained experimentally. Overall, the total mass flux gradually decreases with an increase in water mole fraction in the feed mixture. This trend has been reported in earlier studies for ethanol-selective membranes [37]. Moreover, the total mass flux calculated without the liquid transport parameter (A_{mix}/δ) using equation (5.14) for the pore-flow model or equation (5.27) for the modified pore-flow model fails to correlate with the experimental data satisfactorily. On the other hand, there is an excellent agreement between the experimental data and the data calculated using equation (5.13) and equation (5.26) when the A_{mix}/δ term is included for both the pore-flow and modified pore-flow models. This situation indicates that the assumption of the evaporation occurring at the pore inlet for the negation of the liquid transport parameter (A_{mix}/δ), which has been commonly used to predict the total flux in previous studies [45], is not necessarily applicable to the PVDF hollow fiber membranes utilized in this study. This discrepancy may be due to the fact that most membranes used in earlier studies [23,37,42,45] possess mean pore sizes of less than 15 Å while the membrane pore sizes in this study are in the scale of nanometers.

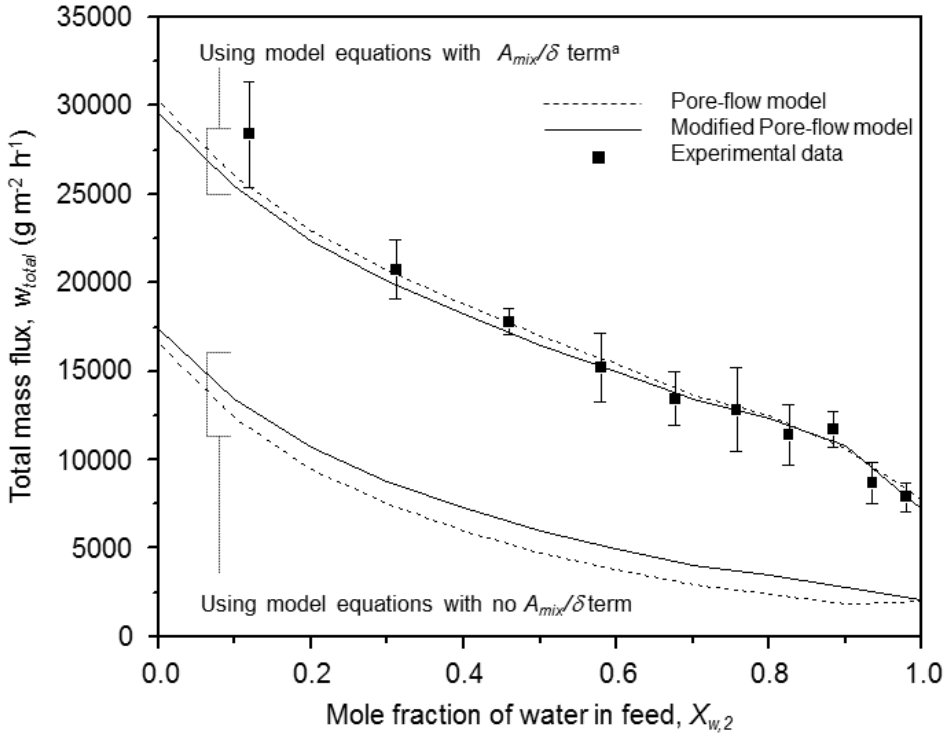

[a] A_{mix}/δ = 9.56 x 10^{-7} mol m^{-2} s^{-1} Pa^{-1} for the pore-flow model and A_{mix}/δ = 8.53 x 10^{-7} mol m^{-2} s^{-1} Pa^{-1} for the modified pore-flow model; The calculation of A_{mix}/δ with the respective models is given in Appendix A.3

Figure 5.6 Comparison of total mass flux obtained from experiment with that predicted from pore-flow and modified pore-flow models. Upstream pressure, P_2 = 101325 Pa, Downstream pressure, P_3 = 0 Pa, Temperature = 40 °C.

The δ_a/δ ratio as mentioned previously can also be used to support the result. Since the ratios (δ_a/δ = 0.20 for water, δ_a/δ = 0.68 for ethanol) are not equal to zero, it implies that the evaporation of ethanol/water mixture takes place between the δ_a/δ ratio varying from 0.20 to 0.68. Thus, there may be a more dominant effect of liquid transport in membranes with a larger pore size, while liquid transport in membranes with smaller pore sizes may be negligible. In addition, at a low water mole fraction in feed ($X_{w,2}$ < 0.10), the predicted data deviates more from the experimental data and this may be attributed to the greater swelling of fibers in high ethanol contents.

The modified pore-flow model offers a more accurate prediction of the composition of the permeate as well as the total mass flux for PVDF hollow fiber membranes. As discussed above, experimental results have proven that the absence of Knudsen flow in the pore-flow model is adequately applicable for predicting the mass transport of such membranes with a small pore size typically in the Angstrom region. However, a significant contribution of Knudsen flow in vapor transport, as stated in the modified pore-flow model, cannot be neglected for the membrane with a larger pore size roughly in nano- or sub-micro regions like PVDF asymmetric hollow fiber membranes employed in this study.

Another support for the contribution of Knudsen gas flow mechanism in our proposed modified pore-flow model may be considered from the gas transport in porous membranes which arises principally from Knudsen and viscous flow patterns [46]. Figure 5.7 shows the contributions of Knudsen flow, viscous flow and surface flow mechanisms to the molar flux at various membrane pore sizes. The Knudsen flow and viscous flow are calculated based on their definitions with the appropriate parameters and conditions of water as used in this pervaporation study, whereas the surface flow is acquired from the experiment. The water system is chosen for the consideration of calculating the Knudsen and viscous parameters in order to neglect the effect of swelling of membranes in ethanol, which was found to cause serious deviations between the predicted model data and the experimental data. Considering the molar flux at membrane pore sizes of 4.4-4.9 $x10^{-10}$ m obtained from liquid and vapor transport parameters in water system (referred to Table 5.7), it can be observed that the molar flux calculated from Knudsen flow is comparable to the molar flux estimated from surface flow and its effect cannot be ignored, while the viscous flow can be

regarded as a minor effect. Therefore, this feature also supports the postulation that there should be a coupling effect of Knudsen and surface flows, as proposed in the modified pore-flow model.

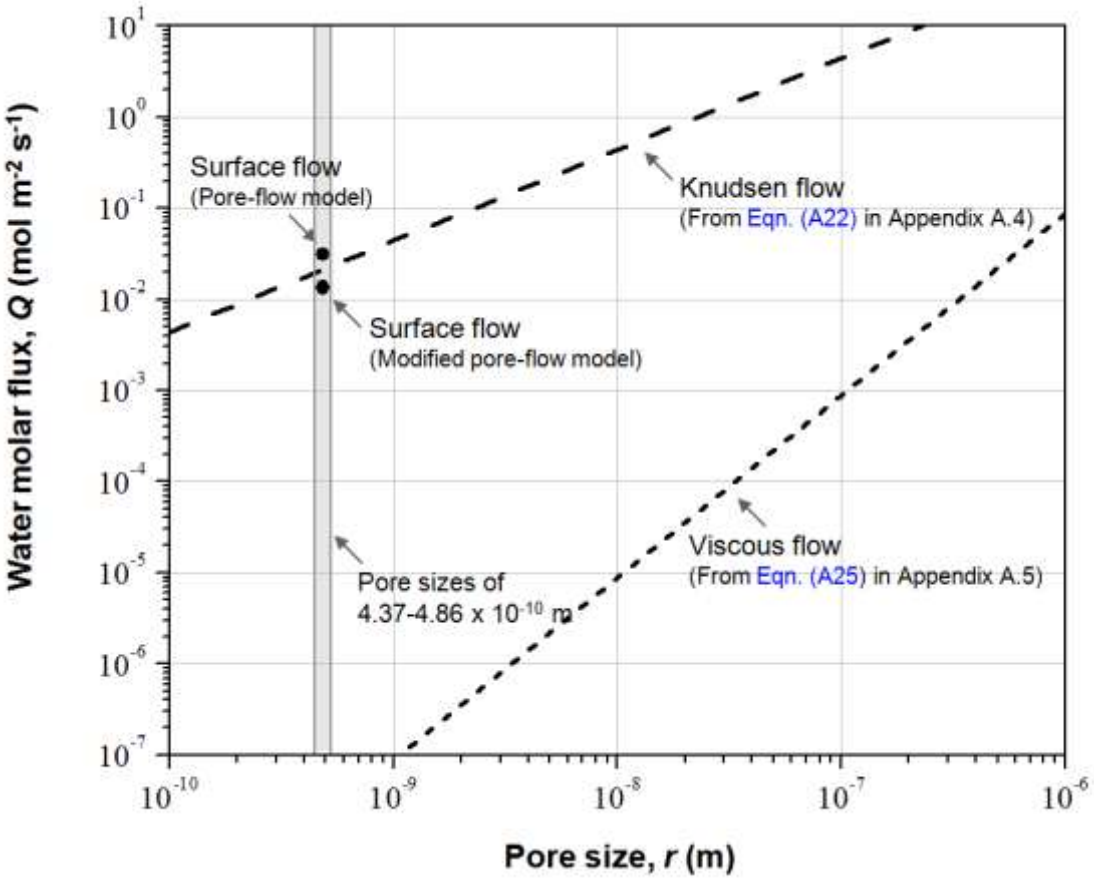

Figure 5.7 The contribution of various gas flow mechanisms to the molar flux at different membrane pore sizes.

We have demonstrated that the modified pore-flow model is preferred for predicting the pervaporation performance for membranes possessing a large pore size with an expected low selectivity through the use of PVDF hollow fiber membranes with a sub micron pore size. The model is also expected to apply for membranes with good selectivity. As discussed previously, the unique feature of the modified pore-flow model from the original pore-flow is the inclusion of Knudsen flow contribution in

vapor transport, a dominant mechanism for membranes possessing a large pore size with an expected low selectivity. In other words, the modified pore-flow model in this study is an extension to the original pore-flow model proposed by Okada and Matsuura [23] but covers a wider spectrum of pores. For membranes with a higher selectivity, which usually consist of tiny or small pore size, the influence of Knudsen flow contribution in the modified pore-flow model can be neglected and the model transport equations will be reduced to be the same form as the pore-flow model. The predictability of pore-flow model has been proven through many previous studies [37, 42, 45] using membranes with a high selectivity made of different membrane materials (typical pore size is < 1.5 nm) in various pervaporation applications.

The modified pore flow model offers several advantages over the original pore flow model as follows; (1) the model exhibits a better prediction for the permeate compositions as well as the total mass flux for membranes with a larger pore size, (2) since the contribution of Knudsen flow is incorporated, the model is applicable to describe the transition gap between pervaporation and membrane distillation (the surface flow is prevailing in membrane pervaporation while the Knudsen flow is prevailing in membrane distillation) and (3) the model is principally valid for membranes with a wider range of pore size.

5.5 Conclusions

The pore-flow model and the modified pore-flow model have been applied to analyze the mass transport in the pervaporation of ethanol/water mixtures through PVDF hollow

fiber membranes with a sub-micron pore size. Based on the results and observations in this study, the following conclusions can be drawn:

(1) The curve characteristic in the pervaporation of pure water and pure ethanol verifies with the mass transport concept of pore-flow model. Each curve consists of two segments: the curved portion corresponds to the combination of liquid and vapor transports, while the straight line portion corresponds to liquid transport. The inflection point corresponds to the saturation vapor pressure of the component.

(2) All liquid and vapor transport parameters (A/δ), B/δ, C/δ) presented in the pore-flow model and the modified pore-flow model are obtained by fitting experimental data from the pure component experiments to the transport equations in the respective models. The large difference in liquid transport parameters (A/δ) for water and ethanol systems may be attributed to the hydrophobicity and the swelling property of PVDF membranes.

(3) The pore size estimated from the liquid transport parameter is smaller (4.9×10^{-10} m) in the water system and bigger (6.3×10^{-9} m) in the ethanol system. This trend supports that the pore size as well as membrane surface morphology change significantly depending on the solvent system in contact.

(4) The modified pore-flow model demonstrates a better prediction for the permeate composition than the pore-flow model particularly at relatively low water content in feed. Both models demonstrate an excellent prediction in the total

weight flux once the liquid transport parameter for a binary component (A_{mix}/δ) is incorporated.

(5) The unique feature of the modified pore-flow model from the pore-flow model is the inclusion of Knudsen flow contribution to the vapor transport. The significance of Knudsen flow is further substantiated from the theoretical viewpoint when comparing the effects of Knudsen, viscous and surface flows to permeation flux at different pore sizes.

REFERENCES

[1] H.L. Fleming, C.S. Slater, Pervaporation, in: W.S. Ho, K.K. Sirkar (Eds.), Membrane handbook, Kluwer Academic Publishers, New York, 1992, p. 103.

[2] P.A. Kober, Pervaporation, perstillation and percrystallization, J. Am. Chem. Soc. 39 (1917) 944-948.

[3] L. Farber, Application of pervaporation, Science 82 (1935) 158.

[4] R.C. Binning, R.J. Lee, J.F. Jennings, E.C. Martin, Separation of liquid mixtures by permeation, Ind. Eng. Chem. 53 (1961) 45-50.

[5] L.Y. Jiang, Y. Wang, T.S. Chung, X.Y. Qiao, J.Y. Lai, Polyimides membranes for pervaporation and biofuels separation, Prog. Polym. Sci. 34 (2009) 1135-1160.

[6] L.M. Vane, A review of pervaporation for product recovery from biomass fermentation processes, J. Chem. Technol. Biotechnol. 80 (2005) 603-629.

[7] B. Smitha, D. Suhanya, S. Sridhar, M. Ramakrishna, Separation of organic-organic mixtures by pervaporation-A review, J. Membr. Sci. 241 (2004) 1-21.

[8] F. Xiangli, Y. Chen, W. Jin, N. Xu, Polydimethylsiloxane (PDMS)/ceramic composite membrane with high flux for pervaporation of ethanol-water mixtures, Ind. Eng. Chem. Res. 46 (2007) 2224-2230.

[9] J.G. Wijmans, R.W. Baker, The solution-diffusion model: A review, J. Membr. Sci. 107 (1995) 1-21.

[10] X. Feng, R.Y.M. Huang, Liquid separation by membrane pervaporation: A review, Ind. Eng. Chem. Res. 36 (1997) 1048-1066.

[11] F.W. Greenlaw, R.A. Shelden, E.V. Thompson, Dependence of diffusive permeation rates on upstream and downstream pressures, J. Membr. Sci. 2

(1977) 333-348.

[12] S.J. Doong, W.S. Ho, R.P. Mastondrea, Prediction of flux and selectivity in pervaporation through a membrane, J. Membr. Sci. 107 (1995) 129-146.

[13] M.Y. Teng, K.R. Lee, D.J. Liaw, J.Y. Lai. Preparation and pervaporation performance of poly(3-alkylthiophene) membrane, Polymer 41 (2000) 2047-2052.

[14] C. Vallieres, E. Favre, D. Roizard, J. Bindelle, D. Sacco, New insights into pervaporation mass transport under increasing downstream pressure conditions: critical role of inert gas entrance, Ind. Eng. Chem. Res. 40 (2001) 1559-1565.

[15] W.F. Guo, T.S. Chung, T. Matsuura, Pervaporation study on the dehydration of aqueous butanol solutions: A comparison of flux vs. permeance, separation factor vs. selectivity, J. Membr. Sci. 245 (2004) 199-210.

[16] R. Liu, X. Qiao, T.S. Chung, The development of high perfornance P84 co-polyimide hollow fibers for pervaporation dehydration of isopropanol, Chem. Eng. Sci. 60 (2005) 6674-6686.

[17] X. Qiao, T.S. Chung, Diamine modification of P84 polyimide membranes for pervaporation dehydration of isopropanol, AIChE J. 52 (2006) 3462-3472.

[18] P. Shao, R.Y.M. Huang, Polymeric membrane pervaporation, J. Membr. Sci. 287 (2007) 162-179.

[19] M. Mujiburohman, X. Feng, Permselectivity, solubility and diffusivity of propyl propionate/water mixtures in poly(ether block amide) membranes, J. Membr. Sci. 300 (2007) 95-103.

[20] L.Y. Jiang, T.S. Chung, R. Rajagopalan, Matrimid®/MgO mixed matrix membranes for pervaporation, AIChE J. 53 (2007) 1745-1757.

[21] Y. Wang, L.Y. Jiang, T. Matsuura, T.S. Chung, S.H. Goh, Investigation of the

fundamental differences between polyamide-imide (PAI) and polyetherimide (PEI) membranes for isopropanol dehydration via pervaporation, J. Membr. Sci. 318 (2008) 217-226.

[22] Y. Huang, R.W. Baker, Bioethanol production using pervaporation and vapour permeation membranes, Presentation at International Congress on Membrane and Membrane Process, Honolulu, USA, July 2008.

[23] T. Okada, T. Matsuura, A new transport model for pervaporation, J. Membr. Sci. 59 (1991) 133-149.

[24] R.K. Tyagi, Transport studies in pervaporation, Ph.D. Thesis, University of Ottawa, Ottawa, Canada, 1993.

[25] P.T. Sumesh, P.K. Bhattacharya, Analysis of phase change during pervaporation with single component permeation, Colloids Surf., A, 290 (2006) 263-272.

[26] J.J. Shieh, R.Y.M. Huang, A Pseudophase-change solution-diffusion model for pervaporation I Single component permeation, Sep. Sci. Technol., 33 (1998) 767-785.

[27] J.J. Shieh, R.Y.M. Huang, A Pseudophase-change solution-diffusion model for pervaporation II Binary mixture permeation. Sep. Sci. Technol., 33 (1998) 933-957.

[28] R.W. Baker, Membrane technology and applications, John Wiley & Sons Ltd., New York, 2004.

[29] T. Matsuura, Synthetic Membranes and Membrane Separation Processes, CRC Press, Boca Raton, FL, 1993.

[30] H. Strathmann, K. Kock, The formation mechanism of phase inversion membranes, Desalination 21 (1977) 241-255.

[31] M. Mulder, Basic Principle of Membrane Technology, Khuwer Academic,

Boston, 1996.

[32] M.L. Yeow, Y.T. Liu, K. Li, Morphological study of poly(vinylidene fluoride) asymmetric membranes: Effects of the solvent, additive, and dope temperature, J. Appl. Polym. Sci. 92 (2004) 1782-1789.

[33] K. Jian, P.N. Pintauro, Integral asymmetric poly(vinylidene fluoride) (PVDF) pervaporation membranes, J. Membr. Sci. 85 (1993) 301-309.

[34] K. Jian, P.N. Pintauro, R. Ponangi, Separation of dilute organic/water mixtures with asymmetric poly(vinylidene fluoride) membranes, J. Membr. Sci. 117 (1996) 117-133.

[35] K. Jian, P.N. Pintauro, Asymmetric PVDF hollow-fiber membranes for organic/water pervaporation separations, J. Membr. Sci. 135 (1997) 41-53.

[36] P. Sukitpaneenit, T.S. Chung, Molecular Elucidation of morphology and mechanical properties of PVDF hollow fiber membranes from aspects of phase inversion, crystallization and rheology, J. Membr. Sci. 340 (2009) 192-205.

[37] T. Okada, M. Yoshikawa, T. Matsuura, A study on the pervaporation of ethanol/water mixtures on the basis of pore flow model, J. Membr. Sci. 59 (1991) 151-168.

[38] N. Widjojo, T.S. Chung, W.B. Krantz, A morphological and structural study of Ultem/P84 copolyimide dual-layer hollow fiber membranes with delamination-free morphology, J. Membr. Sci. 294 (2007) 132-146.

[39] D. Li, T.S. Chung, R. Wang, Morphological aspects and structure control of dual-layer asymmetric hollow fiber membranes formed by a simultaneous co-extrusion approach, J. Membr. Sci. 243 (2004) 155-175.

[40] S. Bonyadi, T.S. Chung, Highly porous and macrovoid-free PVDF hollow fiber membranes for membrane distillation by a solvent-dope solution co-extrusion

approach, J. Membr. Sci. 331 (2009) 66-74.

[41] J.M. Smith, H.C. Van Ness, M.M. Abbott, Introduction to Chemical Engineering Thermodynamics, McGraw-Hill, Singapore, 2005.

[42] S. Deng, B. Shiyao, S. Sourirajan, T. Matsuura, A study of the pervaporation of isopropyl alcohol/water mixtures by cellulose acetate membranes, J. Colloid Interface Sci. 136 (1990) 283-291.

[43] T. Kokugan, Kaseno, E. Yoshimoto, H. Kikukawa, A consideration of pervaporation by porous hydrophobic membranes for dilute ethanol solution, J. Chem. Eng. Japan 31 (1998) 153-156.

[44] A. Sharma, S.P. Thampi, S.V. Suggala, P.K. Bhattacharya, Pervaporation from a dense membrane: Roles of permeant-membrane interactions, Kelvin effect, and membrane swelling, Langmuir 20 (2004) 4708-4714.

[45] T. Okada, T. Matsuura, Predictability of transport equations for pervaporation on the basis of pore-flow mechanism, J. Membr. Sci. 70 (1992) 163-175.

[46] K. Li, J.F. Kong, D. Wang, W.K. Teo, Tailor-made asymmetric PVDF hollow fibers for soluble gas removal, AIChE J. 45 (1999) 1211-1219.

CHAPTER SIX

MOLECULAR DESIGN OF THE MORPHOLOGY AND PORE SIZE OF PVDF HOLLOW FIBER MEMBRANES FOR ETHANOL-WATER SEPARATION EMPLOYING THE MODIFIED PORE-FLOW CONCEPT

6.1 Introduction

Escalating population growth, rising energy demand in the modern lifestyle of people, fossil fuel shortages as well as changing climate conditions due to global warming are pressing issues faced by many countries globally. Shifting society's dependence on petroleum oil to alternative energy resources is considered an essential step in developing a sustainable industrial society and effectively controlling greenhouse gas emission. Among several alternative energy resources, Bioethanol, one of the main biofuels, has emerged as one of strategically sustainable fuel sources in many countries as it is renewable, economical and environmentally friendly. In recent years, many developed and developing countries have launched programs and legislation to use bioethanol on a broad scale [1-4]. For instance, ethanol today constitutes about 15% of U.S. gasoline consumption and the ethanol market penetration is predicted to attain up to 53 % of U.S. gasoline demand in 2030 [5].

Bioethanol is typically converted from biomass via a fermentation process. Depending on the choice of biomass sources, microorganism types and hydrolysis procedures, the fermentation process usually produces an ethanol concentration varying from 1 to 15 wt% [6,7]. The relatively low-yield of ethanol in fermentation broths is due to the inhibition of the microorganism's ability by the ethanol produced and accumulated in

the system [8,9]. Thus, in order to meet the standard fuel-grade ethanol (> 99.5 wt% ethanol), a large amount of water of 85-99 wt% needs to be removed. It has been reported that "*this separation and purification stage*" alone accounts for at least 40% (up to 80%) of the entire production cost [10]. To date, a traditional distillation is the dominant refinery separation scheme. However, it may no longer be economical and practical as the principal operation for biofuel separation and purification because of its high energy intensive nature.

A promising alternative separation process to distillation is pervaporation. It utilizes a membrane to separate various liquid mixtures such as dehydration of organic solvents, recovery of organic compounds from aqueous solutions and separation of organic mixtures [11-15]. Some of the benefits of this membrane-based separation technique over distillation are low energy consumption, minimum contamination and compact operation unit space. The advantages of pervaporation over a simple distillation process for recovering ethanol from fermentation broths or dilute mixtures are recently reviewed by Vane [16]. In terms of energy efficiency, pervaporation is able to compete with a standard distillation, especially in a cellulosic ethanol process (and/or other non-food biomass) in which the ethanol content in broths is relatively low. In addition, the unique advantage of pervaporation includes the potential to be integrated with the existing processes [17-22]. In the recent work by Ding et al. [22], integrating membrane pervaporation with a fermentor resulted in the improvement of ethanol productivity in addition to the benefits of saving energy and having less contaminant products. They employed membranes possessing ethanol-water separation factors of 5-7.2 and fluxes of 300-690 g m^{-2} h^{-1} for the process evaluation. It is expected that membranes with a higher flux could provide better ethanol productivity in the

fermentation process because the ethanol product which becomes an inhibitor for the cells at relatively high concentrations in the broth can be removed constantly.

In principle, two categories of pervaporation membranes that are (1) water-permselective (hydrophilic) membranes and (2) ethanol-permselective (hydrophobic or organophilic) membranes, can be used as a coupled process in series to produce pure ethanol. So far numerous studies have been conducted on the water-permselective membranes and broad range of proficient material candidates are developed for industrial applications [23-25]. Conversely, fewer investigations as well as research and breakthroughs have been performed on the ethanol-permselective membranes. The ethanol-permselective membranes that have been investigated in previous studies are based on hydrophobic elastomeric or rubbery polymers. Polydimethylsiloxane (PDMS), often known as silicone rubber, is the most widely used because it possesses an ethanol-water separation factor ranging from 4.4 to 10.8 [21]. In general, PDMS membranes produce a low permeation flux since the membranes have a relatively dense and symmetric structure. Moreover, several modification attempts; namely, grafting and cross-linking of PDMS with other materials, can only enhance the separation performance marginally yet suffer a significant loss of permeation flux occurred in most cases [21,26]. To overcome the aforementioned drawbacks, PDMS composite membrane comprising a thin layer of PDMS coated on a porous support made of a stronger material, has been developed. However, these membranes require complex fabrication procedures and are lack of chemical and thermal resistance properties [27-28].

Afterward, several attempts have been given for searching other non-elastomeric polymeric materials, which may result in pervaporation membranes with a better separation performance and good thermal, mechanical and chemical stability. Poly [1-(trimethylsilyl)-1-propyne) (PTMSP), a high free volume glassy polymer, has gained much attention as the PTMSP membrane exhibits a higher separation factor and flux than the PDMS membrane [21,29]. However, its unstable performance due to the intrinsic PTMSP properties hindered its development. As a consequence, PDMS or silicone rubber is still regarded as the current benchmark membrane material, which has been known as a representative ethanol- and alcohols-permselective membrane material for the recovery of alcohols from aqueous solutions.

As one of promising polymeric membrane materials for various applications, Poly(vinylidene fluoride) (PVDF) may have great potential in ethanol-water separation due to its outstanding chemical and physical properties. The key advantages of PVDF include its highly hydrophobic nature and excellent chemical resistance [30], which are essential requirements for pervaporation membranes as they come into contact with liquid mixtures. In addition to these superior properties, the ease of fabricating it into hollow fibers via phase inversion process makes PVDF more attractive. Compared to flat-sheet membranes, hollow fiber membranes have the following advantages: (1) a larger membrane area per unit membrane module volume, resulting in a higher permeation flow per unit volume; (2) self-supporting structure, allowing the membrane to be a self-contained vacuum channel where the feed can be supplied from the shell side while vacuum is applied on the lumen side; and (3) good flexibility and ease of handling during module fabrication and system operation. To date, PVDF asymmetric hollow fiber membranes have been explored in diverse membrane-based separation

applications e.g. micro/nano/ultra-filtration [31-32], membrane distillation [33-35], membrane gas absorption [36] and pervaporation [37]. However, relatively lesser studies are devoted to the development of PVDF asymmetric hollow fiber membranes for ethanol-water separation.

It is not an easy task to fabricate asymmetric hollow fiber membrane with a high ethanol-water separation performance. In fact, in-depth understanding in membrane formation is required to design and optimize spinning conditions to achieve membranes with desirable morphology, mechanical integrity and separation performance. Many previous studies on flat sheet and hollow fiber membranes related to PVDF membrane formation proved that there are two competing mechanisms during a membrane formation; (1) liquid-liquid demixing and (2) solid-liquid demixing (accompanying crystallization) [38-42]. Due to its semi-crystalline nature, the solid-liquid demixing accompanying with crystallization always exists but can be significantly suppressed if the phase inversion is rapid enough to favor a liquid-liquid demixing. In hollow fiber spinning, a liquid-liquid demixing results in membranes having a finger-like macrovoids with a cellular microstructure and a relatively dense skin surface as well as a better mechanical strength; whereas a solid-liquid demixing tends to create membranes possessing a macrovoid-free with a globular microstructure and a relatively porous skin surface and a lower mechanical integrity [41]. The former mechanism results in membranes which can potentially be applied for pervaporation while the latter mechanism fails in the initial stage due to its low mechanical strength to stand under the pervaporation operation. Therefore, it is still challenging to fabricate PVDF asymmetric hollow fiber with favorable macrovoid-free structure by means of controlling liquid-liquid demixing in the precipitation. Jian and Pintauro [37]

demonstrated that with the utilization of PVDF/dimethylacetamide (DMAc)/acetone as the polymer solution, water/acetone or water/acetone/DMAc as the bore-fluid, and acetone/water as the coagulation bath, the instantaneous liquid-liquid demixing was enhanced at the inner surface side during membrane formation. The resultant PVDF asymmetric hollow fibers had the inner selective layer with pore sizes varying from 58 to 850 Å. The membranes exhibited an outstanding pervaporation performance in separating very dilute organic compounds, i.e., benzene, toluene, chloroform and butanol from water. Nonetheless, the fabrication method is complicated since it requires a multi-component (polymer/solvent/non-solvent) polymer dope and a high-volatile non-solvent component external coagulation bath. On the other hand, it would be interesting and more challenging if the PVDF asymmetric hollow fiber with a macrovoid-free structure comprising a cellular sponge-like structure made of liquid-liquid demixing controlling can be achieved from using a binary component (polymer/solvent) dope and water used as an external coagulant, which are preferable in industrial-scale fabrication because of high dope stability, low cost and environmental friendly [43]. Alternatively, the roles of bore-fluid, air-gap distance and take-up speed on membrane formation and pervaporation performance, which have yet explored in our previous studies and rarely discussed in the open literature, are attractive.

Recently, we explored and reported preliminary result on the pervaporation performance of PVDF hollow fibers for ethanol-water separation [44]. The membrane possessing a pore size of 50-66 nm exhibited a separation factor of 5 and a total permeation flux of 8,000 g m^{-2} h^{-1} at 5 wt% ethanol feed solution at 40 °C. The separation performance characteristic of the PVDF hollow fibers reported can be

attributed to the large surface pore size and effective surface porosity (pore size distribution) whereby the pervaporation mass transport in the membrane can be satisfactorily predicted via a modified pore-flow model; the smaller the pore size as well as the narrower the pore size distribution lead to better membrane selectivity. In other words, the pore size and pore size distribution could play a crucial role on membrane separation performance. The modified pore-flow could explain the same phenomenon with the consideration of the competing contribution from two vapor transport phenomena namely surface flow and Knudsen flow; at a larger pore, the vapor transport via Knudsen flow is more prevailing rather than surface flow; leading to the enhancement of the permeability but the selectivity is sacrificed [44]. Nevertheless, supporting evidence and understanding on how pore size and pore size distribution really control the contributions of surface and Knudsen flows, and determine the membrane performance are insufficient. This present work may help to provide a better understanding on the physical meaning of the modified pore-flow model.

Therefore, as a continuation to the previous study, the primary objective of this paper is to further study the feasibility on the science of fabricating PVDF asymmetric hollow fiber membranes for ethanol-water separation using the concept of a modified-pore flow model. The desirable PVDF hollow fibers should have the following characteristics: (1) macrovoids-free with a cellular microstructure (2) relatively dense selective skin with a mean pore size lesser than 0.066 μm (as compared to our previous data) (3) porous substructure with minimal transport resistance. A systematic investigation on the effects of bore-fluid compositions, air-gap distances and take-up speeds on membrane morphology and separation performance will be performed to

obtain the optimized conditions for fabricating such membranes. The other aim is to elucidate the influence of pore size and pore size distribution on pervaporation transport from the modified pore-flow model, which has not yet been emphasized previously. A correlation among membrane morphology, pore size, pore size distribution and separation performance with in-depth science will be established. To our best knowledge, our study is a pioneer work not only developing novel PVDF asymmetric hollow fiber membranes for ethanol-water separation, but also elaborating the fundamental science bridging pore size and pore size distribution, and pervaporation characteristics.

6.2 Experimental

6.2.1 Polymer dope composition and spinning condition

The preparation of homogeneous PVDF dope solutions and hollow fiber membranes was based on the method and procedures provided earlier in Chapter 3. Table 6.1 summarizes the spinning parameters and conditions of PVDF hollow fiber membranes in this study, which includes the effect of bore-fluids, air-gap distances and take-up speeds. After spinning, the as-spun hollow fibers were immersed in water for 3 days to ensure thorough removal of residual NMP solvent. Subsequently, the hollow fibers were freeze dried for 24 h before further characterization.

Table 6.1 Spinning parameters and conditions of PVDF hollow fiber membranes

Spinning code	Spinning condition[a]		
	NMP/water bore-fluid composition (wt%)	Air-gap distance (cm)	Take-up speed (m min^{-1})
The effect of bore-fluid compositions			
BF-90	90/10		
BF-70	70/30	1	Free flow
BF-50	50/50		
The effect of air-gap distances			
AG-5		5	
AG-10	70/30	10	Free flow
AG-20		20	
The effect of take-up speeds			
TK-7	70/30	1	7.0
TK-10			10.5

[a] Polymer dope composition: 15 wt% PVDF/NMP; bore-fluid flow rate: 0.6 cm^3 min^{-1}; dope flow rate: 2.0 cm^3 min^{-1}; free flow: ≤ 3.5 m min^{-1}; external coagulant: tap water; spinneret dimensions (OD/ID): 1.2/0.8 mm; external coagulant bath and spinning temperatures: 25 °C; relative humidity: 65%.

6.2.2 Membrane pore size distribution and data analyses

Figure 6.1 illustrates a typical pattern of the pore size distribution obtained from the characterization of the PVDF hollow fiber membrane spun with a mixture of 70/30 wt% NMP/water as the bore-fluid. Two discrete regions can be observed; a lower frequency percentage represents the "large pore region" while a higher frequency percentage represents the "small pore region". All membranes exhibited a similar pore size distribution pattern but differed in pore sizes and percentages of the large and small pore regions.

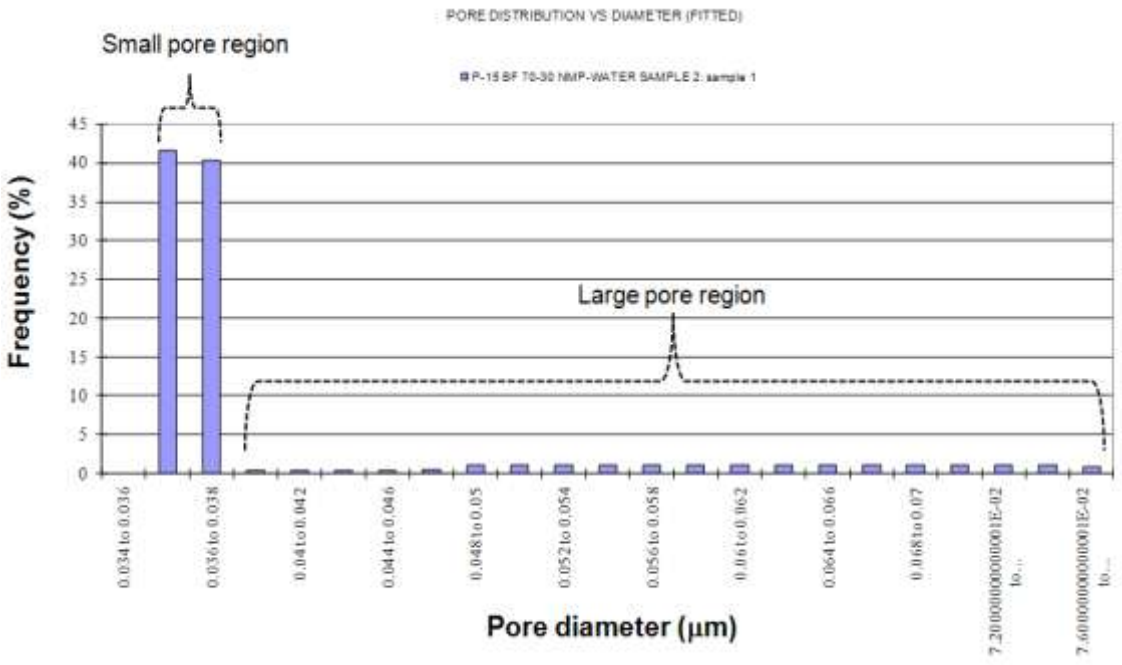

Figure 6.1 An example of pore size distribution data obtained from Capillary Flow Porometer.

6.2.3 Pervaporation experiment

In this study, at least three modules with same fabrication conditions were examined for each pervaporation condition. Two liters of 5 wt% ethanol/water mixture with a recirculation rate of 30 l h^{-1} was used as the feed solution. The operating temperature was maintained at 50 °C throughout the experiment. Details on module fabrication and other operating procedure and conditions can be found in the previous Chapter 3.

6.3 Results and discussion

6.3.1 Membrane morphology and surface characterizations

Figures 6.2, 6.3 and 6.4 disclose the effects of bore-fluid composition, air-gap and take-up speed on membrane morphology, respectively. In all cases, the resulting

membranes have an asymmetric structure, a thick and porous substrate integrally bonded to a thin and relatively dense selective layer at the outer surface. It is apparent that these three key parameters can alter the PVDF hollow fiber membrane morphology significantly. Figure 6.2 illustrates the influence of NMP/water bore-fluid composition on membrane morphological structure under free flow conditions and an air-gap distance of 1 cm. When a NMP/water mixture of 90/10 wt% is used as the bore-fluid, the resultant membrane has finger-like macrovoids crossing the entire cross-section (the 2nd row of Figure 6.2a) and big holes (the 3rd row of Figure 6.2a) in the inner surface. Such holes existing in the inner surface are connected through those finger-like macrovoids. This cross-sectional morphology may result from the combined effects of the use of a relatively high solvent content as the bore-fluid and a rapid phase inversion induced by water at the outer skin [50]. As a result, the high NMP content in the bore-fluid induces a delayed demixing resulting in a very soft inner skin which could not withstand the rapid intrusion of water into the nascent as-spun fiber during phase inversion. On the contrary, when 70/30 wt% and 50/50 wt% NMP/water mixtures are employed, it is found that the water intrusion is suppressed to a certain extent and a finger-like macrovoid structure near the lumen side of the hollow fiber disappears and is replaced by a sponge-like structure (the 2nd row of Figures 6.2b and c). Furthermore, no large holes in the inner surface are observed for both cases (the 3rd row of Figures 6.2b and c). Instead, a uniform and highly porous structure is obtained for 70/30 wt% NMP/water whereas a relatively denser structure is observed when 50/50 wt% NMP/water is used.

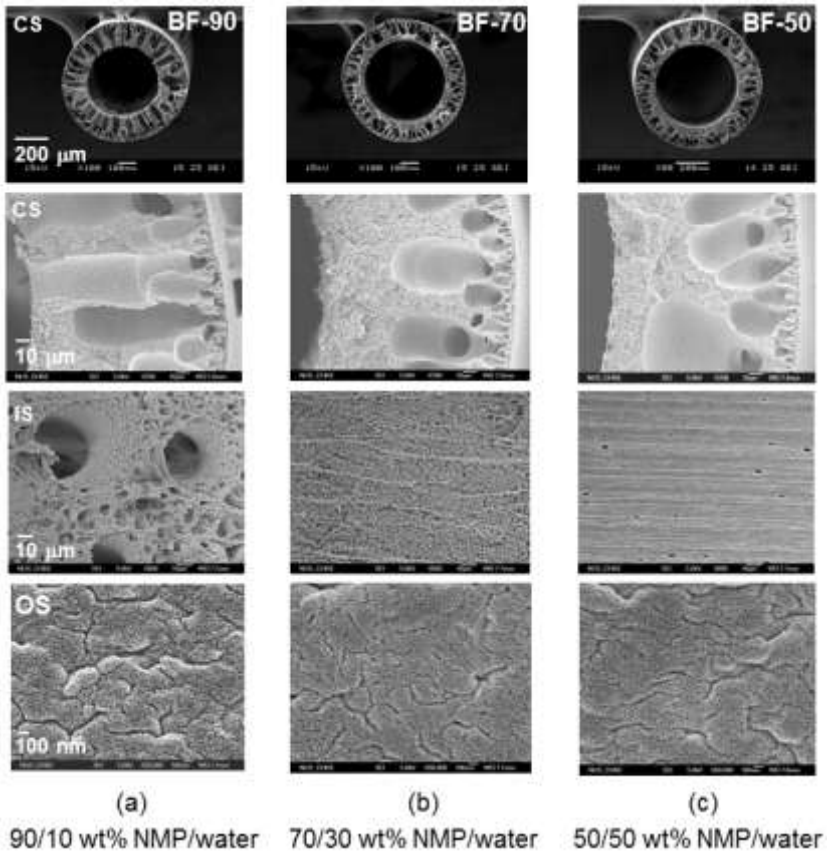

Figure 6.2 The membrane morphology of PVDF hollow fiber membranes spun from different NMP/water bore-fluid (BF) compositions (a) BF-90 (i.e., 90 wt% NMP), (b) BF-70, and (c) BF-50 (CS = cross-section, IS = inner surface, OS = outer surface).

At elevated air-gap distances or take-up speeds, the fiber is unable to form continuously when 90/10 wt% NMP/water bore-fluid is introduced during the fiber spinning. On the other hand, the use of 50/50 wt% NMP/water bore-fluid, a relatively strong internal coagulant for PVDF/NMP dopes, results in a seemingly dense inner surface with irregular fiber shape once high air-gap length and take-up speed are applied. Such inner structure typically results in membranes with a lower flux and a weaker mechanical strength [51]. A fixation of bore-fluid composition at the 70/30 NMP/water mixture is therefore chosen. A uniform and highly porous inner structure is obtained from the 70/30 NMP/water mixture bore-fluid that is favorable as its

substructure resistance is minimized [52]. The separation performance results also support this statement and will be discussed later on.

Figures 6.3 and 6.4 demonstrate the overall cross-section, inner surface and outer surface morphologies of PVDF hollow fibers spun from various air-gap distances and take-up speeds, respectively, using 70/30 wt% NMP/water mixtures as the bore-fluid. An increase in the air-gap length or take-up speed further suppresses the formation of macrovoids and aids the creation of sponge-like structure. The same phenomenon of dependence of macrovoids on air-gap or take-up speed has been reported and discussed through our previous studies on many polymeric membrane materials [53-56]. The reduction of macrovoids may be attributed to the rapid shrinkage process of fiber diameter occurring during the elongation tension by its own gravity (for the case of air-gap) or the elongation stretch by the take-up unit. It may induce a radial outflow (i.e., negative normal stress) which hinders the capillary intrusion of coagulant diffusion, thus eliminates the chance of forming macrovoids [57-58]. As observed from the overall cross-section morphology, an almost macrovoid-free structure is attained when the membranes are spun with a long air-gap length i.e. air gap of 20 cm (referred as AG-20) or a high take-up speed of 10.5 m/min (referred as TK-10). Upon closer scrutiny, the enlarged cross-section morphology of PVDF hollow fibers spun from different air-gap lengths and take-up speeds as respectively depicted in Figures. 5 and 6 reveals that such a macrovoid-free structure actually comprises an array of very small pores beneath the outer surface.

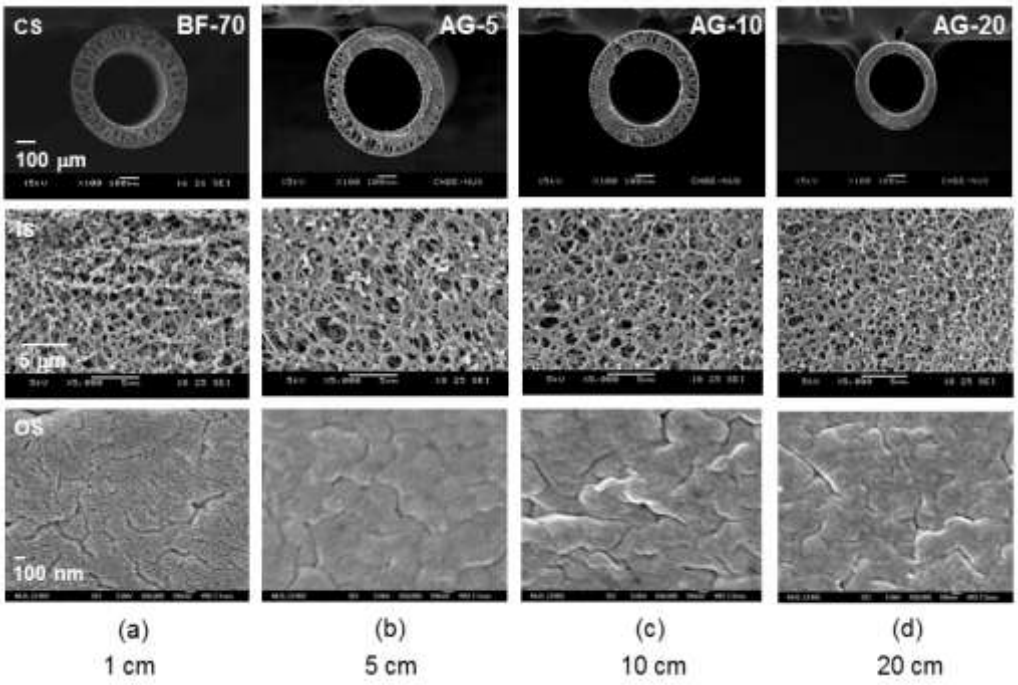

Figure 6.3 The membrane morphology of PVDF hollow fiber membranes with various air-gap (AG) distances (a) BF-70 (b) AG-5 (i.e., 5 cm), (c) AG-10, and (d) AG-20 (CS = cross-section, IS = inner surface, OS = outer surface).

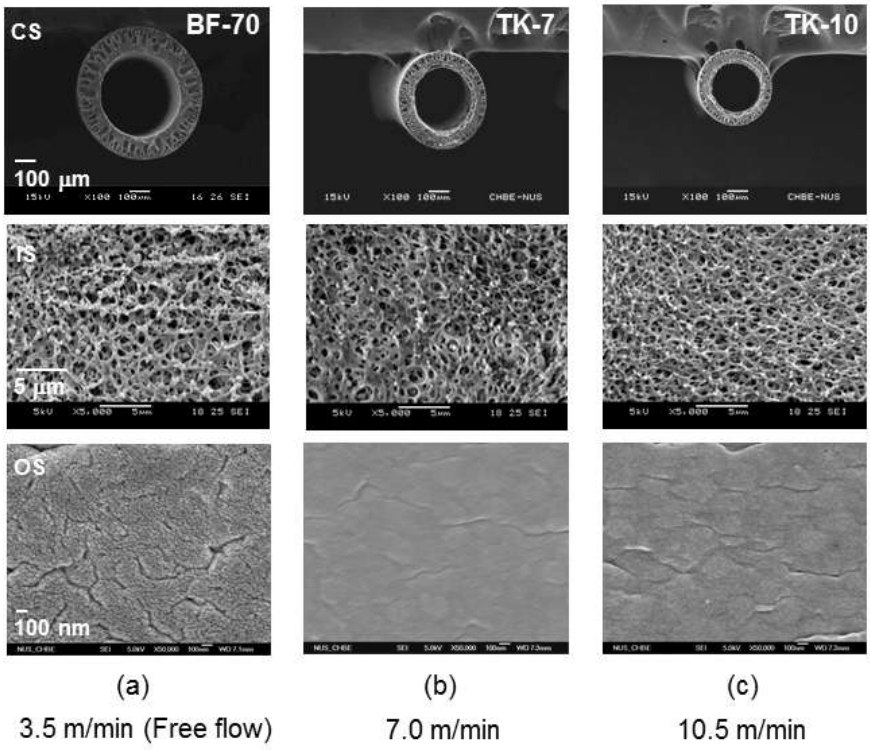

Figure 6.4 The membrane morphology of PVDF hollow fiber membranes spun from different take-up (TK) speeds (a) BF-70, (b) TK-7, and (c) TK-10 (CS = cross-section, IS = inner surface, OS = outer surface).

The resultant PVDF asymmetric hollow fiber membranes with a nearly-perfect macrovoid-free morphology in this study are essentially different from those reported in many previous studies, including our previous work [40,41,59]. The membranes with macrovoid-free morphology produced in most studies typically consist of interlinked PVDF semi-crystalline particles (or globular structure), a result of solid-liquid demixing phase inversion. Interestingly, all membranes presented in this study compose of an interconnected-cellular structure as illustrated through the enlarged cross-section morphological images in Figures 6.5 and 6.6. This kind of morphology usually occurs when the phase invasion is controlled by a liquid-liquid demixing mechanism. As mentioned earlier, the macrovoid-free with a cellular structure made of liquid-liquid demixing is preferable as it has a better mechanical strength than those constructed with PVDF-globule networks.

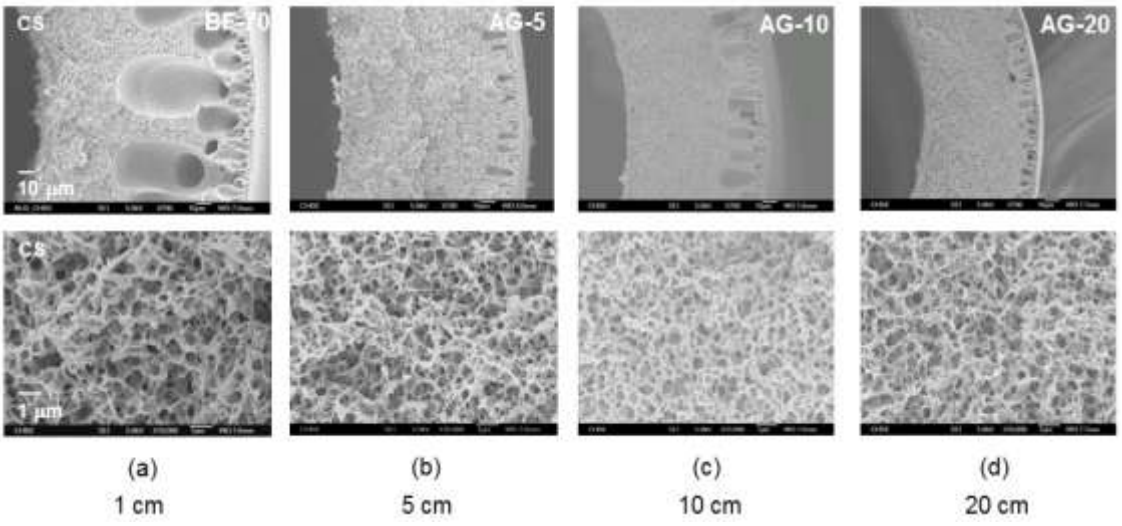

Figure 6.5 The enlarged cross-section morphology of PVDF hollow fiber membranes with various air- gap distances (a) BF-70 (b) AG-5 (c) AG-10 and (d) AG-20 (CS = cross-section).

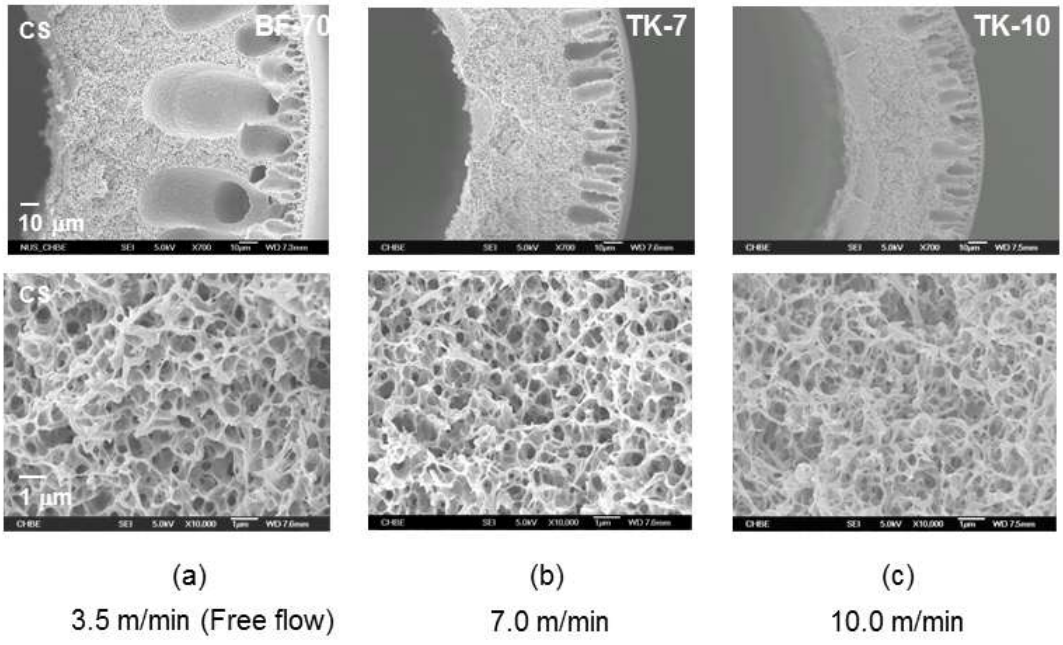

Figure 6.6 The enlarged cross-section morphology of PVDF hollow fiber membranes spun from different take-up speeds (a) BF-70 (b) TK-7 and (c) TK-10 (CS = cross-section).

The trend of increasing air-gap distance or take-up speed towards promoting the liquid-liquid demixing is also supported by the XRD characterization (Figure 6.7). The degree of crystallinity seems to be related to the air-gap length or take-up speed; the membranes spun with a higher air-gap distance or take-up speed exhibit a lower degree of crystallinity. Thus, these results evidently imply that introducing the external elongation stress via either increasing air-gap distance or take-up speed is one of possible effective approaches to facilitate liquid-liquid demixing (suppress solid-liquid demixing) and produce a useful membrane for pervaporation applications.

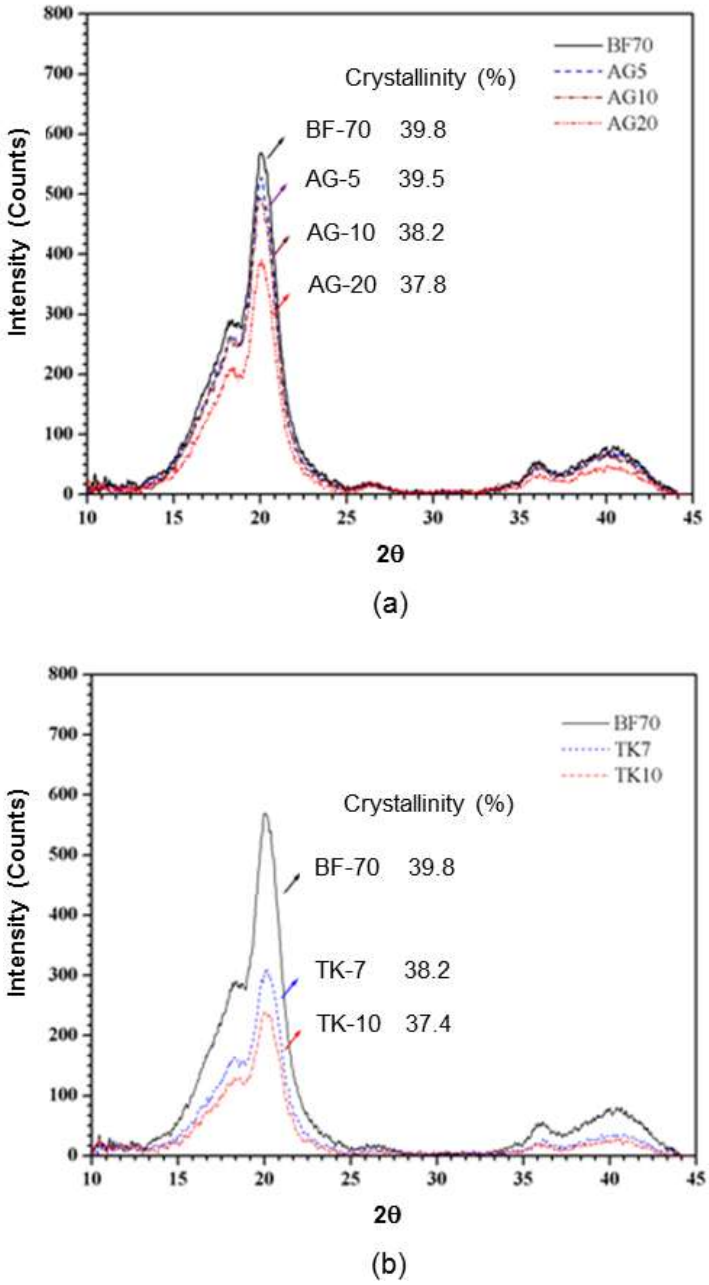

Figure 6.7 XRD patterns and crystallinity of the resultant PVDF hollow fiber membranes spun as a function of (a) air-gap distance and (b) take-up speed.

Figure 6.8 depicts the AFM images of the outer surface topology and surface roughness of as-spun hollow fiber membranes as functions of air-gap distance and take-up speed. Overall, membranes spun with either elevated air-gap lengths (i.e. AG-5, AG-10) or take-up speeds (i.e. TK-7, TK-10) display relatively smaller nodule sizes and lower roughness compared to the original one (BF-70). By observing the three-dimensional

surface topology, there is a difference in the outer surface of the respective membranes; increasing air-gap distance tends to produce an outer surface with a relatively uniform nodule distribution and pores (darker yellow) created at nodule edge. This surface of small-size nodule with a uniform distribution is probably generated due to moisture-induced phase inversion during the air-gap region exposure [53,54]. In contrast, the increment of take-up speed results in smoother outer surface (nodules become flatten) and pores are created and elongated along the same direction as the spinning direction.

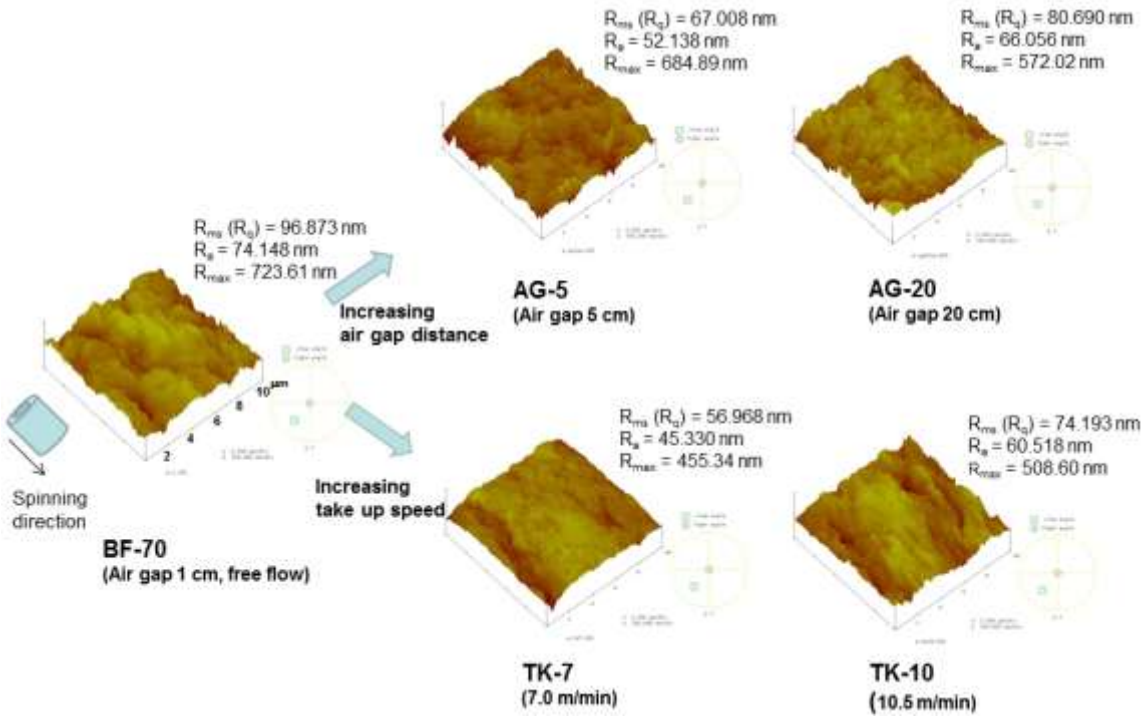

Figure 6.8 AFM images of the outer surface of PVDF hollow fiber membranes spun at different air-gap distances and take-up speeds.

The mean roughness and water contact angle of as-spun PVDF hollow fibers with different air-gap distances and take-up speeds are listed in Table 6.2. One may observe that the higher the roughness of the membrane, the greater the contact angle. Furthermore, both the roughness and the contact angle measurements show a similar

trend; they first decrease and then increase with an increase in air-gap length and take-up speed.

Table 6.2 Roughness and water contact angle at outer surface of PVDF hollow fiber membranes

Spinning code	Mean roughness, R_a (nm)	Water contact angle θ (°)
The effect of bore-fluid compositions		
BF-70	74.148	84.2 ±1.0
The effect of air-gap distances		
AG-5	52.138	81.9 +0.3
AG-10	62.058	84.1 +0.5
AG-20	66.056	86.1 +0.8
The effect of take-up speeds		
TK-7	45.330	81.3 ±1.0
TK-10	60.518	84.7 ±0.5

In general, a higher contact angle, which indicates a higher hydrophobicity, is advantageous as the membrane would have an affinity with ethanol rather than water, usually leading to higher membrane selectivity. Hence, the pristine membrane (BF-70) would represent a better selectivity than those spun at a moderate air-gap length or take-up speed (AG-5, AG-10, TK-7), while membranes spun with a high air-gap distance (AG-20) or take-up speed (TK-10) would show a better separation performance than the pristine membrane (BF-70), which will be discussed later on. This information implies that there would be another critical parameter playing a crucial role in determining the PVDF membrane performance.

6.3.2 Pore size, pore size distribution and overall porosity of PVDF hollow fiber membranes

As pointed out in the previous section, small pores lying beneath a dense skin appear for all the membranes regardless of spinning conditions. Another evident support can be deduced from the outer surface morphology; there are small voids or defects presented at the edge of nodules on the rough surface (see Figures 6.2, 6.3 and 6.4, the bottom row). In our previous study, by considering these voids or surface defects as pores on the membrane surface, we are able to predict the pervaporation mass transport via the modified pore-flow model [44]. Therefore, in the present study, the same pore size characterization by means of a porometer was carried out in order to compare the result with the previous data.

Table 6.3 shows the membrane pore size information of the resultant PVDF hollow fibers which includes the maximum pore size, mean pore size, pore size distribution and overall membrane porosity. The interesting facet is the significant effect of those spinning conditions on membrane surface pore and pore size distribution. First, it can be seen that the bore-fluid composition plays the most crucial role on pore size and pore size distribution. At BF-90, the membrane possesses a mean pore size of 0.0659 μm which is close to its maximum pore size of 0.0775 μm because the large pore region is the prevailing contributor to its pore size distribution. When a lower NMP content is used (i.e. BF-70, BF-50), a significant reduction in mean pore size and a shift of pore size distribution towards smaller pore size region are observed. For instance, at BF-70, the resulting membrane has a membrane mean pore of 0.0302 μm (a reduction of nearly twice the amount compared to BF-90) and the small pore region

is dominant (75.54%). The influence of air-gap distances and take-up speeds on membrane pore size and pore size distribution is of interest. The increased air-gap length or take-up speed results in membranes with reduced pore sizes, i.e. 0.0189 μm at AG-20, 0.0194 μm at TK-10 compared to 0.0302 μm at BF-70. This finding is consistent with previous studies; hollow fiber membranes spun at a high air-gap or take-up speed tends to have a smaller pore size with minimum defects [60-61]. However, there is a limitation in the amount of air-gap or take-up speed applied so as to prevent defects being recreated. Thus, one may see from Table 6.3 that though the small pore region is still regarded as a dominant contributor to pore size distribution as it accounts to 64-82 %, the ratio of large pore contribution increases gradually as a function of air-gap or take-up speed. The reduction in overall porosity due to (1) the decrease in macrovoids because of the use of a higher water amount in bore-fluid, and (2) the increase in air-gap distance or take-up speed is in agreement with previous studies [58,61].

Table 6.3 Maximum and mean pore size, pore size distribution and overall porosity of PVDF hollow fiber membranes spun from different bore-fluid compositions, air-gap distances and take-up speeds

Spinning code	Bubble point (max pore size) (μm)	Mean pore size (μm)	Pore size distribution				Overall porosity[a] (%)
			Large pore region	Contribution (%)	Small pore region	Contribution (%)	
The effect of bore-fluid compositions							
BF-90	0.0775	0.0659	0.0540-0.0775	68.95	0.0500-0.0540	31.05	82.3 ±0.8
BF-70	0.0776	0.0302	0.0320-0.0776	24.46	0.0280-0.0320	75.54	77.8 ±0.3
BF-50	0.0777	0.0220	0.0240-0.0777	19.33	0.0200-0.0240	80.67	76.4 ±0.1
The effect of air gap distances							
AG-5	0.0776	0.0258	0.0260-0.0776	24.01	0.0256-0.0260	75.99	72.6 ±0.7
AG-10	0.0775	0.0207	0.0200-0.0775	24.50	0.0180-0.0200	75.50	70.4 ±0.3
AG-20	0.0775	0.0189	0.0200-0.0775	35.33	0.0180-0.0200	64.67	66.7 ±0.9
The effect of take up speeds							
TK-7	0.0774	0.0192	0.0200-0.0774	18.14	0.0180-0.0200	81.86	69.5 ±0.9
TK-10	0.0775	0.0194	0.0200-0.0775	35.90	0.0180-0.0200	64.10	67.6 ±0.9

[a] The overall porosity is determined by impregnating hollow fibers with kerosene for two days

The evolution of smaller pore size and sharper pore size distribution by increasing the air-gap lengths or take-up speeds may likely arise from three possible factors: (1) the properties of the spinning solution may change under high spinning conditions. Besides the shear stress at the spinneret, many studies have proven that the elongation stress significantly affect the properties of the solution, the phase separation process and the formation of macrovoids and pores [41,58,61]. (2) The external elongation stresses probably create extra phase instability and facilitate a liquid-liquid demixing via spinnodal decomposition mechanism [62]. In our recent work by Sun et al. [61], the spinnodal decomposition is a prevailing mechanism relative to nucleation and growth under high elongation stresses and resulting in the formation of the nano-pore morphological structure of polyamide-imide hollow fiber membranes. (3) The rapid shrinkage of the fiber diameter during the elongation stretch induces radial outflow of solvents, hence retarding the non-solvent intrusion. This not only suppresses the bulk macrovoids (as discussed in the previous section), the formation of large pores during membrane formation could also possibly be limited.

Another important finding is related to the presence of maximum pore size and large pore region in all cases. This implies that although a proper choice of bore-fluid composition, air-gap distance or take-up speed can help effectively to reduce the amount of large pores or defects resulting in a smaller pore size in dominant, it is very difficult to completely remove skin defects. This may be attributed to (1) the slow phase inversion characteristic of PVDF resulting in a strong intrusion of non-solvent during polymer precipitation (2) the semi-crystalline nature of PVDF whereby the solid-liquid demixing mechanism tends to always create some relative big pores or defects at the surface [40]. Based on these findings, it would be possible to rationale that the

evolution of two discrete pore sizes may be due to the competition of liquid-liquid and solid-liquid demixing mechanisms during the phase inversion. The former mechanism is an instantaneous process which could inhibit the pore growth, yielding relative small pores whereas the latter is a critical factor contributing to the formation of large pores because of its intrinsic delayed process.

6.3.3 The pervaporation performance of PVDF hollow fiber membranes

The pervaporation study of the resultant PVDF hollow fiber membranes for ethanol-water separation is explored. The pervaporation performance of the PVDF hollow fibers spun with different spinning conditions and a 5 wt% ethanol-water mixture as a feed model solution is summarized in Table 6.4.

Table 6.4 Pervaporation performance of PVDF hollow fiber membranes with various spinning conditions

Spinning code	Pervaporation performance[a]					
	Permeate composition (% wt)		Separation factor, $\alpha_{ethanol/water}$	Total flux, W_{total} (g m^{-2} h^{-1})	Ethanol permeate flux, $W_{ethanol}$ (g m^{-2} h^{-1})	Water permeate flux, W_{water} (g m^{-2} h^{-1})
	Ethanol	Water				
The effect of bore-fluid compositions						
BF-90	20.75	79.25	4.95	8795	1843	6952
BF-70	26.63	73.37	6.22	8101	2157	5944
BF-50	22.98	77.02	5.55	7805	1794	6011
The effect of air-gap distances						
AG-5	26.92	73.08	7.05	6260	1685	4574
AG-10	29.45	70.55	7.15	4286	1262	3023
AG-20	30.06	69.94	7.57	3536	1063	2473
The effect of take-up speeds						
TK-7	32.43	67.57	7.79	3961	1285	2676
TK-10	31.65	68.35	7.42	3617	1145	2472

[a] Feed solution: 5 wt% ethanol/water mixture; feed flow rate: 30 l h^{-1}; operating temperature: 50 °C

Overall, the membranes possess separation factor of 5-7.8 (21-32.5 wt% ethanol) and flux of 3,500-8,800 g m^{-2} h^{-1}. There is a close relationship among membrane morphology, pore size and pore distribution and separation performance. The membranes possessing a long finger-like macrovoid structure like BF-90 exhibit a low separation factor ($\alpha_{ethanol/water}$= 4.95, 21 wt% ethanol) but a relatively high permeation flux (8,795 g m^{-2} h^{-1}). The membranes spun from 70/30 and 50/50 NMP/water bore-fluid (BF-70 and BF-90) are typical examples of membranes with moderate separation factors as well as comparable fluxes compared to the previous types (BF-90). Their corresponding membrane morphology comprises a certain finger-like macrovoids and sponge-like structure. Although BF-70 and BF-90 membranes are similar in their apparent cross-section morphology, the higher separation factor and flux for the case of BF-70 may be attributed to the inner surface morphology. As demonstrated through many studies, a sponge-like structure together with a highly porous and uniform porous inner structure (BF-70) is desirable because it provides a better channel for vacuum facility, which could act as a non-swollen layer suppressing membrane swelling (i.e., losing selectivity) and enhancing mass transport (i.e., enhancing flux). An increase in air-gap length or take-up speed tends to produce membranes with lesser finger-like macrovoids and almost entire macrovoid-free morphology. Similarly, the membrane spun at a certain air-gap (AG-5) possessing a certain finger-like macrovoids with thicker sponge-like structure exhibit an enhanced separation factor ($\alpha_{ethanol/water}$= 7.05, 26.92 % wt ethanol) and a satisfactory flux (6,260 g m^{-2} h^{-1}). The nearly macrovoid-free morphology of those membranes fabricated with relatively high air-gap lengths (AG-10. AG-20) or with take-up speeds significantly enhance separation factor (up to $\alpha_{ethanol/water}$

=7.79, 32.43 wt% ethanol). The schematic drawing of relationship between membrane morphology and separation performance is illustrated in Figure 6.9.

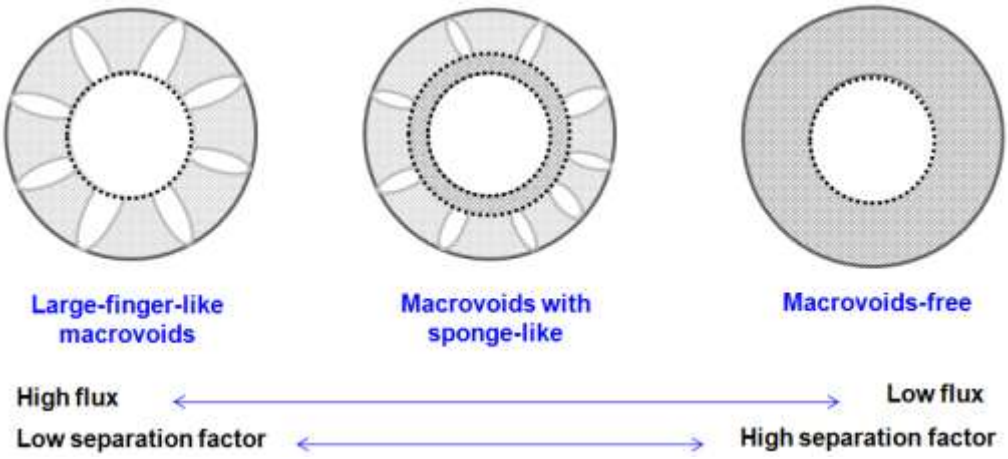

Figure 6.9 Schematic drawing of the significant relationship between membrane morphology and separation performance of PVDF asymmetric hollow fiber membranes.

The membranes having a greater hydrophobicity tend to exhibit a better selectivity but this is not applicable for all cases. The typical examples can be found for the case of AG-5 and TK-7 hollow fibers compared to the controlled membrane (BK-70). On the other hand, to a greater extent, the membrane performance appears to be determined by pore size and pore size distribution which apparently can be tailored by adjusting the bore-fluid composition, air-gap length and take-up speed as discussed earlier.

Figure 6.10 illustrates the influence of mean pore size on pervaporation performance. With the reference to Figure 6.10(a), only slight enhancements in ethanol permeate content and separation factor are observed when the mean pore size decreases from 0.067 μm to 0.03 μm. On the other hand, membrane's separation factor and ethanol permeate concentration can be significantly improved when the mean pore size is less than 0.03 μm. One of possible reasons can be drawn by examining the permeate water

and ethanol fluxes as demonstrated in Figure 6.10(b). The water flux drops more rapidly as compared to the ethanol flux when the mean pore size is lower than 0.03 μm. This finding implies that there should be an optimal pore size in which the water transport through pores is hindered while maintaining the ethanol transport.

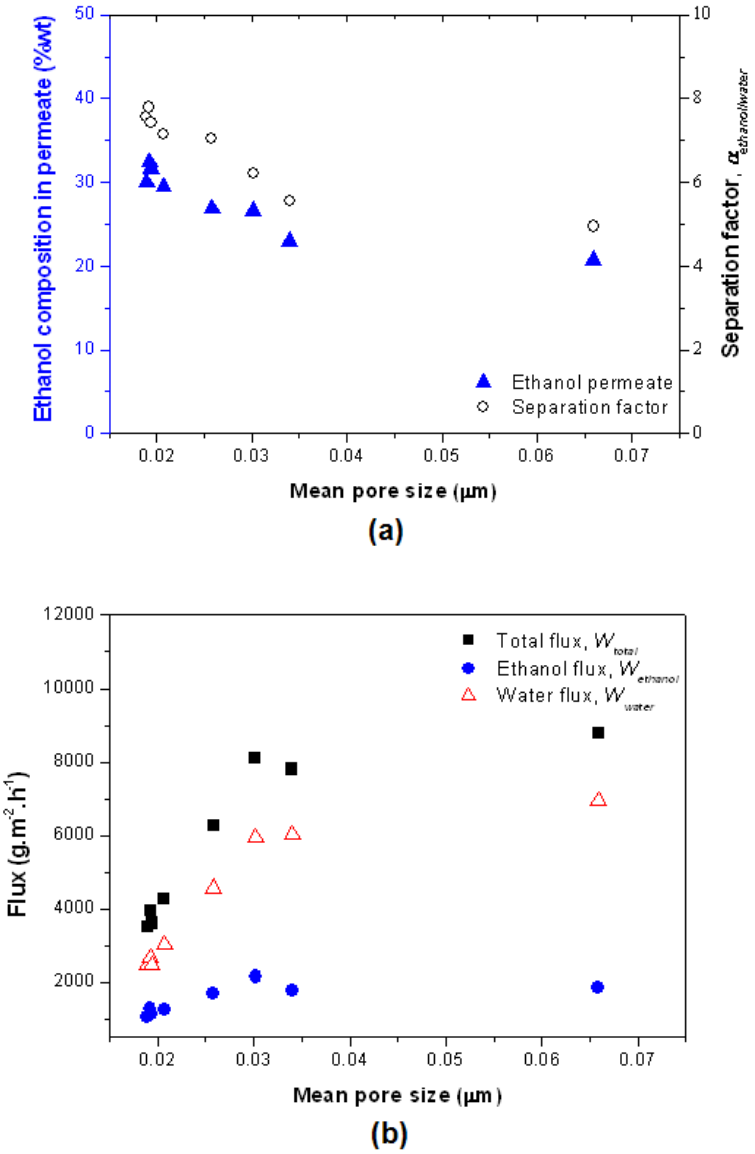

Figure 6.10 The effect of mean pore sizes of PVDF hollow fiber membranes on pervaporation performance using a 5 wt% ethanol aqueous feed solution at 50 °C; (a) ethanol permeate composition and separation factor and (b) ethanol, water and total permeation fluxes.

It is interesting to highlight that the excellent correlation between pore size, pore size distribution and membrane separation performance is in agreement with the conceptual of the modified pore-flow model as proposed in our previous studies [44]. Figure 6.11 demonstrates the schematic representation of pervaporation characteristics on the basis of the modified pore-flow model.

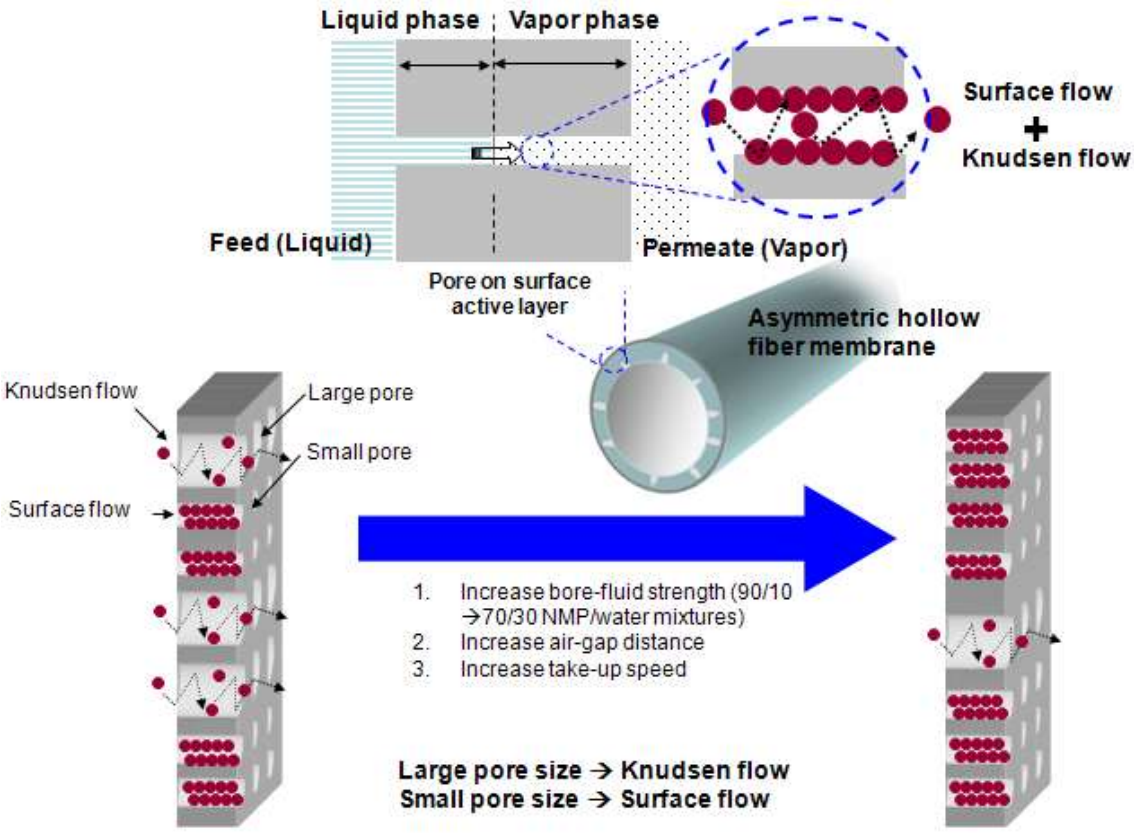

Figure 6.11 Schematic representation of the concept of modified pore flow model in pervaporation transport within asymmetric hollow fiber membranes.

In the modified pore-flow model, there are two vapor transport mechanisms competing at different pore sizes; namely surface flow and Knudsen flow. In fact, it may be possible that in the vapor phase, the surface flow is more prevailing in smaller pores whereas the Knudsen flow is more prevailing in bigger pores. Consequently, the small pores may help in achieving a better separation factor whereas the big pores may result

in a lower separation factor. This concept is consistent with our results and observations; all hollow fiber membranes consist of two discrete pore size regions, termed as small pore size region and large pore size region. In other words, the membranes with large pore sizes (e.g. BF-90) should be a good example of the modified pore-flow where the Knudsen flow is more dominant compared to the surface flow. Such membranes exhibit a high flux with a relatively low separation factor. By controlling membrane pore size via increasing bore-fluid strength (BF-70, BF-50), air-gap distance or take-up speed, the membranes tend to have a smaller pore size and lesser contribution from a large pore region. The surface flow is more dominant where the performance characteristic can be predicted with the reduced form of the modified pore flow model, which is similar to the pore flow model [63-64]. A better separation factor would be expected from these membranes.

6.3.4 Comparison of pervaporation performance of PVDF hollow fiber membranes with other polymeric membranes for ethanol-water separation

A comparison of pervaporation performance of the PVDF hollow fiber membranes explored in this study with other polymeric membranes in open literature for ethanol-water separation is given in Figure 6.12 and the detailed information of each membrane is listed in Table 6.5. One may notice that the PDMS-based membranes with a flat-sheet configuration are the most widely investigated. The membrane possesses an average separation factor around 5-10 with the total flux ranging from 10-1,000 g m^{-2} h^{-1} depending on the modification introduced. In comparison to the most conventional polymeric-based membranes, the developed PVDF hollow fiber membranes exhibit an acceptable separation factor ($\alpha_{ethanol/water}$ 5-8) with a remarkable flux (3,500-8,800 g m^{-2}

h^{-1}). Although the equivalent membrane performance can be achieved in the case of PDMS/ceramic composite (refers to the references [79] and [80]), the newly developed PVDF hollow fiber membrane may be more favorable in terms of simple fabrication and modification.

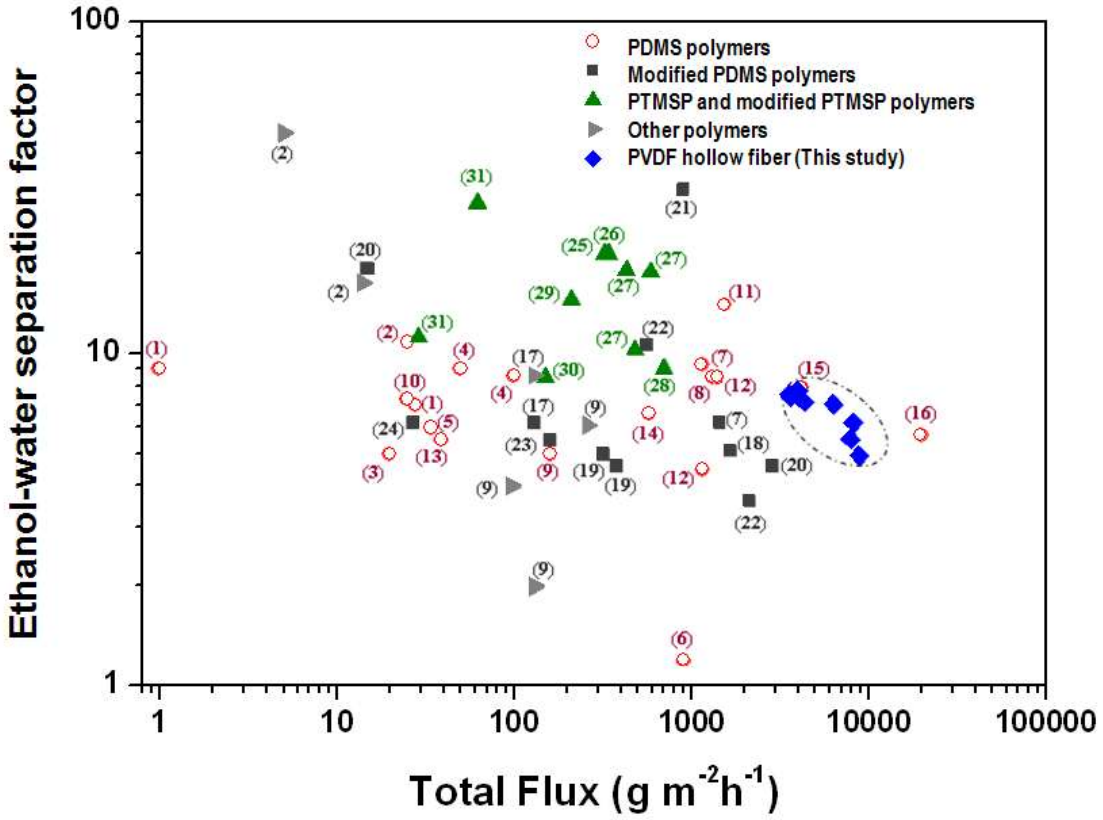

Figure 6.12 Graphical representation of polymeric membrane performance for ethanol recovery as presented in Table 6.5 (The number near the data point refers to the cited reference).

Table 6.5 Ethanol-water separation of polymeric membranes via pervaporation

Membrane	Configuration	Ethanol/water feed composition (wt%)	Temp (°C)	Separation factor, $\alpha_{ethanol/water}$	Total flux (g m^{-2} h^{-1})	Reference and referring number in Figure 6.12	
PDMS polymers							
PDMS	Flat sheet	11.9/88.1	25	9.0	1	[65]	1
PDMS	Flat sheet	8/92	30	10.8	25.1	[66]	2
PDMS	Flat sheet	10/90	30	5.0	20	[67]	3
PDMS	Flat sheet	6/94	35	9.0	50	[68]	4
PDMS (GE 615 membrane)	Flat sheet	6/94	50	8.6	100	[68]	4
PDMS (Sulzer membrane)	Flat sheet	6/94	35	6.0	34	[69]	5
PDMS on cellulose acetate support	Flat sheet	3/97	30	1.2	900	[70]	6
PDMS on cellulose acetate support	Flat sheet	5/95	40	9.3	1139.6	[71]	7
PDMS on cellulose acetate support	Flat sheet	5/95	40	8.5	1300	[72]	8
PDMS on polyvinyl fluoride support	Flat sheet	11.9/88.1	20	7	28	[65]	1
PDMS on Nylon support	Flat sheet	10/90	40	5.0	160	[73]	9
PDMS on polyetherimide support	Flat sheet	7/93	22	7.3	25	[74]	10
PDMS on PTFE support	Flat sheet	6/94	20	14.0	1530	[75]	11
PDMS on polyamide support	Flat sheet	4/96	40	8.5	1400	[76]	12
PDMS on polysulfone support	Flat sheet	4/96	40	4.5	1150	[76]	12

Table 6.5 Ethanol-water separation of polymeric membranes via pervaporation (Cont'd)

Membrane	Configuration	Ethanol/water feed composition (wt%)	Temp (°C)	Separation factor, $\alpha_{ethanol/water}$	Total flux (g m^{-2} h^{-1})	Reference and referring number in Figure 6.12	
PDMS on microporous support (MTR membrane)	Flat sheet	6/94	25	5.5	39	[77]	13
PDMS/polysulfone composite	Hollow fiber	8/92	50	6.6	576	[78]	14
PDMS on ZrO2/Al2O3 ceramic support	Tubular	4.2/95.8	60	7.93	4190	[79]	15
PDMS on ZrO2/Al2O3 ceramic support	Tubular	4.3/95.7	70	5.7	19500	[80]	16
Modified PDMS polymers							
PPMS on cellulose acetate support	Flat sheet	5/95	40	6.2	1432.6	[71]	7
PDMS-styrene graft copolymer on PTFE support	Flat sheet	8.1/91.9	60	6.2	130	[81]	17
Plasma-Induced grafted PDMS/PVDF composite	Flat sheet	10/90	35	5.1	1650	[82]	18
PDMS (Plasma-polymerized Tetramethoxysilane monomers)	Flat sheet	4/96	25	4.6	380	[83]	19
PDMS (Plasma-polymerized Hexamethyltrisiloxane monomers)	Flat sheet	4/96	25	5.0	320	[83]	19
PDMS (Plasma-polymerized hexamethyltrisiloxane PDMS membranes and treated with Octadecyldiethoxymethylsilane)	Flat sheet	4/96	25	18.0	15	[83]	19
Plasma-Induced grafted TMVS/PVDF , coating by phosphate ester containing silicone copolymer	Multi-layer flat sheet	10/90	30	31	900	[85]	21
PDMS-imide copolymers (synthesized from ODMS and PMDA)	Flat sheet	10/90	40	10.6	560	[86]	22

Table 6.5 Ethanol-water separation of polymeric membranes via pervaporation (Cont'd)

Membrane	Configuration	Ethanol/water feed composition (wt%)	Temp (°C)	Separation factor, $\alpha_{ethanol/water}$	Total flux (g m^{-2} h^{-1})	Reference and referring number in Figure 6.12	
PDMS-imide copolymers (synthesized from ODMS and 6FDA)	Flat sheet	10/90	40	3.6	2120	[86]	22
PDMS-polystyrene interpenetrating polymer network on polyethersulfone ultrafiltration support	Flat sheet	10/90	60	5.5	160	[87]	23
PDMS-polysulfone block copolymers	Flat sheet	10/90	25	6.2	27	[88]	24
PTMSP polymers							
PTMSP	Flat sheet	6/94	30	19.9	340	[89]	25
PTMSP	Flat sheet	6/94	30	19.9	325	[90]	26
PTMSP	Flat sheet	6/94-7/93	50	10.3	480	[91]	27
PTMSP	Flat sheet	6/94	75	9	700	[92]	28
PTMSP	Flat sheet	10/90	50	14.5	210	[93]	29
PTMSP	Flat sheet	10/90	50	8.5	150	[94]	30
PTMSP	Flat sheet	7/93	30	11.2	29	[95]	31
Modified PTMSP polymers							
PTMSP/PDMS graft copolymer	Flat sheet	7/93	30	28.3	62	[95]	31
Trimethylsilyl substituted PTMSP	Flat sheet	6/94-7/93	50	17.6	590	[91]	27
n-Decane substituted PTMSP	Flat sheet	6/94-7/93	50	17.8	430	[91]	27

Table 6.5 Ethanol-water separation of polymeric membranes via pervaporation (Cont'd)

Membrane	Configuration	Ethanol/water feed composition (wt%)	Temp (°C)	Separation factor, $\alpha_{ethanol/water}$	Total flux (g m^{-2} h^{-1})	Reference and referring number in Figure 6.12	
Other polymers							
Styrene-fluoroalkyl acrylate graft copolymer on PDMS support	Flat sheet	8/92	30	16.3-45.9	5-14	[66]	2
Polyorganophosphazene containing $-OC_2H_5$ pendant group on Nylon support	Flat sheet	10/90	40	2.0	130	[73]	9
Polyorganophosphazene containing $-OCH_2CF_3$ pendant group on Nylon support	Flat sheet	10/90	40	6.1	260	[73]	9
Polyorganophosphazene containting $-OCH_2CF_2CF_2CF_2H$ pendant group on Nylon support	Flat sheet	10/90	40	4.0	96	[73]	9
Polyurethaneurea containing PDMS	Flat sheet	10/90	40	8.6	130	[81]	17
PVDF with an asymmetric structure	**Hollow fiber**	**5/95**	**50**	**5-8**	**3500-8800**	**This study**	

6.4 Conclusions

By employing the concept of the modified-flow model, PVDF asymmetric hollow fiber membranes were fabricated and studied for ethanol–water pervaporation separation. The effects of bore-fluid composition, air-gap distance and take-up speed on membrane morphology and separation performance have been studied. The following conclusion can be drawn from this study:

(1) By optimizing bore-fluid composition, high air-gap distance or take-up speed, the membrane morphology changes from a large finger-like macrovoid structure to a macrovoid-free structure. An increase in air-gap distance and take-up speed results in nearly macrovoid-free membranes with a sponge-like structure comprising cellular microstructure due to the acceleration of the liquid–liquid demixing mechanism during phase inversion.

(2) The pore size, pore size distribution and porosity are strongly dependent on spinning conditions. An increment in air-gap length or take-up speed effectively produces membranes with a smaller pore size, narrower pore size distribution and lesser overall porosity. The resultant membranes possess amean pore size in a sub-micron range between 0.0189 and 0.0659 μm with different contributions from the large and small pore regions. The overall porosity is of 66–82%.

(3) The enhancement in membrane selectivity is essentially contributed from (1) the creation of cellular sponge-like structure and (2) the reduction of membrane pore size and the shift towards the small-pore region distribution. The increase in a permeation flux is mainly attributed to the

presence of large macrovoids, large pore region and increased overall porosity. The role of pore size and pore size distribution affecting the separation performance and mass transport is satisfactorily explained via the concept of the modified pore-flow model.

(4) The resulting PVDF asymmetric hollow fiber membranes have separation factors of 5–8 and total fluxes of 3500–8800 gm−2 h−1. In comparison to other previous studies, the newly developed membranes possess an acceptable separation factor with outstanding permeation flux.

REFERENCES

[1] M. Balat, H. Balat, C. Oz, Progress in bioethanol processing, Prog. Energy Combust. Sci. 34 (2008) 551.

[2] S.K. Hoekman, Biofuels in the U.S.-challenges and opportunities, Renewable Energy 34 (2009) 14.

[3] E.D. Larson, Biofuel production technologies: status, prospects and implications for trade and development, Report no. UNCTAD/DITC/TED/2007/10. United Nations Conference on Trade and Development, New York and Geneva (2008).

[4] T. Wiesenthal, G. Leduc, P. Christidis, B. Schade, L. Pelkmans, L. Govaerts, P. Georgopoulos, Biofuel support policies in Europe: lessons learnt for the long way ahead, Renewable Sustainable Energy Rev. 13 (2009) 789.

[5] K.R. Szulczyk, B.A. McCarl, G. Cornforth, Market penetration of ethanol, Renewable Sustainable Energy Rev. 14 (2010) 394.

[6] L.M. Vane, F.R. Alvarez, A.P. Mairal, R.W. Baker, Separation of vapor-phase alcohol/water mixtures via fractional condensation using a pilot-scale dephlegmator: Enhancement of the pervaporation process separation factor, Ind. Eng. Chem. Res. 43 (2004) 173.

[7] L.M. Vane, V. V. Namboodiri, T.C. Bowen, Hydrophobic zeolite-silicone rubber mixed matrix membranes for ethanol-water separation: Effect of zeolite and silicone component selection on pervaporation performance, J. Membr. Sci. 308 (2008) 230.

[8] P.S. Nigam, A. Singh, Production of liquid biofuels from renewable resources, Prog. Energy Combust. Sci. 37 (2011) 52.

[9] F. Taylor, M.J. Kurantz, N. Goldberg, J.C. Craig, Continuous fermentation and stripping of ethanol, Biotechnol. Prog. 11 (1995) 693.

[10] A.J. Ragauskas, C.K. Williams, B.H. Davison, G. Britovsek, J. Cairney, C.A. Eckert, W.J. Frederick Jr., J.P. Hallett. D.J. Leak, C.L. Liotta, J.R. Mielenz, R. Murphy, R. Templer, T. Tschaplinski, The path forward for biofuels and biomaterials, Science 311 (2006) 484.

[11] I. Blume, J.G. Wijmans, R.W. Baker, The separation of dissolved organics from water by pervaporation, J. Membr. Sci. 49 (1990) 253.

[12] X. Feng, R.Y.M. Huang, Liquid separation by membrane pervaporation: A review, Ind. Eng. Chem. Res. 36 (1997) 1048.

[13] Y. Huang, R.W. Baker, Bioethanol production using pervaporation and vapour permeation membranes. Presentation at International Congress on Membrane and Membrane Process, Honolulu, USA (2008).

[14] L.Y. Jiang, Y. Wang, T.S. Chung, X.Y. Qiao, J.Y. Lai, Polyimides membranes for pervaporation and biofuels separation, Prog. Polym. Sci. 34 (2009) 1135.

[15] B. Smitha, D. Suhanya, S. Sridhar, M. Ramakrishna, Separation of organic-organic mixtures by pervaporation-A review, J. Membr. Sci. 241 (2004) 1.

[16] L.M. Vane, Review: Separation technologies for the recovery and dehydration of alcohols from fermentation broths, Biofuels, Bioprod. Bioref. 2 (2008) 553.

[17] W.J. Groot, M.R. Kraayenbrink, R.G.J.M. van der Lans, K.C.H.A.M. Luyben, Ethanol production in an integrated fermentation/membrane system. Process simulations and economics, Bioprocess. Eng. 8 (1993) 189.

[18] H.J. Huang, S. Ramaswamy, U.W. Tschirner, B.V. Ramarao, A review of separation technologies in current and future biorefineries, Sep. Purif. Technol. 62 (2008) 1.

[19] F. Lipnizki, Membrane process opportunities and challenges in the bioethanol industry, Desalination 250 (2010) 1067.

[20] F. Lipnizki, S. Hausmanns, G. Laufenberg, R.W. Field, B. Kunz, Use of pervaporation-bioreactor hybrid processes in biotechnology, Chem. Eng. Technol. 23 (2000) 569.

[21] L.M. Vane, A review of pervaporation for product recovery from biomass fermentation processes, J. Chem. Technol. Biotechnol. 80 (2005) 603.

[22] W.W. Ding, Y.T. Wu, X.Y. Tang, L. Yuan, Z.Y. Xiao, Continuous ethanol fermentation in a closed-circulating system using an immobilized cell coupled with PDMS membrane pervaporation, J. Chem. Technol. Biotechnol. 86 (2011) 82.

[23] P.D. Chapman, T. Oliveira, A.G. Livingston, K. Li, Review: Membranes for the dehydration of solvents by pervaporation, J. Membr. Sci. 318 (2008) 5.

[24] Y. Huang, J. Ly, D. Nguyen, R.W. Baker, Ethanol dehydration using hydrophobic and hydrophilic polymer membranes, Ind. Eng. Chem. Res. 49 (2010) 12067.

[25] C.Y. Tu, Y.L. Liu, K.R. Lee, J.Y. Lai, Hydrophilic surface-grafted poly(tetrafluoroethylene) membranes using in pervaporation dehydration processes, J. Membr. Sci. 274 (2006) 47.

[26] D. Beaumelle, M. Marin, H. Gibert, Pervaporation with organophilic membranes: state of the art, Trans. Inst. Chem. Eng. 71 (C) (1993) 77.

[27] P.N. Pintauro, K. Jian, Integral asymmetric fluoropolymer pervaporation membranes and method of making the same, US Patent 5,387,378 (1995).

[28] J.G. Wijmans, J. Kaschemekat, J.E. Davidson, R.W. Baker, Treatment of organic-contaminated wastewater streams by pervaporation, Environ. Prog. 9

(1990) 262.

[29] B.T. Low, Y. Wang, T.S. Chung, Polymeric membranes for energy applications, Encyclopedia of Polymer Science and Technology, New York: John Wiley & Sons, (2010).

[30] A.J. Lovinger, in: D.C. Bassett (Ed.), Poly(vinylidene fluoride), Development in Crystalline Polymers, vol. 1, London: Applied Science, (1982).

[31] C. Güell, R.H. Davis, Membrane fouling during microfiltration of protein mixtures, J. Membr. Sci. 119 (1996) 269.

[32] M. Khayet, C.Y. Feng, K.C. Khulbe, T. Matsuura, Preparation and characterization of polyvinylidene fluoride hollow fiber membranes for ultrafiltration, Polymer 43 (2002) 3879.

[33] K. Schneider, T.S. Van Gassel, Membrane distillation, Chem. Eng. Technol. 56 (1984) 514.

[34] M.M. Teoh, T.S. Chung, Membrane distillation with hydrophobic macrovoid-free PVDF-PTFE hollow fiber membranes, Sep. Purif. Technol. 66 (2009) 229.

[35] K.Y. Wang, T.S. Chung, M. Gryta, Hydrophobic PVDF hollow fiber membranes with narrow pore size distribution and ultraskin for the fresh water production through membrane distillation, Chem. Eng. Sci. 63 (2008) 371.

[36] K. Li, J.F. Kong, D. Wang, W.K. Teo, Tailor-made asymmetric PVDF hollow fibers for soluble gas removal, AIChE J. 45 (1999) 1211.

[37] K. Jian, P.N. Pintauro, Asymmetric PVDF hollow-fiber membranes for organic/water pervaporation separations, J. Membr. Sci. 135 (1997) 41.

[38] M.G. Buonomenna, P. Macchi, M. Davoli, E. Drioli, Poly(vinylidene fluoride) membranes by phase inversion: the role the casting and coagulation conditions play in their morphology, crystalline structure and properties, Eur. Polym. J. 43

(2007) 1557.

[39] L.P. Cheng, D.J. Lin, C.H. Shih, A.H. Dwan, C.C. Gryte, PVDF membrane formation by diffusion-induced phase separation-morphology prediction based on phase behavior and mass transfer modeling, , J. Poly. Sci. Part B: Polym. Phys. 37 (1999) 2079.

[40] S.H. Choi, F. Tasselli, J.C. Jansen, G. Barbieri, E. Drioli, Effect of the preparation conditions on the formation of asymmetric poly(vinylidene fluoride) hollow fibre membranes with a dense skin, Eur. Polym. J. 46 (2010) 1713.

[41] P. Sukitpaneenit and T.S. Chung, Molecular elucidation of morphology and mechanical properties of PVDF hollow fiber membranes from aspects of phase inversion, crystallization and rheology, J. Membr. Sci. 340 (2009) 192.

[42] T.H. Young, L.P. Cheng, D.J. Lin, L. Fane, W.Y. Chuang, Mechanisms of PVDF membrane formation by immersion-precipitation in soft (1-octanol) and harsh (water) nonsolvents, Polymer 40 (1999) 5315.

[43] T.S. Chung, Fabrication of hollow fiber membranes by phase inversion, in: N. Li et al (Eds.), Advanced Membrane Technology and Applications, New York: Wiley, (2008), p 821.

[44] P. Sukitpaneenit, T.S. Chung, L.Y. Jiang, Modified pore-flow model for pervaporation mass transport in PVDF hollow fiber membranes for ethanol-water separation, J. Membr. Sci. 362 (2010) 393.

[45] X. Qiao, T.S. Chung, K.P. Pramoda, Fabrication and characterization of BTDA-TDI/MDI (P84) co-polyimide membranes for the pervaporation dehydration of isopropanol, J. Membr. Sci. 264 (2005) 176.

[46] D.J. Lin, H.H. Chang, T.C. Chen, Y.C. Lee, L.P. Cheng, Formation of porous poly(vinylidene fluoride) membranes with symmetric or asymmetric

morphology by immersion precipitation in the water/TEP/PVDF system, Eur. Polym. J. 42 (2006) 1581.

[47] K.Y. Wang, S.W. Foo, T.S. Chung, Mixed matrix PVDF hollow fiber membranes with nanoscale pores for desalination through direct contact membrane distillation, Ind. Eng. Chem. Res. 48 (2009) 4474.

[48] A. Jena, K. Gupta, Flow Porometry: What can flow porometry do for us?, Porous Materials, Inc., Ithaca, NY, USA, 2002.

[49] L.Y. Jiang, T.S. Chung, R. Rajagopalan, Dehydration of alcohols by pervaporation through polyimide Matrimid® asymmetric hollow fibers with various modifications, Chem. Eng. Sci. 63 (2008) 204.

[50] K.Y. Wang, T.S. Chung, R. Rajagopalan, Novel Polybenzimidazole (PBI) nanofiltration membranes for the separation of sulfate and chromate from high alkalinity brine to facilitate the chlor-alkali process, Ind. Eng. Chem. Res. 46 (2007) 1572.

[51] Y.E. Santoso, T.S. Chung, K.Y. Wang, M. Weber, The investigation of irregular inner skin morphology of hollow fiber membranes at high-speed spinning and the solutions to overcome it, J. Membr. Sci. 282 (2006) 383.

[52] Y. Wang, S.H. Goh, T.S. Chung, N. Peng, Polyamide-imide/polyetherimide dual-layer hollow fiber membranes for pervaporation dehydration of C1-C4 alcohols, J. Membr. Sci. 326 (2009) 222.

[53] T.S. Chung, X. Hu, Effect of air-gap distance on the morphology and thermal properties of polyethersulfone hollow fibers, J. Appl. Polym. Sci. 66 (1997) 1067.

[54] R. Liu, X. Qiao, T.S. Chung, The development of high performance P84 co-polyimide hollow fibers for pervaporation dehydration of isopropanol, Chem.

Eng. Sci. 60 (2005) 6674.

[55] N. Peng, T.S. Chung, K.Y. Wang, Macrovoid evolution and critical factors to form macrovoid-free hollow fiber membranes, J. Membr. Sci. 318 (2008) 363.

[56] K.Y. Wang, T.S. Chung, Polybenzimidazole nanofiltration hollow fiber for cephalexin separation, AIChE J. 52 (2006) 1363.

[57] D.F. Li, T.S. Chung, R. Wang, Morphological aspects and structure control of dual-layer asymmetric hollow fiber membranes formed by a simultaneous co-extrusion approach, J. Membr. Sci. 243 (2004) 155.

[58] K.Y. Wang, D.F. Li, T.S. Chung, S.B. Chen, The observation of elongation dependent macrovoid evolution in single and dual-layer asymmetric hollow fiber membranes, Chem. Eng. Sci. 59 (2004) 4657.

[59] S. Rajabzadeh, T. Maruyama, T. Sotani, H. Matsuyama, Preparation of PVDF hollow fiber membrane from a ternary polymer/solvent/nonsolvent system via thermally induced phase separation (TIPS) method, Sep. Purif. Technol. 63 (2008) 415.

[60] M. Khayet, The effects of air gap length on the internal and external morphology of hollow fiber membranes, Chem. Eng. Sci. 58 (2003) 3091.

[61] S.P. Sun, K.Y. Wang, D. Rajarathnam, T.A. Hatton, T.S. Chung, Polyamide-imide nanofiltration hollow fiber membranes with elongation induced nano-pore evolution, AIChE J. 56 (2010) 1481.

[62] T. S. Chung, The limitations of using Flory-Huggins equation for the states of solutions during asymmetric hollow fiber formation, J. Membr. Sci. 126 (1997) 19.

[63] T. Okada, T. Matsuura, A new transport model for pervaporation, J. Membr. Sci. 59 (1991) 133.

[64] T. Okada, M. Yoshikawa, T. Matsuura, A study on the pervaporation of ethanol/water mixtures on the basis of pore flow model, J. Membr. Sci. 59 (1991) 151.

[65] Z. Changluo, L. Moe, X. Wei, Separation of ethanol-water mixtures by pervaporation-membrane separation process, Desalination 62 (1987) 299.

[66] I. Kazuhiko, M. Kiyohide, Pervaporation of ethanol-water mixture through composite membranes composed of styrene-fluoroalkyl acrylate graft copolymers and crosslinked polydimethylsiloxane membrane, J. Appl. Polym. Sci. 34 (1987) 437.

[67] M.C. Conclaves, G.S.S Marquez, F. Galembeck, Pervaporation and dialysis of water-ethanol solution by using silicone rubber-membrane, Sep. Sci. Technol. 18 (1983) 893.

[68] B. Moermans, W.D. Beuckelaer, I.F.J. Vankelecom, R. Ravishankar, J.A. Martens, P.A. Jacobs, Incorporation of nano-sized zeolites in membranes, Chem. Commun. 24 (2000) 2467.

[69] I.F.J. Vankelecom, D. Depré, S.D. Beukelaer, J.B. Uytterhoeven, Influence of zeolites in PDMS membranes: Pervaporation of water/alcohol mixtures. J. Phys. Chem. 99 (1995) 13193.

[70] T. Mohammadi, A. Aroujalian, A. Bakhshi, Pervaporation of dilute alcoholic mixtures using PDMS membrane, Chem. Eng. Sci. 60 (2005) 1875.

[71] Y. Luo, S. Tan, H. Wang, F. Wu, X. Liu, L. Li, Z. Zhang, PPMS composite membranes for the concentration of organics from aqueous solutions by pervaporation, Chem. Eng. J., 137 (2008) 496.

[72] L. Li, Z. Xiao, S. Tan, L. Pu, Z. Zhang, Composite PDMS membrane with high flux for the separation of organics from water by pervaporation, J. Membr. Sci.

243 (2004) 177.

[73] Y. Huang, J. Fu, Y. Pan, X. Huang, X. Tang, Pervaporation of ethanol aqueous solution by polyphosphazene membranes: Effect of pendant groups, Sep. Purif. Technol. 66 (2009) 504.

[74] M.D. Jia, K.V. Peinemann, R.D. Behling, Preparation and characterization of thin-film zeolite-PDMS composite membranes, J. Membr. Sci. 73 (1992) 119.

[75] Y. Mori, T. Inaba, Ethanol production from starch in a pervaporation membrane bioreactor using clostridium thermohydrosulfuricum, Biotechnol. Bioeng. 36 (1990) 849.

[76] E. Shi, W. Huang, Z. Xiao, D. Li, M. Tang, Influence of binding interface between active and support layers in composite PDMS membranes on permeation performance, J. Appl. Polym. Sci. 104 (2007) 2468.

[77] S.L. Schmidt, M.D. Myers, S.S. Kelley, J.D. McMillan, N. Padukone, Evaluation of PTMSP membranes in achieving enhanced ethanol removal from fermentations by pervaporation, Appl. Biochem. Biotech. 63-65 (1997) 469.

[78] J. Guo, G. Zhang, W. Wu, S. Ji, Z. Qin, Z. Liu, Dynamically formed inner skin hollow fiber polydimethylsiloxane/polysulfone composite membrane for alcohol permselective pervaporation, Chem. Eng. J. 158 (2010) 558.

[79] F. Xiangli, W. Wei, Y. Chen, W. Jin, N. Xu, Optimization of preparation conditions for polydimethylsiloxane (PDMS)/ceramic composite pervaporation membranes using response surface methodology, J. Membr. Sci. 311 (2008) 23.

[80] X. Fenjuan, C. Yiwei, J. Wangin, X. Nanping, Polydimethylsiloxane (PDMS)/ceramic composite membrane with high flux for pervaporation of ethanol-water mixtures, Ind. Eng. Chem. Res. 46 (2007) 2224.

[81] S. Takegemi, H. Yamada, S. Tusujii, Pervaporation of ethanol/water mixture

using novel hydrophobic membrane containing polydimethylsiloxane., J. Membr. Sci. 75 (1992) 93.

[82] C.L. Chang, P.Y. Chang, Performance enhancement of silicone/PVDF composite membranes for pervaporation by reducing cross-linking density of the active silicone layer, Desalination 192 (2006) 241.

[83] T. Kashiwagi, K. Okabe, K. Okita, Separation of ethanol from ethanol/water mixtures by plasma-polymerized membranes from silicone compounds, J. Membr. Sci. 36 (1988) 353.

[84] C.L. Chang, M.S. Chang, Preparation of composite membranes of functionalised silicone polymers and PVDF for pervaporation of ethanol-water mixture, Desalination 148 (2002) 39.

[85] C.L. Chang, M.S. Chang, Preparation of multi-layer silicone/PVDF composite membranes for pervaporation of ethanol aqueous solutions, J. Membr. Sci. 238 (2004) 117.

[86] M. Krea, D. Roizard, N. Moulai-Mostefa, D. Sacco, New copolyimide membranes with high siloxane content designed to remove polar organics from water by pervaporation, J. Membr. Sci. 241 (2004) 55.

[87] L. Liang, E. Ruckenstein, Pervaporation of ethanol-water mixtures through polydimethylsiloxane-polystyrene interpenetrating polymer network supported membranes, J. Membr. Sci. 114 (1996) 227.

[88] K. Okamoto, A. Butsuen, S. Tsuru, S. Nishioka, K. Tanaka, H. Kita, S. Asakawa, Pervaporation of water-ethanol mixtures through polydimetylsiloxane block-copolymer membranes, Polym. J. 19 (1987) 747.

[89] V.V. Volkov, A.G. Fadeev, V.S. Khotimsky, E.G. Litvinova, Y.A. Selinskaya, J.D. McMillan, S.S. Kelly, Effects of synthesis conditions on the pervaporation

properties of Poly[1-(Trimethylsilyl)-1-Propyne] useful for membrane bioreactors, J. Appl. Polym. Sci. 91 (2004) 2271.

[90] A.G. Fadeev, S.S. Kelley, I.D. McMillan, Y.A. Selinskaya, V.S. Khotimsky, V.V. Volkov, Effect of yeast fermentation by-products on poly[1-(trimethylsilyl)-1-propyne] pervaporative performance, J. Membr. Sci. 214 (2003) 229.

[91] Y. Nagase, Y. Takamura, K. Matsui, Chemical modification of Poly(substituted-acetylene). V. Alkylsilylation of Poly(1-Trimethylsilyl-1-propyne) and improved liquid separating property at pervaporation, J. Appl. Polym. Sci. 42 (1991) 185.

[92] J.R. Gonzalez-Velasco, J.A. Gonzalez-Marcos, C. Lopez-Dehesa, Pervaporation of ethanol-water mixtures through poly(1-trimethylsilyl-1-propyne) (PTMSP) membranes, Desalination 149 (2002) 61.

[93] S. Claes, P. Vandezande, S. Mullens, R. Leysen, K.D. Sitter, A. Andersson, F.H.J. Maurer, H. Van den Rul, R. Peeters, M.K. Van Bael, High flux composite PTMSP-silica nanohybrid membranes for the pervaporation of ethanol/water mixtures, J. Membr. Sci. 351 (2010) 160.

[94] J.A. Gonzalez-Marcos, C. Lopez-Dehesa, J.R. Gonzales-Velasco, Effect of operation conditions in the pervaporation of ethanol-water mixtures with poly(1-trimethylsilyl-1-propyne) membranes, J. Appl. Polym. Sci. 94 (2004) 1395.

[95] Y. Nagase, K. Ishihara, K. Matsui, Chemical modification of poly(substituted-acetylene): II. Pervaporation of ethanol/water mixture through poly(1-trimethylsilyl-1-propyne)/poly(dimethylsiloxane) graft copolymer membrane, J. Poly. Sci. Part B: Polym. Phys. 28 (1990) 377.

CHAPTER SEVEN

PVDF/NANO-SILICA DUAL-LAYER HOLLOW FIBERS WITH ENHANCED SELECTIVITY AND FLUX AS NOVEL MEMBRANES FOR ETHANOL RECOVERY

7.1 Introduction

Biofuel like bioethanol is one of the most successful renewable and sustainable fuels alternatives to fossil-fuels [1-4]. To date, commercial bioethanol is typically produced from the fermentation of corn and sugar-based feedstocks. This leads to controversial issues regarding the competitive usage of land and price of these food crop feedstocks with agricultural aspects. Recently, cellulosic ethanol, derived from lignocellulosic based biomass, has emerged to address the above-mentioned issues concerning starch-based foods [5, 6]. This next-generation biofuel is expected to play a promising role in sustainable development. Hence, there is a great interest in developing a cost-effective technology for extracting ethanol derived from non-food lignocellulosic feedstocks.

One of the challenges faced by such feedstocks is that lignocellulose-based fermentations typically produce a more dilute concentration of ethanol than that from corn or sugarcane based fermentations [7,8]; 1 to 6 wt% from lignocellulosic feedstocks, while 8-15 wt% from starch-based feedstocks. The low concentration of ethanol poses a problem for conventional distillation processes; distillation energy requirements (and cost) increase exponentially at low ethanol feed concentrations [9, 10]. Furthermore, questions concerning the net environmental impact of bioethanol purified by distillation have been raised [11]. A more efficient and greener separation

process is under demand to significantly reduce the energy footprint of bioethanol production from lignocellulosic feedstocks, and even for starch-based feedstocks. This circumstance signifies a clear view that alongside tremendous efforts devoted to the advancements in biosciences and bioengineering on the design and engineering of the genetic transformation of biomass into biofuel [12], a major breakthrough in the separation and purification of biofuel from fermentation products is of paramount importance.

Pervaporation is a membrane-based separation process that has the potential to provide energy and cost-effective alternative to a traditional distillation for the recovery of alcohols from fermentation broths [10,11,13,14]. In pervaporation, the liquid containing dilute ethanol is brought into contact with one side of the membrane while a vacuum or gas purge is applied on the other side to produce a permeate vapor on the other side of the membrane [15]. In a recent review on various separation technologies for alcohols recovery by Vane [10], pervaporation could be a promising choice to compete with a standard distillation in terms of energy efficiency, in particular for a cellulosic ethanol process in which the ethanol content in broths is relatively low. In addition, the unique advantage of pervaporation includes the potential to be integrated with the existing processes [16-18]. In a recent work by Ding et al. [19], integrating membrane pervaporation with a fermentor resulted in the improvement of ethanol productivity. Besides the above-mentioned benefits, other attractive features of pervaporation include minimum contamination, compact operation unit space and its environmental friendliness.

Despite its apparent economic and environmental advantages and great application potential, the absence of desirable membrane materials that combine a high selectivity-high flux separation characteristic with a cost-effective fabrication is a significant obstacle hindering further advancement of this technology in the industrial practice. Vane's evaluation of the energy efficiency of pervaporation to replace a current standard distillation suggested that membranes with an ethanol-water separation factor greater than of 20 are necessary in order to achieve its energy saving proficiency [10, 20].

To date, several membrane materials ranging from polymeric, inorganic and composite (mixed-matrix) materials have been extensively investigated but have yet received a breakthrough in the development. Poly(dimethylsiloxane) (PDMS) or well known as 'silicone rubber' is a benchmark material and the most widely studied for ethanol recovery. Tremendous effort has been given to enhance the ethanol-water separation factor of PDMS via chemical modifications such as grafting and cross-linking with other materials. However, only a marginal improvement in the separation performance has been achieved with a significant loss in the total flux. Other polymeric materials such as polyimide [14], poly[1-(trimethylsilyl)-1-propyne] (PTMSP) [21-23], styrene-fluoroalkyl acrylate graft copolymer [24], polyorganophosphazene [25], polyurethaneurea [26], polyether block amide [27], styrene-butadiene-styrene block copolymers [28] have also been investigated. Most of the membranes show a trade-off relationship in the separation performance; they possess either an improved separation factor with a significantly reduced flux or an enhanced flux with a lack of selectivity.

Inorganic membranes based on silicalite-1 and hydrophobic zeolites typically exhibit a greater ethanol/water separation factor and flux relative to polymeric membranes. However, zeolite and silicalite-1 membranes are more difficult and costly to fabricate than polymeric membranes. An idea of incorporating zeolite/silicalite-1 into the polymer matrix is therefore of great recent interest as it combines the benefits of both materials; the exceptional high separation properties and thermal resistance of silicalite-1/zeolites with the desirable mechanical integrity, the low price and ease of membrane fabrication of polymers [29-30]. The incorporation of silicalite-1 or hydrophobic zeolites into PDMS polymer matrix have been intensively studied [31-34]. Besides mixed-matrix membranes based silicalite-1 or zeolite, new hybrid or composite membranes containing other different fillers such as polyphosphazene nanotubes [35] and carbon black [36], silica [37] have been studied, and their separation performances mostly fall in between PDMS and silicalite-1 /PDMS membranes. At present, PDMS and silicalite-1/PDMS composite membranes have been manufactured by many companies such as Sulzer Chemtech (Neunkirchen, Germany), SolSep BV (Apeldoorn, Netherlands), Pervatech BV (Enter, Netherlands) [38]. However, the limited efficacy in a high selectivity with an elevated flux and membrane stability of available membrane materials has yet to compete with distillation for ethanol recovery. Without the development of an appropriate membrane, pervaporation is unlikely to materialize as a viable alternative ethanol recovery technique.

Recently, the potential of PVDF membranes as alternative membrane materials for ethanol-water separation has been explored [39]. The key advantages of PVDF over most conventional polymers such as PDMS include its highly hydrophobic nature,

good mechanical property and excellent chemical resistance, which are vital requirements for pervaporation membranes as they come into contact with liquid mixtures. Additionally, its hollow fiber configuration offers many advantages such as a higher permeation flow per unit volume, self-contained vacuum channel on the lumen side, and ease of handling during module fabrication and system operation. Compared with polymeric membranes available in the literature, the PVDF hollow fibers exhibited a remarkable high flux of 3,500-8,800 g m^{-2} h^{-1} and reasonable ethanol-water separation factor up to 8. However, as mentioned earlier, the membrane selectivity must be improved at least up to separation factor of 20 to meet its potential applications.

The success of membrane development is not only relied on the advancements in membrane materials and fabrication techniques but also requires a proper understanding in the mass transport across the membrane. Our previous studies [39-40] have proved that the pervaporation transport in PVDF hollow fiber membranes for ethanol/water separation can be satisfactorily described via a modified pore-flow concept, rather than a solution-diffusion model which is widely employed in the majority of the studies. Hence, this leads to different strategies in developing membrane structure and operating conditions. For example, in the solution-diffusion approach, the ideal membranes are dense and a thin-selective layer is therefore required to maximize the membrane selectivity and flux, respectively [41-42]. Conversely, the membranes following the modified pore-flow model have a relatively porous structure whereby the pore size, surface porosity and hydrophobicity play a crucial role in determining the separation performance. In fact, a thin hydrophobic porous selective skin composing fine pores and high surface porosity is the preferential

membrane structure for the modified pore-flow concept. Recent studies have proven that the incorporation of finely dispersed organic and inorganic particles, i.e. Organophilic clay [43-44], PTFE (Teflon) [45], SiO_2 [46-48], TiO_2 [49-50], Al_2O_3 [51], and ZrO_2 [52] in the PVDF polymer matrix is a very useful approach in altering the membrane surface properties. For instance, adding silica into the PVDF polymer matrix possibly resulted in the formation of fine pore size, high porosity, strong membranes, as well as the alteration of membrane surface hydrophobicity. Meanwhile, the advanced fabrication of hollow fibers by means of the co-extrusion technology can help to accomplish a relative thin selective porous skin in addition to the benefit of saving material cost [44, 53-54].

Besides the different approaches in designing a favorable membrane structure, the identification of appropriate operating conditions for each type of membranes is also important in particular the role of downstream pressure. In the last 30 years, only very limited publications have been given to discuss the significance of downstream pressure on pervaporation [55-58], but most of them were based on dense membranes with the solution-diffusion mechanism approach. Typically, the downstream pressure is suggested to be kept as low as possible (most often reported under vacuum conditions of 0-100 Pa) in order to create the maximum driving force of mass transport across the membrane [59]. This practice has been widely adopted to conduct experiments in academic research despite the fact that it would be more reasonable and cost effective to examine the pervaporation process at relatively higher downstream pressures (up to several thousand Pa) due to the technical difficulty of achieving and keeping relatively low vacuum in the industrial practical scale [57]. However, the same practice may not be appropriate for the pore-flow membranes where the pressure

gradient may significantly interfere the mass transport in the selective pore which involves the evaporation/liquid-vapor phase change. It would be worthwhile to investigate and understand the influence of downstream pressure from the modified pore-flow model, which has yet to be reported in the literature.

Therefore, the objective of this work is to molecularly design PVDF/nano-silica dual-layer hollow fiber membranes with an enhanced selectivity (ethanol-water separation factor up to 29) and a high total flux for ethanol recovery via tuning membrane morphology and controlling the operating downstream pressure employing the modified pore-flow concept. The desirable membranes should have the following characteristics: (1) a relative thin PVDF/nano-silica composite outer layer; (2) a highly porous and sponge-like inner layer and (3) delamination-free at the interface. In this regard, the incorporation of hydrophobic silica nanoparticles and optimization of spinning parameters such as air-gap, take-up speed, and outer-dope flow rate were studied. A relationship among corresponding membrane morphology, pore size, porosity, hydrophobicity and separation performance was elaborated. The significance of downstream pressure on membrane separation and pervaporation mass transport was investigated and the modified pore-flow model was further employed to predict and understand such separation-downstream pressure dependent phenomenon. A comparison of the separation performance of developed hollow fiber membranes with various membranes available in the literature was highlighted. To our best knowledge, this work not only establishes the development of high performance pervaporation membranes for ethanol recovery, but also provides the fundamental science and understanding of tunable pervaporation characteristics from the aspects of membrane morphological design and downstream pressure control.

7.2 Experimental

7.2.1 Spinning dope formulation and hollow fiber spinning

The PVDF/NMP dope solutions with and without silica were employed as outer layer and inner layer membrane materials, respectively in the fabrication of PVDF/silica dual-layer hollow fiber membranes using a dry-jet wet spinning process via the co-extrusion of polymer dopes through a dual-layer spinneret. Figure 7.1 depicts the schematic of the dual-layer spinneret and its dimension used in this study. Table 7.1 lists the sample identification, dope compositions and spinning conditions of hollow fiber membranes with various air-gap lengths, take-up speeds and outer-dope flow rate. The dope with 20 wt% silica loading (i.e., the weight ratio of silica to the sum of silica and PVDF polymer) was deliberately chosen in this work due to the composition being able to accommodate the highest silica loading while preserving the appropriate dope viscosity (spinnability) simultaneously. From our experimental observation, the dope prepared with a higher silica loading (>20%) exhibited an excessively high viscosity, an inhomogeneous solution and a difficulty for spinning at room temperature.

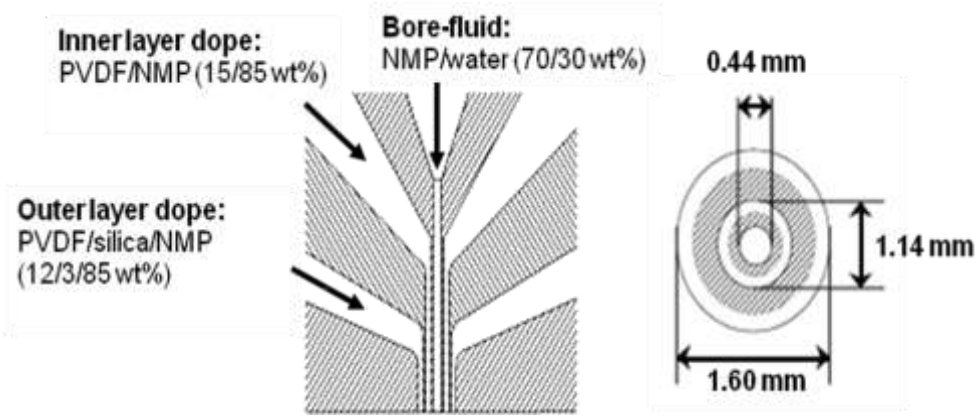

Figure 7.1 Schematic diagram of spinneret for dual-layer hollow fiber spinning

Table 7.1 Spinning conditions and parameters of PVDF/nano-silica dual-layer hollow fiber membranes with a thin composite outer-layer

Spinning code	Parameter[a]				
	Outer-layer dope composition (wt%)	Inner-layer dope composition (wt%)	Outer-layer dope flow rate (cm^3 min^{-1})	Air-gap distances (cm)	Take-up speed (m min^{-1})
The effect of air-gap distance					
DL_{AG-20}	PVDF/nano-silica/NMP 12/3/85	PVDF/NMP 15/85	0.2	20	Free flow
The effect of take-up speed					
DL_{TK-7}	PVDF/nano-silica/NMP 12/3/85	PVDF/NMP 15/85	0.2	1	7
The effect of outer-dope flow rate					
$DL_{AG-20-ODR-0.1}$	PVDF/nano-silica/NMP 12/3/85	PVDF/NMP 15/85	0.1	20	Free flow
$DL_{AG-20-ODR-0.4}$			0.4		

[a] Inner-dope flow rate: 2.0 cm^3 min^{-1}; bore-fluid composition: 70/30 wt% water/NMP; bore-fluid flow rate: 0.6 cm^3 min^{-1}; external coagulant: tap water; coagulant bath and spinning temperature: 25 °C; relative humidity: 65%.

The spinning conditions at an elevated air-gap of 20 cm and high take-up speed of 7 m min^{-1} were adopted from our previous study to facilitate the suppression of macrovoids and large defects/pore formation during membrane precipitation [39,60]. Other spinning parameters were kept constant throughout the spinning process. The as-spun hollow fibers were immersed in water for at least 3 days to ensure thorough removal of residual NMP solvent. Subsequently, the hollow fibers were freeze dried for 24 h before further characterization.

7.2.2 Modified pore-flow model for pervaporation transport analyses

The modified-pore flow model was proposed in our previous study [40] and was established based on the assumptions that there are a bundle of straight cylindrical pores penetrating across the selective layer of the membranes and that all the pores are

operating under an isothermal condition. The mass transport in the pore can be considered as a combination of liquid-phase and vapor-phase transport in series where the vapor transport is governed by surface flow and Knudsen flow mechanisms. According to the model, the mass transport in terms of total molar flux of a pure component system can be represented as

$$Q_{total} = Q_{liquid} + Q_{surface} + Q_{knudsen} \tag{7.1}$$

$$Q_{total} = \frac{A}{\delta}(P_2 - P_*) + \frac{B}{\delta}(P_*^2 - P_3^2) + \frac{C}{\delta}(P_* - P_3) \quad when\ P_3 < P_* \tag{7.2}$$

$$Q_{total} = \frac{A}{\delta}(P_2 - P_3) \quad when\ P_3 \geq P_* \tag{7.3}$$

The details on theoretical background and equation derivations can be found in Chapter 5.

The prediction of the mole fraction of water at the permeate side in a binary system using the transport parameters from pure component systems can be obtained by the following equation

$$Y_{w,3} = \frac{\frac{B_w}{\delta}(P_{w,*}^2 - P_{w,3}^2) + \frac{C_w}{\delta}(P_{w,*} - P_{w,3})}{\frac{B_w}{\delta}(P_{w,*}^2 - P_{w,3}^2) + \frac{C_w}{\delta}(P_{w,*} - P_{w,3}) + \frac{B_e}{\delta}(P_{e,*}^2 - P_{e,3}^2) + \frac{C_e}{\delta}(P_{e,*} - P_{e,3})} \tag{7.4}$$

To be expressed in terms of downstream pressure (P_3), the equation (7.4) can be rewritten as

$$Y_{w,3} = \frac{\frac{B_w}{\delta}[P_{w,*}^2 - (P_3 Y_{w,3})^2] + \frac{C_w}{\delta}[P_{w,*} - (P_3 Y_{w,3})]}{\frac{B_w}{\delta}[P_{w,*}^2 - (P_3 Y_{w,3})^2] + \frac{C_w}{\delta}[P_{w,*} - (P_3 Y_{w,3})] + \frac{B_e}{\delta}[P_{e,*}^2 - (P_3(1-Y_{w,3}))^2] + \frac{C_e}{\delta}[P_{e,*} - (P_3(1-Y_{w,3}))]} \quad (7.5)$$

where $Y_{w,3}$ is the water mole fraction in the permeate side, B_w/δ and B_e/δ (mol $m^{-1}s^{-1}Pa^{-2}$) are the vapor transport coefficients contributed by the surface flow of water and ethanol components, respectively. C_w/δ and C_e/δ (mol m^{-1} s^{-1} Pa^{-1}) are the vapor transport coefficients contributed by the Knudsen flow of water and ethanol components, respectively. $P_{w,*}$ and $P_{e,*}$ (Pa) are the partial vapor pressures of the water and ethanol components in the saturated vapor, respectively.

From the equation (7.5), the permeate water mole fraction ($Y_{w,3}$) under various downstream pressures can be calculated using the mathematics computation (MATLAB computing software) whereby all transport parameters and saturation vapor pressures for respective pure component systems can be attained by fitting the experimental data to equations (7.2) and (7.3). Figure 7.2 illustrates a typical pattern of curve characteristics in the pervaporation of pure water (Figure 7.2a) and pure ethanol (Figure 7.2b) systems for hollow fiber membranes spun with air-gap 20 cm (DL_{AG-20}). All membranes exhibited a similar curve pattern but differed in values of the transport parameters and saturation vapor pressures.

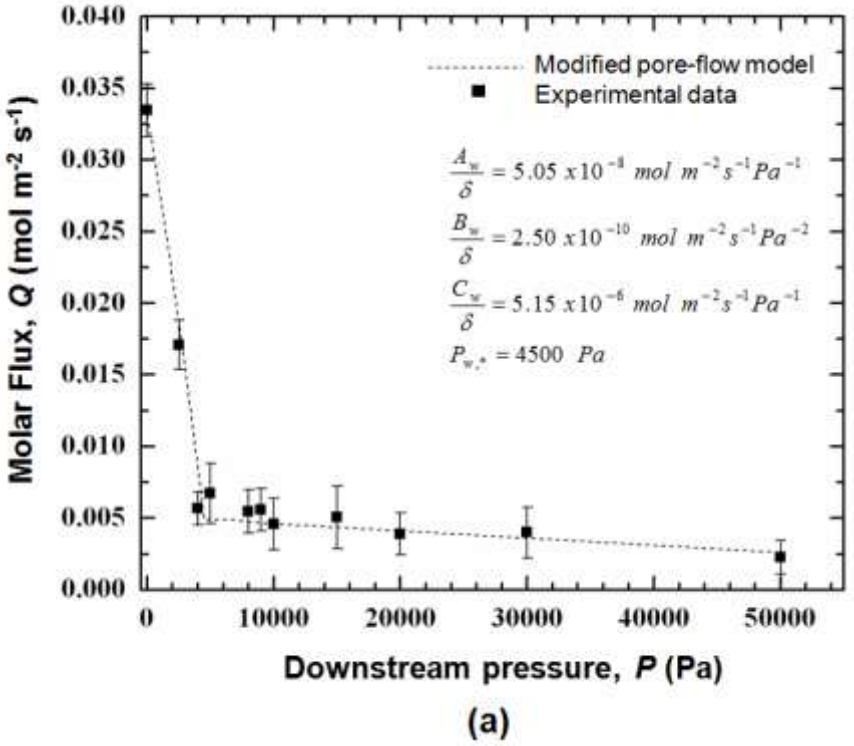

(a)

.

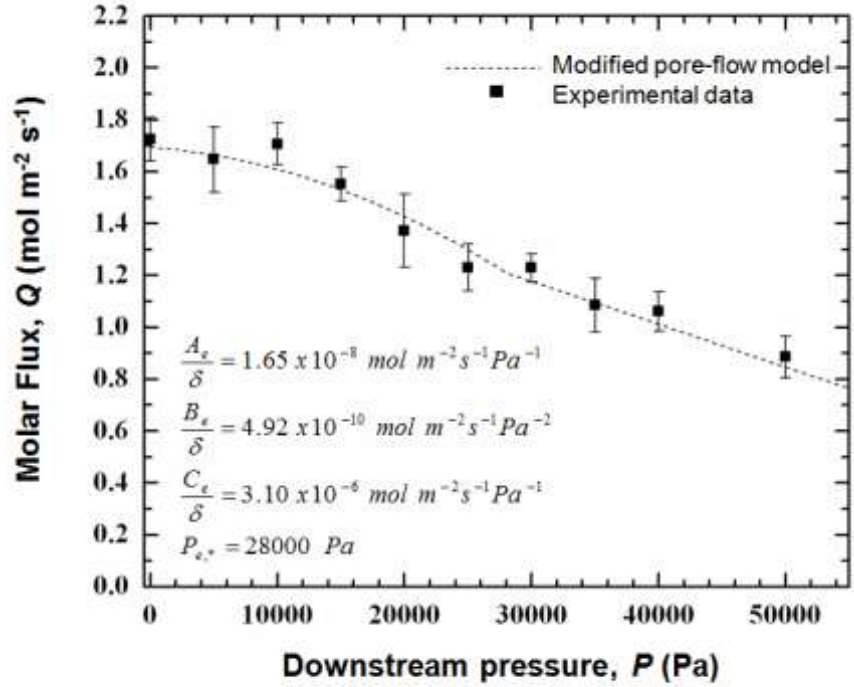

(b)

Figure 7.2 The estimation of transport parameters in the modified pore-flow model from the pervaporation data of pure component systems at 50 °C (a) pure water and (b) pure ethanol (spinning code: $DL_{AG\text{-}20}$).

7.3 Results and discussion

7.3.1 Membrane characterizations

A typical morphology of PVDF/nano-silica dual layer hollow fiber membranes spun with an air-gap of 20 cm (DL_{AG-20}) is shown in Figure 7.3. The cross section morphology reveals that the membrane consists of a fully porous PVDF inner layer, a relatively thin PVDF/nano-silica composite outer layer, and a delamination-free interface. The surface and bulk morphologies of the inner layer of the hollow fiber has a highly porous structure which is desirable for minimizing the substructure resistance [39,60].

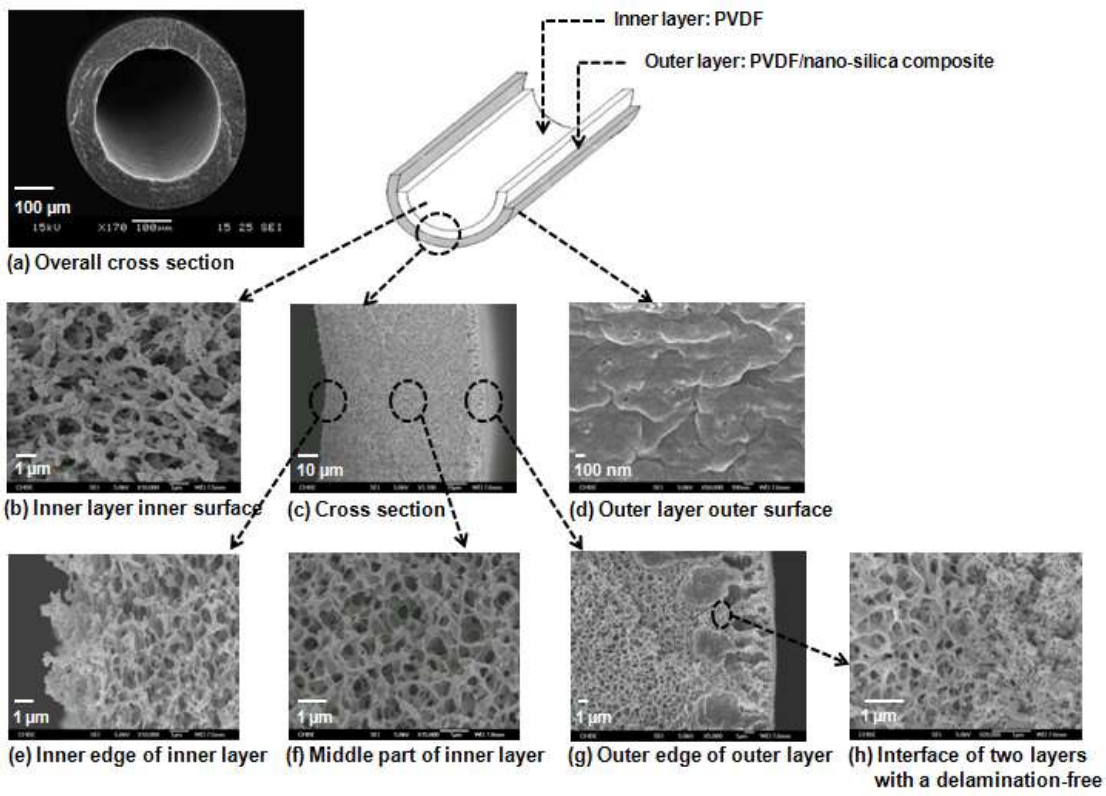

Figure 7.3 SEM and FESEM images of different bulk and surface morphologies of PVDF/nano-silica composite dual-layer hollow fiber membranes (Spinning code: DL_{AG-20})

The outer surface of the outer layer made of the PVDF/nano-silica composite (Figure 7.3d) is relatively dense and seemingly comprises tiny voids formed at the nodular edge and the surrounding area of dispersed silica particles. Upon closer scrutiny, the enlarged cross-section morphology (Figure 7.3g) depicts very small pores beneath the outer layer surface. With the consideration of these voids or defects as pores on the membrane surface, the developed membrane structural feature is identical with the conceptual structure in the modified pore-flow concept. Similar bulk and surface morphologies as discussed above are obtained for the hollow fibers spun with other conditions.

The distribution of filler particles in the polymer matrix is another major concern in fabricating the nanocomposite or mixed-matrix membranes. In this study, the distribution of nano-silica in the dual-layer hollow fiber membrane morphology was monitored by EDX-SEM, as shown in Figure 7.4. A typical silica distribution through the cross section and outer surface morphologies of the hollow fiber condition DL_{AG-20} is presented in Figure 7.4(a). It can be qualitatively observed that the silica was dispersed thoroughly across the composite layer and the outer surface of the membrane. Figure 7.4(b) displays the silica distribution profile in a line-scan mode of hollow fibers spun with different air-gap length, take-up speed and outer-dope flow rate. A sharp appearance of high silica intensity in the profile not only confirms the existence of nano-silica in the outer layer but also allows us to estimate the thickness of the composite outer layer. Depending upon the spinning conditions, the thickness of composite layer falls in the range of 3-18 μm. The high take-up speed or low outer-dope flow rate results in a reduced composite outer layer thickness. The EDX result also supports the achievement of membranes consisting of a thin PVDF/nano-silica composite layer bonded on a thick fully porous substructure.

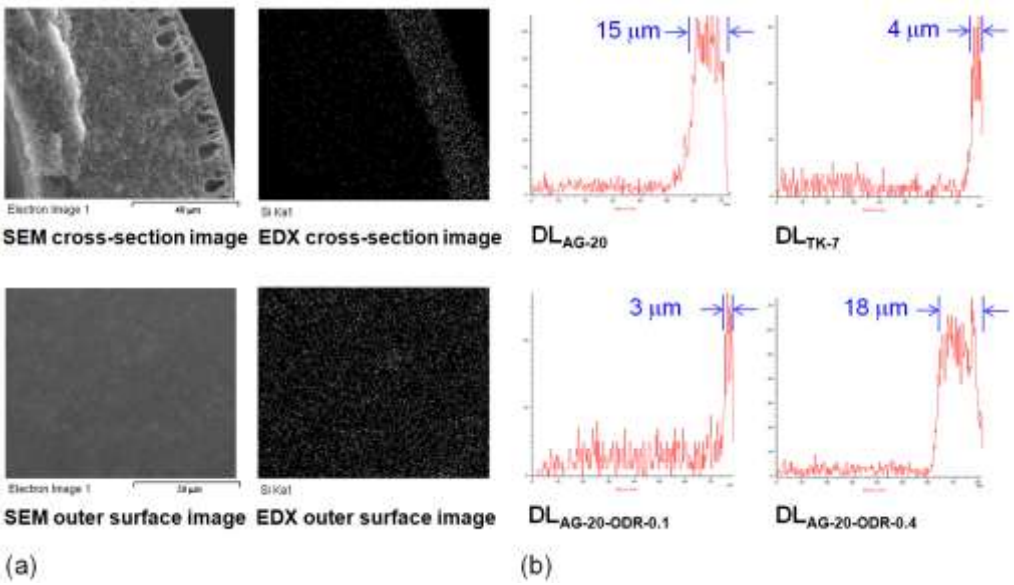

Figure 7.4 The distribution of silica and the estimation of composite layer thickness of PVDF/nano-silica dual-layer hollow fibers using EDX-SEM characterization:

(a) Typical silica distribution profile in cross-section and outer surface morphologies (DL_{AG-20})

(b) The effect of air-gap distance, take-up speed and outer dope flow rate on the silica distribution profile and the corresponding nanocomposite outer-layer thickness.

Table 7.2 tabulates the membrane properties of as-spun PVDF/nano-silica hollow fiber membranes which includes the mean pore size, effective surface porosity, overall porosity and water contact angle.

Table 7.2 Membrane properties of PVDF/silica dual-layer hollow fiber membranes

Membrane	Mean pore size, r (nm)	Effective surface porosity, ε_s/δ (m^{-1})	Overall porosity (%)	Water contact angle, θ (°)
The effect of air-gap distance				
DL_{AG-20}	62.2 ±0.6	(6.41 ±0.62) x 10^2	68.0 ±0.5	99.0 ±2.8
The effect of take-up speed				
DL_{TK-7}	55.0 ±0.3	(3.94 ±0.56) x 10^2	67.0 ±2.1	88.2 ±1.8
The effect of outer-dope flow rate				
$DL_{AG-20-ODR-0.1}$	50.3 ±1.2	(8.61 ±0.18) x 10^2	68.3 ±1.3	95.7 ±3.9
$DL_{AG-20-ODR-0.4}$	53.1 ±0.7	(5.83 ±0.30) x 10^2	67.4 ±0.8	96.7 ±3.1

It can be seen that all resultant membranes possess a mean pore size in the range of 50-62 nm with an effective surface porosity in the magnitude of 10^2 and overall bulk porosity nearly of 69%. Such pore characteristics may be attributed to the combination effect of (1) the incorporation of nano-silica into the PVDF matrix which could help in achieving a small pore size with a high surface porosity [61] and (2) the elongation stress via spinning at a high-air gap or high take-up speed, which has been discussed in our previous studies [39]. Additional evidence can be drawn from the fact that the membranes with a thinner composite outer-layer thickness resulting from the higher elongation stress (i.e. $DL_{TK\text{-}7}$ and $DL_{AG\text{-}20\text{-}ODR\text{-}0.1}$) tends to have a smaller mean pore size with a higher effective surface porosity compared to membranes having a thicker outer-layer thickness i.e. $DL_{AG\text{-}20}$ and $DL_{AG\text{-}20\text{-}ODR\text{-}0.4}$.

The hydrophobicity of fabricated hollow fibers with various spinning conditions employed was evaluated by determining the water contact angle at the membrane outer surface. In most cases, membranes show a high water contact angle of 90-100°, thus reflecting the improvement of the membrane hydrophobicity compared to the pristine single-layer PVDF hollow fibers (contact angle of 81-86°). This observation implies that the existence of nano-silica could play an essential role on the enhanced hydrophobicity. It is presumably because of its highly hydrophobic nature (contact angle of 105°) in addition to the significant effect on surface porosity as mentioned previously. However, it should be noted that for the case of high take-up speed spinning ($DL_{TK\text{-}7}$), a moderate increment of water contact angle is observed which is possibly due to the lower in surface porosity. The same phenomenon has also reported in previous studies [39].

7.3.2 Pervaporation performance of PVDF/nano-silica composite dual-layer hollow fiber membranes

The pervaporation tests of PVDF/nano-silica dual-layer hollow fibers spun with different spinning conditions were first carried out using a 5 wt% ethanol feed solution, operating temperature of 50 °C and downstream pressure of ~ 0 Pa. The corresponding separation performance in terms of permeation composition, ethanol-water separation factor and total flux of the membranes is summarized in Table 7.3. The membranes spun at a high air-gap length of 20 cm regardless of different outer-dope flow rates (i.e. DL_{AG-20}, $DL_{AG-20-ODR-0.1}$ and $DL_{AG-20-ODR-0.4}$) show a relatively better ethanol-water separation factor compared to the membrane prepared at a high take-up speed (DL_{TK-7}). This may be attributed to the fact that the DL_{TK-7} membranes possess a lower hydrophobicity even though they have comparable pore sizes with other membranes.

Table 7.3 Pervaporation performance of PVDF/nano-silica dual-layer hollow fiber membranes with various spinning conditions

Spinning code	Permeate composition (wt%)		Pervaporation performance[a]	
	Ethanol	Water	Separation factor, $\alpha_{ethanol/water}$	Total flux, W_{total} (g m^{-2} h^{-1})
The effect of air-gap distance				
DL_{AG-20}	32.37 ±0.60	67.63 ±0.60	8.51 ±0.23	4321 ±161
The effect of take-up speed				
DL_{TK-7}	29.75 ±0.02	70.25 ±0.02	7.59 ±0.01	2639 ±291
The effect of outer-dope flow rate				
$DL_{AG-20-ODR-0.1}$	31.58 ±1.0	68.42 ±1.0	8.61 ±0.44	4255 ±269
$DL_{AG-20-ODR-0.4}$	31.77 ±1.0	68.23 ±1.0	8.74 ±0.29	4111 ±387

[a] Feed solution: 5 ±0.5 wt% ethanol/water mixture; feed flow rate: 30 l h^{-1}; operating temperature: 50 °C; downstream pressure: 0 Pa

The membrane surface porosity has a huge influence on the total flux of the membranes in all cases. Membranes with a higher effective surface porosity/overall porosity tend to produce a greater total permeation flux. The surface porosities presented in Table 7.2 seem to offer a clearer understanding of its influence on the flux enhancement in comparison to the bulk porosities. Overall, all resultant membranes exhibit ethanol-water separation factors of 7.6-8.74 (30-33 wt% ethanol) and total fluxes of 2,640-4,320 g m^{-2} h^{-1}. Despite the fact that the membranes display a remarkably high flux, the membrane selectivity is still lower than our target which at least ethanol-water separation factor of 20 is preferable to compete with distillation as stated earlier in the introduction.

Figure 7.5 illustrates the effect of downstream pressure on pervaporation performance of PVDF/nano-silica dual layer hollow fibers using a 5 wt% ethanol as the feed solution at 50 °C. Interestingly, the alteration of downstream pressure shows a great effect on both flux and separation factor behaviors. With the reference to Figure 7.5(a), the total flux decreases considerably at first and then further declines gradually with an increase in downstream pressure for all cases. The curve characteristic on the flux-downstream pressure dependence is somewhat consistent with the curve pattern in the modified pore-flow model. In addition, the declining pattern of total flux as a function of downstream pressures is found to be different for each membrane, particularly at relatively low downstream pressures, while approaching at a high downstream pressure the linear relationship with comparable flux values is observed for all membranes.

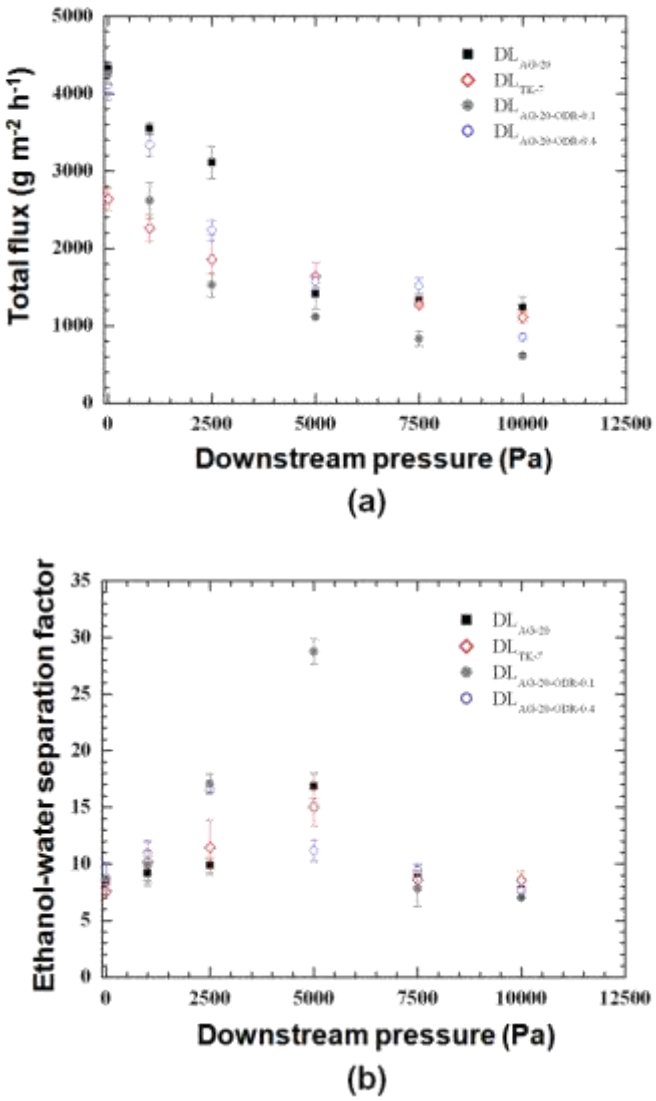

Figure 7.5 The effect of downstream pressure on pervaporation performance of PVDF/silica nanocomposite dual-layer hollow fiber membranes at 5 ±0.5 wt% ethanol feed solution and 50 °C: (a) Total flux (b) Separation factor

The significance of downstream pressure on membrane selectivity or separation factor is revealed in Figure 7.5(b). While only a slight difference in ethanol-water separation factor for all membranes (in a range of 7-9) is found at the downstream pressure ~ 0 Pa, the enrichment in the separation factor is clearly observed by increasing downstream pressure. Interestingly, the membrane selectivity can be achieved with ethanol-water separation factor as high as 29 at the downstream pressure of 5 kPa for the membrane spun at the 20 cm air-gap and the 0.1 outer- dope flow rate ($DL_{AG\text{-}20\text{-}ODR\text{-}0.1}$). For the

membranes with other spinning conditions (DL_{AG-20}, DL_{TK-7} and $DL_{AG-20-ODR-0.4}$), the incremental separation factors of 15-18 is observed with the different downstream pressures; namely 2.5 kPa for DL_{TK-7}, and 5 kPa for DL_{AG-20} and $DL_{AG-20-ODR-0.4}$. Another interesting finding is that when the downstream pressure was applied beyond the optimal pressure, a significant drop in the membrane selectivity is obvious in all membranes with the remaining separation factor of 7-9. Based on our observations during experiments, a further increase in downstream pressure results in a continuous reduction of separation factor coupled with a serious drop of total flux.

7.3.3 The role of downstream pressures on pervaporation transport and its predictability via the modified pore-flow model

It is clear that the downstream pressure could play a very crucial role on mass pervaporation transport in PVDF/nano-silica dual-layer hollow fiber membranes, which turns out to provide a great opportunity to enhance the membrane selectivity. In this study, the modified pore-flow model is employed to further verify and understand the selectivity-downstream pressure dependence phenomenon. Table 7.4 lists the transport parameters and saturation pressure for all membranes obtained from the pure water and pure ethanol system and used in the model equation. It can be seen that the same magnitude in each A/δ, B/δ and C/δ transport parameters is presented for all membranes. However, the liquid transport parameters (A/δ) for pure ethanol (magnitude of 10^{-5}) are greater than those for pure water (magnitude of 10^{-8}), which indicates the high hydrophobic and swelling properties of hollow fiber membranes [40].

Table 7.4 Liquid and vapor transport parameters of the pure component system based on the modified pore-flow model

Membrane	Parameters in model equations							
	Pure water				Pure Ethanol			
	Liquid transport	Vapor transport		Saturation vapor pressure	Liquid transport	Vapor transport		Saturation vapor pressure
	A_w/δ (mol m^{-2} s^{-1} Pa^{-1})	B_w/δ (mol m^{-2} s^{-1} Pa^{-2})	C_w/δ (mol m^{-2} s^{-1} Pa^{-1})	$P_{w,s}$ (Pa)	A_e/δ (mol m^{-2} s^{-1} Pa^{-1})	B_e/δ (mol m^{-2} s^{-1} Pa^{-2})	C_e/δ (mol m^{-2} s^{-1} Pa^{-1})	$P_{e,s}$ (Pa)
DL_{AG-20}	5.05×10^{-8}	2.50×10^{-10}	5.15×10^{-6}	4500	1.65×10^{-5}	4.92×10^{-10}	3.10×10^{-6}	28000
DL_{TK-7}	4.82×10^{-8}	2.05×10^{-10}	4.86×10^{-6}	5000	1.58×10^{-5}	2.25×10^{-10}	3.26×10^{-6}	35000
$DL_{AG-20-ODR-0.1}$	4.95×10^{-8}	2.73×10^{-10}	5.90×10^{-6}	4000	1.55×10^{-5}	3.92×10^{-10}	3.85×10^{-6}	35000
$DL_{AG-20-ODR-0.4}$	5.25×10^{-8}	1.83×10^{-10}	5.12×10^{-6}	2500	1.67×10^{-5}	4.93×10^{-10}	3.50×10^{-6}	25000

This information is consistent with the observation during experiments where the fibers showed no swelling in pure water but exhibited high swelling in pure ethanol. The vapor transport parameter, B/δ, which refers to the surface flow mechanism obtained in pure ethanol is always higher than the one in pure water. For the vapor transport parameter, C/δ, which represents Knudsen diffusion contribution, the opposite trend is observed, the calculated C/δ of pure water is higher than that of pure ethanol. From this finding, it possibly infers that the water may preferentially transport by Knudsen diffusion rather than surface flow whereas the ethanol may favorably transport via surface flow rather than Knudsen diffusion.

The saturation vapor pressures (P*) attained for pure water are in range of 2.5-5 kPa for pure water and 28-35 kPa for pure ethanol, which is found to be strongly dependent on each membrane. Compared to the saturation vapor pressure of water (12.4 kPa) and ethanol (29.5 kPa) at 50 °C as calculated by the Antoine equation [62], the significant

difference in the values can be observed in particular for the case of water. This can be understood from the fact that in the pore-flow model, the evaporation phenomenon occurring in the pore can be more complicated for cases especially when the pore is very small, leading to a strong interaction between absorbed vapor and membrane pore. In such a case, the saturation vapor pressure simulated by the pore-flow concept can be different from the literature values [63,64]. In other words, the saturation vapor pressure of water derived from the modified pore-flow model is lower than that of predicted from a simple evaporation prediction using the Antoine equation most likely due to the nano- pore size, great hydrophobicity and non-swelling property in water of the dual-layer hollow fiber membranes.

Table 7.5 summarizes the pore size and total saturation vapor pressure estimated from transport parameters listed in Table 7.4. It can be observed that the pore size (2.1-3.1 nm) predicted from the liquid transport parameter from pure water tests is smaller than that (50-62 nm) determined from gas permeation tests, whereas the pure ethanol system tests resulted in much larger pore size (74-114 nm). The pore size expansion in pure ethanol may be due to the preferential affinity of ethanol and the strong swelling in the hydrophobic membranes [40,65]. For both pure component systems, the pore size predicted from the vapor parameter is similar to that obtained from gas permeation tests. This may be attributed to the similarity in the gas/vapor phase where the strong membrane swelling is compromised compared to the liquid in contact.

Table 7.5 Estimation of pore size and total saturation vapor pressure by the modified pore-flow model

Membrane	Pore size (nm) (Gas permeation test)	Pore size from transport parameters (nm)[a, b]				Total saturation vapor pressure for a binary system, $P_{*,\text{ethanol-water}}$ (Pa)
		Pure water		Pure ethanol		
		Calculated from A_w/δ	Calculated from C_w/δ	Calculated from A_e/δ	Calculated from C_e/δ	
DL_{AG-20}	62.2	2.51	52.5	91.2	50.5	4970
DL_{TK-7}	55.0	3.12	80.6	114	86.4	5600
$DL_{AG-20-ODR-0.1}$	50.3	2.14	44.8	76.3	46.7	4620
$DL_{AG-20-ODR-0.4}$	53.1	2.68	57.4	96.2	62.7	2950

[a] For A_w/δ and A_e/δ, the pore size is calculated from $r=\left[\left(\frac{A}{\delta}\right)\frac{8\eta M}{\rho}\frac{1}{(\varepsilon_s/\delta)}\right]^{-1/2}$; the detailed calculations for water and ethanol systems are given in Appendix B.1

[b] For C_w/δ and C_e/δ, the pore size is calculated from $r=\frac{3}{2}\left(\frac{C}{\delta}\right)\left(\frac{\pi M}{8RT}\right)^{1/2}\frac{RT}{(\varepsilon_s/\delta)}$; the detailed calculations for water and ethanol systems are given in Appendix B.2

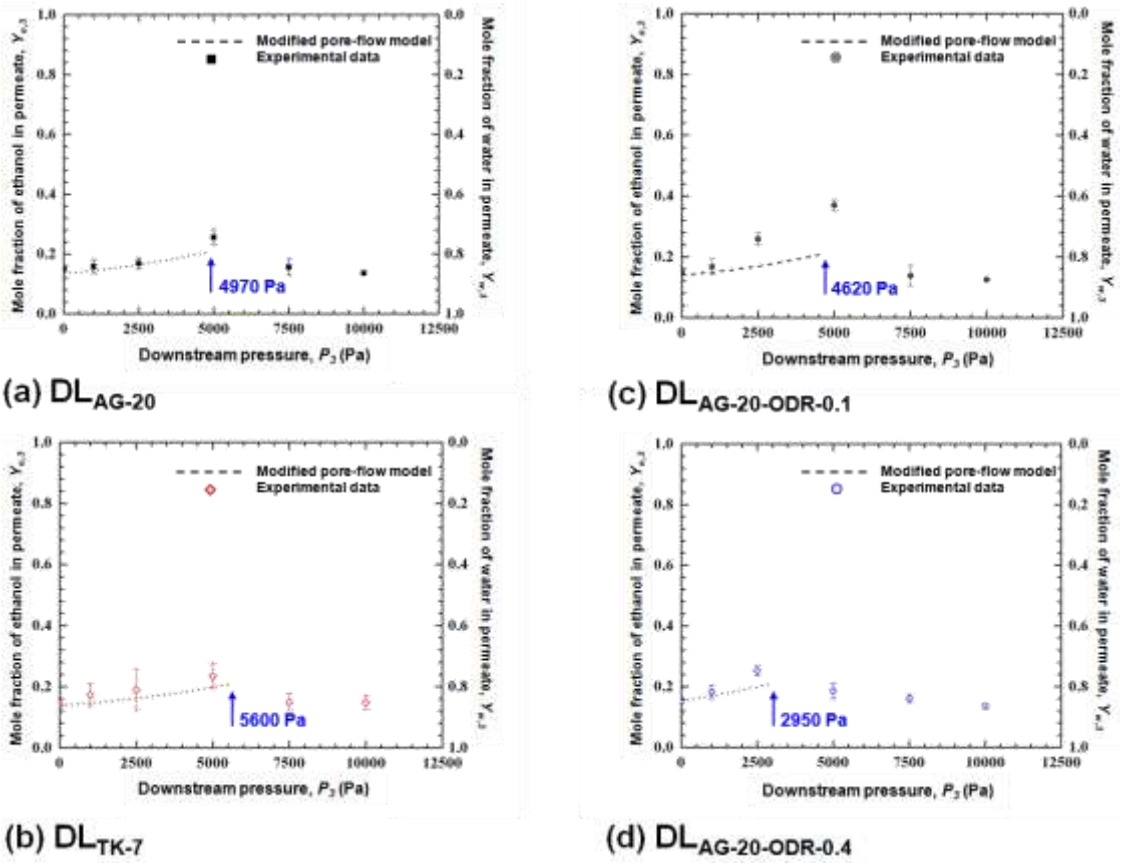

Figure 7.6 Comparison of ethanol mole fraction at the permeate side as a function of downstream pressures from experiments and theoretical predictions from the modified pore-flow model for various hollow fiber membranes (a) DL_{AG-20} (b) DL_{TK-7} (c) $DL_{AG-20-ODR-0.1}$ and (d) $DL_{AG-20-ODR-0.4}$.

Figure 7.6 compares the ethanol mole fraction of the permeate as a function of downstream pressure obtained from experiments with the prediction from the modified pore-flow model using all transport parameters listed in Table 7.4. From the result, there is a fair agreement between the modified pore-flow model and the experimental data. In any case, the model is able to predict the increment of ethanol permeate mole fraction (ethanol selectivity). However, one may see that the influence of downstream pressure on membrane separation can be more complicated in particular for the membrane possessing a high ethanol-water separation factor e.g. $DL_{AG\text{-}20\text{-}ODR\text{-}0.1}$ where the modified pore-flow shows somewhat deviation for predicting mole fraction of the ethanol permeate at the downstream pressure greater than 1 kPa. This indicates that there may be other separation mechanisms or altered permeate/membrane interactions that facilitate the ethanol transport and meanwhile hinder the water transport. Even though the explicit separation mechanism has yet well understood, this existing phenomenon has been demonstrated in several studies [66-68]. Ghofar and Kokugan [68] reported the same phenomenon that the ethanol can be enriched exceed its vapor-liquid equilibrium composition through hydrophobic porous membranes. They suggested that an increase in downstream pressure towards to the saturation pressure of the dilute ethanol solution could aid the enhancement of the strong interaction between ethanol permeate and hydrophobic membranes.

Another important finding is with regards to the downstream pressure value that the membranes display the maximal ethanol mole fraction (ethanol selectivity). As shown in Figure 7.6, there is a close correlation between the total saturation vapor pressure predicted from the modified pore-flow model and the optimal pressure point for each membrane. Previous studies reported that the enriched ethanol on permeate side can be

achieved when the downstream pressure is increased and approaches the saturated vapor pressure of the feed mixture. Similarly, this study suggests that the modified pore-flow model is adequate to predict the actual total saturation vapor pressure of the system which typically corresponds to the chance in achieving the optimal separation selectivity. In other words, this finding suggests operating at a downstream pressure which can adequately be predicted via the modified pore-flow model and is close to the saturated vapor pressure of the system.

7.3.4 Comparison of pervaporation performance with the literature

Figure 7.7 illustrates the ethanol-water separation performance in terms of separation factor and flux of various membrane materials reported in the literature, including PVDF/nano-silica dual-layer hollow fiber membranes developed in this study. Table 7.6 tabulates the status of ethanol-water separation performance for polymeric membranes, Table 7.7 for inorganic membranes and Table 7.8 for mixed-matrix or organic-inorganic membranes. Most polymeric membranes reported in previous studies have a relatively low selectivity with a wide range of permeation flux. Silicalite-1 or hydrophobic zeolite membranes exhibit both high selectivity and flux while the pervaporation performance of mixed-matrix or hybrid membranes, which mostly are silicalite-1/PDMS membranes, is spatially scattered in the transition gap between both respective materials.

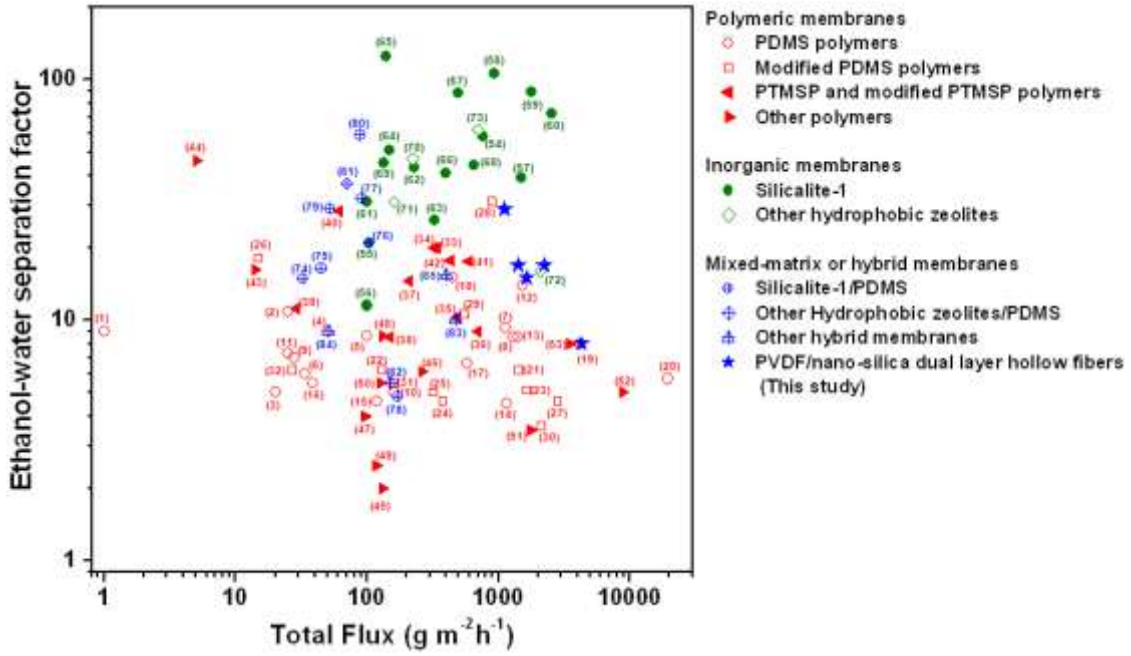

Figure 7.7 Graphical representation of separation performance of PVDF/nano-silica dual-layer hollow fiber membranes for ethanol recovery in a comparison with various membranes in the literature

It can be seen that the developed PVDF/nano-silica dual-layer hollow fibers display an outstanding ethanol-water separation factor and a sustainable flux compared to most prior art of polymeric and hybrid membranes even including the commercially available ones [71,72,77]. The best performance observed with the separation factor 29 and total flux of 1,100 g m^{-2} h^{-1} is found in the same region with the separation characteristic of inorganic membranes. With such encouraging separation performance and together with the benefits of membrane fabrication and process operation at a practical industrial-scale vacuum system, the newly developed PVDF/nano-silica dual-layer hollow fiber can be a promising candidate for ethanol recovery.

Table 7.6 Polymeric membranes for ethanol recovery via pervaporation

Membrane material	Configuration	Feed composition (wt%)	T (°C)	Separation factor, $\alpha_{ethanol/water}$	Total flux (g m^{-2} h^{-1})	Reference and referring number in Figure 7.7	
PDMS polymers							
PDMS	Flat sheet	11.9/88.1	25	9.0	1	Changluo et al. (1987) [69]	1
PDMS	Flat sheet	8/92	30	10.8	25.1	Kazuhiko and Kiyohide (1987) [24]	2
PDMS	Flat sheet	10/90	30	5.0	20	Conclaves et al. (1983) [70]	3
PDMS	Flat sheet	6/94	35	9.0	50	Moermans et al. (2000) [71]	4
PDMS (GE 615 membrane)	Flat sheet	6/94	50	8.6	100	Moermans et al. (2000) [71]	5
PDMS (Sulzer membrane)	Flat sheet	6/94	35	6.0	34	Vankelecom et al (1995) [72]	6
PDMS on cellulose acetate support	Flat sheet	5/95	40	9.3	1139.6	Luo et al. (2008) [73]	7
PDMS on cellulose acetate support	Flat sheet	5/95	40	8.5	1300	Li et al. (2004) [74]	8
PDMS on polyvinyl fluoride support	Flat sheet	11.9/88.1	20	7	28	Changluo et al. (1987) [69]	9
PDMS on Nylon support	Flat sheet	10/90	40	5.0	160	Huang et al. (2009) [25]	10
PDMS on polyetherimide support	Flat sheet	7/93	22	7.3	25	Jia et al. (1992) [32]	11
PDMS on PTFE support	Flat sheet	6/94	20	14.0	1530	Mori and Inaba (1990) [75]	12
PDMS on polyamide support	Flat sheet	4/96	40	8.5	1400	Shi et al. (2007) [76]	13
PDMS on polysulfone support	Flat sheet	4/96	40	4.5	1150	Shi et al. (2007) [76]	14
PDMS on polyimide support	Flat sheet	3/97	41	4.6	120	Dobrak et al. (2010) [28]	15
PDMS on microporous support (MTR membrane)	Flat sheet	6/94	25	5.5	39	Schmidt et al. (1997) [77]	16

Table 7.6 Polymeric membranes for ethanol recovery via pervaporation (Cont'd)

Membrane material	Configuration	Feed composition (wt%)	T (°C)	Separation factor, $\alpha_{ethanol/water}$	Total flux (g m^{-2} h^{-1})	Reference and referring number in Figure 7.7	
PDMS polymers							
PDMS/polysulfone composite	Hollow fiber	8/92	50	6.6	576	Guo et al. (2010) [78]	17
PDMS/PVDF/non-woven-fiber, multi-layer configuration	Flat sheet	5/95	60	15	450	Zhan et al. (2010) [79]	18
PDMS on ZrO_2/Al_2O_3 ceramic support	Tubular	4.2/95.8	60	7.93	4190	Xiangli et al. (2008) [80]	19
PDMS on ZrO_2/Al_2O_3 ceramic support	Tubular	4.3/95.7	70	5.7	19500	Fenjuan et al. (2007) [81]	20
Modified PDMS polymers							
PPMS on cellulose acetate support	Flat sheet	5/95	40	6.2	1432.6	Luo et al. (2008) [73]	21
PDMS-styrene graft copolymer on PTFE support	Flat sheet	8.1/91.9	60	6.2	130	Takegemi et al. (1992) [26]	22
Plasma-induced grafted PDMS/PVDF composite	Flat sheet	10/90	35	5.1	1650	Chang and Chang (2006) [82]	23
PDMS (Plasma-polymerized Tetramethoxysilane monomers)	Flat sheet	4/96	25	4.6	380	Kashiwagi et al. (1988) [83]	24
PDMS (Plasma-polymerized Hexamethyltrisiloxane monomers)	Flat sheet	4/96	25	5.0	320	Kashiwagi et al. (1988) [83]	25
PDMS (Plasma-polymerized hexamethyltrisiloxane PDMS membranes and treated with Octadecyldiethoxymethylsilane)	Flat sheet	4/96	25	18.0	15	Kashiwagi et al. (1988) [83]	26
Plasma-induced grafted TMVS/PVDF, coating by phosphate ester containing silicone copolymer	Flat sheet	10/90	30	4.6	2850	Chang and Chang (2002) [84]	27
Plasma-induced grafted TMVS/PVDF, coating by phosphate ester containing silicone copolymer	Multi-layer flat sheet	10/90	30	31	900	Chang and Chang (2004) [85]	28

Table 7.6 Polymeric membranes for ethanol recovery via pervaporation (Cont'd)

Membrane material	Configuration	Feed composition (wt%)	T (°C)	Separation factor, $\alpha_{ethanol/water}$	Total flux (g m^{-2} h^{-1})	Reference and referring number in Figure 7.7	
Modified PDMS polymers							
PDMS-imide copolymers (synthesized from ODMS and PMDA)	Flat sheet	10/90	40	10.6	560	Krea et al. (2004) [86]	29
PDMS-imide copolymers (synthesized from ODMS and 6FDA)	Flat sheet	10/90	40	3.6	2120	Krea et al. (2004) [86]	30
PDMS-polystyrene interpenetrating polymer network on polyethersulfone ultrafiltration support	Flat sheet	10/90	60	5.5	160	Liang and Ruckenstein (1996) [87]	31
PDMS-polysulfone block copolymers	Flat sheet	10/90	25	6.2	27	Okamoto et al. (1987) [88]	32
PTMSP polymers							
PTMSP	Flat sheet	6/94	30	19.9	340	Volkov et al. (2004) [21]	33
PTMSP	Flat sheet	6/94	30	19.9	325	Fadeev et al. (2003) [89]	34
PTMSP	Flat sheet	6/94-7/93	50	10.3	480	Nagase et al. (1991) [90]	35
PTMSP	Flat sheet	6/94	75	9	700	Gonzalez-Velasco et al. (2002) [22]	36
PTMSP	Flat sheet	10/90	50	14.5	210	Claes et al. (2010) [37]	37
PTMSP	Flat sheet	10/90	50	8.5	150	Gonzalez-Marcos et al. (2004) [91]	38
PTMSP	Flat sheet	7/93	30	11.2	29	Nagase et al. (1990) [23]	39

Table 7.6 Polymeric membranes for ethanol recovery via pervaporation (Cont'd)

Membrane material	Configuration	Feed composition (wt%)	T (°C)	Separation factor, $\alpha_{ethanol/water}$	Total flux (g m^{-2} h^{-1})	Reference and referring number in Figure 7.7	
Modified PTMSP polymers							
PTMSP/PDMS graft copolymer	Flat sheet	7/93	30	28.3	62	Nagase et al. (1990) [23]	40
Trimethylsilyl substituted PTMSP	Flat sheet	6/94-7/93	50	17.6	590	Nagase et al. (1991) [90]	41
n-Decane substituted PTMSP	Flat sheet	6/94-7/93	50	17.8	430	Nagase et al. (1991) [90]	42
Other polymers							
Styrene-fluoroalkyl acrylate graft copolymer on PDMS support	Flat sheet	8/92	30	16.3-45.9	5-14	Kazuhiko and Kiyohide (1987) [24]	43,44
Polyorganophosphazene containing $-OC_2H_5$ pendant group on Nylon support	Flat sheet	10/90	40	2.0	130	Huang et al. (2009a) [25]	45
Polyorganophosphazene containing $-OCH_2CF_3$ pendant group on Nylon support	Flat sheet	10/90	40	6.1	260	Huang et al. (2009a) [25]	46
Polyorganophosphazene containting $-OCH_2CF_2CF_2CF_2CF_2H$ pendant group	Flat sheet	10/90	40	4.0	96	Huang et al. (2009a) [25]	47
Polyurethaneurea containing PDMS	Flat sheet	10/90	40	8.6	130	Takegemi et al. (1992) [26]	48
PEBA (polyether block amide) PEBAX® 2533, Antofina	Flat sheet	5/95	23	2.5	117.5	Liu et al. (2005) [27]	49
SBS (Styrene-butadiene-styrene) block copolymer, dense	Flat sheet	3/97	41	5.5	125	Dobrak et al. (2010) [28]	50
SBS (Styrene-butadiene-styrene) block copolymer, porous	Flat sheet	3/97	41	3.5	1752	Dobrak et al. (2010) [28]	51
PVDF, asymmetric membrane	Hollow fiber	5/95	50	5-8	3500-8800	Sukitpaneenit and Chung (2011) [39]	52,53

Table 7.7 Silicalite-1 and hydrophobic inorganic membranes for ethanol recovery via pervaporation

Membrane material	Configuration	Feed composition (wt%)	T (°C)	Separation factor, $\alpha_{ethanol/water}$	Total flux (g m^{-2} h^{-1})	Reference and referring number in Figure 7.7	
Silicalite-1							
Silicalite-1 on porous stainless steel support	Flat sheet	4/96	60	58	760	Sano et al. (1994) [92]	54
Silicalite-1 on porous stainless steel support	Flat sheet	5/95 (Fermented ethanol)	30	21	104	Ikegami et al. (2003) [93]	55
Silicalite-1 on Al_2O_3 support	Flat sheet	9.7/90.3	32	11.5	100	Liu et al. (1996) [94]	56
Silicalite-1 on porous α-Al_2O_3 tube support	Tubular	5/95	60	39	1510	Shen et al. (2011) [95]	57
Silicalite-1 on Mullite tubular support	Tubular	5/95	60	106	930	Lin et al. (2003) [96]	58
Silicalite-1 on α-Al_2O_3 tubular support	Tubular	5/95	60	89	1800	Lin et al. (2001) [97]	59
Silicalite-1 on Mullite tubular support	Tubular	10/90	60	72	2550	Lin et al. (2000) [98]	60
Silicalite-1 on Stainless steel support	Flat sheet	10/90 (Fermented ethanol)	30	31	100	Ikegami et al. (2002) [99]	61
Silicalite-1 coated with PDMS on Stainless steel support	Flat sheet	10/90 (Fermented ethanol)	30	43	230	Ikegami et al. (2002) [99]	62
Silicalite-1 on stainless steel support	Flat sheet	4/96	30	26-51	150-330	Matsuda et al. (2002) [100]	63,64
Silicalite-1 coated with PDMS on stainless steel support	Flat sheet	4/96	30	125	140	Matsuda et al. (2002) [100]	65
Silicalite-1 on porous stainless steel disk support	Flat sheet	4.7/95.3	30	41	400	Nomura et al. (2002) [101]	66
Silicalite-1 on porous stainless steel disk support	Flat sheet	4.6/95.4 (Fermented ethanol)	30	88	500	Nomura et al. (2002) [101]	67

Table 7.7 Silicalite-1 and hydrophobic inorganic membranes for ethanol recovery via pervaporation (Cont'd)

Membrane material	Configuration	Feed composition (wt%)	T (°C)	Separation factor, $\alpha_{ethanol/water}$	Total flux (g m^{-2} h^{-1})	Reference and referring number in Figure 7.7	
Silicalite-1							
Silicalite-1 treated with silane, $C_8H_{17}SiCi_3$, on porous stainless steel disk support	Flat sheet	4/96	50	44	650	Sano et al. (1995) [102]	68
Silicalite-1 treated with silane, $C_{18}H_{37}SiCi_3$, on porous stainless steel disk support	Flat sheet	4/96	50	45	133	Sano et al. (1995) [102]	69
Other hydrophobic zeolite							
Ge-ZSM-5, on stainless steel support	Flat sheet	5/95	30	47	223	Li et al. (2003) [103]	70
B-ZSM-5, on Al_2O_3-coated SiC multi-channel monolith support	Flat sheet	5/95	60	31	160	Bowen et al. (2003) [104]	71
Ti-Silicalite, on α-Al_2O_3 capillary support	Tubular	5/95	45	16-62	700-2100	Sebastian et al. (2010) [105]	72,73

Table 7.8 Silicalite-1/PDMS mixed-matrix and other hybrid membranes for ethanol recovery via pervaporation

Membrane material	Particle size (μm)	Particle loading (%)	Feed composition (wt%)	*T* (°C)	Separation factor, $\alpha_{ethanol/water}$	Total flux (g m^{-2} h^{-1})	Reference and referring number in Figure 7.7	
Silicalite-1/PDMS								
Silicalite-1/PDMS	0.5-5	40	5-5.5/94.5-95	22.5	14.9	32.2	Hennepe et al. (1987) [31]	74
Silicalite-1/PDMS	0.5-5	60	5-5.5/94.5-95	22.5	16.5	44.9	Hennepe et al. (1987) [31]	75
Silicalite-1/PDMS	~1	60	5.3/94.7	50	21	105	Yi et al. (2010) [34]	76
Silicalite-1/PDMS	~1	67	5.3/94.7	50	32	90	Yi et al. (2010) [34]	77
Silicalite-1 filled PDMS on polyimide support	0.1-0.23	15	3/97	41	4.8	170	Dobrak et al. (2010) [28]	78
Silicalite-1 (UOP Inc.) /PDMS	1-10	70	7/93	22	29	52	Jia et al. (1992) [32]	79
Silicalite-1/PDMS	0.3-4	77	7/93	22	59	89	Jia et al. (1992) [32]	80
Hydrophobic zeolites/PDMS								
ZSM-5/PDMS (Si/Al = 137)	~2.4	50	5/95	50	37	70	Vane et al. (2008) [33]	81
ZSM-5/PDMS, on polyimide support, CBV 3002 (Si/Al =240)	1-1.5	30	3/97	41	5.5	151	Dobrak et al. (2010) [28]	82
Other hybrid membranes								
PDMS/Polyphosphazene nanotube	50 in length, 0.040 in diameter	10	10/90	40	10	476	Huang et al. (2009) [35]	83
PDMS/carbon black	0.051	10	6/94	35	9	51	Vankelecom et al. (1997) [36]	84
PTMSP/nano-silica	0.0045-0.0065	50	10/90	50	15.3	400	Claes et al. (2010) [37]	85
PVDF/nano-silica dual-layer hollow fiber	**0.016**	**20**	**5/95**	**50**	**8-29**	**1115-4320**	**The present study**	

7.4 Conclusions

In this study, we have developed the novel PVDF/nano-silica dual-layer hollow fiber membranes with desirable membrane morphology and separation performance for ethanol recovery using the concept of the modified pore-flow model. The following conclusions can be drawn from the result of the current work:

(1) By introducing hydrophobic nano-silica with optimizing air-gap distance, take-up speed and outer-dope flow rate, the desirable membrane morphology consisting of a thin skin layer of PVDF/silica composite, a highly sponge-like porous support structure is successfully fabricated. The resultant membranes possess the mean pore size in nano-range with a relative high surface porosity in the magnitude of 10^2 m^{-1}, and the water contact angle can be as high as 99°. The membranes with a smaller pore size and greater hydrophobicity acquire a better membrane selectivity while the total flux is crucially contributed by the effective surface porosity of the membranes.

(2) The downstream pressure plays a critical role in controlling penetrant transports and membrane separation performance in addition to the related morphological and physical properties of membranes i.e., pore size, surface porosity and hydrophobicity. By applying downstream pressure close to the optimum total saturation vapor pressure which can be adequately predicted by the modified pore-flow model, the ethanol enrichment can be accomplished.

(3) The developed PVDF/nano-silica dual-layer hollow fiber membranes have ethanol-water separation factors of 8-29 and total fluxes of 1,100-4,300 g m^{-2} h^{-1} depending upon tailored membrane morphologies and controlled downstream pressures. In a

comparison with various types of membranes available in the literature, the accomplished high separation factor up to 29 and total flux 1,100 g m^{-2} h^{-1} is approachable the separation characteristic of inorganic membranes.

RFERENCES

[1] M. Balat, H. Balat, C. Oz, Progress in bioethanol processing, Prog. Energy Combust. Sci. 34 (2008) 551.

[2] S.K. Hoekman, Biofuels in the U.S.-challenges and opportunities, Renew. Energy 34 (2009) 14.

[3] T. Wiesenthal, G. Leduc, P. Christidis, B. Schade, L. Pelkmans, L. Govaerts, P. Georgopoulos, Biofuel support policies in Europe: lessons learnt for the long way ahead, Renew. Sustain. Energy Rev. 13 (2009) 789.

[4] K.R. Szulczyk, B.A. McCarl, G. Cornforth, Market penetration of ethanol, Renewable Sustainable Energy Rev. 14 (2010) 394.

[5] C. Somerville, H. Youngs, C. Taylor, S.C. Davis, S.P. Long, Feedstocks for lignocellulosic biofuels, Science 329 (2010) 790.

[6] L.R. Lynd, C.H.B. Cruz, Make way for ethanol, Science 330 (2010) 1176.

[7] M. Larrson, G. Zacchi, Production of ethanol from dilute glucose solution. A technical-economic evaluation of various refining alternatives, Bioprocess Eng. 15 (1996) 125.

[8] T. Eggeman, R.T. Elander, Process, economic analysis of pretreatment technologies, Bioresource Technol. 96 (2005) 2019.

[9] B.L. Maiorella, Ethanol, in: M. Moo-Young (Ed.), Comprehensive Biotechnology, vol. 3, New York: Pergamon Press (1985) 861.

[10] L.M. Vane, Review: Separation technologies for the recovery and dehydration of alcohols from fermentation broths, Biofuels Bioprod. Biorefin. 2 (2008) 553.

[11] C.A. Cardona, O.J. Sànchez, Fuel ethanol production: process design trends and integration opportunities, Bioresource Technol. 98 (2007) 2415.

[12] G. Stephanopoulos, Challenges in engineering microbes for biofuels production, Science 315 (2007) 801.

[13] Y. Huang, R.W. Baker, Bioethanol production using pervaporation and vapour permeation membranes, Presentation at International Congress on Membrane and Membrane Process, Honolulu, USA (2008).

[14] L. Y. Jiang, Y. Wang, T. S. Chung, X. Y. Qiao, J. Y. Lai, Polyimides for pervaporation membranes and biofuels separation, Prog. Polym. Sci. 34 (2009) 1135.

[15] H.L. Fleming, C.S. Slater, Pervaporation, in: Ho, W.S., Sirkar, K.K. (Eds.), Membrane Handbook, New York: Kluwer Academic Publishers (1992) 103.

[16] W.J. Groot, M.R. Kraayenbrink, R.G.J.M. van der Lans, K.C.H.A.M. Luyben, Ethanol production in an integrated fermentation/membrane system. Process simulations and economics, Bioprocess. Eng. 8 (1993) 189-201.

[17] D.J. O'Brien, L.H. Roth, A.J. McAloon, Ethanol production by continuous fermentation-pervaporation: A preliminary economic analysis, J. Membr. Sci. 166 (2000) 105.

[18] H.J. Huang, S. Ramaswamy, U.W. Tschirner, B.V. Ramarao, A review of separation technologies in current and future biorefineries, Sep. Purif. Technol. 62 (2008) 1.

[19] W.W. Ding, Y.T. Wu, X.Y. Tang, L. Yuan, Z.Y. Xiao, Continuous ethanol fermentation in a closed-circulating system using an immobilized cell coupled with PDMS membrane pervaporation, J. Chem. Technol. Biotechnol. 86 (2011) 82.

[20] L.M. Vane, A review of pervaporation for product recovery from biomass fermentation processes, J. Chem. Technol. Biotechnol. 80 (2005) 603.

[21] V.V. Volkov, A.G. Fadeev, V.S. Khotimsky, E.G. Litvinova, Y.A. Selinskaya, J.D. McMillan, S.S. Kelly, Effects of synthesis conditions on the pervaporation properties of Poly[1-(Trimethylsilyl)-1-Propyne] useful for membrane bioreactors, J. Appl. Polym. Sci. 91 (2004) 2271.

[22] J.R. Gonzalez-Velasco, J.A. Gonzalez-Marcos, C. Lopez-Dehesa, Pervaporation of ethanol-water mixtures through poly(1-trimethylsilyl-1-propyne) (PTMSP) membranes, Desalination 149 (2002) 61.

[23] Y. Nagase, K. Ishihara, K. Matsui, Chemical modification of poly(substituted-acetylene): II. Pervaporation of ethanol/water mixture through poly(1-trimethylsilyl-1-propyne)/poly(dimethylsiloxane) graft copolymer membrane, J. Poly. Sci. Part B: Polym. Phys. 28 (1990) 377.

[24] I. Kazuhiko, M. Kiyohide, Pervaporation of ethanol-water mixture through composite membranes composed of styrene-fluoroalkyl acrylate graft copolymers and crosslinked polydimethylsiloxane membrane, J. Appl. Polym. Sci. 34 (1987) 437.

[25] Y. Huang, J. Fu, Y. Pan, X. Huang, X. Tang, Pervaporation of ethanol aqueous solution by polyphosphazene membranes: Effect of pendant groups, Sep. Purif. Technol. 66 (2009) 504.

[26] S. Takegemi, H. Yamada, S. Tusujii, Pervaporation of ethanol/water mixture using novel hydrophobic membrane containing polydimethylsiloxane, J. Membr. Sci. 75 (1992) 93.

[27] F. Liu, L. Liu, X. Feng, Separation of acetone-butanol-ethanol (ABE) from dilute aqueous solutions by pervaporation, Sep. Purif. Technol. 42 (2005) 273.

[28] A. Dobrak, A. Figoli, S. Chovau, F. Galiano, S. Simone, I.F.J. Vankelecom, E. Drioli, B. Van der Bruggen, Performance of PDMS membranes in pervaporation:

Effect of silicalite fillers and comparison with SBS membranes, J. Colloid Interf. Sci. 346 (2010) 254.

[29] S. Kulprathipanja, R.W. Nousil, N.N. Li, Separation of fluids by means of mixed matrix membranes in gas permeation, US Patent No. 4,740,219 (1998).

[30] T. S. Chung, L. Y. Jiang, Y. Li, S. Kulprathipanja, Mixed matrix membranes (MMMs) comprising organic polymers with dispersed inorganic fillers for gas separation, Prog. Polym. Sci. 32 (2007) 483.

[31] H.J.C. te Hennepe, D. Bargeman, M.H.V. Mulder, C.A. Smolders, Zeolite-filled silicone rubber membranes Part 1. Membrane preparation and pervaporation results, J. Membr. Sci. 35 (1987) 39.

[32] M.D. Jia, K.V. Peinemann, R.D. Behling, Preparation and characterization of thin-film zeolite-PDMS composite membranes, J. Membr. Sci. 73 (1992) 119.

[33] L.M. Vane, V.V. Namboodiri, T.C. Bowen, Hydrophobic zeolite-silicone rubber mixed matrix membranes for ethanol-water separation: Effect of zeolite and silicone component selection on pervaporation performance, J. Membr. Sci. 308 (2008) 230.

[34] S. Yi, Y. Su, Y. Wan, Preparation and characterization of vinyltriethoxysilane (VTES) modified silicalite-1/PDMS hybrid pervaporation performanceand its application in ethanol separation from dilute aqueous solution, J. Membr. Sci. 360 (2010) 341.

[35] Y. Huang, P. Zhang, J. Fu, Y. Zhou, X. Huang, X. Tang, Pervaporation of ethanol aqueous solution by polydimethylsiloxane/polyphosphazene nanotube nanocomposite membranes, J. Membr. Sci. 339 (2009) 85.

[36] I.F.J. Vankelecom, J.D. Kinderen, B.M. Dewitte, J.B. Uytterhoeven, Incorporation of hydrophobic porous fillers in PDMS membranes for use in pervaporation, J. Phys. Chem. B 101 (1997) 5182.

[37] S. Claes, P. Vandezande, S. Mullens, R. Leysen, K.D. Sitter, A. Andersson, F.H.J. Maurer, H. Van den Rul, R. Peeters, M.K. Van Bael, High flux composite PTMSP-silica nanohybrid membranes for the pervaporation of ethanol/water mixtures, J. Membr. Sci. 351 (2010) 160.

[38] P. Peng, B. Shi, Y. Lan, A review of membrane materials for ethanol recovery by pervaporation, Sep. Sci. Technol. 46 (2011) 234.

[39] P. Sukitpaneenit, T.S. Chung, Molecular design of the morphology and pore size of PVDF hollow fiber membranes for ethanol-water separation employing the modified pore-flow concept, J. Membr. Sci. 374 (2011) 67.

[40] P. Sukitpaneenit, T.S. Chung, L.Y. Jiang, Modified pore-flow model for pervaporation mass transport in PVDF hollow fiber membranes for ethanol-water separation, J. Membr. Sci. 362 (2010) 393.

[41] X. Feng, R.Y.M. Huang, Liquid separation bymembranepervaporation: a review, Ind. Eng. Chem. Res. 36 (1997) 1048.

[42] J.G. Wijmans, R.W. Baker, The solution-diffusion model: a review. J. Membr. Sci. 107 (1995) 1.

[43] K.Y. Wang, S.W. Foo, T.S. Chung, Mixed matrix PVDF hollow fiber membranes with nanoscale pores for desalination through direct contact membrane distillation, Ind. Eng. Chem. Res. 48 (2009) 4474.

[44] S. Bonyadi, T.S. Chung, Flux enhancement in membrane distillation by fabrication of dual layer hydrophilic-hydrophobic hollow fiber membranes, J. Membr. Sci. 306 (2007) 134.

[45] M.M. Teoh, T.S. Chung, Membrane distillation with hydrophobic macrovoid-free PVDF-PTFE hollow fiber membranes, Sep. Purif. Technol. 66 (2009) 229.

[46] L.Y. Yu, Z.L. Xu, H.M. Shen, H. Yang, Preparation and characterization of PVDF-SiO2 composite hollow fiber UF membrane by sol-gel method, J. Membr. Sci. 337 (2009) 257.

[47] H.L. Shen, H. Liao, C.F. Xiao, Formation mechanism and properties of polyvinylidene fluoride (PVDF)/nano-silica hybrid membranes, Advanced Materials Research, 123-125 (2010) 93.

[48] N.A. Hashim, Y. Liu, K. Li, Preparation of PVDF hollow fiber membranes using SiO2 particles: The effect of acid and alkali treatment on the membrane performances, Ind. Eng. Chem. Res. 50 (2011) 3035.

[49] S.J. Oh, N. Kim, Y.T. Lee, Preparation and characterization of PVDF/TiO_2 organic-inorganic composite membranes for fouling resistance improvement, J. Membr. Sci. 345 (2009) 13.

[50] X. Cao, J. Ma, X. Shi, Z. Ren, Effect of TiO_2 nanoparticle size on the performance of PVDF membrane, Appl. Surf. Sci. 253 (2006) 2003.

[51] L. Yan, Y.S. Li, C.B. Xiang, Preparation of poly(vinylidene fluoride) (PVDF) ultrafiltration membrane modified by nano-sized alumina (Al_2O_3) and its antifouling research, Polymer 46 (2005) 7701.

[52] A. Bottino, G. Capannelli, A. Comite, Preparation and characterization of novel porous PVDF-ZrO_2 composite membrane, Desalination 146 (2002) 35.

[53] L.Y. Jiang, T.S. Chung, S. Kulprathipanja, Fabrication of mixed matrix hollow fibers with intimate polymer-zeolite interface for gas separation, AIChE J. 52 (2006) 2898.

[54] Y. Li, T.S. Chung, Z. Huang, S. Kulprathipanja, Dual-layer polyethersulfone (PES)/BTDA-TDI/MDI co-polyimide (P84) hollow fiber membranes with a submicron PES-zeolite beta mixed matrix dense-selective layer for gas separation, J. Membr. Sci. 277 (2006) 28.

[55] F.W. Greenlaw, W.D. Prince, R.A. Shelden, E.V. Thompson, Dependence of diffusive permeation rates on upstream and downstream pressures. II. Two component permeate, J. Membr. Sci. 2 (1977) 333.

[56] P.K. Ten, R.W. Field, Organophilic pervaporation: an engineering science analysis of component transport and the classification of behavior with reference to the effect of permeate pressure, Chem. Eng. Sci. 55 (2000) 1425.

[57] C. Vallieres, E. Favre, D. Roizard, J. Bindelle, D. Sacco, New insights into pervaporation mass transport under increasing downstream pressure conditions: critical role of inert gas entrance, Ind. Eng. Chem. Res. 40 (2001) 1559.

[58] Y. Wang, T. S. Chung, B. W. Neo, M. Gruender, Processing and engineering of pervaporation dehydration of ethylene glycol via dual-layer polybenzimidazole (PBI) /polyetherimide (PEI) Membranes, J. Membr. Sci. 378 (2011) 339.

[59] R.Y.M. Huang, J.W. Rhim, Separation characteristics of pervaporation membrane separation processes, in text book edited by R.Y.M. Huang: Pervaporation membrane separation processes, Amsterdam: Elsevier Science Publishers B.V. (1991).

[60] P. Sukitpaneenit and T.S. Chung, Molecular elucidation of morphology and mechanical properties of PVDF hollow fiber membranes from aspects of phase inversion, crystallization and rheology, J. Membr. Sci. 340 (2009) 192.

[61] H.L. Shen, H. Liao, C.F. Xiao, Formation mechanism and properties of polyvinylidene fluoride (PVDF)/nano-silica hybrid membranes, Adv. Mater. Res. 123-125 (2010) 93.

[62] J.M. Smith, H.C. Van Ness, M.M. Abbott, Introduction to Chemical Engineering Thermodynamics. Singapore: McGraw-Hill (2005).

[63] T. Okada, T. Matsuura, A new transport model for pervaporation, J. Membr. Sci. 59 (1991) 133.

[64] T. Matsuura, Synthetic Membranes and Membrane Separation Processes, CRC Press, Boca Raton, FL (1993).

[65] A. Sharma, S.P. Thampi, S.V. Suggala, P.K. Bhattacharya, Pervaporation from a dense membrane: Roles of permeant-membrane interactions, Kelvin effect, and membrane swelling, Langmuir 20 (2004) 4708.

[66] E. Hoffmann, D.M. Pfenning, E. Philippsen, P. Schwahn, M. Sieber, R. When, D. Woermann, G. Wiedner, Evaporation of alcohol/water mixtures through hydrophobic porous membranes, J. Membr. Sci. 34 (1987) 199.

[67] T. Kokugan, Kaseno, E. Yoshimoto, H. Kikukawa, A consideration of pervaporation by porous hydrophobic membranes for dilute ethanol solution, J. Chem. Eng. Jpn. 31 (1998) 153.

[68] A. Ghofar, T. Kokugan, The pervaporation mechanism of dilute ethanol solution by hydrophobic porous membranes, Biochem. Eng. J. 18 (2004) 235.

[69] Z. Changluo, L. Moe, X. Wei, Separation of ethanol-water mixtures by pervaporation-membrane separation process, Desalination 62 (1987) 299.

[70] M.C. Conclaves, G.S.S Marquez, F. Galembeck, Pervaporation and dialysis of water-ethanol solution by using silicone rubber-membrane, Sep. Sci. Technol. 18 (1983) 893.

[71] B. Moermans, W.D. Beuckelaer, I.F.J. Vankelecom, R. Ravishankar, J.A. Martens, P.A. Jacobs, Incorporation of nano-sized zeolites in membranes, Chem. Commun. 24 (2000) 2467.

[72] I.F.J. Vankelecom, D. Depré, S.D. Beukelaer, J.B. Uytterhoeven, Influence of zeolites in PDMS membranes: Pervaporation of water/alcohol mixtures. J. Phys. Chem. 99 (1995) 13193.

[73] Y. Luo, S. Tan, H. Wang, F. Wu, X. Liu, L. Li, Z. Zhang, PPMS composite membranes for the concentration of organics from aqueous solutions by pervaporation, Chem. Eng. J., 137 (2008) 496.

[74] L. Li, Z. Xiao, S. Tan, L. Pu, Z. Zhang, Composite PDMS membrane with high flux for the separation of organics from water by pervaporation, J. Membr. Sci. 243 (2004) 177.

[75] Y. Mori, T. Inaba, Ethanol production from starch in a pervaporation membrane bioreactor using clostridium thermohydrosulfuricum, Biotechnol. Bioeng. 36 (1990) 849.

[76] E. Shi, W. Huang, Z. Xiao, D. Li, M. Tang, Influence of binding interface between active and support layers in composite PDMS membranes on permeation performance, J. Appl. Polym. Sci. 104 (2007) 2468.

[77] S.L. Schmidt, M.D. Myers, S.S. Kelley, J.D. McMillan, N. Padukone, Evaluation of PTMSP membranes in achieving enhanced ethanol removal from fermentations by pervaporation, Appl. Biochem. Biotech. 63-65 (1997) 469.

[78] J. Guo, G. Zhang, W. Wu, S. Ji, Z. Qin, Z. Liu, Dynamically formed inner skin hollow fiber polydimethylsiloxane/polysulfone composite membrane for alcohol permselective pervaporation, Chem. Eng. J. 158 (2010) 558.

[79] X. Zhan, J. Li, J. Huang, C. Chen, Enhanced pervaporation performance of multi-layer PDMS/PVDF composite membrane for ethanol recovery from aqueous solution, Appl. Biochem. Biotechnol. 160 (2010) 632.

[80] F. Xiangli, W. Wei, Y. Chen, W. Jin, N. Xu, Optimization of preparation conditions for polydimethylsiloxane (PDMS)/ceramic composite pervaporation membranes using response surface methodology, J. Membr. Sci. 311 (2008) 23.

[81] X. Fenjuan, C. Yiwei, J. Wangin, X. Nanping, Polydimethylsiloxane (PDMS)/ceramic composite membrane with high flux for pervaporation of ethanol-water mixtures, Ind. Eng. Chem. Res. 46 (2007) 2224.

[82] C.L. Chang, P.Y. Chang, Performance enhancement of silicone/PVDF composite membranes for pervaporation by reducing cross-linking density of the active silicone layer, Desalination 192 (2006) 241.

[83] T. Kashiwagi, K. Okabe, K. Okita, Separation of ethanol from ethanol/water mixtures by plasma-polymerized membranes from silicone compounds, J. Membr. Sci. 36 (1988) 353.

[84] C.L. Chang, M.S. Chang, Preparation of composite membranes of functionalised silicone polymers and PVDF for pervaporation of ethanol-water mixture, Desalination 148 (2002) 39.

[85] C.L. Chang, M.S. Chang, Preparation of multi-layer silicone/PVDF composite membranes for pervaporation of ethanol aqueous solutions, J. Membr. Sci. 238 (2004) 117.

[86] M. Krea, D. Roizard, N. Moulai-Mostefa, D. Sacco, New copolyimide membranes with high siloxane content designed to remove polar organics from water by pervaporation, J. Membr. Sci. 241 (2004) 55.

[87] L. Liang, E. Ruckenstein, Pervaporation of ethanol-water mixtures through polydimethylsiloxane-polystyrene interpenetrating polymer network supported membranes, J. Membr. Sci. 114 (1996) 227.

[88] K. Okamoto, A. Butsuen, S. Tsuru, S. Nishioka, K. Tanaka, H. Kita, S. Asakawa, Pervaporation of water-ethanol mixtures through polydimetylsiloxane block-copolymer membranes, Polym. J. 19 (1987) 747.

[89] A.G. Fadeev, S.S. Kelley, I.D. McMillan, Y.A. Selinskaya, V.S. Khotimsky, V.V. Volkov, Effect of yeast fermentation by-products on poly[1-(trimethylsilyl)-1-propyne] pervaporative performance, J. Membr. Sci. 214 (2003) 229.

[90] Y. Nagase, Y. Takamura, K. Matsui, Chemical modification of Poly(substituted-acetylene). V. Alkylsilylation of Poly(1-Trimethylsilyl-1-propyne) and improved liquid separating property at pervaporation, J. Appl. Polym. Sci. 42 (1991) 185.

[91] J.A. Gonzalez-Marcos, C. Lopez-Dehesa, J.R. Gonzales-Velasco, Effect of operation conditions in the pervaporation of ethanol-water mixtures with poly(1-trimethylsilyl-1-propyne) membranes, J. Appl. Polym. Sci. 94 (2004) 1395.

[92] T. Sano, H. Yanagishita, Y. Kiyozumi, F. Mizukami, K. Haraya, Separation of ethanol/water mixture by silicalite membrane on pervaporation, J. Membr. Sci. 95 (1994) 221.

[93] T. Ikegami, D. Kitamoto, H. Negishi, K. Haraya, H. Matsuda, Y. Nitanai, N. Koura, T. Sano, H. Yanagishita, Drastic improvement of bioethanol recovery using a pervaporation separation technique employing a silicone rubber-coated silicalite membrane, J. Chem. Tech. Biotechnol. 78 (2003) 1006.

[94] Q. liu, R.D. Noble, J.L. Falconer, H.H. Funke, Organics/water separation by pervaporation with a zeolite membrane, J. Membr. Sci. 117 (1996) 163.

[95] D. Shen, W. Xiao, J. Yang, N. Chu, J. Lu, D. Yin, J. Wang, Synthesis of silicalite-1 membrane with two silicon source by secondary growth method and its pervaporation performance, Sep. Purif. Technol. 76 (2011) 308.

[96] X. Lin, X. Chen, H. Kita, K. Okamoto, Synthesis of silicalite tubular membranes by in situ crystallization, AIChE J. 49 (2003) 237.

[97] X. Lin, H. Kita, K.I. Okamoto, Silicalite membrane preparation, characterization and separation performance, Ind. Eng. Chem. Res. 40 (2001) 4069.

[98] X. Lin, H. Kita, K.I. Okamoto, A novel method for the synthesis of high performance silicalite membranes, Chem. Comm. (2000) 1889.

[99] T. Ikegami, H. Yanagishita, D. Kitamoto, H. Negishi, K. Haraya, T. Sano, Concentration of fermented ethanol by pervaporation using silicalite membranes coated with silicone rubber, Desalination 149 (2002) 49.

[100] H. Matsuda, H. Yanagishita, H. Negishi, D. Kitamoto, T. Ikegami, K. Haraya, T. Nakane, Y. Idemoto, N. Koura, T. Sano, Improvement of ethanol selectivity of silicalite membrane in pervaporation by silicone rubber coating, J. Membr. Sci. 210 (2002) 433.

[101] M. Nomura, T. Bin, S.I. Nakao, Selective ethanol extraction from fermentation broth using a silicalite membrane, Sep. Purif. Technol. 27 (2002) 59.

[102] T. Sano, M. Hasegawa, S. Ejiri, Y. Kawakami, H. Yanagishita, Improvement of the pervaporation performance of silicalite membranes by modification with a silane coupling reagent, Microporous Mater. 5 (1995) 179.

[103] S. Li, V.A. Tuan, J.L. Falconer, R.D. Noble, Properties and separation performance of Ge-ZSM-5 membranes, Micropor. Mesopor. Mat. 58 (2003) 137.

[104] T.C. Bowen, H. Kalipcilar, J.L. Falconer, R.D. Noble, Pervaporation of organic/water mixtures through B-ZSM-5 zeolite membranes on monolith supports, J. Membr. Sci. 215 (2003) 235.

[105] V. Sebastian, J. Motuzas, R.W.J. Dirrix, R.A. Terpstra, R. Mallada, A. Julbe, Synthesis of capillary titanosilicalite TS-1 ceramic membranes by MW-assisted hydrothermal heating for pervaporation application, Sep. Purif. Technol. 75 (2010) 249.

CHAPTER EIGHT

CONCLUSIONS AND RECOMMENCATIONS

8.1 Conclusions

The development of hollow fiber membranes with desirable morphology and separation performance for ethanol recovery by pervaporation is of crucial importance and challenge. Therefore, in this study, a systematic investigation on the key factors involved in the fabrication of PVDF hollow fiber membranes was investigated. The separation performance and mass transport phenomena in pervaporation process through PVDF hollow fiber membranes were explored. In order to enhance the pervaporation performance, the PVDF/nano-silica composite dual layer hollow fiber membranes were further developed for ethanol recovery. Based on above studies, the following conclusions can be drawn.

8.1.1 Molecuar elucidation of morphology and mechanical properties of PVDF hollow fibers from aspects of phase inversion, crystallization and rheology

This study explores the fundamental science of fabricating poly(vinylidene fluoride) (PVDF) hollow fiber membranes as well as elucidates the correlation among membrane morphology, crystallinity and mechanical properties as functions of non-solvent additives and dope rheology in the phase inversion process. A series of non-solvents (i.e. water, methanol, ethanol, isopropanol) are used either as nonsolvent additives in the dope or as a component in the external coagulant. Depending on the strength of the non-solvent, the phase inversion of semi-crystalline PVDF membranes

is dominated by liquid–liquid demixing or solid–liquid demixing accompanying crystallization. As a result, the membrane morphology transforms from an interconnected-cellular type to an interconnected-globule transition type with lower mechanical strengths when adding water, methanol, ethanol, or isopropanol into the spinning dopes or into the coagulation bath. The precipitation mechanisms drastically influence the resultant morphology and mechanical integrity of the membranes. The crystallinity and size of spherulitic globules in the morphology are controlled by the amounts of non-solvents presented in the systems. The rheological behavior of dope solutions is explored and the relationship between elongation viscosity and mechanical properties has been elaborated. Analytical methods and molecular dynamics simulations are employed to provide insights mechanisms from the views of thermodynamic and kinetic aspects as well as the state of polymer chains involved in the phase inversion process. Importantly, the conventional perspective of macrovoid-free membranes yielding better mechanical properties may not be applicable for semi-crystalline polymers like PVDF.

8.1.2 Modified pore-flow model for pervaporation mass transport in asymmetric PVDF hollow fiber membranes for ethanol-water separation

The mass transport phenomenon in pervaporation of the ethanol/water system via PVDF asymmetric hollow fiber membranes has been demonstrated through the pore-flow model and a newly modified pore-flow model has been proposed. The modified pore-flow model differs from the pore-flow model by factoring the contribution of Knudsen flow to vapor transport, which was neglected by the pore-flow model. All transport parameters involved in the model equations are determined from the

pervaporation experimental data of pure water and pure ethanol. The liquid transport parameter is strongly influenced by the hydrophobic and swelling properties of the PVDF polymer in the pure component system. The correlation of transport parameters to membrane pore size is explored and it is found that the pore size expansion (including the change of membrane surface morphology) is strongly dependent on the solvent in contact. The applicability of the pore-flow model and the modified pore-flow model is compared in predicting the pervaporation performance in terms of the permeate composition and the total mass flux in a water/ethanol mixture system. The modified pore-flow model shows a better prediction for the permeate composition than the pore-flow model and both models exhibit an excellent prediction of total permeate mass flux. The significance of Knudsen flow contribution in vapor phase transport as stated in the modified pore-flow model is discussed from the experimental and theoretical aspects.

8.1.3 Molecular design of the morphology and pore size of PVDF hollow fiber membranes for ethanol-water separation employing the modified pore-flow concept

In this study, we have established the fundamental science and engineering of fabricating poly(vinylidene fluoride) (PVDF) asymmetric hollow fiber membranes for ethanol–water separation and elucidated the complicated relationship among membrane morphology, pore size, pore size distribution and separation performance using the concept of the modified pore-flow model proposed in the previous work. The variation of bore-fluid composition, air-gap distance and take-up speed results in membranes with various morphologies ranging from large-finger-like macrovoid to nearly perfect macrovoid-free structures. Interestingly, an increase in air-gap distance

or take-up speed not only effectively suppress the formation of macrovoids but also results in the reduction of membrane pore size and the narrowing of pore size distribution, hence leading to the enhancement of membrane performance. The permeation flux is found to be mainly controlled by the overall porosity and the contribution of large pore sizes of the membrane, while the selectivity or separation factor is greatly determined by membrane pore size and pore size distribution, which is consistent with the modified pore-flow model proposed in our previous works. The newly developed PVDF asymmetric hollow fiber membranes demonstrates remarkable high fluxes of 3500–8800 g m^{-2} h^{-1} and reasonable ethanol–water separation factors of 5–8 compared to existing polymeric-based pervaporation membranes.

8.1.4 PVDF/nano-silica dual-layer hollow fibers with enhanced selectivity and flux as novel membranes for ethanol recovery

We have demonstrated the design and engineering of poly(vinylidene fluoride) (PVDF)/nano-silica dual-layer hollow fibers as novel pervaporation membranes for ethanol recovery. The newly developed dual-layer hollow fiber membrane can exhibit a high separation factor of up to 29 with a sustainable high flux of 1,100 g m^{-2} h^{-1}, which is equivalent to the separation performance regime of inorganic membranes. Central to this performance achievement is the synergy of (1) desirable membrane morphology, nano- pore size and high surface porosity of a thin-PVDF/nano-silica composite on a fully porous substrate accomplished by the dual-layer co-extrusion technology, and (2) optimal operating downstream pressure with the aid of controlled pervaporation transport. The membrane selectivity-downstream pressure dependence of PVDF/nano-silica hybrid membranes is comprehensible via a modified pore-flow

model. This study may represent a new class of membranes for ethanol-water separation.

8.2 Recommendations and future work

Based on the experimental results obtained, discussions presented and conclusions drawn from this research, the following recommendations may provide further insight for future investigations related to the development of membrane materials with potentially high separation properties and the innovation of membrane fabrication technology.

1. Exploring the membrane separation performance with real fermentation broths and other valued biofuel products such as acetone/n-butanol/ethanol (ABE) broths. A further investigation on the membrane performance and long-term stability under actual fermentation environments is recommended to bring the know-how technology close to industrial practices. In addition to ethanol as fuel, butanol has gained significant attention recently due to it possesses several important characteristics such as high octane value, gasoline blending, distribution and refueling, and good compatibility with the existing petroleum infrastructure. Acetone is also an important sovent in many chemical industries.

2. Fabricating novel mixed-matrix membranes by incorporating other active nano-particles such as zeolites, Metal-Organic Frameworks (MOFs), polyhedral oligomeric silsesquoxanes (POSS), polytetrafluoroethylene (PTFE), cyclodextrin, carbon nano-tube materials, metal oxides, and paticles based rubbers or elastomers

into PVDF membranes to explore the potentially practical feasilibity in pervaporation.

3. Investingating other possible modifications e.g. plasma modification, approaches to enhance the membrane separation performance.

4. Expending the present study to other organic/water mixture separations and organic-organic separations by pervaporation.

APPENDIX A

THE DERIVATION OF EQUATIONS AND PARAMETERS FOR MODIFIED PORE-FLOW MODEL (CHAPTER FIVE)

A.1 The derivation of $r = \left[(\frac{A}{\delta}) \frac{8\eta_L M}{\rho} \frac{1}{(\varepsilon_s / \delta)} \right]^{1/2}$ for water and ethanol systems

From equation (5.1), the parameter A can be deduced as

$$A = \frac{\pi r^4 \rho N_t}{8\eta_L M} \tag{A1}$$

Dividing δ by both sides of equation (A1)

$$\frac{A}{\delta} = \frac{\pi r^4 \rho N_t}{8\eta_L M \delta} \tag{A2}$$

$$\frac{A}{\delta} = \frac{\pi r^4 \rho}{8\eta_L M \delta} \frac{\varepsilon_s}{\pi r^2} \qquad where\ N_t = \frac{\varepsilon_s}{\pi r^2} \tag{A3}$$

$$\frac{A}{\delta} = \frac{r^2 \rho}{8\eta_L M} \frac{\varepsilon_s}{\delta} \tag{A4}$$

Rearranging the equation (A4) yields the pore size as follows

$$r = \left[(\frac{A}{\delta}) \frac{8\eta_L M}{\rho} \frac{1}{(\varepsilon_s / \delta)} \right]^{1/2} \tag{A5}$$

For pure water at 40 °C; ρ = 992 kg m^{-3}, η_L = 6.53x10^{-4} Pa s, M = 0.018 kg mol^{-1}

$\frac{\varepsilon_s}{\delta}$ = 3.31x10^4 m^{-1} (from Table 5.5) and $\frac{A}{\delta}$ = 8.25x10^{-8} mol m^{-2} s^{-1} Pa^{-1} (from Table 5.7)

Therefore, the pore size obtained for the pure water system is

$$r = \left[(8.25\times10^{-8}) \times \frac{8\times6.53\times10^{-4}\times0.018}{992} \frac{1}{(3.31\times10^4)} \right]^{1/2} = 4.86\times10^{-10}\,\text{m} \tag{A6}$$

Similarly, for pure ethanol at 40 °C; ρ =785 kg m^{-3}, η_L = 1.08x10^{-3} Pa s, M = 0.046 kg mol^{-1}, $\frac{\varepsilon_s}{\delta} = 3.31\times10^{4}$ m^{-1}(from Table 5.5) and $\frac{A}{\delta} = 2.56\times10^{-6}$ mol m^{-2} s^{-1} Pa^{-1} (from Table 5.7)

Thus, the pore size obtained for the pure ethanol system is

$$r = \left[(2.56\times10^{-6})\times\frac{8\times1.08\times10^{-3}\times0.046}{785}\frac{1}{(3.31\times10^{4})}\right]^{1/2} = 6.26\times10^{-9}\,\text{m} \qquad \text{(A7)}$$

A.2 The derivation of $r = \frac{3}{2}\left(\frac{C}{\delta}\right)\left(\frac{\pi M}{8RT}\right)^{1/2}\frac{RT}{(\varepsilon_s/\delta)}$ for water and ethanol systems

From equation (5.16), the parameter C can be rearranged as

$$C = \frac{2}{3}\left(\frac{8RT}{\pi M}\right)^{1/2}\frac{\pi r^3 N_t}{RT} \qquad \text{(A8)}$$

Similar to the derivation of equations (A2) to (A4), the equation (A8) can be rewritten as

$$\frac{C}{\delta} = \frac{2}{3}\left(\frac{8RT}{\pi M}\right)^{1/2}\frac{1}{RT}\frac{r\varepsilon_s}{\delta} \qquad \text{(A9)}$$

Hence, the pore size can be expressed as

$$r = \frac{3}{2}\left(\frac{C}{\delta}\right)\left(\frac{\pi M}{8RT}\right)^{1/2}\frac{RT}{(\varepsilon_s/\delta)} \qquad \text{(A10)}$$

For pure water at 40 °C; M = 0.018 kg mol^{-1}, T = 313 K, R = 8.314 m^3 Pa mol^{-1} K^{-1}, $\frac{\varepsilon_s}{\delta} = 3.31\times10^{4}$ m^{-1} (from Table 5.5) and $\frac{C}{\delta} = 2.25\times10^{-6}$ mol m^{-2} s^{-1} Pa^{-1} (from Table 5.7)

Therefore, the calculated pore size for pure water system is

$$r = (2.25x10^{-6})\frac{3}{2}\left(\frac{3.14\times0.018}{8\times8.314\times313}\right)^{1/2}\frac{(8.314\times313)}{(3.31\times10^{4})} = 4.37x10^{-10}\,\text{m} \qquad \text{(A11)}$$

For pure ethanol at 40 °C; M = 0.046 kg mol^{-1}, T = 313 K, R = 8.314 m^3 Pa mol^{-1} K^{-1}

$\frac{\varepsilon_s}{\delta} = 3.31\times10^4$ m^{-1} (from Table 5.5) and $\frac{C}{\delta} = 1.08\times10^{-6}$ mol m^{-2} s^{-1} Pa^{-1} (from Table 5.7)

As a result, the pore size for pure ethanol system is

$$r = (1.08\times10^{-6})\cdot\frac{3}{2}\left(\frac{3.14\times0.046}{8\times8.314\times313}\right)^{1/2}\frac{(8.314\times313)}{(3.31\times10^4)} = 3.35x10^{-10}\ \text{m} \qquad \text{(A12)}$$

A.3 The calculation of A_{mix}/δ for the pore-flow model

From the equation (5.13),

$$W_{total} = \left[\frac{A_{mix}}{\delta}(P_2 - P_*) + \frac{B_w}{\delta}(P_{w,*}^2 - P_{w,3}^2) + \frac{B_e}{\delta}(P_{e,*}^2 - P_{e,3}^2)\right]\times\left(M_w Y_{w,3} + M_e Y_{e,3}\right) \qquad \text{(A13)}$$

where the i^{th} and j^{th} components are water and ethanol, respectively.

For the pervaporation data of 45 wt% ethanol/water mixture; W_{total} = 3.558 g m^{-2} s^{-1}, P_2 = 101,325 Pa, P_* = 10060 Pa, $P_{w,*}$ = 4833.86 Pa, $P_{e,*}$ = 5220.13 Pa; $Y_{w,3}$=0.4811; $Y_{e,3}$ = 0.5189; M_w = 18 g mol^{-1}, M_e = 46 g mol^{-1}, B_w/δ = 4.28x10^{-10} mol m^{-2} s^{-1} Pa^{-2} (from Table 5.6), B_e/δ = 4.45x10^{-10} mol m^{-2} s^{-1} Pa^{-1} (from Table 5.6). Thus, the A_{mix}/δ can be calculated as

$$3.558 = \left[\frac{A_{mix}}{\delta}(101325-10060) + 4.28\times10^{-10}(4833.86^2 - 0^2) + 4.45x10^{-10}(5220.13^2 - 0^2)\right]\times \left[(18\times0.4811) + (46\times0.5189)\right] \qquad \text{(A14)}$$

$$\frac{A_{mix}}{\delta} = 9.56\times10^{-7}\ \text{mol m}^{-2}\ \text{s}^{-1}\ \text{Pa}^{-1} \quad \text{(for the pore-flow model)} \qquad \text{(A15)}$$

Similarly, the calculation of A_{mix}/δ for the modified pore-flow model can be derived from equation (5.26),

$$W_{total} = \left[\begin{array}{l} \frac{A_{mix}}{\delta}(P_2 - P_*) + \frac{B_w}{\delta}(P_{w,*}^2 - P_{w,3}^2) + \frac{C_w}{\delta}(P_{w,*} - P_{w,3}) + \\ \frac{B_e}{\delta}(P_{e,*}^2 - P_{e,3}^2) + \frac{C_e}{\delta}(P_{e,*} - P_{j,3}) \end{array} \right] \times \left(M_w Y_{w,3} + M_e Y_{e,3} \right) \quad \text{(A16)}$$

where the i^{th} and j^{th} components are water and ethanol, respectively.

For the pervaporation data of 45 wt% ethanol/water mixture; W_{total} = 3.518 g m^{-2} s^{-1}, B_w/δ = 1.86x10^{-10} mol m^{-2} s^{-1} Pa^{-2} (from Table 5.6), B_e/δ = 3.95x10^{-10} mol m^{-2} s^{-1} Pa^{-1} (from Table 5.6), C_w/δ = 2.25x10^{-6} mol m^{-2} s^{-1} Pa^{-1} (from Table 5.6), C_e/δ = 1.08x10^{-6} mol m^{-2} s^{-1} Pa^{-1} (from Table 5.6), and all other parameters obtained in the calculation of the equation (A14) remains the same. Therefore, the A_{mix}/δ can be determined as

$$3.558 = \left[\begin{array}{l} \frac{A_{mix}}{\delta}(101325 - 10060) + 1.86\times10^{-10}(4833.86^2 - 0^2) + 2.25\times10^{-6}(4833.86 - 0) + \\ 3.95\times10^{-10}(5220.13^2 - 0^2) + 1.08\times10^{-6}(5220.13 - 0) \end{array} \right] \times \left[(18\times0.4811) + (46\times0.5189) \right] \quad \text{(A17)}$$

$$\frac{A_{mix}}{\delta} = 8.53x10^{-7} \text{ mol } m^{-2} \text{ } s^{-1} \text{ } Pa^{-1} \quad \text{(for the modified pore-flow model)} \quad \text{(A18)}$$

A.4 The derivation of $Q_{Knudsen} = \frac{2}{3}\left(\frac{8RT}{\pi M}\right)^{1/2} \frac{1}{RT} \frac{r\varepsilon_s}{\delta} \times (P_* - P_3)$

The definition of Knudsen flow in the unit of mol m^{-2} s^{-1} can be expressed as

$$Q_{Knudsen} = \frac{2}{3}\left(\frac{8RT}{\pi M}\right)^{1/2} \frac{1}{RT}\frac{\pi r^3}{\delta} \times (P_* - P_3) \times N_t \quad \text{(A19)}$$

Since $N_t = \frac{\varepsilon_s}{\pi r^2}$ (A20)

$$Q_{Knudsen} = \frac{2}{3}\left(\frac{8RT}{\pi M}\right)^{1/2} \frac{1}{RT}\frac{\pi r^3}{\delta} \times (P_* - P_3) \times \frac{\varepsilon_s}{\pi r^2} \quad \text{(A21)}$$

$$Q_{Knudsen} = \frac{2}{3}\left(\frac{8RT}{\pi M}\right)^{1/2} \frac{1}{RT}\frac{r\varepsilon_s}{\delta} \times (P_* - P_3) \quad \text{(A22)}$$

An example of the calculation at pore size of $1x10^{-8}$ m in the water system; M = 0.018 kg mol^{-1}, T = 313 K, R = 8.314 m^3 Pa mol^{-1} K^{-1}, $\frac{\varepsilon_s}{\delta} = 3.31\times10^4\ m^{-1}$ (from Table 5.5), r = $1.0x10^{-8}$ m, P_* = 8500 Pa, P_3 = 0 Pa. Therefore, the molar flux contributed from Knudsen flow can be calculated as

$$Q_{Knudsen} = \frac{2}{3}\left(\frac{8\times8.314\times313}{3.14\times0.018}\right)^{1/2} \frac{1}{8.314\times313} \times 1x10^{-8} \times 3.31x10^4 \times (8500-0) = 0.44 \text{ mol } m^{-2}s^{-1} \quad \text{(A23)}$$

A.5 The derivation of $Q_{viscous} = \frac{1}{8\eta_g RT}\frac{r^2 P_m \varepsilon_s}{\delta} \times (P_* - P_3)$

The definition of viscous flow in the unit of $mol.m^{-2}.s^{-1}$ can be expressed as

$$Q_{viscous} = \frac{1}{8\eta_g RT}\frac{\pi r^4 P_m}{\delta} \times (P_* - P_3) \times N_t \qquad where\ N_t = \frac{\varepsilon_s}{\pi r^2} \quad \text{(A24)}$$

$$Q_{viscous} = \frac{1}{8\eta_g RT}\frac{r^2 P_m \varepsilon_s}{\delta} \times (P_* - P_3) \quad \text{(A25)}$$

An example of the calculation at pore size 1.0×10^{-8} m in a water system; M = 0.018 kg mol^{-1}, η_g = 6.53×10^{-4} Pa s, T = 313 K, R = 8.314 m^3 Pa mol^{-1} K^{-1}, $\frac{\varepsilon_s}{\delta} = 3.31 \times 10^4$ m^{-1} (from Table 5.5), r = 1×10^{-8} m, P_* = 8500 Pa, P_m= 4250 Pa, P_3 = 0 Pa. Therefore, the molar flux contributed from Knudsen flow can be estimated as

$$Q_{viscous} = \frac{1}{8 \times 6.53 \times 10^{-4} \times 8.314 \times 313} \times (1.0 \times 10^{-8})^2 \times 4250 \times 3.31 \times 10^4 \times (8500 - 0) = 8.80 \times 10^{-6}$$

mol m^{-2} s^{-1} (A26)

APPENDIX B

THE DERIVATION OF EQUATIONS AND PARAMETERS FOR THE MODIFIED PORE-FLOW MODEL (CHAPTER SEVEN)

B.1 The sample estimation of pore size using liquid transport parameters for pure water (A_w/δ) and pure ethanol (A_e/δ) systems

According to the modified pore-flow model, the pore size can be determined by following equation

$$r = \left[\left(\frac{A}{\delta}\right) \frac{8\eta_L M}{\rho} \frac{1}{(\varepsilon_s/\delta)} \right]^{1/2} \quad \text{(B1)}$$

For pure water at 50 °C; ρ = 988 kg m^{-3}, η_L = 5.47x10^{-4} Pa s, M_w = 0.018 kg mol^{-1} and the membrane (DL$_{AG\text{-}20}$) with following properties; $\frac{\varepsilon_s}{\delta} = 6.41x10^{2}$ m^{-1} (from Table 7.2) and $\frac{A_w}{\delta} = 5.05x10^{-8}$ mol m^{-2} s^{-1} Pa^{-1} (from Table 7.4)

Therefore, the pore size obtained for the pure water system is

$$r = \left[(5.05x10^{-8}) \times \frac{8 \times 5.47x10^{-4} \times 0.018}{988} \frac{1}{(6.41x10^{2})} \right]^{1/2} = 2.51x10^{-9} \text{ m} = 2.51 \text{ nm} \quad \text{(B2)}$$

Similarly, for pure ethanol at 50 °C; ρ = 763 kg m^{-3}, η_L = 6.70x10^{-4} Pa s, M_e = 0.046 kg mol^{-1}, $\frac{\varepsilon_s}{\delta} = 6.41x10^{2}$ m^{-1} (from Table 7.2) and $\frac{A_e}{\delta} = 1.65x10^{-5}$ mol m^{-2} s^{-1} Pa^{-1} (from Table 7.4)

Thus, the pore size obtained for the pure ethanol system is

$$r = \left[(1.65x10^{-5}) \times \frac{8 \times 6.70x10^{-4} \times 0.046}{763} \frac{1}{(6.41x10^{2})} \right]^{1/2} = 9.12x10^{-8}\,\text{m} = 91.2\ \text{nm} \qquad \text{(B3)}$$

B.2 The sample estimation of pore size using vapor transport parameters for pure water (C_w/δ) and pure ethanol (C_e/δ) systems

According to the modified pore-flow model, the pore size can be expressed as

$$r = \frac{3}{2}\left(\frac{C}{\delta}\right)\left(\frac{\pi M}{8RT}\right)^{1/2} \frac{RT}{(\varepsilon_s/\delta)} \qquad \text{(B4)}$$

For pure water at 50 °C; M_w = 0.018 kg mol^{-1}, T = 323 K, R = 8.314 m^3 Pa mol^{-1} K^{-1} and the membrane ($DL_{AG\text{-}20}$) with following properties; $\frac{\varepsilon_s}{\delta} = 6.41x10^{2}\,\text{m}^{-1}$ (from Table 7.2) and $\frac{C_w}{\delta} = 5.15x10^{-6}$ mol m^{-2} s^{-1} Pa^{-1} (from Table 7.4)

Hence, the calculated pore size for pure water system is

$$r = (5.15x10^{-6})\frac{3}{2}\left(\frac{3.14 \times 0.018}{8 \times 8.314 \times 323}\right)^{1/2} \frac{(8.314 \times 323)}{(6.41 \times 10^{2})} = 5.25x10^{-8}\,\text{m} = 52.5\ \text{nm} \qquad \text{(B5)}$$

For pure ethanol at 50 °C; M_e = 0.046 kg mol^{-1}, T = 323 K, R = 8.314 m^3 Pa mol^{-1} K^{-1} $\frac{\varepsilon_s}{\delta} = 6.41x10^{2}\,\text{m}^{-1}$ (from Table 7.2) and $\frac{C_e}{\delta} = 3.10x10^{-6}$ mol m^{-2} s^{-1} Pa^{-1} (from Table 7.4)

As a result, the pore size for pure ethanol system is

$$r = (3.10x10^{-6})\frac{3}{2}\left(\frac{3.14 \times 0.046}{8 \times 8.314 \times 323}\right)^{1/2} \frac{(8.314 \times 323)}{(6.41x10^{2})} = 5.05x10^{-8}\ \text{m} = 50.5\ \text{nm} \qquad \text{(B6)}$$

PUBLICATIONS

Journal Papers:

1. **P. Sukitpaneenit**, T.S. Chung, Molecular elucidation of morphology and mechanical properties of PVDF hollow fiber membranes from aspects of phase inversion, crystallization and rheology, Journal of Membrane Science, 340 (2009) 192.
2. **P. Sukitpaneenit**, T.S. Chung, L.Y. Jiang, Modified pore-flow model for pervaporation mass transport in PVDF hollow fiber membranes for ethanol-water separation, Journal of Membrane Science, 362 (2010) 393.
3. **P. Sukitpaneenit**, T.S. Chung, Molecular design of the morphology and pore size of PVDF hollow fiber membranes for ethanol-water separation employing the modified pore-flow concept, Journal of Membrane Science, 374 (2011) 67.
4. **P. Sukitpaneenit**, T.S. Chung, PVDF/nano-silica dual-layer hollow fibers with enhanced selectivity and flux as novel membranes for ethanol recovery, Industrial & Engineering Chemistry Research, Accepted.
5. N. Peng, N. Widjojo, **P. Sukitpaneenit**, M.M. Teoh, T.S. Chung, J.Y. Lai. Review article: Molecular design of polymeric hollow fibers as sustainable technologies: Past, Present, and Future. (Revised manuscript in preparation for Progress in Polymer Science)
6. Y. Wang, S.S. Hosseini, **P. Sukitpaneenit**, T.S. Chung. Review article: Polymeric membrane separation technology for sustainable energy development. (Manuscript in preparation for Energy & Environmental Science)

Conference Papers:

1. **P. Sukitpaneenit**, T.S. Chung, PVDF hollow fiber membrane formation: Fundamental study on the roles of phase inversion, crystallization and rheology on morphology and mechanical properties, AIChE Annual Meeting, Nashville, Tennessee, USA. Nov. 8-13, 2009.
2. **P. Sukitpaneenit,** T.S. Chung, Fundamental science and engineering of fabricating PVDF hollow fiber membranes for alternative energy and water, Nanomemcourse 2010: Nano-structured materials and Membranes for Health and Sustainable Water, University of Twente, Enschede, April 7-16, 2010.
3. **P. Sukitpaneenit,** T.S. Chung, Design and tailoring of chemistry and morphology of PVDF hollow fiber membranes for various separation applications, The 4th Materials Research Society of Singapore (MRS-S) conference on Advanced Materials, Institute of Materials Research and Engineering (IMRE), Singapore, March 17-19, 2010.
4. **P. Sukitpaneenit**, T.S. Chung, Advances in membrane fabrication and separation technologies for biofuel-sustainable energy, The 11th APRU Doctoral Students Conference, University of Indonesia, Indonesia, July 11-16, 2010.
5. T.S. Chung, N. Peng, N. Widjojo, **P. Sukitpaneenit,** J. Su, Y. Wang, The Fabrication Technologies of Polymeric Hollow Fiber Membranes: Past, Present, and Future, International Congress on Membranes and Membrane Processes (ICOM), Amsterdam, The Netherlands, July 23-29, 2011.